

MODELING THE EFFECT OF PRECISE SHORT-CHAIN BRANCH PLACEMENT
IN ETHYLENE-CO-PROPYLENE AND ETHYLENE-CO-BUTYLENE MATERIALS:
SYNTHESIS, THERMAL BEHAVIOR, AND MORPHOLOGICAL
CHARACTERIZATION

By

JASON ALAN SMITH

A DISSERTATION PRESENTED TO THE GRADUATE SCHOOL
OF THE UNIVERSITY OF FLORIDA IN PARTIAL FULFILLMENT
OF THE REQUIREMENTS FOR THE DEGREE OF
DOCTOR OF PHILOSOPHY

UNIVERSITY OF FLORIDA

2002

For my mother, Brenda, and my father, Franklin. It is they who instilled all that is good in me. I will be forever grateful for the love, encouragement, and support they have given me during my academic career. I love them both more than words could ever express. This dissertation is a testament to them.

ACKNOWLEDGMENTS

There are a great number of individuals who have given me their support, encouragement, and friendship during the course of my dissertation work. First and foremost, I must thank my parents, Franklin D. and Brenda C. Smith. Their tender love, devotion, and moral standards have made me the man that I am today. Without them, I would be incomplete.

I would like to acknowledge the people that shaped and molded my career as a student of chemistry before coming to graduate school. Mr. Ken Hastings, my high school chemistry teacher, is the best chemistry instructor that I have ever had. Perhaps it is because he was first, but more so, it was because of his excellent teaching abilities and his love of chemistry that made me first become interested in the field.

Sincere gratitude also goes to Dr. Joseph W. Kolis, my undergraduate advisor at Clemson University. I have never met his equal in the enthusiasm he expresses for chemistry. Dr. Kolis made my undergraduate research career an extremely rewarding experience, and through his teachings, support, and encouragement, I attained a better understanding and love of chemistry.

I would also like to express my sincere thanks to Dr. James E. Rodgers, my supervisor at the Monsanto (Solutia) Chemical Company in Pensacola, Florida. His attention to detail, dedication to true science, and amazing work ethic were genuinely a sight to behold. I will always be indebted to the support and friendship he has given me over the past eight years and still continues to give to this day.

I am extremely grateful to Dr. George B. Butler and his wife Josephine for establishing the Butler Polymer Laboratory. It has truly been both a unique and wonderful place at which to work and study.

The Butler Polymer Floor is made up of a pool of extremely talented people, and I am fortunate to have made friendships with many of its members over the years. There are so many people on the Butler Polymer Floor that have enriched my life, both inside and outside of the laboratory—sincere thanks are extended to Wagener group members, past and present, including Dr. John D. Anderson, Dr. James H. Pawlow, Dr. Kystyna Brzezinska, Dr. Mark D. Watson, Dr. Dominick J. Valenti, Dr. Tammy A. Davidson, Dr. Debra ‘Debby’ Tindall, Dr. P. Shane Wolfe, Dr. A. Cameron (Church) Pawlow, John Sworen, Tim Hopkins, Patrick O’Donnell, John Schwendeman, and Ed Lehman.

Specifically, I wish to thank Dr. Dominick Valenti for initiating this research project and providing valuable advice during my first year as a graduate student. I also feel very fortunate to have been trained in the ways of ADMET by Drs. Krystyna Brzezinska and Mark Watson. Krystyna helped me immensely in the beginning of my dissertation work, a debt that I can never repay in kind, but for which I am eternally grateful. She is a true friend, gracious soul, skilled professional, and perhaps the most talented synthetic chemist with which I have ever been associated. I am so very fortunate to have shared the lab with Mark Watson; he is also an extremely talented chemist, good friend, and true “Southern Gentleman.” The floor was never the same for me after the departure of Mark and his wife, Kim. In addition, I express my gratitude to Mr. John C. Sworen, who will continue the work presented in this dissertation. The last year spent in the laboratory with him has been a complete joy, and I regret not having had

more time to spend with him. He is a good man and a fine chemist, and my life is richer for having known and worked with him.

I must also thank several other members of the floor who have all touched my life in a positive manner. My experience at the University of Florida would not have been complete without making the acquaintances of Dr. Anil Kumar, Dr. Peter Balanda, Drs. David and Jennifer Irvin, Dr. Dean Welsh, Dr. Michael Ramey, Mr. Carl Gaupp, and Mr. C. J. "The Raging Cajun" DuBois. In particular, I would like to thank Carl for being the best lab mate that anyone could possibly imagine. I hope that our paths cross again one day. I must once more mention Mike Ramey; he and I came to the Butler Polymer Floor together as first year graduate students. He is a fine man, and I feel proud to call him my friend. I will always have fond memories of the times we had while attending U.F.

Enough thanks cannot be expressed to Mrs. Lorraine Williams, Mrs. Donna Balkcom, and Mrs. Lori Clark for taking care of all the administrative issues associated with graduate school. No matter what the situation, they always handled it with an unparalleled amount of grace, caring, and understanding. I will miss all of them because they could all turn any of my bad days around by simply smiling and telling me that everything would be okay. Sure enough, it always worked out due to their labors. Specifically, I owe many debts of gratitude to the efforts and friendship of Lorraine Williams—the Butler Polymer Floor would be lost without her. She is the heart and soul of the Polymer Floor, and I will never forget her.

I will be eternally grateful to Professor Dr. Gerhard Wegner for inviting me into his group in order to study x-ray diffraction and microscopy at the Max-Planck-Institut für Polymerforschung (MPI-P) in Mainz, Germany. My time there was the most rewarding

experience I have had to this point in my young life, both scientifically and culturally. Professor Wegner is a wonderful man and the most intelligent scientist that I have ever met. The times spent discussing chemistry and life with him will always be cherished.

Many people at the MPI-P greatly impacted and/or contributed to the work presented in this dissertation. I owe sincere thanks to Dr. Günter Lieser, Dr. Wolfgang Meyer, Dr. Volker Enkelmann, Herr Michael Steiert, Herr Gunnar Glaßer, Frau Katrin Kirschhoff, Frau Petra Räder, Herr Bernhard Zimmer, and Herr Walter Scholdei. Their friendship, technical support, and helpful discussions are fondly remembered and greatly appreciated.

Specifically, I would like to extend my heartfelt thanks Dr. Günter Lieser, who served as my project leader during my time at the MPI-P. Dr. Lieser was, is, and always will be the “truest scientist” that I have ever had the pleasure of knowing. He is a consummate professional and the fruits of his ideas and labor make up the heart of Chapters 3 and 4 in this dissertation. I wish that I could express to him how much he has helped me as a young scientist, but alas, I know there is no way to do so because there isn’t a word for it, in English or German (Aber, vielen Dank für alles, Herr Lieser.). He is a truly the most talented scientist with whom I have had the pleasure of working, and my time and experiences with him will remain special to me for as long as I shall live.

I have been deeply blessed with a number of funding sources throughout my graduate career. Therefore, for financial support, I would like to give thanks to the National Science Foundation; National Science Foundation Dissertation Enhancement Fellowship and the Eastman Fellowship (from the Eastman Chemical Company), both of

which funded my exploits during the period spent at the MPI-P; and the University of Florida for providing me with numerous teaching assistantships.

Many thanks are extended to the members of my committee—Professors John R. Reynolds, J. Eric Enholm, James M. Boncella, and Anthony B. Brennan. Their efforts in reading and discussing the material presented in this dissertation have been instrumental in making it a stronger document.

In closing, I must express my sincere appreciation to my research director and chairman of my committee, Dr. Kenneth B. Wagener. I am grateful for his encouragement, guidance, patience, and understanding during the course of my graduate career. I would like to thank him for giving me the freedom to explore science and make my own mistakes as I climbed the ladder of being a student to becoming a chemist. He has not only filled the role of my advisor but has also become a dear friend of mine. I owe him debts of gratitude that I can never repay, much the same as child can never repay the love extended by his or her parents. He is truly an amazing man, both professionally and personally, and I am a better person for having known him.

TABLE OF CONTENTS

	<u>page</u>
ACKNOWLEDGMENTS	iii
LIST OF TABLES	xii
LIST OF FIGURES	xiv
ABSTRACT	xx
 CHAPTER	
1 ADMET—A NON-TRADITIONAL STEP-GROWTH POLYMERIZATION	1
1.1 Introduction	1
1.1.1 Historical Perspective	1
1.1.2 Metathesis Catalysts	3
1.1.3 Requirements for ADMET Polymerization	6
1.1.4 Applications	7
1.2 Overview of Chemistry and Analytical Techniques	8
1.2.1 Chemistry and Catalysis	8
1.2.1.1 Brief history	8
1.2.1.2 Importance of catalyst selection	11
1.2.2 Experimental Methods	13
1.2.2.1 Purification of monomers, reagents, and solvents	14
1.2.2.2 General metathesis polymerization conditions	15
1.2.2.3 ADMET polymerization of 1,9-decadiene	16
1.2.3 Characterization of ADMET Polymers	17
1.3 Structure-Property Relationships	21
1.3.1 General Considerations	21
1.3.2 Influence of Precise Branching on Polymer Microstructure	22
1.4 Dissertation Purpose	24
 2 SYNTHESIS AND CHARACTERIZATION OF ETHYLENE/PROPYLENE MODEL COPOLYMERS WITH PRECISE METHYL BRANCH PLACEMENT	 26
2.1 Introduction	26
2.2 Results and Discussion	28
2.2.1 Monomer and Polymer Synthesis and Design	28
2.2.2 ADMET Polymerization and Hydrogenation Chemistry	29

2.2.3	Molecular Weight Analysis of Fully Hydrogenated ADMET Polyethylenes	31
2.2.4	Structural Determination Data.....	33
2.2.5	Thermal Analysis: Comparative Polyethylene Thermal Data	37
2.2.6	Methyl Branched ADMET Polyethylene Melting Behavior.....	39
2.2.7	The Glass Transition Behavior of Methyl Branched ADMET Polyethylene	45
2.3	Conclusions	47
2.4	Experimental	48
2.4.1	Instrumentation and analysis.....	48
2.4.2	Materials.	51
2.4.3	Characterization of starting materials.	52
2.4.4	Symmetrical monomer synthesis and characterization.....	54
2.4.5	ADMET polymerizations of symmetrical methyl branch monomers....	66
2.4.6	Hydrogenation of polymers 2a-2e. Watson's supported catalyst.	69
2.4.7	Hydrogenation of polymer 2ds. Modified diimide method.	73
3	THERMAL BEHAVIOR OF MODEL ETHYLENE/PROPYLENE COPOLYMERS WITH PRECISE METHYL BRANCH PLACEMENT	74
3.1	Introduction.....	74
3.2	Experimental.....	77
3.2.1	Materials.....	77
3.2.2	Differential Scanning Calorimetry (DSC).....	77
3.2.2.1	Initial studies on HP9, HP11, HP15, HP19, and HP21.....	77
3.2.2.2	Extended studies on HP9, HP15, HP21.	78
3.2.2.3	Crystallinity determination.	80
3.2.2.4	Scan rate dependence versus melting/crystallization temperature.....	81
3.2.2.5	Thermal history.....	81
3.2.2.6	Isothermal crystallization (annealing) time effect.	82
3.3	Results and Discussion	83
3.3.1	Influence of Comonomer Content on Thermal Behavior and Morphology.	83
3.3.2	Initial Calorimetry Data for ADMET Model EP Systems with Precise Methyl Branch Placement.....	87
3.3.3	Extended Thermal Behavior Studies for HP9, HP15, and HP21.	89
3.3.4	Dependence of Melting/Crystallization Temperature on Scan Rate.	93
3.3.5	Indication of Multiple Melting Endotherms for HP9.	98
3.3.6	Annealing Behavior.....	101
3.3.7	Importance of Choosing Proper Annealing Condition.....	112
3.4	Conclusions.....	114
4	X-RAY DIFFRACTION AND MICROSCOPY INVESTIGATIONS OF MODEL ETHYLENE/PROPYLENE COPOLYMERS WITH PRECISE METHYL BRANCH PLACEMENT	117
4.1	Structure of Solids—Historical Perspective	117
4.2	X-ray Diffraction of Crystals.....	120

4.3	Towards the Structure of Polyethylene—Linear Paraffins	122
4.4	Structural Morphology of Linear Polyethylene	124
4.5	Long Range Order in Linear Polyethylene	126
4.6	Wide-Angle X-ray Diffraction (WAXD): Powder Diffraction—The Debye-Scherrer Technique	130
4.7	Small-Angle X-ray Scattering (SAXS).....	133
4.8	Three-Dimensional Structure Determination in Polymeric Materials—Additional Techniques.....	135
4.9	Introduction—Morphological Studies of EP Copolymers Containing Precise Methyl Branching	136
4.10	Experimental	141
4.10.1	Materials.....	141
4.10.2	Differential Scanning Calorimetry (DSC).....	141
4.10.3	Wide-Angle X-ray Diffraction (WAXD).....	143
4.10.3.1	Debye-Scherrer camera.....	143
4.10.3.2	ENRAF-NONIUS Diffractus 586.....	143
4.10.4	Small-Angle X-ray Scattering (SAXS)	143
4.10.4.1	Sample preparation—annealing.....	143
4.10.4.2	Kiessig camera.....	144
4.10.5	Optical (Light) Microscopy.....	144
4.10.5.1	Sample preparation	144
4.10.5.2	Instrumentation	144
4.10.6	Transmission Electron Microscopy (TEM) and Electron Diffraction.....	145
4.10.6.1	Sample preparation	145
4.10.6.2	Instrumentation	145
4.10.7	Infrared (IR) Spectroscopy.....	145
4.10.8	Raman Spectroscopy	146
4.11	Results and Discussion	146
4.11.1	Thermal Behavior.....	146
4.11.2	X-ray Diffraction.....	152
4.11.2.1	Debye-Scherrer camera—powder diff (WAXD).....	154
4.11.2.2	ENRAF-NONIUS Diffractus 586—powder diff (WAXD).....	159
4.11.2.3	Small-angle x-ray scattering (SAXS)—Kiessig camera.....	167
4.11.2.4	Small-angle x-ray scattering (SAXS)—Long-period	177
4.11.3	Optical Microscopy (OM) of HP15 and HP21	179
4.11.4	Transmission Electron Microscopy (TEM) and Electron (e ⁻) Diffraction of HP15 and HP21.....	185
4.11.5	Raman and Infrared (IR) Spectroscopy of HP15 and HP21.	193
4.11.5.1	Raman spectroscopy	193
4.11.5.2	Infrared spectroscopy.....	200
4.12	Final Comments on the Structure of the Hexagonal Phase Determined for ADMET EP Copolymers Containing Precise Methyl Branching.....	208

5 SYNTHESIS AND THERMAL BEHAVIOR OF A MODEL ETYLENE/BUTYLENE COPOLYMER WITH PRECISE ETHYL BRANCH PLACEMENT	211
5.1 Introduction.....	211
5.2. Results and Discussion	213
5.2.1 Monomer Synthesis and Design.....	213
5.2.2 Continuing Research in Regard to Ethyl Monomer Synthesis.....	220
5.2.3. ADMET Polymerization and Hydrogenation Chemistry.....	224
5.2.4. Molecular Weight Analysis.....	224
5.2.5. Structural Determination Data.....	225
5.2.6. Thermal Analysis	232
5.3. Conclusions.....	235
5.4. Experimental	236
5.4.1. Instrumentation and Analysis.....	236
5.4.2. Materials.....	239
5.4.3. Characterization of Starting Materials.....	239
5.4.4. Symmetrical Monomer Synthesis and Characterization.....	240
5.4.4.1. Step 1: Dialkylation of ethyl acetoacetate.....	240
5.4.4.2. Step 2: Decarboxylation of the disubstituted β -keto ester.....	240
5.4.4.3. Step 3: Reduction of the alkyl methyl ketone to the alcohol.....	242
5.4.4.4. Step 4 (Tosylation of the alcohol).....	243
5.4.4.5. Step 5: Reduction of the tosylate to the ethyl branch monomer.....	244
5.4.4.6. General Metathesis Conditions.....	246
5.4.4.7. Polymerization of 3-(4-pentenyl)-7-octene (1) to give UPEB9 (2).....	247
5.4.4.8. Hydrogenation of UPEB9 (2) to produce HPEB9 (3).....	248
REFERENCES	250
BIOGRAPHICAL SKETCH	273

LIST OF TABLES

<u>Table</u>	<u>page</u>
2-1. Molecular Weight Data for Unsaturated and Saturated Branched ADMET Polyethylene Polymers.	30
2-2. The Effect of Molecular Weight on Thermal Properties for Linear and Methyl Branched ADMET Polyethylene Polymers.	33
2-3. Thermal Data for a Number of Polyethylene Systems.	38
2-4. DSC Data for Fully Hydrogenated ADMET Polyethylene Methyl-Branched Model Polymers.	41
2-5. Glass Transition Data for ADMET Polyethylene Model Polymers.	46
3-1. DSC and Crystallinity Data for ADMET EP Copolymer Models with Precise Methyl Branching.	89
3-2. DSC and Percent Crystallinity Data for ADMET E/P Models with Precise Methyl Branching—In Depth Analysis/Comparison.	90
3-3. Peak Melting Temperatures and Crystallinity after Annealing at Room Temperature for Extended Time Periods.	106
4-1. Optimized Peak Melting Temperatures and Crystallinity Found After Annealing Experiments for Extended Time Periods.	148
4-2. Lamella Thickness (L): Theoretical Calculation Based on the Thomson-Gibbs Equation.	151
4-3. Debye-Scherrer Scattering Data for EP Copolymer with Random Methyl Branching.	155
4-4. Debye-Scherrer Scattering Data for HP15: EP Copolymer with Precise Methyl Branching (67 methyls/1000 carbons).	156
4-5. Debye-Scherrer Scattering Data for HP21: EP Copolymer with Precise Methyl Branching (48 methyls/1000 carbons).	157
4-6a. Kiessig Camera: SAXS of HP15, 100 mm Exposure Distance: EP Copolymer with Precise Methyl Branching (67 methyls/1000 carbons).	169

4-6b.	Kiessig Camera: SAXS of HP15, 200 mm Exposure Distance: Copolymer with Precise Methyl Branching (67 methyls/1000 carbons).....	EP 170
4-7a.	Kiessig Camera: SAXS of HP21, 100 mm Exposure Distance: EP Copolymer with Precise Methyl Branching (48 methyls/1000 carbons).	174
4-7b.	Kiessig Camera: SAXS of HP21, 200 mm Exposure Distance: Copolymer with Precise Methyl Branching (48 methyls/1000 carbons).....	EP 174
4-8.	SAXS Long-Spacing Measurements for ADMET Model EP Copolymers with Precise Methyl Branching.....	178
4-9.	Raman Frequency Assignments for EP Copolymer Models with Precise Methyl Branching.	196
4-10.	Methylene Sequence Length Needed to Obtain Planar—Zigzag PE Chains	199
4-11.	Infrared Frequency Assignments for Solution and Melt Crystallized EP Copolymer Models with Precise Methyl Branching.....	203
5-1.	Decarboxylation of Compound 4 to Yield 5: Representative Optimization Reactions.....	217
5-1.	Continued.....	218
5-2.	Reduction of the Secondary Tosylate (4) to Ethyl-Branched (1) and Eliminated (8) Monomers with Various Hydride Reducing Agents.	219
5-3.	Molecular Weight Data for Unsaturated and Saturated Ethyl Branched ADMET Polyethylene Polymers	224
5-4.	Observed and Calculated Chemical Shifts for an ADMET Model EB Copolymer with an Ethyl Branch on Every 9 th Carbon.....	229

LIST OF FIGURES

<u>Figure</u>	<u>page</u>
1-1. The four types of metathesis reactions.	2
1-2. Dall'Asta's ROMP polymerization of cyclopentene.....	3
1-3. Wagener's ADMET of 1,9-decadiene using Schrock's [W] catalyst.....	4
1-4. Metathesis catalysts systems.	5
1-5. Various polymers produced by ADMET in the Wagener group.....	8
1-6. General catalytic cycle for acyclic diene metathesis (ADMET).	10
1-7. 2 nd generation of ADMET polymerization glassware	14
1-8. ADMET polymerization of 1,9-decadiene.	16
1-9 (a) 200-MHz ¹ H NMR of linear poly(octenamer) produced by ADMET polymerization of 1,9-decadiene. (b) 50-MHz ¹³ C NMR of linear poly(octenamer) produced by ADMET polymerization of 1, 9-decadiene..	18
1-10. GPC Analysis of poly(octenamer) (10) and hydrogenated poly(octenamer) in trichlorobenzene at 135 °C.....	19
1-11. DSC (Endo Down) of poly(octenamer) (10) [dashed] and hydrogenated poly(octenamer) [bold].	21
2-1. A pictorial representation of the difference in branch placement for PE Produced by: a) ADMET chemistry and b) typical chain processes.	27
2-2. General synthetic scheme for synthesis of symmetrical methyl branched ethylene/propylene (EP) copolymer models by ADMET.....	28
2-3. Synthetic pathway to produce methyl-branched biene with symmetrical methylene spacing for both alkenyl substituents.	29
2-4. ¹ H NMR for a) monomer, 8f b) unsaturated polymer, 2e c) saturated polymer, 3e.	35
2-5. ¹³ C NMR Spectra for a) unsaturated polymer, 2e b) saturated polymer, 3e.....	36

2-6.	Typical DSC plot illustrating melting endotherm and crystallization exotherm. DSC for 3e (methyl branch every 21 st carbon).....	40
2-7.	DSC visual overlay of melt transitions for ADMET polyethylene with precisely placed methyl branches presented in Table 2-4.	43
2-8.	Flory equation treatment for the impact of comonomer (defect) content on the melting point.	44
2-9.	Glass transition curve for methyl branched ADMET polyethylene with a methyl branch on each and every 9 th carbon (3a).	47
3-1.	Retro-Synthetic Methodology to Produce E/P Model Copolymers via ADMET. .	77
3-2.	DSC trace comparison of (a) UHMWPE, (b) HDPE, and (c) LDPE samples	84
3-3.	DSC trace comparison of (a) BASF 1800D and (b) 1810H	85
3-4.	Expanded view of multiple a) endotherms and b) exotherms for branched PEs..	86
3-5.	Initial DSC traces illustrating melting endotherm and crystallization exotherm for ADMET EP copolymer models with precise branching: a) HP9 b) HP15 and c) HP21.....	88
3-6.	Extended DSC analysis for ADMET EP copolymer models with precise methyl branching: a) HP9 b) HP15 and c) HP21	90
3-7.	Expanded view of secondary exotherm event observed in Figure 3-6.....	91
3-8.	DSC melting curves as a function of heating rate.	94
3-9.	Linear regression plot for the influence of scan rate on peak melting temperature.	96
3-10.	Linear regression plot for the influence of scan rate on peak crystallization temperature.	97
3-11.	Magnified View of Bimodal Melting Process Observed for HP9.....	99
3-12.	Annealing at room temperature for extended time periods—HP15 (3-12a) vs. HP21 (3-12b).	103
3-13.	Annealing at room temperature for HP15 at extended time periods—expanded view.....	104
3-14.	Annealing at room temperature for HP21 at extended time periods—expanded view.....	105

3-15. Annealing at room temperature for time periods on the order of 1 day to 1 week—HP21	108
3-16. Optimizing crystallinity through isothermal annealing: a) HP15 at 20 °C versus b) HP21 at 43 °C.....	109
3-17. Optimizing crystallinity through isothermal annealing—HP15 at 20 °C. Expanded view	110
3-18. Optimizing crystallinity through isothermal annealing. HP21 at 43 °C. Expanded view.....	111
3-19. Importance of choosing proper annealing temperature—HP15 annealed at 28 °C for 5 days.	113
4-1. Geometry of a generalized unit cell.....	117
4-2. The fourteen crystal (Bravais) lattices.....	118
4-3. Crystallographic planes in the body-centered cubic lattice.	119
4-4. Bragg's theory of x-ray constructive interference.	121
4-5. Bond distances and angles in a completely aliphatic-based chain: (a) all trans (b) occurrence of a cis linkage.....	123
4-6. PE orthorhombic unit cell (ab face shown in plane).	125
4-7. Fringed-micelle model for the crystalline-amorphous composite interface found in polymeric materials.	127
4-8. Two-dimensional pictorial representation of possible fold surfaces in polymer lamellae.	128
4-9. Chain-folded lamellae in linear polyethylene—top and side view of the weave-like pattern formed by polymeric stems	129
4-10. Debye-Scherrer powder diffraction camera, [mounted (left); un-mounted, opposite view (right)].	131
4-11. Reflected cones generated by the Debye-Scherrer powder method.	132
4-12. Geometry of a Debye-Scherrer Camera and relation to interplanar spacings found on exposed photographic film.....	133
4-13. Kiessig camera.....	135
4-14. EP copolymers possessing precise methyl branch placement.	139

4-15.	2-Dimensional representation of possible fold surfaces postulated for ADMET model EP copolymers prior to x-ray studies.....	140
4-16.	Optimizing crystallinity through isothermal annealing: HP15 (4-16a) at 20 °C vs. HP21 (4-16b) at 43 °C.....	150
4-17.	WAXD—Debye-Scherrer film from powder diffraction of an EP copolymer with random methyl branching.	154
4-18.	WAXD—Debye-Scherrer film from powder diffraction of HP15 (theoretically 67 methyls/1000 carbons).....	156
4-19.	WAXD—Debye-Scherrer Film from Powder Diffraction of HP21 (theoretically 48 methyls/1000 carbons).....	157
4-20.	DiffraX Model 586—Powder Diffraction (WAXD).	158
4-21.	WAXD—Powder diffraction of HP15 versus HP21 at room temperature.	160
4-22.	WAXD—Temperature dependent measurements during cooling for HP15.....	161
4-23.	WAXD—Temperature dependent measurements during cooling for HP21.....	162
4-24.	WAXD—Suggested evidence for an ordered mesophase in the amorphous region (HP21).....	165
4-25.	WAXD—Further evidence for a secondary ordered mesophase in the amorphous region (HP15 at 78 °C vs. HP21 at 100 °C).....	167
4-26.	SAXS of HP15.....	169
4-27.	Possible periodic distances for HP15.	171
4-28.	SAXS of HP21.....	173
4-29.	Possible periodic distances for HP21.	176
4-30.	Long-spacing measurement from SAXS (a) HP15 (b) HP21.....	177
4-31.	Representative optical microscopy images for HP15.....	181
4-32.	Representative optical microscopy images for HP21.....	182
4-33.	Representative transmission electron microscopy images for HP15.....	186
4-34.	Representative transmission electron microscopy images for HP21.....	187
4-35.	Representative electron diffraction image for HP15.....	189

4-36. Representative electron diffraction image for HP21.	190
4-37. Raman spectral data for (a) HP15 (b) HP21. Samples crystallized from the melt and analyzed at room temperature.	195
4-38. Examples of molecular vibrations encountered in the infrared absorption spectroscopy for simple hydrocarbon-based materials.	200
4-39. IR Spectroscopy of HP21—fingerprint region (700 to 1200 cm^{-1}).	201
4-40. IR Spectroscopy of HP21—entire middle IR spectrum (600 to 4000 cm^{-1}).	202
4-41. Defect conformations: (a) double gauche, GG and (b) kink, GTG* defects with all trans (planar zigzag) polymer chains on either side.	208
5-1. General scheme for the synthesis of precisely branched ethylene/ α -olefin copolymer models by ADMET.	212
5-2. Synthesis of the first ADMET model ethylene/butylene (EB) copolymer.	213
5-3. Synthetic pathways attempted in route to the target symmetrical α,ω -diene monomer with symmetrical ethyl branch placement.	213
5-4. Synthesis of an ADMET α,ω -diene monomer with a symmetrically placed ethyl branch.	214
5-5. Mechanism for the decarboxylation of compound 4.	216
5-6. Ethyl monomer synthesis via decyanation chemistry.	220
5-7. Possible resonance structures for anion formation in compound 10.	221
5-8. Proposed ring closing mechanism for the decyanation reaction of 11.	222
5-9. ^1H NMR: (a) monomer, 1; (b) unsaturated polymer, 2; (c) saturated polymer, 3.	226
5-10. ^{13}C NMR: (a) monomer, 1; (b) unsaturated polymer, 2; (c) saturated polymer, 3.	227
5-11. Generalized nomenclature for ^{13}C NMR analysis of branched polyethylenes.	228
5-12. IR split spectrum of (a) UPEB9: unsaturated polymer with ethyl branch on every 9 th carbon (2) and (b) HPEB9 saturated polymer with ethyl branch on every 9 th carbon (3).	230
5-13. DSC comparison of unsaturated polymer (2) to fully hydrogenated EB copolymer model (3). Relaxations are given as onset glass transition values.	233

- 5-14. DSC comparison of 1) HPEP9: ADMET model ethylene/propylene copolymer with a methyl on each and every 9th carbon and 2) HPEB9: ADMET model ethylene/butylene copolymer with an ethyl on each and every 9th carbon.234

Abstract of Dissertation Presented to the Graduate School
of the University of Florida in Partial Fulfillment of the
Requirements for the Degree of Doctor of Philosophy

MODELING THE EFFECT OF PRECISE SHORT-CHAIN BRANCH PLACEMENT
IN ETHYLENE-CO-PROPYLENE AND ETHYLENE-CO-BUTYLENE MATERIALS:
SYNTHESIS, THERMAL BEHAVIOR, AND MORPHOLOGICAL
CHARACTERIZATION

By

Jason Alan Smith

August 2002

Chair: Professor Kenneth B. Wagener
Major Department: Chemistry

By far, ethylene-based materials (homo and copolymers) constitute the highest volume of synthetically produced macromolecules in the world today. Although such factors as mode of polymerization (radical, Ziegler-Natta, etc.), choice of catalyst, temperature of reaction, and molecular weight are of extreme importance, the distribution and amount of the short-chain branching (SCB) content are the most influential factors for determining the final materials properties for ethylene/ α -olefin copolymers.

Chapter 2 describes the first synthetic approach to attain precisely controlled methyl branching in ethylene-*co*-propylene (EP) materials created via acyclic diene metathesis (ADMET) chemistry. In Chapters 2 and 3, differential scanning calorimetry (DSC) was employed to examine the thermal behavior of five model EP copolymers

wherein a methyl branch was placed on each and every 9th, 11th, 15th, 19th, and 21st carbon along the backbone.

Chapter 4 details the first secondary structural data for these model EP copolymers via a variety of techniques including wide-angle x-ray diffraction (WAXD), small-angle x-ray scattering (SAXS), optical microscopy (OM), transmission electron microscopy (TEM), electron diffraction, infrared (IR) spectroscopy, and Raman scattering. The crystalline regions in these systems were found to be pseudo-hexagonal and consist of parallel-packed arrays of conformationally disordered (Condis) hydrocarbon chains. This is the first verified existence of the pseudo-hexagonal phase for an ethylene-based material without having initially applied high pressures/temperatures to the sample and/or stretching the material prior to analysis.

Chapter 5 presents the synthetic methodology used to create the first ADMET model ethylene-*co*-butylene (EB) materials in which the ethyl branches are set into a precise methylene sequence length (MSL). In particular, details are provided in regard to monomer/polymer syntheses, characterization, and initial thermal behavior findings for a single model EB copolymer in which the ethyl branch has been placed on each and every 9th carbon along the polymer backbone.

Comparisons of these model polymers with industrial polyethylene samples demonstrate that this polycondensation approach provides a significant opportunity to better understand the morphology, crystalline structure, and thermodynamics of the crystallization process for the most abundant synthetic macromolecule in the world, polyethylene.

CHAPTER 1

ADMET—A NON-TRADITIONAL STEP-GROWTH POLYMERIZATION

1.1 Introduction

Olefin metathesis, an expression coined by Calderon et al. in 1967,¹ has been accurately described in Ivin and Mol's seminal text *Olefin Metathesis and Metathesis Polymerization* as "the (apparent) interchange of carbon atoms between a pair of double bonds."² This remarkable conversion can be divided into four types of reactions as illustrated in Figure 1-1.

These reactions have been used extensively in the synthesis of a broad range of both macromolecules and small molecules;³ this chapter focuses on acyclic diene metathesis (ADMET) polymerization as a versatile route for the production of a wide range of functionalized polymers.

1.1.1 Historical Perspective

The history of metathesis chemistry dates back over 50 years⁴ to the development of Ziegler-Natta-type transition metal catalysts for olefin polymerization in the late 1940s.⁵ While olefin exchange reactions were observed by several research groups using such catalysts, the exact nature of the active catalyst species and mechanism were not understood at the time. Most early metathesis catalyst systems, similar to either Phillips-type (supported metal oxides at high temperatures) or Ziegler-Natta-type (metal halide/alkyl aluminum mixtures at low temperatures) catalysts for the polymerization of α -olefins and ethylene, involved the *in situ* formation of the catalyst. Such nebulous, multi-component systems are complicated, and as a result, difficult to study and

understand. Only after detailed labeling studies by Dall'Asta and coworkers was it conclusively proven that in metathesis, the olefin double bond is cleaved and reassembled by the active catalyst.⁶

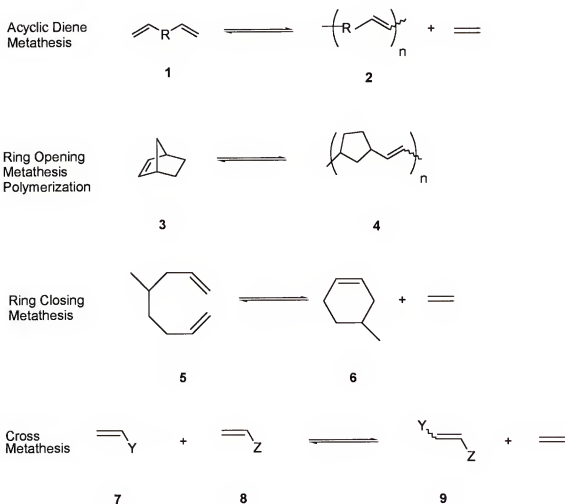
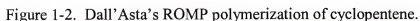


Figure 1-1. The four types of metathesis reactions.

The mechanism of such cleavage remained unknown until Herrison and Chauvin solved it in 1970.^{1e} Chauvin proposed that the metathesis reaction involves a metallacyclobutane ring intermediate, which is formed by the interaction of a metal carbene with an olefin. This is the key step in metathesis chemistry and is common to all

The discovery and preparation of organometallic carbene complexes in 1964 provided not only a vital clue for the determination of the metathesis mechanism but also has subsequently led to the deliberate design of improved, later generation catalysts. A brief overview is presented here for several catalytic systems used for metathesis polymerization, and in particular acyclic diene metathesis (ADMET) polymerization. The most important catalysts (determined by usage and numbers of publications) are based on ten elements in the transition metal series of the periodic table: Mo, W, Ru, Re, V, Zr, Cr, Co, Rh, and Tc. It is uncommon to observe metathesis activity with non-transition metal elements. It was not until 1963 that Dall'Asta⁶ was able to prepare high molecular weight polymers via ROMP of the strained cyclic olefin cyclopentene (**10**), producing polypentenemer (**11**) (Figure 1-2).



Even more challenging was the synthesis of step-growth polymers using acyclic dienes, since high conversions (>99%) are mandatory for high molecular weight polymers to be produced.³ Initially, attempts to prepare such polymers failed and research into this area became quite limited. It was not until 1990, following the discovery of active, acid-free, single site tungsten-based alkylidenes by Schrock's group,⁷

that Wagener and coworkers were able to successfully perform the ADMET reaction using 1,9-decadiene (**12**) as the monomer, producing poly(octenamer) (**13**) (Figure 1-3).⁸

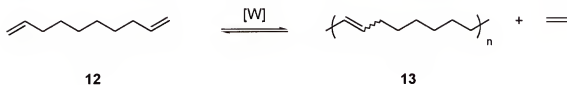


Figure 1-3. Wagener's ADMET of 1,9-decadiene using Schrock's $[W]$ catalyst.

We now know that three catalyst systems are viable in ADMET polymerization: "classical" catalysts (**14**),² Schrock-type alkylidenes (**15**),⁷ and Grubbs-type carbenes (**16**, **17**).^{9,10} Each catalyst type has advantages and limitations, and the choice of catalyst is dependent on the nature of the diene to be polymerized (monomer functionalities present, physical properties of the polymer formed, and so forth). "Classical" catalysts (**14**) are, in reality, ill-defined catalytic mixtures containing two or more components in which the active species (alkylidene) is generated *in situ*.² Typically, a classical catalyst is composed of an early transition metal halide such as WCl_6 reacted with an alkylating agent or activator, such as Bu_4Sn or $EtAlCl_2$. Such catalysts are rather effective under certain conditions, such as high temperatures (100 °C), and proceed with reasonable rates. A practical disadvantage to such catalytic mixtures is their ill-defined nature; the active species often cannot be isolated, or in some cases are unable to be identified—even by spectroscopic means. Consequently, catalyst concentration cannot be easily quantified and monitored during the course of a reaction.

These limitations were overcome with the introduction of the well-defined, single-component tungsten and molybdenum (**17**) alkylidenes in 1990. (Figure 1-4).⁷ Schrock's

discovery revolutionized the metathesis field and vastly increased the utility of this reaction. The Schrock alkylidenes are particularly reactive species, have no detectable side reactions, and are quite effective as polymerization catalysts for both ROMP and ADMET. Due to the oxophilicity of molybdenum, these alkylidenes are moisture and air sensitive, so all reactions using these catalysts must be performed under anaerobic conditions, requiring Schlenk and/or glovebox techniques.

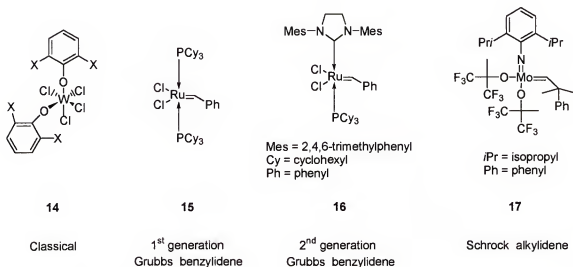


Figure 1-4. Metathesis catalysts systems.

Grubbs-type carbenes (**15**, **16**) based on the late transition metal ruthenium are more tolerant to air, moisture, and most functional groups.⁹ The original Grubbs' carbene (**15**) is kinetically slower compared to Schrock's [Mo] catalyst (**17**). A significant improvement to [Ru] carbene catalysts was discovered in 1999 by the Herrmann group, with the introduction of the N-heterocyclic carbene ligand.¹¹ Similar catalysts using this type of ligand, such as **16**,¹⁰ have enabled the [Ru] catalysts to match or exceed the reaction rate of the Schrock alkylidenes, at least in several ADMET and ROMP reactions. This enhancement, when combined with the functional group tolerance of these carbenes,

has led to its increased use in organic synthesis, particularly in ring closing metathesis (RCM).¹⁰

1.1.3 Requirements for ADMET Polymerization

ADMET of α,ω -dienes has been a focus of research in the Wagener laboratories for many years now, where this chemistry has been explored for its viability in synthesizing polymers possessing both precisely designed microstructures as well as a variety of functionalities. The requirements for this reaction, such as steric and electronic factors, functionalities allowed, appropriate choice of catalyst, and the necessary length or structure of the diene have been examined.^{3,12-14} A detailed discussion will be presented later in this chapter with a brief synopsis of the basic requirements needed for a successful ADMET polymerization reaction to take place.

Like most polycondensation reactions, ADMET is most effective under bulk (neat) reaction conditions with the monomer itself acting as both reactant and solvent. Doing so maximizes the monomer concentration and promotes a shift in the reaction equilibrium (*vide supra*) towards unsaturated polymer formation. Similar to polycondensation reactions, ADMET is typically performed under reduced pressure ($< 10^{-2}$ mm Hg) to remove the condensate—ethylene. This irreversibly shifts the monomer/polymer equilibrium towards polymer formation, promoting faster monomer conversion and raising the molecular weight of the product. ADMET is a true step-growth polymerization reaction exhibiting the typical kinetic behavior and molecular weight distribution ($M_w/M_n \cong 2.0$) commonly observed for this class of polymerization.¹² In order to suppress monomer cyclization via the RCM route (cyclization is common in polycondensation chemistry), the α,ω -diene must consist of a chain of ten atoms or

greater to favor ADMET polymerization. Shorter chain dienes have an increased propensity to form stable five-, six-, and seven-membered rings. This thermodynamically controlled phenomenon is known as the Thorpe-Ingold effect.¹⁵ Since ADMET polymerization is performed over extended time periods under equilibrium conditions, it is ultimately thermodynamics rather than kinetics that determine the choice between a selected diene monomer undergoing either polycondensation or cyclization.

1.1.4 Applications

ADMET is one of the most flexible transition metal catalyzed polymerization routes studied to date. With the introduction of new, functionality-tolerant robust catalysts, the primary limitation of this chemistry involves the synthesis and cost of the diene monomer that is used. ADMET gives the chemist a powerful tool for the creation of polymers not easily accessible via other means. Herein, the synthetic techniques required to perform this reaction are detailed and a discussion is made concerning the wide range of properties observed from the variety of polymers that can be synthesized. For example, branched and functionalized polymers produced by this route provide excellent models (after quantitative hydrogenation) for the study of many large volume commercial copolymers; and the synthesis of reactive carbosilane polymers provides a flexible route to solvent resistant elastomers with variable properties. Telechelic oligomers can also be made which offer an excellent means for polymer modification or incorporation into block copolymers. All of these examples illustrate the versatility of ADMET.

1.2 Overview of Chemistry and Analytical Techniques

1.2.1 Chemistry and Catalysis

1.2.1.1 Brief history

As mentioned earlier, the chemistry and mechanism surrounding the olefin metathesis reaction (Figure 1-1) have been points of intense interest since their discovery over 50 years ago.^{1,2} In the late 1980s, research by the Wagener group demonstrated approaches to meet the stringent requirements of step polymerization.¹³ Defining the opportunity has been the direct result of revolutionary developments of the single-site metathesis catalysts described earlier; and subsequently, a series of high molecular weight polymers possessing various functionalities have been made by ADMET (Figure 1-5).¹⁴

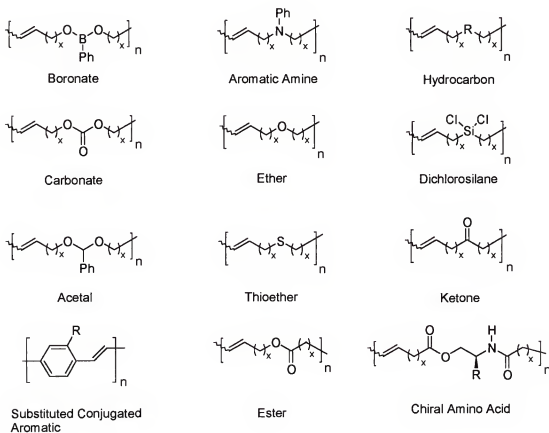


Figure 1-5. Various polymers produced by ADMET in the Wagener group.

At this point, it is appropriate to discuss the mechanism for ADMET, because ADMET polymerization is more mechanistically complex than its chain polymerization counterpart—ROMP. Figure 1-6 illustrates the accepted mechanistic pathway which leads to productive metathesis polymerization, as first described by Wagener, Boncella, and Nel.^{14a} A general model reaction between an α,ω -diene with a metal alkylidene initiator is presented here for simplicity, and upon examination of this polymerization cycle, several interesting features become apparent. Since each and every reaction step in this cycle is in equilibrium, the ultimate driving force of the polymerization is the removal of a small olefinic species, typically ethylene, in the case of terminal dienes. Therefore, ADMET is an equilibrium, step-growth condensation-type polymerization (generally known as polycondensation) that displays typical kinetics and molecular weight distributions (~ 2.0) for this type of polymerization.¹²

As is the case for other polycondensation reactions, internal interchange reactions are possible for ADMET, similar to that of polyesters and polyamides.¹⁶ Interchange reactions involve a catalyst molecule on a polymer chain-end reacting with an internal double bond in another polymer chain. The result is two new polymer chains; however, no change in the molecular weight distribution is observed from that expected for a random polymerization. The distribution observed is the Flory, or most probable, distribution.

Another factor in step-growth polymerizations is cyclization versus linear polymerization.^{15, 16} Since ADMET is a step-growth polymerization, most reactions are carried out in the bulk, using high concentrations of the reactant in order to suppress most cyclic formation. A small percentage of cyclic species is always present but is dependent upon thermodynamic factors, typical of any polycondensation reaction.

1.2.1.2 Importance of catalyst selection

The obviation of side reactions is essential to the success of ADMET, and this can be realized if the proper catalyst is chosen. Catalyst choice must avoid the possibility of cation formation,¹³ vinyl addition, and/or formation of multiple catalytic species, all of which are detrimental to clean metathesis chemistry. Over the past 10 years, the Wagener group has utilized a variety of catalyst moieties, several of which are illustrated in Figure 1-4.

Presently, the two most commonly used single-site catalysts for ADMET are 1) Schrock's alkylidene catalysts of the type $M(\text{CHR}')(\text{NAr}')(\text{OR})_2$ where $M = [\text{W}]$ or $[\text{Mo}]$, $\text{Ar}' = 2,6\text{-C}_6\text{H}_3\text{-}i\text{-Pr}_2$, $\text{R}' = \text{CMe}_2\text{Ph}$, and $\text{R} = \text{CMe}(\text{CF}_3)_2$ (**17**)⁷ and 2) Grubbs' ruthenium-based catalyst, $\text{RuCl}_2(=\text{CHPh})(\text{PCy}_3)_2$ (**15**) where $\text{Cy} = \text{cyclohexyl}$.⁹ While

both catalysts meet the requirements to be successful in ADMET, they are markedly different in their reactivity and in the results each can produce.

Kinetic studies using 1,9-decadiene and 1,5-hexadiene in comparison with catalyst **17** and catalyst **15** demonstrate an order of magnitude difference in their rates of polymerization, with **17** being the faster of the two.¹² Further, this study shows that different products are produced when the two catalysts are reacted with 1,5-hexadiene. Catalyst **17** generates principally linear polymer with the small amount of cyclics normally observed in step-condensation chemistry, while **15** produces only small amounts of linear oligomers with the major product being cyclics such as 1,5-cyclooctadiene.¹² Catalyst **15**, a late transition metal benzyldiene (carbene), has vastly different steric and electronic factors compared to catalyst **17**, an early transition metal alkylidene. Since the results were observed after extended reaction time periods and no catalyst quenching or kinetic product isolation was performed, this anomaly is attributed to mechanistic differences between these two catalysts under identical reaction conditions.

Another difference between these catalysts is found in their functional group tolerance. Catalysts such as **15** are more robust to most functionalities (except sulfur and phosphorus), moisture, oxygen, and impurities enabling them to easily polymerize dienes containing functional groups such as esters, alcohols, and ketones.⁹ On the other hand, catalyst **17** is more tolerant of sulfur based functionalities.⁷ The researcher must choose the appropriate catalyst by considering the chemical interactions between monomer and catalyst as well as the reaction conditions needed.

1.2.2 Experimental Methods

A discussion of this polymerization method would not be complete without mention of the development of specialized glassware utilized over the years. It has evolved from very elaborate, sophisticated, and specially designed glassware to fairly simple setups. Initially, elaborate break-seal technology was used to complete the entire polymerization process,^{14a} similar to anionic polymerization methodology.¹⁷ Break-seal techniques were employed to fully understand many monomer structure/reactivity relationships; these techniques are no longer needed.

Today, the glassware required consists of either a round bottom flask or a Schlenk tube serving as the reaction chamber. This chamber is equipped with a magnetic stirbar and a Teflon high-vacuum valve (or glass stopcock) which allows easy vacuum control after attachment to a vacuum line (Figure 1-7). Figure 1-7b illustrates the vessel used when the monomer is very volatile (high vapor pressure). This design prevents low boiling monomer from being lost under reduced pressure conditions due to the presence of a cold finger/trap, which usually contains a cooling mixture of dry ice/isopropanol ($-78\text{ }^{\circ}\text{C}$). This set-up also can be used when a monomer is a solid, and solvent must be added in small quantities in order to facilitate the polymerization. In these cases care must be taken to utilize *many intermittent vacuum cycles* to ensure the formation of a viscous polymer product before full vacuum ($<10^{-2}$ mm Hg) is employed. Figure 1-7a and 1-7c illustrate the glassware used when the monomer remains a stirrable, non-volatile liquid under normal vacuum conditions at room temperature.

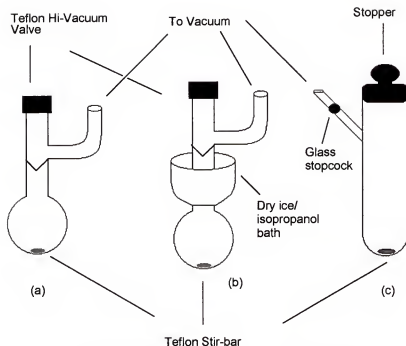


Figure 1-7. 2nd generation of ADMET polymerization glassware

1.2.2.1 Purification of monomers, reagents, and solvents

Care must be taken in the preparation of any reagent or monomer that comes in contact with the catalyst. All reagents and chemicals that are purchased or that are synthesized must be of high purity (>99% is preferred). Typical methods of monomer purification that have been used include the following: recrystallization; simple, vigreux, or spinning band distillation; flash chromatography; and high performance liquid chromatography (HPLC).¹⁸ If catalyst **17** is used, then care must be taken to ensure absolute dryness and an oxygen-free atmosphere. Monomers used for these reactions usually are further purified and degassed by three freeze-pump-thaw cycles prior to polymerization. The N-heterocyclic-carbene-ligated ruthenium catalyst (**16**) requires substantially less stringent conditions.¹⁰

1.2.2.2 General metathesis polymerization conditions

Usually ADMET polymerizations are conducted in the bulk state (neat) to maximize the molar concentration of the olefin, and so the examples discussed in this chapter describe bulk polymerization conditions.

For a typical ADMET polymerization, all monomers, reagents, and solvents are purified as described earlier and degassed. The glassware is dried in an oven for at least 4 hours and taken into an argon (or nitrogen) glovebox. The monomer is placed in a tared reaction vessel, and then the appropriate catalyst is weighed out. Typical monomer to catalyst ratios are on the order of 500-1000:1 (**17**), 100-500:1 (**15**), and 100-500:1 (**16**). Catalyst is then added to monomer in order to initiate the polymerization reaction, which is characterized by visible bubbling (evolution of ethylene). The reaction vessel is sealed off to the atmosphere, removed from the glovebox, and immediately connected to an evacuated vacuum line. Intermittent vacuum cycles are carried out until the viscosity increases enough to hinder or completely stop stirring.

The temperature of the oil bath in the initial stages and throughout the course of the polymerization is monomer and catalyst dependent. As a general rule, low boiling, volatile monomers are initially begun at room temperature (20-25 °C), whereas higher boiling substrates may be initiated at 30-40 °C. Polymerizations using catalyst **17** should be started at lower temperatures (20-30 °C) compared to reactions with **15** (30-40 °C). This is primarily due to the possibility of decomposition when using Schrock's catalyst at higher temperatures, but it also takes into account the differences in relative reactivity of the two catalysts (rate of polymerization: Schrock's [Mo] > Grubbs' [Ru]). *The best laboratory scale ADMET reaction is a slow and controlled one, progressively building*

up the molecular weight of the product. Rapid reactions splatter monomer inside the upper walls of the reaction vessel, which can lead to decreased conversions.

After several intermittent vacuum cycles, the reaction mixture becomes viscous (bubbling of ethylene is less vigorous) and full, continuous vacuum ($<10^{-2}$ mm Hg) may then be applied. The reaction temperature is slowly ramped to ultimately reach temperatures of 50-55 °C when using **17**, 60-70 °C for **15**, and 70-90 °C with **16**. Once the evolution of ethylene is complete, the reaction vessel is cooled to room temperature and the catalyst is quenched by either exposure to the atmosphere, addition of a terminating agent (benzaldehyde or ethyl vinyl ether), or by the introduction of non-purified, lab grade solvent (usually benzene, chloroform, toluene, etc.). Polymers are isolated from the dissolved solution by precipitation into a non-solvent such as methanol, isopropanol, or hexanes. Several successive precipitations may be required to reduce the level of catalyst residue to acceptable levels. Alternative methods have been developed for Grubbs' catalyst removal using chelating phosphines.¹⁹ As a reference, provided below is an example of the ADMET of 1,9-decadiene Figure 1-8.

1.2.2.3 ADMET polymerization of 1,9-decadiene (**9**)

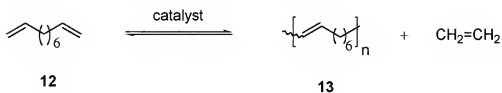


Figure 1-8. ADMET polymerization of 1,9-decadiene.

The following steps are performed in an argon atmosphere glovebox. In a 50 mL round bottom flask equipped with a Teflon magnetic stirbar, 2.03 g (14.7 mmol) of previously distilled and degassed 1,9-decadiene (**12**) (Aldrich) and 27.6 mg (3.61×10^{-2}

mmol) of Schrock's catalyst (**17**) [400:1] are combined. In a matter of seconds, catalyst is dissolved into the monomer and the vigorous evolution of ethylene is observed. The flask is sealed with a Teflon vacuum adapter and removed from the drybox. The polymerization vessel is immediately connected to the vacuum line, placed into an oil-bath, and stirred at 30 °C. Intermittent vacuum cycles are performed until the evolution of ethylene slows and the increased viscosity of the polymer solution makes stirring very difficult. At this point, 1,9-decadiene is exposed to full vacuum ($<10^{-2}$ mm Hg) after 1.5 h, and the temperature is increased slowly, over a period of days, to a final level 50 °C. After 3-5 days total reaction time, the polymerization is cooled to room temperature and quenched by exposure to air. The poly(octenamer) (**13**) is isolated in high yield (95%) by dissolving in toluene and precipitating into methanol. The dissolved polymer may be purified by flash chromatography through a short silica gel column in order to remove a large portion of decomposed catalyst residue. However, trace amounts of residue are still present even after this process, which may lead to slight discoloration of the polymer. After this precipitation and subsequent drying under vacuum, the polymer is characterized using typical analytical techniques (see section 1.2.3).

1.2.3 Characterization of ADMET Polymers

ADMET polymers are easily characterized using the common analysis techniques available to the chemist, including nuclear magnetic resonance (^1H and ^{13}C NMR), infrared (IR) spectra, elemental analysis, gel-permeation chromatography (GPC), vapor pressure osmometry (VPO), membrane osmometry (MO), thermal gravimetric analysis (TGA), and differential scanning calorimetry (DSC). The preparation of poly(octenamer) (**13**) via the metathesis of 1,9-decadiene (**12**) is an excellent model polymerization to study ADMET, since the monomer is readily available and the polymer is well known.²¹

The NMR characterization data (Figure 1-9) for the hydrogenated versions of poly(octenamer) illustrate the clean and selective nature of ADMET.

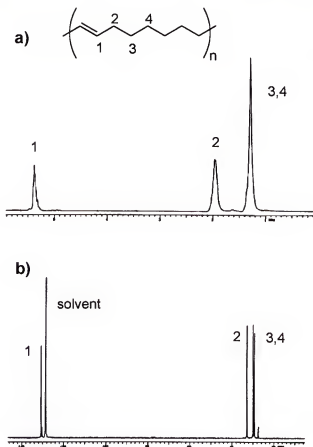


Figure 1-9 (a) 200-MHz ^1H NMR of linear poly(octenamer) produced by ADMET polymerization of 1,9-decadiene.^{14a} (b) 50-MHz ^{13}C NMR of linear poly(octenamer) produced by ADMET polymerization of 1,9-decadiene. Reproduced with permission from *Macromolecules* **1991**, 24, 2649-2657. Copyright 1991 Am. Chem. Soc.

These spectra not only support the primary structure of the polymer's repeat unit but also strongly suggest that no side reactions are detectable within the limitations of the instrument. In the ^{13}C NMR spectrum (*vide supra*) all resonances can be unequivocally assigned, demonstrating the clean nature of the ADMET reaction. The ^{13}C NMR spectrum also allows the scientist to distinguish between *cis* and *trans* internal sp^2 carbons as well as the allylic carbon, which is adjacent to the internal vinyl position.

Using quantitative ^{13}C NMR analysis, the integration of the peak intensities between the allylic carbon resonances and those of the internal vinyl carbons gives the percentage of *trans/cis* stereochemistry that is present for the polymer.²² Empirically, the ratio of *trans* to *cis* linkages in ADMET polymers has typically been found to be 80:20. Elemental analysis results of polymers produced via ADMET demonstrate excellent agreement between experimental and theoretical values as well.

Membrane osmometry, vapor pressure osmometry, gel permeation chromatography, light scattering, and intrinsic viscosity have been used to determine the molecular weight for a series of linear poly(octenamer) samples made via ADMET and have been examined elsewhere.^{14a} For simplicity, only the example of GPC analysis is given here (Figure 1-10).

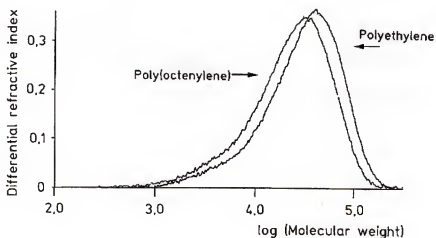


Figure 1-10. GPC analysis of poly(octenamer) (**13**) and hydrogenated poly(octenamer) in trichlorobenzene at 135 °C.²³ Reproduced with permission from *Macromol. Chem., Rapid Commun.* **1993**, *14*, 657-662. Copyright 1993 Wiley-VCH.

This GPC trace shows that hydrogenation does little to affect the molecular weight distribution of poly(octenamer). Further it is important to note that the polydispersity index (M_w/M_n) for polymers produced by ADMET typically approaches 2.0 (within the

normal range for step-condensation chemistry), and characteristic molecular weights for ADMET polymers are in the range of $M_n = 10\,000$ to $70\,000$.

Thermogravimetric analysis is used to determine the stability of a compound to decomposition upon heating, and DSC is employed to measure glass transitions (amorphous domain), melting/crystallization behavior (polymers with crystalline domains), and the effects of thermal history or annealing in a polymer sample. Figure 1-11 illustrates the dramatic effect that hydrogenation has on a sample—the melting point is increased from $69\text{ }^{\circ}\text{C}$ to $134\text{ }^{\circ}\text{C}$, a typical value for high-density polyethylene. This is due to an increase in the relative percent crystallinity or order in the hydrogenated version (linear polyethylene) compared to its unsaturated parent. Additionally, the melting transitions for both the unsaturated (13) and saturated versions of the ADMET polymer of 1,9-decadiene (12) are rather sharp and clean compared to polymers of a similar backbone in the literature, which usually show broad melting curves that extend over a wide temperature range. The sharpness of the melting transition is another characteristic that points to the clean microstructures of polymers made using ADMET. The next section examines the effect this precise control has on the final structural property relationships of a given polymer. In particular, focus will center on polymers that model branching effects in polyethylene (PE).

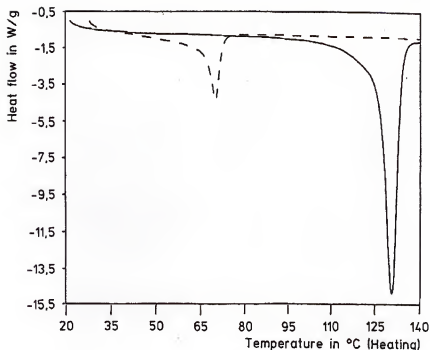


Figure 1-11. DSC (Endo Down) of poly(octenamer) (13) [dashed] and hydrogenated poly(octenamer) [bold].²³ Reproduced with permission from *Macromol. Chem., Rapid Commun.* 1993, **14**, 657-662. Copyright 1993 Wiley-VCH.

1.3 Structure-Property Relationships

1.3.1 General Considerations

What can ADMET offer in terms of tailoring the properties of a given polymer? The answer lies in the clean chemistry of metathesis. If a metathesis-active α,ω -diene can be synthesized, then a known polymer microstructure can be produced. Few other polymerization techniques are so versatile, yet so precise. In recent years, the Wagener group has focused attention towards modeling polymers and copolymers made from ethylene, and in particular, the effect of precise placement of alkyl and polar branches sequentially along the backbone of polyethylene has been examined.

1.3.2 Influence of Precise Branching on Polymer Microstructure

Polyethylene's structural simplicity has made it one of the most thoroughly studied polymeric materials; however, it is still pertinent to study its structure-property relationships, thermal behavior, morphology, and the effects of adding branches and functional groups to the polymer backbone.

Polyethylene is usually thought of as a linear, straight chain macromolecule. In reality, it is a hydrocarbon backbone with variable branching. Purely linear polyethylene has been produced by both the catalytic decomposition of diazomethane²⁴ and ADMET of 1,9-decadiene followed by hydrogenation.²³ However, these are not the methods of choice to produce polyethylene industrially. Polyethylene is commonly synthesized via chain propagation chemistry using free-radical initiation,²⁵ Ziegler-Natta catalysis,²⁶ metallocene catalysis,²⁷ and most recently, late transition metal single-site catalysts.²⁸ Inevitably, both intra- and intermolecular chain transfer occurs in all of these systems causing varying degrees of random branching. This creates polyethylenes with ill-defined, randomly branched microstructures, which have been used to an advantage industrially, creating a wider materials response.

In fact, there exist a number of materials that make up one of the largest families of ethylene-based materials—these are referred to as linear low-density polyethylenes (LLDPEs). LLDPE is made via the copolymerization of ethylene with a 1-alkene, typically with a Ziegler-Natta or metallocene-based catalyst. The completion of such reactions yields a polymer with a known branch length. For example, the copolymerization of ethylene with propene, butene, hexene, or octene, etc. yields a material with methyl, ethyl, butyl, or hexyl branches, respectively. The production of such materials has gained a noticeable share of the commercial market in recent years, mainly

due to the ability to fine-tune the final physical properties of the material by placing a finite amount of known branch points along the PE backbone. Despite being able to tailor the branch length, current commercial techniques used to synthesize LLDPEs do not offer the ability to place a given branch into a set sequence length (i.e. precise placement). So, LLDPE, like LDPE, is a statistically branched material.

What is so important about branching in polyethylene, and why would scientists like to study it or better yet, to control it? The extent of branching content in polyethylene is dependent on many factors, such as the method of polymerization and reaction temperature. The overall branch density may approach 15-30 branches per 500 *mer* units. Numerous studies using chain propagation chemistry have focused on delineating the effect of these irregularities in polyethylene random copolymers²⁹ with both alkyl³⁰ and polar pendant groups.³¹ The studies have produced a consensus that the melting point is decreased with increasing frequency and steric bulk of the imperfections. Branching sequence distributions also play a major role in the final material properties of the polymer. Copolymerization of ethylene with different comonomers (usually α -olefins, LLDPEs) is the best way to examine this phenomenon; however, due to differing reactivity ratios between monomers, it is not trivial to prepare polymers with precise placement of desired irregularity/branch point. In order to generate a valid study concerning the exact impact an individual branch has on polymeric materials response, it is necessary to find a method to precisely place a pendant group into a set sequence length. Consequently, strategically designed ethylene-based copolymers with highly defined microstructures should prove extremely valuable as material models.

Ethylene copolymers with strict *mer* sequences (pendant group on every 5th carbon) have previously been prepared using an indirect method, accomplished by a perfectly alternating copolymerization of butadiene with vinyl monomers, followed by hydrogenation.³² In order to further understand the impact of precise pendant group placement, the Wagener group began to synthesize a number of similar ethylene copolymers. Utilizing ADMET, model alkyl-branched polyethylenes with highly defined microstructures have been produced. Ethylene/functional-olefin copolymers with several commercially relevant substituents have also been synthesized, thereby increasing the possible avenues with which to model the exact materials response change(s) caused by alkyl or polar functionalities that are precisely placed along the polyethylene backbone.

By designing the repeat unit into the parent diene (containing either an alkyl branch or functionality), only a single type of repeat unit is formed upon polymerization, giving pure polymer microstructures. To date, perfectly controlled ADMET ethylene/copolymers have included ethylene/CO,³³ ethylene/vinyl alcohol,³⁴ ethylene/vinyl acetate,³⁵ and ethylene/propylene.²⁰

1.4 Dissertation Purpose

This dissertation will present the findings concerning ethylene/propylene (EP) copolymer models in which the short-chain branches are set into finite methylene sequence lengths along the backbone of PE. In particular, the synthesis (Chapter 2) and thermal behavior (Chapter 2 and 3) will be presented for a series of five EP copolymers in which the methyl branches have been precisely placed. Additional characterization data for these EP copolymer models has been gathered through the use of x-ray diffraction, microscopy, infrared spectroscopy, and Raman scattering (Chapter 4), thereby obtaining the first detailed, secondary structural information for any ADMET-

produced polymeric material. From these results, it has been possible to deduce the unit cell geometry and morphological characteristics for two of these materials (Chapter 4).

Further, a brief report is given for the monomer and polymer syntheses that enable production of the first ADMET ethylene/butylene (EB) copolymer models. The initial characterization and thermal behavior for the singular model EB copolymer, examined to date, is presented within (Chapter 5), and a cursory attempt has been made to compare this material to its EP copolymer model counterpart(s).

CHAPTER 2

SYNTHESIS AND CHARACTERIZATION OF ETHYLENE/PROPYLENE MODEL COPOLYMERS WITH PRECISE METHYL BRANCH PLACEMENT

2.1 Introduction

Polyethylene (PE) is the highest volume macromolecule produced in the world today, with over 88 billion pounds produced in 1996 and an estimated demand of 109 billion pounds in 2000.³⁶ Consequently, it is still of interest to study the structure-property relationships, thermal behavior, and morphology of this polymer. The polymer is synthesized via chain propagation chemistry using free-radical initiation,²⁵ heterogeneous Ziegler-Natta catalysis,²⁶ metallocene-based catalysis,²⁷ and most recently, late transition metal catalytic systems.²⁸ Inevitably, chain transfer occurs to varying degrees in these polymerization schemes leading to a randomly branched polymer microstructure, a phenomenon which is exploited to create a wider materials response. Branching in polyolefins has been examined for more than 60 years,^{30,37,38} including numerous studies designed to better understand branching in polyethylene.^{30b,30f,32e,37c,38}

Recently, we have found a way to avoid the random nature of branching in polyethylene. This has been accomplished via the elimination of chain transfer during propagation by using step polymerization rather than chain polymerization techniques. The work began by demonstrating that linear ADMET polyethylene²³ (no branches) could be synthesized by condensing linear 1,9-decadiene into its polymer, followed by exhaustive saturation with hydrogen. The use of metathesis polycondensation is important here, for it is mild chemistry that obviates chain transfer and operates via

essentially one mechanism. The consequence is that only a single type of repeat unit is formed leading to pure polymer microstructures. This early work was followed by the first known example of introducing a precisely controlled methyl “branch” on each and every ninth carbon along the polymer backbone.³⁹ Figure 2-1 compares the two types of microstructure under discussion, i.e., that with precision branching as compared with random placement.

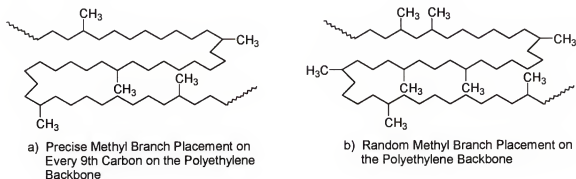


Figure 2-1. A pictorial representation of the difference in branch placement for PE Produced by: a) ADMET chemistry and b) typical chain processes used to date.

We now report the synthesis of a series of polyethylenes possessing *precisely controlled* methyl branch points where we have examined the effect of branching on the thermal behavior of these model polymers. The synthetic strategy for this new class of polyethylene also involves ADMET polycondensation chemistry and is illustrated in Figure 2-2.^{13,40}

Polymerization of the appropriate methyl branched α,ω -diene monomer via step polycondensation (ethylene is removed) produces unsaturated polymers, where the microstructure is controlled completely by the symmetrical nature of the monomer. Monomer symmetry is the key to this methodology. Exhaustive hydrogenation produces a fully saturated, precisely branched polymer and these macromolecules, which we term ADMET polyethylene, are described herein.

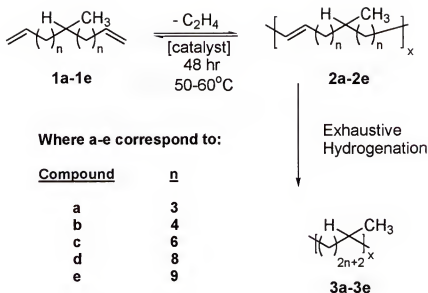


Figure 2-2. General synthetic scheme for synthesis of symmetrical methyl branched ethylene/propylene (EP) copolymer models by ADMET.

2.2 Results and Discussion

2.2.1 Monomer and Polymer Synthesis and Design

Two synthetic pathways proved useful in the preparation of the symmetrical monomers needed for this work, choosing either an acetoacetate based route³⁹ or by using alkenyl halide/carboxylic acid chemistry;^{41,42} this report describes the former route in some detail (Figure 2-3). Ethyl acetoacetate is reacted with an alkenyl bromide possessing appropriate methylene spacing to produce the disubstituted β -keto product (**4a-4f**), which is deacylated by retro-Claisen condensation to yield the ester (**5a-5f**). Reduction using lithium aluminum hydride yields the alcohol (**6a-6f**), which is tosylated (**7a-7f**), then reduced via hydride displacement to produce the symmetrical diene of interest. Six symmetrical monomers were prepared in this manner where $n = 3, 4, 6, 8, 9$ and 2 (Figure 2-3), (**1a-1f**).

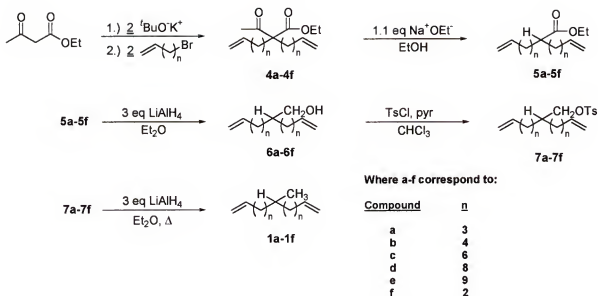


Figure 2-3. Synthetic pathway to produce methyl-branched biene with symmetrical methylene spacing for both alkenyl substituents.

2.2.2 ADMET Polymerization and Hydrogenation Chemistry

All six symmetrical monomers in this study were exposed to Grubbs' ⁹ or Schrock's ⁷ catalyst under mild ADMET step polymerization conditions. The chemistry proceeds cleanly to produce linear, unsaturated polymers possessing only one type of repeat unit plus the usual small quantity (<1%) of cyclics found in bulk polycondensation conversions. No side reactions are detectable via TLC and NMR analysis. Number average molecular weights (\overline{M}_n 's) range from 8 000 to 78 000 grams/mole, typical for polycondensation chemistry as are the polydispersity indices (PDI's), which range from 1.7 to 2.0 (Table 2-1). Only monomer **1f** failed to produce high polymer due to its propensity to cyclize under bulk reaction conditions, a result of the Thorpe-Ingold Effect ^{15,43,44} in which thermodynamically favored cyclization is driven by the presence of the methyl group.

Table 2-1. Molecular Weight Data for Unsaturated and Saturated Branched ADMET Polyethylene Polymers.

methyl branched ADMET PE	methyl branch on every n^{th} carbon	unsaturated polymer \overline{M}_n (10^3 g/mole) ^a	polydispersity index (P.D.I.)	saturated polymer \overline{M}_n (10^3 g/mole) ^a	polydispersity index (P.D.I.)
	n				
3a	9	22.8	2.0	17.5	1.7
3b	11	8.0	1.7	8.5	1.8
3c	15	15.7	1.7	17.1	1.7
3d	19	11.3	1.9	17.4	1.6
3ds	19 ^b	78.1	1.9	72.0	1.9
3e	21	20.2	1.7	20.2	1.7

^a Molecular weight data taken using chloroform as solvent and is relative to polystyrene standards. ^b Polymerized using Schrock's [Mo] alkylidene.

These unsaturated polymers were converted to model ethylene/propylene (EP) copolymers via exhaustive hydrogenation, where one of two methods was applied to this procedure. Exhaustive hydrogenation is crucial to this examination; for otherwise, the comparisons with "chain-made" polyethylene would be incorrect. Consequently, two methods for hydrogenation have been examined in this work—one involving a heterogeneous supported hydrogenation catalyst and the other involving homogeneous stoichiometric diimide reduction.

The heterogeneous supported catalysis method uses Grubbs' ruthenium catalysis for both metathesis and hydrogenation.^{33,45} The unsaturated polymer is mixed with dry silica in toluene under inert conditions, pressurized with 125 psi of H₂, stirred for 48 h, and the resultant suspension filtered and concentrated to produce the series of fully saturated

polymers (**3a-3e**). The fully hydrogenated polymer is isolated by precipitation into CH₃OH and dried *in vacuo* for a 24 h period in the melt; molecular weight data for these polymers is also found in Table 2-1. We find this tandem homogeneous metathesis/heterogeneous hydrogenation procedure to be an efficient method of producing ADMET PE. The stoichiometric diimide method is based on chemistry described by Hahn⁴⁶ and also gives excellent results. This is accomplished by successive additions of toluenesulfonylhydrazide (TSH) and tripropylamine (TPA), 3 equivalents of each, to the unsaturated polymer in *o*-xylene. The mixture is refluxed; TSH and TPA are added once again (3 eq) and brought to reflux once again. After cooling, the saturated polymer (**3ds**) is recovered by precipitation into CH₃OH.

Interestingly, during this study, it was found that combining [Mo] metathesis catalysis with [Ru] supported hydrogenation gives very poor saturation results; **2ds** could not be hydrogenated using the heterogeneous catalysis system (silica, Grubbs' catalyst). After exposing **2ds** to these conditions, it was found that only 15-20% hydrogenation had occurred (via NMR integration); consequently, this hydrogenation technique was not pursued further.

2.2.3 Molecular Weight Analysis of Fully Hydrogenated ADMET Polyethylenes

Table 2-1 shows that hydrogenation does not alter the molecular weight of the unsaturated polymers in this study, an observation noted in our earlier experiments.³⁹ Polydispersities are somewhat narrower than for the unsaturated analogs principally due to a small degree of fractionation upon precipitation, but the values still reflect a polycondensation scheme. Since the ADMET polyethylene models exhibit polydispersity indices (PDI's) in the range of 2.0, they are excellent models for similar ethylene based polymers produced via metallocene catalysis.^{47a}

The molecular weight analysis of these ADMET EP copolymer models is an important issue to delineate, for metathesis polycondensation chemistry produces PE-based samples with lower molecular weights than observed for the usual chain techniques. Clearly there exists a molecular weight dependence of the melting behavior in polymeric materials,⁴⁸ and because of potential penultimate effects, the question becomes evident whether or not these macromolecules are of sufficient size to model the thermal behavior of conventional materials.

We have addressed this question in two ways, the data for which is displayed in Table 2-2. First, linear ADMET polyethylene samples (no branches) were prepared in a range between $\overline{M}_n = 2\,400$ to 15 000 grams/mole. These samples increased in melting point from 130.7 °C to 133.9 °C; whereas, further changes in melting behavior with molecular weight were very gradual. The penultimate effect on melting in the $\overline{M}_n = 15\,000$ grams/mole sample may be present, but only to a small degree, certainly less than is important for comparisons with the methyl branched samples. Further, this sample's T_m of 133.9 °C and its heat of fusion compare favorably with commercial linear PE prepared using Ziegler-Natta chemistry.

Second, we prepared two samples possessing dramatically different molecular weights of polyethylene possessing a methyl branch precisely placed on each and every 19th carbon along the chain (this chemistry used to accomplish this is described in the experimental section), both with an \overline{M}_n greater than 15 000 grams/mole (samples **3d** and **3ds**, Table 2-2). A sharp melting endotherm of 57 °C is observed for both of them, one with an $\overline{M}_n = 17\,400$ grams/mole and the other 72 000 grams/mole. This data suggests

that a minimum number average molecular weight of approximately 15 000 grams/mole is sufficient for comparison between samples in this study.

Table 2-2. The Effect of Molecular Weight on Thermal Properties for Linear and Methyl Branched ADMET Polyethylene Polymers.

ADMET polyethylene	methyl branch on every n^{th} carbon	\overline{M}_n (g/mole)	polydispersity index (P.D.I.)	T_m (°C) (peak)	Δh_m (J/g)
n					
linear ADMET PE ^a	--	2400	2.4	130.7	252
linear ADMET PE ^a	--	7600	2.4	131.3	213
linear ADMET PE ^a	--	11 000	1.9	132.0	221
linear ADMET PE ^a	--	15 000	2.6	133.9	204
branched ADMET PE ^b 3d	18	17 400	1.6	57	96
branched ADMET PE ^c 3ds	18	72 000	1.9	57	84

^a Synthesized by ADMET of 1,9-decadiene. GPC analyses performed in 1,2,4-trichlorobenzene at 135 °C with respect to polyethylene standards.²³ ^b Polymerized with Grubbs' [Ru] benzylidene. GPC analysis performed in chloroform with respect to polystyrene standards. ^c Polymerized with Schrock's [Mo] alkylidene. GPC analysis performed in chloroform with respect to polystyrene standards.

2.2.4 Structural Determination Data

Figure 2-4 shows the ¹H NMR spectra for a typical conversion of monomer **1e**, 12-methyl-1,22-trieicosadiene, to its unsaturated polymer **2e**, and then to its saturated ADMET polyethylene methyl branch polymer **3e**. The olefin region illustrates the conversion of monomer to unsaturated polymer with the disappearance of the terminal

olefin at 4.96 and 5.81 ppm in the monomer and the subsequent growth of internal olefin resonance at 5.37 ppm in the unsaturated polymer **2e**. Upon exhaustive hydrogenation, these olefin resonances completely disappear. The ^{13}C NMR spectra (Figure 2-5) further supports the conclusion of exhaustive hydrogenation; note that the sp^2 resonances in the unsaturated polymer (trans: 130.36 ppm, cis: 129.90 ppm) completely disappear after hydrogenation giving **3e**. These spectra are typical for all the ADMET polyethylenes synthesized in the series, and they illustrate the degree of structure control that is possible.

Further, the ^{13}C NMR data exhibited in Figure 2-5 reveal that six sp^3 carbon signals are present in this polymer, which contains a methyl branch on every 21st carbon, an observation made earlier for the ADMET polyethylene sample possessing a methyl branch every 9th carbon.³⁹ The chemical shifts observed for polymer **3e** were 19.73, 27.11, 29.73, 30.05, 32.75, and 37.11 ppm, values which are in very good agreement with the values predicted by Carman, Tarpley, and Goldstein for a series of branched alkanes.⁴⁹ Resolution of chemical shifts apparently extends only to this point since the entire series of saturated polymers produced in this study, regardless of the number of methylene spacers, yields the same six chemical shifts. Higher field NMR experiments, which may further resolve these signals, are presently being investigated.

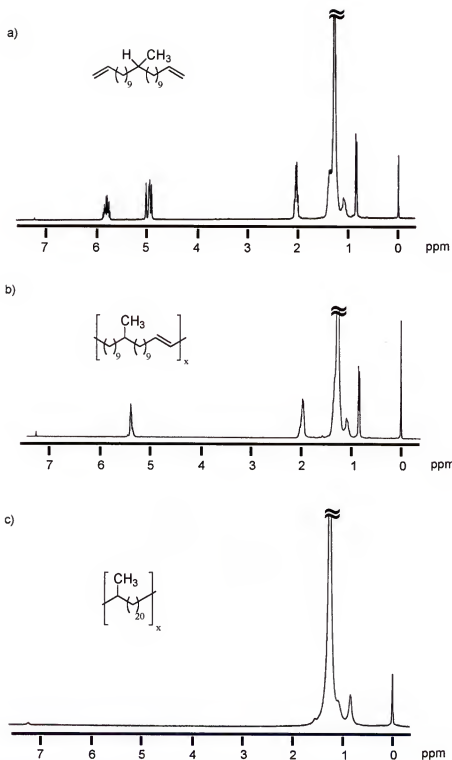
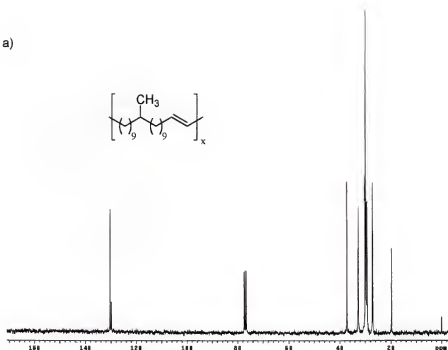


Figure 2-4. ^1H NMR for a) monomer, **8f** b) unsaturated polymer, **2e** c) saturated polymer, **3e**.

a)



b)

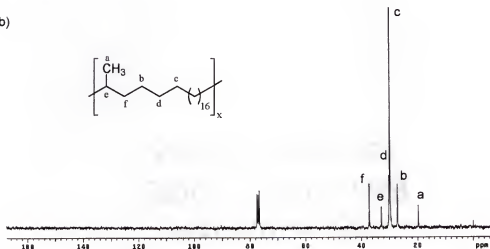


Figure 2-5. ^{13}C NMR spectra for a) unsaturated polymer, 2e b) saturated polymer, 3e.

These spectral data not only support the primary structure of the repeat unit but also suggest that no side reactions are detectable within the limitations of the NMR instrument. Elemental analysis results also show good agreement between theoretical and experimental values, as do bromine uptake experiments, sensitive to the presence of

any unsaturation. Infrared spectroscopy of these materials also shows no evidence for the presence of residual internal olefin, that if present would generate a strong fundamental absorption between $967\text{--}969\text{ cm}^{-1}$, which corresponds to the out-of-plane (oop) C—H bending in the alkene.

Do these methyl branched ADMET polyethylenes possess tacticity? Traditionally, tacticity in synthetic polymers describes the nature of successive stereocenters placed on every second or third carbon in the polymer backbone. In this work, the methyl branches are widely spaced from one another (from 9 to 21 carbons apart) and so the issue of tacticity is less important. Even so, strictly speaking the tacticity issue applies; however, the nature of the ADMET polymerization mechanism yields a completely random distribution of *R* and *S* stereocenters which makes these model systems atactic by definition. Nevertheless, as the thermal data demonstrates, the regular placement of the methyl branch has given these materials a level of order that allows crystallization to occur, even in materials with highest levels of branch content. Again, higher field ^{13}C NMR as well as x-ray crystallography should allow for a better understanding of the imposed order in these model systems.

2.2.5 Thermal Analysis: Comparative Polyethylene Thermal Data

Many different types of PE have been produced since its commercial inception in the 1930s; however, each type has a unique mode of initiation that leads to distinct differences in branch identity and branch content. This variation in branching gives rise to striking differences in the thermal properties of these materials that in turn becomes very important during materials processing. For the sake of comparison, Table 2-3, *vide infra*, compares these various types of PEs descending from the theoretical (infinitely

long chain, no branching) to varying degrees of branching. Included in this table are two types of ADMET polyethylene, linear and methyl branched.

Table 2-3. Thermal Data for a Number of Polyethylene Systems.

type of polyethylene	\overline{M}_n (10^3 g/mole)	methyl branches per 1000 carbon atoms	T_m (°C)	Δh_m (J/g)
theoretical PE ^e	24-114	0	141.5-146.5	293
ADMET PE ^c	2-15	0	131-134	204-252
metallocene PE ^d	30-1500	0.9-1.2	137-140	
HDPE ^e	50-250	1-6	133-138	219-245
Brookhart PE ^a	14-65	1.2-74	97-132	
ethylene/propylene copolymers ^b	20-70	2-100	80-133	--
LDPE ^e	20-100	30-60	105-115	95-141
MB ADMET PE ^f	8-72	48-111	-14-62	28-103

^a See ref 28i: M. Brookhart's new late transition metal systems using Pd and Ni. ^b See ref 30a: EP copolymers from the work of Wunderlich. ^c See ref 23: J. E. O'Gara and K. B. Wagener; PE produced by ADMET polycondensation. ^d See ref 47: Kaminsky, Cecchin, and Zucchini's work reviews on metallocene PE catalysis. ^e See ref 50: J. D. Hoffman's equilibrium values derived for an infinitely long PE chain. ^f Work in this study—PE model polymers made by ADMET with precise placement of methyl branches along the backbone.

Differences in melting points are quite interesting to compare. Hoffman's^{50a} theoretical polyethylene melt is the highest, followed by linear versions (no branching, or nearly so), then followed by materials possessing low quantities of random branches [metallocene PE, high density polyethylene (HDPE), Brookhart PE, then to purposely branched polymers such as ethylene/propylene (EP) copolymers and low density polyethylene (LDPE)]. Finally, precisely methyl branched ADMET polyethylene appears in the table. While the Brookhart polyethylenes are new, the others have been examined extensively, and in general, the endotherm for a branched polyethylene made

by chain techniques is broadened in shape and melts at lower temperatures as the methyl branch content increases.

The situation is decidedly different for precisely branched, ADMET polyethylene. By comparison, all these endotherms are considerably sharper—some very sharp. Further, while linear ADMET PE melts in a manner similar to metallocene and HDPE materials, methyl branched ADMET polyethylene melts at dramatically lower temperatures, clearly lower than any of the commercially produced polymers. This change in behavior is attributed to its significantly different, precisely controlled microstructure where only methyl branches are present; these methyl branches are precisely—exactly—placed along the backbone. Of course, PE made by chain propagation possesses randomly placed branches of differing identity (methyls, longer alkyls, vinyls, allyls, etc.).

2.2.6 Methyl Branched ADMET Polyethylene Melting Behavior

DSC analyses were performed using a Perkin-Elmer DSC 7 at a scan rate of 2 °C/minute. Calibrations were accomplished using indium and *p*-nitrotoluene as standards for both peak temperature transitions and heats of fusion. In order to erase thermal history, each sample was annealed for 5h at 50 °C above the peak melting point found in initial scans. Complete details of exact scanning procedures may be found in the experimental section.

Differential scanning calorimetry was employed to determine the melting behavior of the ADMET polyethylene series, since a great deal of DSC data is present in the literature for comparison. The random copolymers, such as those made from ethylene and propylene via Ziegler-Natta catalysis,^{30a} exhibit a broad, indistinct melting behavior when the percentage of propylene exceeds approximately 15%.^{30a,38h} In comparison, the

exact placement of a methyl group in ADMET EP copolymer model materials produces both sharp melting endotherms and recrystallization exotherms; as illustrated in Figure 2-6 for polymer sample **3e**. This sample possesses a methyl branch on each and every 21st carbon along the PE backbone (48 methyl branches per 1000 carbon atoms); and it is important to emphasize that all of the ADMET PEs in this series show similar endotherm and exotherm shapes.

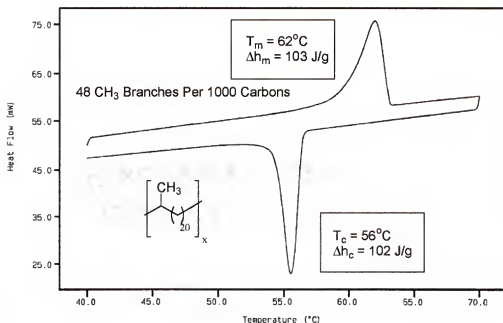


Figure 2-6. Typical DSC plot illustrating melting endotherm and crystallization exotherm. DSC for **3e** (methyl branch every 21st carbon).

Table 2-4 lists DSC data obtained for the methyl branched ADMET model EP copolymers studied to date. Note that the melting temperatures (Table 2-4) are reported as onsets and peak maximums, and enthalpy values are quantitative thermodynamic measurements and are reported in relation to the unit weight.

Several interesting results are observed concerning the melting point behavior of these precisely placed methyl branched polymers. While the T_m for perfectly linear

ADMET PE approaches that of other highly linear PEs made by commercial routes,^{51,52,53} the precisely placed methyl group on every 9th carbon, polymer (**3a**), depresses the peak melting point to -14 °C with a Δh_m of 28 J/g. This polymer melts approximately 150 °C lower than linear ADMET polyethylene and exhibits a heat of fusion approximately approximately 1 order of magnitude smaller.²³

Table 2-4. DSC Data for Fully Hydrogenated ADMET Polyethylene Methyl-Branched Model Polymers.

ADMET polyethylenes ^a	methyl branch on every n^{th} carbon	methyl branches per 1000 carbon atoms	T_m (°C) (onset)	T_m (°C) (peak)	Δh_m (J/g)
	n				
3a	9	111	-18	-14	28
3b	11	91	-3	11	66
3c	15	67	35	39	82
3d	19	53	53	57	96
3ds	19	53	49	57	84
3e	21	48	57	62	103
linear ADMET polyethylene ^b	--	0	--	134	204

^a **3a-3e** polymerized with Grubbs' [Ru] benzylidene; however, **3ds** was prepared using Schrock's [Mo] alkylidene. ^b Made by ADMET of 1,9-decadiene.²³

As the methylene spacing increases between branch points for the methyl branched ADMET PE series, melting points and heats of fusion increase. This is to be expected, for as the frequency of comonomer content (methyl/methine mole fraction) decreases, the percent crystallinity of the polymer sample should increase. The increase in T_m and Δh_m with a decrease in comonomer content indicates that the relative percent crystallinity is

increasing but still quite distant from the corresponding values for linear ADMET polyethylene.

The mere presence of a distinct melting point for any of the methyl branched polymers, and particularly for sample **3a**, is a surprising result. Alamo and Mandelkern have shown that the lack of regularity in ethylene run lengths impacts the nature of the melting temperature transition,^{30d} and model studies by others using chain propagation techniques illustrate that a completely amorphous polymer is formed when the frequency of methyl branch is an average of 150 or greater branches per 1000 carbon atoms.^{30a,32c} However, in the case of ADMET polyethylene possessing precise spacing, a branch frequency of 111 methyl branches per 1000 carbon atoms (sample **3a**) yields a material possessing a distinct, sharp melting point. In fact, the breadth of all melt transitions for the entire series of polymers in Table IV are narrower than those reported for poly(ethylene-copropylene) samples with comparable comonomer content.^{30a,54} Figure 2-7 provides a DSC visual overlay for all of the polymer samples described herein.

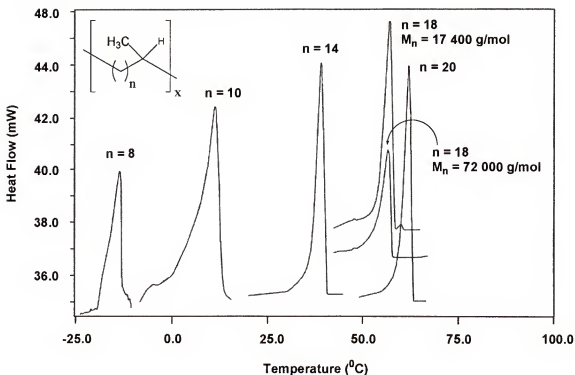


Figure 2-7. DSC visual overlay of melt transitions for ADMET polyethylene with precisely placed methyl branches presented in Table 2-4.

This trend in melting point behavior for methyl branched ADMET polyethylene illustrates the dependence of melting point on comonomer composition, and this data is plotted in Figure 2-8 using the Flory equation (Eq. 2-1, below).⁵⁵

$$T_m = T_m^* \left(1 - \frac{RT_m^*}{\Delta H_m^*} [\chi_{CHCH_3}] \right) \quad \text{Equation [2-1]}$$

The equilibrium melting point T_m^* of theoretical polyethylene is assumed to be 145.5 °C; the equilibrium enthalpy of melting, ΔH_m^* is taken as 4.1 kJ/mole of methylene groups; and χ_{CHCH_3} is the mole fraction of methyl branch moiety in the polymer. Theoretical data is plotted in comparison with ADMET polymer data that was derived from a series of five differing comonomer contents.

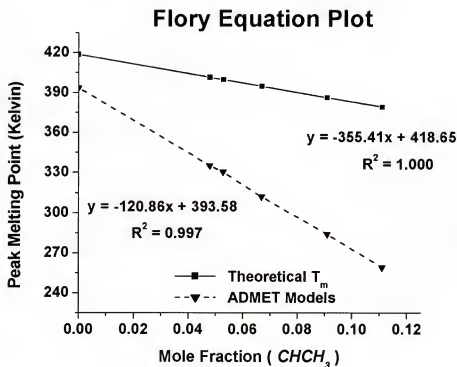


Figure 2-8. Flory equation treatment for the impact of comonomer (defect) content on the melting point.

Just as the theoretical model predicts, the methyl branched ADMET polyethylene models give a linear relationship when plotting the melting point depression versus the increase in comonomer content ($CHCH_3$). However, the slope and intercept of the line for methyl branched ADMET polyethylene samples studied here is distinctly different when compared to the theoretical model for random branching. The discrepancy between experimental and theoretical data can be expected, for the Flory equation accounts not for the chemical nature of the comonomer units but only the number of these units in the polyethylene chain. Nevertheless, the correlation coefficient of 0.998 indicates that these ADMET polyethylene polymers provide an effective tool for modeling precise methyl branch placement along the backbone of polyethylene.

2.2.7 The Glass Transition Behavior of Methyl Branched ADMET Polyethylene

While the relaxation spectra of linear and branched polyethylene have been extensively examined,⁵⁶⁻⁶³ debate continues on the exact transitions which can be called the glass transition temperature for this polymer.^{57,63} Thermal expansion, calorimetric, and dynamic mechanical measurements on branched polyethylene all have shown three distinct relaxation regimes termed α , β , and γ , respectively.

Work completed by various researchers have reported the α relaxation^{59,60} at 70 +/- 10 °C, the β relaxation⁶¹ at -30 +/- 15 °C and the γ relaxation^{57,62} at -125 +/- 5 °C. Most investigators agree that these three transitions exist but cannot agree on the true T_g for polyethylene. The α relaxation is thought to arise from motions in the crystalline regions of the polymer (long-spacing growth), while the β transition is attributed to the relaxation of chain branch regions of the polymer. The γ relaxation origin is a topic of considerable debate; however, it is often described as the consequence of a crankshaft type motion along a small number of methylene units in the amorphous domains of PE. A study concerning the relative magnitudes of the β and γ relaxation in dynamic mechanical measurements showed a marked increase in the intensity of the β relaxation as the number of chain branches increased.⁵⁶ This and other observations on ethylene containing copolymers led experimentalists to view the β relaxation as the primary T_g of branched, semicrystalline polyethylene, a result supported by work done by Stehling and Mandelkern in 1970.⁵⁷

Given that methyl branched ADMET polyethylene likely possesses a high amorphous content, three such polymers—**3a**, **3b**, and **3e**—ranging from 48 methylys to

111 methyl branches per 1000 carbon atoms were examined for their glass transition behavior in the β relaxation region, and the results are displayed in Table 2-5.

Table 2-5. Glass Transition Data for ADMET Polyethylene Model Polymers.

polymer	methyl branch on every n^{th} carbon	T_g (°C)	ΔC_p (J/g°C)
	n		
3a	9	-44	29
3b	11	-44	28
3e	21	-43	27

The T_g 's and changes in specific heat average are -44 °C and 29 J/g °C, respectively, and are the same for all three samples regardless of running length of the polyethylene between branch points. This β relaxation is particularly evident in the DSC spectra of these precisely spaced methyl branched polyethylenes. Figure 2-9 shows one of the DSC curves, which is essentially identical to what is observed for the other two. The likely explanation for this behavior relates to the probability that relaxation about the branch point is quite local in scope such that running polyethylene lengths are not a factor. These initial glass transition findings are quite intriguing.

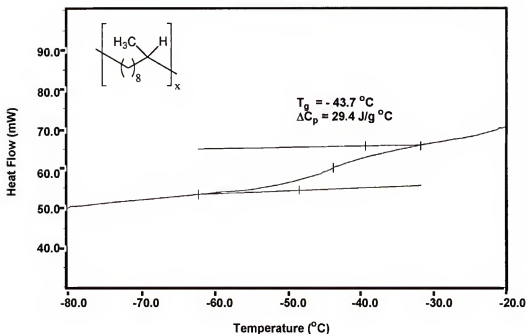


Figure 2-9. Glass transition curve for methyl branched ADMET polyethylene with a methyl branch on each and every 9th carbon (3a).

2.3 Conclusions

The perfect control of methyl branch placement along the backbone of polyethylene has a profound influence on the thermal behavior of these PE model materials. As the methylene spacing between branch points increases, the melting point and heat of fusion increase. The data correlate well with the Flory relationship, suggesting that the ADMET polycondensation approach to model branching in polyethylene offers a sound analytical basis, despite the lower molecular weight ranges for these step polymers. Initial glass transition data show the β relaxation for polyethylene is independent of the frequency of branching.

Presently we are continuing this research by gathering x-ray and other scattering data for these methyl-substituted polymers. Our intention is to better understand the secondary and tertiary structure of these models. We also are preparing other ADMET

polyethylenes possessing longer branches (ethyl, butyl, hexyl, etc) in order to model other common materials such as linear low density PE, metallocenes and the like. Further, we are probing the glass transition data in more detail.

ADMET chemistry represents the only method to precisely control the identity and distribution of branches along the backbone of polyethylene. *This research will provide the basis for a better understanding of the morphology, crystalline structure, and thermodynamics of the crystallization process of the most abundant synthetic macromolecule in the world, polyethylene.*

2.4 Experimental

2.4.1 Instrumentation and analysis.

All ^1H NMR (300 MHz) and ^{13}C NMR (75 MHz) spectra were recorded on either a General Electric QE-Series NMR Superconducting spectrometer system or Varian Associates Gemini 300 spectrometer. Chemical shifts for ^1H and ^{13}C NMRs were referenced to residual signals from CDCl_3 with 0.03% v/v TMS as an internal standard. Reaction conversions and relative purity of crude reactions were monitored by chromatography. Gas chromatography (GC) was performed on a Hewlett-Packard HP5880A gas chromatograph equipped with a methyl silicone capillary column and flame ionization detector. Thin layer chromatography (TLC) was performed on WatmanTM aluminum backed, 250 mm silica gel coated plates. TLC plates were developed with mixtures of hexanes and ethyl acetate as the mobile phase. TLC plates for UV inactive olefin monomers were stained with either potassium permanganate (2%) in an aqueous solution of sodium bicarbonate (4%) or phosphomolybdic acid (10%) in ethanol after development to produce a visible signature. Low and high resolution mass spectral (LRMS and HRMS) data were obtained on a Finnegan 4500 gas

chromatograph/mass spectrometer using the electron ionization (EI) mode. Elemental analyses were carried out by Atlantic Microlabs Inc., Norcross, GA.

Ester and alcohol intermediates were purified by vacuum distillation from calcium hydride. Initial purification of monomer was accomplished by simple short path vacuum distillation. Final purification to yield pure monomer was accomplished by either flash chromatography⁶⁴ using 100% hexanes as the eluent or high performance liquid chromatography (HPLC) using 99.5% hexanes and 0.5% ethyl acetate as the mobile phase. HPLC was accomplished using a Ranin instrument equipped with Dynamax SD1 pumps, Dynamax UV-1 variable wavelength UV/VIS absorbance detector and a Varian Star 9042 Refractive Index (RI) detector in series, and Dynamax FC-1 fraction collector. Two columns were utilized: 1) analytical or scout scale column with dimensions of 10.0 mm (inner diameter) by 250.0 mm and 2) preparative scale with dimensions of 41.4 mm (inner diameter) by 250.0 mm. Both columns were silica packed with a particle size of 8 μ m and a pore size of 60 Å. Crude samples were diluted in a 25% solution (w/v) of HPLC grade hexanes and filtered before injection.

Gel permeation chromatography (GPC) was performed using a Waters Associates liquid chromatography U6K equipped with a tandem ABI Spectroflow 757 UV absorbance detector and a Perkin-Elmer LC-25 RI detector. All molecular weights are relative to polystyrene standards. Polymer samples were dissolved in HPLC grade CHCl_3 (approximately 0.1% w/v) and filtered before injection (a volume of 20-40 μL). The GPC was equipped with an Ultrastaygel linear mixed-bed column. HPLC grade chloroform was used as the eluent at a constant flow rate of 1.0 mL/min. Retention times were calibrated against narrow molecular weight polystyrene standards (Scientific

Polymer Products, Inc.). All standards were selected to produce M_p or M_w values well beyond the expected polymer's range. A minimum of five data points was acquired to produce an adequate calibration curve.

Differential scanning calorimetry (DSC) analyses were performed on two separate instruments. Initial results were obtained on a TA Instruments Model 2910 DSC and Model 2850 TGA equipped with a Model 2000 data analysis software program. DSC analyses were obtained at a heating rate of 2 °C/min. Calibrations were made using indium as the standard for both peak temperature transitions and the heats of fusion. All samples were prepared in hermetically sealed pans. Attempts were made to keep a small range on the weight for all polymer samples (approximately 10 mg/sample). Initial scans were performed to determine the onset and peak melting position for each unannealed polymer sample. All samples were analyzed using an empty pan as reference and empty cells as a subtracted baseline. The two lowest melting samples were analyzed from -80 °C to 30 °C, (**3a**, **3b**) and the remainder of the samples (**3c-3e**) were analyzed from 0 °C to 80 °C. These melting points were used as guides for annealing in the subsequent DSC study. Initial melting point and heat of fusion data is given in the experimental for each polymer. Thermogravimetric analysis (TGA) was also performed. All samples were heated from room temperature to 800 °C in nitrogen at a scan rate of 10 °C/min. The onset of weight loss was taken as the initial value.

After initial values for peak melting points were found, a second set of samples were prepared in a similar fashion to the first set. DSC analyses were performed using a Perkin-Elmer DSC 7 at a heating rate of 2 °C/min. Indium and *p*-nitrotoluene were used as standards for peak temperature transitions, while all enthalpy measurements are based

on using indium as the single standard. In order to destroy all thermal history, each sample was annealed for 5h at 50 °C above the peak melting point found in initial scans. Subsequently, the samples were then cooled at 2 °C/min to approximately one degree below the onset melt temperature found in the initial DSC measurements. Each sample was then annealed at this point for 5h. Then, the sample was cooled at 2 °C/min to a point that was approximately 30 °C below the observed recrystallization temperature, followed by cooling at 30 °C below the crystallization temperature for 5 min. After cooling, the sample was heated at 2 °C/min until reaching approximately 30 °C above the observed melting point and isothermally held for 5 min. Finally, the samples were scanned for multiple cycles through the same range to verify the results obtained on the first run. Data collection was taken on the first run. The results are listed in the experimental and in tabular form within the text. Reported values are given as T_m (peak) (melting, first order transition peak position), T_m (onset), T_c (peak)(recrystallization, first order transition peak position). Glass transition temperatures (T_g 's) were taken in the following manner. Each sample was loaded and annealed for five hours at 50 °C above the observed melting temperature. Next the sample was rapidly quenched to -80°C (from 50°C above the melt to -80°C in approximately 4 seconds) and isothermally cooled for fifteen minutes. Finally, the sample was heated at 2 °C/minute from -80 °C to 0 °C. Reported values are given as T_g (glass transition)(second order transition) and C_p (heat capacity in J/g °C).

2.4.2 Materials.

Grubbs' benzyldiene ruthenium catalyst, $\text{RuCl}_2(=\text{CHR})-(\text{PCy}_3)_2$, where Cy = cyclohexyl, and R = phenyl (Figure 2-2), was synthesized using the literature procedure.⁹ Schrock's molybdenum catalyst $[(\text{CF}_3)_2\text{CH}_2\text{CO}]_2(\text{N}-2,6-\text{C}_6\text{H}_3-i\text{-Pr}_2)\text{Mo}=\text{CHC}(\text{CH}_3)_2\text{Ph}$

(Figure 2-1), was also synthesized via literature procedure.⁷ Acrôs 60 mesh silica gel was dried under vacuum ($<10^{-3}$ mm Hg) at 100°C for 24 h and stored in an Argon atmosphere drybox prior to use in the hydrogenation reactions.

Dimethoxyethane (DME), toluene, and diethyl ether (Et₂O) were freshly distilled from Na/K alloy using benzophenone as the indicator. *p*-Toluenesulfonohydrazide (TSH) was purchased from Aldrich and recrystallized from CH₃OH prior to use. Tripropylamine (TPA) and *o*-xylene were purchased from Aldrich and distilled from CaH₂ prior to use. A solution of 2M potassium tert-butoxide (K⁺ O⁻ Bu) was prepared in a flame dried, argon purged Schlenk tube by combining the salt (Aldrich) with DME freshly distilled from Na/K alloy. 5-bromo-1-pentene, 6-bromo-1-hexene, 8-bromo-1-octene (Aldrich), 10-bromo-1-decene (Alfa Aesar, Avocado), and 11-bromo-1-undecene were distilled from CaH₂ prior to use. The 11-bromo-1-decene was synthesized from 10-undecen-1-ol (Alfa Aesar, Avocado) via literature method (see experimental).⁶⁵ Ethyl acetoacetate (Aldrich) was also distilled from CaH₂ prior to use. ¹H NMR and ¹³C NMR spectra for ethyl acetoacetate and all alkenyl bromides are provided under the listing of starting materials. All other reagents mentioned in the experimental were used as received.

2.4.3 Characterization of starting materials.

Ethyl acetoacetate (Aldrich): ¹H NMR (CDCl₃): δ (ppm) 1.29 (t, 3H, -C(O)OCH₂CH₃), 2.29 (s, 3H, -C(O)CH₃), 3.46 (s, 2H), 4.21 (q, 2H, -C(O)OCH₂CH₃), 12.17 (s, 0.06H, enol contributor); ¹³C NMR (CDCl₃): δ (ppm) 14.12 (-C(O)OCH₂CH₃), 30.10 (-C(O)CH₃), 50.10, 61.30 (-C(O)OCH₂CH₃), 167.22 (-C(O)OCH₂CH₃), 200.74 (-C(O)CH₃).

5-bromo-1-pentene (Aldrich): ^1H NMR (CDCl_3): δ (ppm) 1.95 (m, 2H), 2.21 (m, 2H), 3.41 (t, 2H), 5.05 (m, 2H), 5.79 (m, 1H); ^{13}C NMR (CDCl_3): δ (ppm) 31.80, 32.06, 33.06, 115.91, 136.74.

6-bromo-1-hexene (Aldrich): ^1H NMR (CDCl_3): δ (ppm) 1.52 (m, 2H), 1.87 (m, 2H), 2.09 (m, 2H), 3.40 (t, 2H), 5.03 (m, 2H), 5.82 (m, 1H); ^{13}C NMR (CDCl_3): δ (ppm) 27.25, 32.07, 32.65, 33.35, 114.82, 137.93.

8-bromo-1-octene (Aldrich): ^1H NMR (CDCl_3): δ (ppm) 1.38 (m, br, 6H), 1.86 (m, 2H), 2.05 (m, 2H), 3.40 (t, 2H), 4.97 (m, 2H), 5.80 (m, 1H); ^{13}C NMR (CDCl_3): δ (ppm) 28.21, 28.77, 28.91, 32.84, 33.82, 33.88, 114.20, 139.08.

10-bromo-1-decene (Alpha Aesar, Avocado): ^1H NMR (CDCl_3): δ (ppm) 1.38 (m, br, 10H), 1.86 (m, 2H), 2.05 (m, 2H), 3.41 (t, 2H), 4.98 (m, 2H), 5.82 (m, 2H); ^{13}C NMR (CDCl_3): δ (ppm) 28.19, 28.81, 28.94, 29.10, 29.42, 32.87, 33.84, 33.85, 114.19, 139.14.

10-undecene-1-ol (Alpha Aesar, Avocado): ^1H NMR (CDCl_3): δ (ppm) 1.24 (m, br, 12H), 1.58 (m, 2H), 1.82 (s, s, 1H, alcohol), 2.09 (m, 2H), 3.67 (t, 2H), 5.03 (m, 2H), 5.84 (m, 1H); ^{13}C NMR (CDCl_3): δ (ppm) 25.72, 28.90, 29.06, 29.37, 29.50, 32.78, 33.72, 62.94, 114.04, 139.11.

11-bromo-1-undecene.⁶⁵ To a flame dried and Ar purged 500 mL 3-neck flask equipped with a magnetic stir bar were added 20.0 g (117 mmol) of 10-undecen-1-ol and 200-250 mL of anhydrous Et_2O . To this solution was added 77.9 g (235 mmol) CBr_4 . The stirring solution was then cooled to 0 °C and 65.4 g PPh_3 (235 mmol) was added in small increments over a period of 30 min. The solution was allowed to warm to room temperature and stir for 6 h. The solution had manifested a yellow tint at this point and was then filtered and the solvent removed under reduced pressure. The resultant residue

was dissolved in pentane and filtered. The solution was then flash filtered through a short bed of silica gel and the pentane removed under reduced pressure. This solution was distilled under vacuum to yield the alkenyl bromide. Yield of 11-bromo-1-undecene: 82.7% (Isolated). The following spectral properties were observed. ^1H NMR (CDCl_3): δ (ppm) 1.35 (m, br, 12H), 1.85 (m, 2H), 2.04 (m, 2H), 3.39 (t, 2H), 4.96 (m, 2H), 5.80 (m, 1H); ^{13}C NMR (CDCl_3): δ (ppm) 28.20, 28.79, 28.94, 29.11, 29.41, 32.87, 33.83, 33.87, 114.16, 139.13.

2.4.4 Symmetrical monomer synthesis and characterization.

The following set of five monomers were synthesized using an extension of a methodology presented previously.³⁴ A sample procedure is given for the first monomer in the series. *Note: Results for 4-8f are not listed since high polymer was not obtained.*

2.4.4.1 Step 1 (One-Pot, Two-Step Synthesis) (Dialkylation of Ethyl Acetoacetate)

Ethyl-2-acetyl-2-(4-pentenyl)-hept-6-en-oate (4a). A 10.9 g (84 mmol) sample of ethyl acetoacetate and 200-250 mL of dry DME were placed in a flame dried, argon purged 500 mL 3-neck flask equipped with a magnetic stirbar and condenser. A 42 mL portion of a 2M solution of potassium *tert*-butoxide in DME was then added with stirring. Upon addition, the solution turned lime-green in color. Due to the exothermic nature, the reaction mixture was allowed to stand for 30 min. Next, 12.5 g (84 mmol) of dry 5-bromo-1-pentene was slowly added via syringe over the course of 5-6 min. The reaction mixture was slowly raised to reflux becoming an orange-brown in color with salt formation. After 18 h (longer halides in this series require up to 24 h of reaction time as shown by GC), the reaction was allowed to cool to room temperature in preparation for the second addition of halide. At this point, the reaction mixture was pale yellow in color

with a white precipitate. The second addition of 42 mL of a 2M solution of potassium *tert*-butoxide in DME and 12.5 g (84 mmol) of dry 5-bromo-1-pentene was administered in the same manner as described above. The reaction was taken to reflux for a period of 26 h (monitored by GC, note that longer halides in this series require up to 36 h of reaction time for completion). The reaction mixture is cooled to room temperature, quenched with 3N HCl, and extracted three times with Et₂O. The combined ether extracts were washed with DI H₂O, dried over MgSO₄, filtered, and finally evaporated under reduced pressure to yield a yellow-tinted product. **Note:** the disubstituted β -keto product was not purified before proceeding to the next reaction. Yield of **4a**: 80.0% (Crude). The following spectral properties were observed: ¹H NMR (CDCl₃): δ (ppm) 1.17 (m, br, 4H), 1.26(t, 3H, -C(O)OCH₂CH₃), 1.85 (m, br, 4H), 2.05 (q, 4H), 2.11 (s, 3H, -C(O)CH₃), 4.19 (q, 2H, -C(O)OCH₂CH₃), 4.99 (m, 4H, vinyl CH₂), 5.76 (m, 2H, vinyl CH); ¹³C NMR (CDCl₃): δ (ppm) 14.11, 23.22, 26.67, 30.73, 33.62, 33.89, 61.17, 63.38, 115.14 (vinyl CH₂), 138.01 (vinyl CH), 172.57 (-C(O)OCH₂CH₃), 205.26 (-C(O)CH₃); EI/LRMS: [M + 1]⁺ calcd. for C₁₆H₂₆O₃: 267, found: 267.

Ethyl-2-acetyl-2-(5-hexenyl)-oct-7-en-oate (4b). Synthesized as above. Yield of **4b**: 81.2% (Crude). The following spectral properties were observed: ¹H NMR (CDCl₃): δ (ppm) 1.01 (m, br, 4H), 1.26(t, 3H, -C(O)OCH₂CH₃), 1.42 (m, br, 4H), 1.85 (m, br, 4H), 2.03 (q, 4H), 2.16 (s, 3H, -C(O)CH₃), 4.20 (q, 2H, -C(O)OCH₂CH₃), 4.98 (m, 4H, vinyl CH₂), 5.79 (m, 2H, vinyl CH); ¹³C NMR (CDCl₃): not obtained; EI/LRMS: [M + 1]⁺ calcd. for C₁₈H₃₀O₃: 295, found: 295.

Ethyl-2-acetyl-2-(7-octenyl)-dec-9-en-oate (4c). Synthesized as above. Yield of **4c**: 80.1% (Crude). The following spectral properties were observed: ¹H NMR (CDCl₃):

δ (ppm) 1.09 (m, br, 4H), 1.20(t, 3H, $-\text{C}(\text{O})\text{OCH}_2\text{CH}_3$), 1.34 (m, br, 12H), 1.84 (m, br, 4H), 2.03 (q, 4H), 2.10 (s, 3H, $-\text{C}(\text{O})\text{CH}_3$), 4.19 (q, 2H, $-\text{C}(\text{O})\text{OCH}_2\text{CH}_3$), 4.95 (m, 4H, vinyl CH_2), 5.78 (m, 2H, vinyl CH); ^{13}C NMR (CDCl_3): δ (ppm) 14.13, 23.81, 26.63, 28.87, 29.88, 31.22, 33.80, 61.06, 63.50, 114.32 (vinyl CH_2), 138.96 (vinyl CH), 172.69 ($-\text{C}(\text{O})\text{OCH}_2\text{CH}_3$), 205.33 ($-\text{C}(\text{O})\text{CH}_3$); EI/LRMS: $[\text{M} + 1]^+$ calcd. for $\text{C}_{22}\text{H}_{38}\text{O}_3$: 351, found: 351.

Ethyl-2-acetyl-2-(9-decenyl)-dodec-11-en-oate (4d). Synthesized as above Yield of **4d**: 96.2% (Crude). The following spectral properties were observed: ^1H NMR (CDCl_3): δ (ppm) 1.06 (t, br, 3H, $-\text{C}(\text{O})\text{OCH}_2\text{CH}_3$), 1.30 (m, br, 24H), 1.79 (m, 4H), 2.07 (q, 4H), 2.11 (s, 3H, $-\text{C}(\text{O})\text{CH}_3$), 4.19 (q, 2H, $-\text{C}(\text{O})\text{OCH}_2\text{CH}_3$), 4.96 (m, 4H, vinyl CH_2), 5.80 (m, 2H, vinyl CH); ^{13}C NMR (CDCl_3): δ (ppm) 14.12, 23.75, 26.65, 27.38, 28.90, 29.28, 29.38, 29.95, 31.10, 33.79, 61.06, 63.49, 114.15 (vinyl CH_2), 139.16 (vinyl CH), 172.75 ($-\text{C}(\text{O})\text{OCH}_2\text{CH}_3$), 205.62 ($-\text{C}(\text{O})\text{CH}_3$); EI/LRMS: $[\text{M} + 1]^+$ calcd. for $\text{C}_{26}\text{H}_{46}\text{O}_3$: 407, found: 407.

Ethyl-2-acetyl-2-(10-undecenyl)-tridec-12-en-oate (4e). Synthesized as above. Yield of **4e**: 90.3% (Crude). The following spectral properties were observed: ^1H NMR (CDCl_3): δ (ppm) 1.34 (m, br, 31H), 1.84 (m, br, 4H), 2.03 (q, 4H), 2.10 (s, 3H, $-\text{C}(\text{O})\text{CH}_3$), 4.19 (q, 2H, $-\text{C}(\text{O})\text{OCH}_2\text{CH}_3$), 4.97 (m, 4H, vinyl CH_2), 5.79 (m, 2H, vinyl CH); ^{13}C NMR (CDCl_3): δ (ppm) 14.13, 23.81, 26.62, 27.47, 28.99, 29.17, 29.37, 29.52, 30.02, 31.21, 33.86, 61.01, 63.50, 114.18 (vinyl CH_2), 139.10 (vinyl CH), 172.72 ($-\text{C}(\text{O})\text{OCH}_2\text{CH}_3$), 205.35 ($-\text{C}(\text{O})\text{CH}_3$); EI/LRMS: $[\text{M} + 1]^+$ calcd. for $\text{C}_{28}\text{H}_{50}\text{O}_3$: 435, found: 435.

2.4.4.2 Step 2 (Retro-Claisen Condensation)

Ethyl-2-(4-pentenyl)-hept-6-en-oate (5a). A 21.81 g sample of crude **4a** (82 mmol) and 125 mL of anhydrous EtOH (Aldrich) were placed in flame dried, Ar purged 500 mL 3-neck round bottom flask equipped with a condenser and stirbar. 125 mL (1.1 mol) of a 21% w/w NaOEt/EtOH solution (Aldrich) was added via cannula to the solution. The reaction mixture was refluxed 4-6 h (dependent on the monomer). After cooling the solution to room temperature, the reaction was quenched with water (slowly) and 3N HCl. The quenched reaction mixture was extracted three times with Et₂O, washed with DI H₂O, and dried over MgSO₄. Finally, the combined organics were distilled and evaporated under reduced pressure. The product was then placed over CaH₂ and stirred overnight. The crude ester over CaH₂ was then placed into a vigreux distillation apparatus, placed under vacuum, and stirred overnight (<10⁻¹ mm Hg). Crude ester (**5a**) was then distilled with a boiling point of 79-80 °C at 1mm Hg. Yield of ester **5a**: 96.2% (Crude), 62.3% (Isolated). The following spectral properties were observed: ¹H NMR (CDCl₃): δ (ppm) 1.25 (t, 3H, -C(O)OCH₂CH₃), 1.40 (m, br, 6H), 1.61 (m, br, 2H), 2.04 (q, 4H), 2.32 (m, 1H), 4.14 (q, 2H, -C(O)OCH₂CH₃), 4.98 (m, 4H, vinyl CH₂), 5.76 (m, 2H, vinyl CH); ¹³C NMR (CDCl₃): δ (ppm) 14.36, 26.68, 31.93, 33.61, 45.47, 60.02 (-C(O)OCH₂CH₃), 114.65 (vinyl CH₂), 138.48 (vinyl CH), 176.29 (-C(O)OCH₂CH₃); EI/LRMS: [M + 1]⁺ calcd. for C₁₄H₂₄O₂: 225, found: 225; Elemental analysis calcd. for C₁₄H₂₄O₂: 74.94 C, 10.79 H; found: 74.97 C, 10.77 H.

Ethyl-2-(5-hexenyl)-oct-7-en-oate (5b). Synthesized as above. Crude ester (**5b**) was distilled with a boiling point of 93-94 °C at 1mm Hg. Yield of **5b**: 73.5% (Crude), 48.3% (Isolated). The following spectral properties were observed: ¹H NMR (CDCl₃):

δ (ppm) 1.28 (m, br, 11H), 1.65 (m, 4H), 2.02 (q, 4H), 2.31 (m, 1H), 4.15 (q, 2H, -C(O)OCH₂CH₃), 5.01 (m, 4H, vinyl CH₂), 5.79 (m, 2H, vinyl CH); ¹³C NMR (CDCl₃): δ (ppm) 14.02, 14.10, 24.64, 26.67, 28.35, 28.40, 28.45, 28.64, 32.08, 33.30, 34.12, 45.46, 59.84 (-C(O)OCH₂CH₃), 114.12 (vinyl CH₂), 138.54 (vinyl CH), 173.35 (-C(O)OCH₂CH₃); EI/HRMS: [M + 1]⁺ calcd. for C₁₆H₂₈O₂: 252.2089, found: 252.2089; Elemental analysis calcd. for C₁₆H₂₈O₂: 76.14 C, 11.18 H; found: 76.16 C, 11.20 H.

Ethyl-2-(7-octenyl)-dec-9-en-oate (5c). Synthesized as above. Crude ester (**5c**) was distilled with a boiling point of 155-156 °C at 1 mm Hg. Yield of **5c**: 79.5% (Crude), 49.9% (Isolated). The following spectral properties were observed: ¹H NMR (CDCl₃): δ (ppm) 1.14 (m, br, 21H), 1.60 (m, br, 2H), 2.02 (q, 4H), 2.31 (m, 1H), 4.14 (q, 2H, -C(O)OCH₂CH₃), 5.04 (m, 4H, vinyl CH₂), 5.83 (m, 2H, vinyl CH); ¹³C NMR (CDCl₃): δ (ppm) 14.31, 27.33, 28.83, 28.91, 29.35, 32.44, 33.69, 45.72, 59.82 (-C(O)OCH₂CH₃), 114.10 (vinyl CH₂), 139.03 (vinyl CH), 176.33 (-C(O)OCH₂CH₃); EI/HRMS: [M + 1]⁺ calcd. for C₂₀H₃₆O₂: 308.2715, found: 308.2728; Elemental analysis calcd. for C₂₀H₃₆O₂: 77.85 C, 11.77 H; found: 78.00 C, 11.70 H.

Ethyl-2-(9-decenyl)-dodec-11-en-oate (5d). Synthesized as above. Crude ester (**5d**) was distilled with a boiling point of 170-171 °C at 1 mm Hg. Yield of **5d**: 87.2% (Crude), 56.4% (Isolated). The following spectral properties were observed: ¹H NMR (CDCl₃): δ (ppm) 1.33 (m, br, 29H), 1.58 (m, br, 2H), 2.02 (q, 4H), 2.27 (m, 1H), 4.13 (q, 2H, -C(O)OCH₂CH₃), 4.96 (m, 4H, vinyl CH₂), 5.79 (m, 2H, vinyl CH); ¹³C NMR (CDCl₃): δ (ppm) 14.37, 27.44, 28.94, 29.13, 29.43, 29.55, 32.54, 33.83, 45.78, 59.92 (-C(O)OCH₂CH₃), 114.13 (vinyl CH₂), 139.19 (vinyl CH), 176.62 (-C(O)OCH₂CH₃);

EI/HRMS: $[M + 1]^+$ calcd. for $C_{24}H_{44}O_2$: 365.3419, found: 365.3397; Elemental analysis calcd. for $C_{24}H_{44}O_2$: 79.05 C, 12.17 H; found: 79.11 C, 12.05 H.

Ethyl-2-(10-deceny)-tridec-12-en-oate (5e). Synthesized as above. Crude ester (5e) was distilled with a boiling point of 90-91 °C at 0.03 mm Hg. Yield of 5e: 85.9% (Crude), 77.5% (Isolated). The following spectral properties were observed: 1H NMR ($CDCl_3$): δ (ppm) 1.37 (m, br, 33H), 1.59 (m, br, 2H), 2.03 (q, 4H), 2.28 (m, 1H), 4.13 (q, 2H, $-C(O)OCH_2CH_3$), 4.96 (m, 4H, vinyl CH_2), 5.81 (m, 2H, vinyl CH); ^{13}C NMR ($CDCl_3$): δ (ppm) 14.37, 25.01, 27.47, 28.97, 29.17, 29.29, 29.51, 29.55, 32.57, 33.85, 45.81, 59.92 ($-C(O)OCH_2CH_3$), 114.13 (vinyl CH_2), 139.22 (vinyl CH), 176.63 ($-C(O)OCH_2CH_3$); EI/LRMS: $[M + 1]^+$ calcd. for $C_{26}H_{48}O_2$: 393, found: 393.

2.4.4.3 Step 3 (Ester Reduction to the Alcohol)

2-(4-pentenyl)-hept-6-en-1-ol (6a). An 18.1 g (81 mmol) sample of distilled 5a and 200 mL of dry ether were combined in a flame dried, Ar purged three-neck 500 mL round bottom flask equipped with a stir bar and condenser. This mixture was then cooled to 0 °C and stirred for 30 min. To this stirring, cooled solution was added 61 mL (3 eq. of hydride) of 1.0M lithium aluminum hydride (LAH) in Et_2O over a period of 5-10 min. Bubbling was observed during addition. The reaction was allowed to come to room temperature and stirred for a period of 6-12 h. After transferring to a beaker, DI H_2O was added (Caution: dropwise initially) with stirring to quench the reaction. Upon formation of a gel-like solution that hinders stirring, 3N HCl was added to complete the quenching, dissolving all precipitated salts. The reaction mixture was extracted three times with Et_2O , washed with DI H_2O , and dried over $MgSO_4$. The combined organic extracts were filtered and evaporated under reduced pressure. The product was then placed over CaH_2 ,

stirred overnight, and distilled under reduced pressure using a vigreux column ($<10^{-1}$ mm Hg). Crude alcohol (**6a**) was distilled with a boiling point of 97-98 °C at 2.2 mm Hg. Yield of alcohol **6a**: 99.8% (Crude), 58.9% (Isolated). The following spectral properties were observed: ^1H NMR (CDCl_3): δ (ppm) 1.38 (m, br, 9H), 1.74 (s, 1H, $-\text{CH}_2\text{OH}$), 2.04 (q, 4H), 3.53 (d, 2H, $-\text{CH}_2\text{OH}$), 4.98 (m, 4H, vinyl CH_2), 5.81 (m, 2H, vinyl CH); ^{13}C NMR (CDCl_3): δ (ppm) 26.23, 30.40, 34.16, 40.36, 65.48 ($-\text{CH}_2\text{OH}$), 114.46 (vinyl CH_2), 138.90 (vinyl CH); EI/HRMS: $[\text{M} + 1]^+$ calcd. for $\text{C}_{12}\text{H}_{22}\text{O}$: 183.1749, found: 183.1796; Elemental analysis calcd. for $\text{C}_{12}\text{H}_{22}\text{O}$: 79.05 C, 12.17 H; found: 79.11 C, 12.19 H.

2-(5-hexenyl)-oct-7-en-1-ol (6b). Synthesized as above. Crude alcohol (**6b**) was distilled with a boiling point of 89.5-90.5 °C at 1.5mm Hg. Yield of alcohol **6b**: 93.0% (Crude), 80.2% (Isolated). The following spectral properties were observed: ^1H NMR (CDCl_3): δ (ppm) 1.30 (m, br, 13H), 1.83 (s, 1H, $-\text{CH}_2\text{OH}$), 2.08 (q, 4H), 3.54 (d, 2H, $-\text{CH}_2\text{OH}$), 5.06 (m, 4H, vinyl CH_2), 5.84 (m, 2H, vinyl CH); ^{13}C NMR (CDCl_3): δ (ppm) 26.37, 29.30, 30.89, 33.64, 40.61, 65.71 ($-\text{CH}_2\text{OH}$), 114.20 (vinyl CH_2), 138.96 (vinyl CH); EI/HRMS: $[\text{M} + 1]^+$ calcd. for $\text{C}_{14}\text{H}_{26}\text{O}$: 211.2062, found: 211.2070; Elemental analysis calcd. for $\text{C}_{14}\text{H}_{26}\text{O}$: 79.92 C, 12.47 H; found: 79.90 C, 12.47 H.

2-(7-octenyl)-dec-9-en-1-ol (6c). Synthesized as above. Crude alcohol (**6c**) was distilled with a boiling point of 138-139 °C at 1.2 mm Hg. Yield of alcohol **6c**: 90.2% (Crude), 76.6% (Isolated). The following spectral properties were observed: ^1H NMR (CDCl_3): δ (ppm) 1.31 (m, br, 22H), 2.04 (q, 4H), 3.53 (d, 2H, $-\text{CH}_2\text{OH}$), 4.97 (m, 4H, vinyl CH_2), 5.81 (m, 2H, vinyl CH); ^{13}C NMR (CDCl_3): δ (ppm) 26.88, 28.96, 29.16, 29.95, 30.93, 33.83, 40.54, 65.66 ($-\text{CH}_2\text{OH}$), 114.18 (vinyl CH_2), 139.18 (vinyl CH);

EI/HRMS: $[M + 1]^+$ calcd. for $C_{18}H_{34}O$: 266.2610, found: 266.2629; Elemental analysis calcd. for $C_{18}H_{34}O$: 81.12 C, 12.87 H; found: 81.20 C, 12.91 H.

2-(9-decenyl)-dodec-11-en-1-ol (6d). Synthesized as above. Crude alcohol (**6d**) was distilled with a boiling point of 173-174 °C at 1.0 mm Hg. Yield of alcohol **6d**: 90.8% (Crude), 64.3% (Isolated). The following spectral properties were observed: 1H NMR ($CDCl_3$): δ (ppm) 1.37 (m, br, 30H), 2.04 (q, 4H), 3.52 (d, 2H, $-CH_2OH$), 4.96 (m, 4H, vinyl CH_2), 5.81 (m, 2H, vinyl CH); ^{13}C NMR ($CDCl_3$): δ (ppm) 26.91, 28.96, 29.17, 29.52, 29.61, 30.08, 30.93, 33.85, 40.54, 65.67 ($-CH_2OH$), 114.13 (vinyl CH_2), 139.22 (vinyl CH); EI/HRMS: $[M + 1]^+$ calcd. for $C_{22}H_{42}O$: 323.3314, found: 323.3315; Elemental analysis calcd. for $C_{22}H_{42}O$: 81.91 C, 13.13 H; found: 82.05 C, 13.21 H.

2-(10-undecenyl)-tridec-12-en-1-ol (6e). Synthesized as above. Crude alcohol (**6e**) was then distilled with a boiling point of 205-206 °C at 1.0 mm Hg. Yield of alcohol **6e**: 94.3% (Crude), 60.7% (Isolated). The following spectral properties were observed: 1H NMR ($CDCl_3$): δ (ppm) 1.30 (m, br, 33H), 1.91 (s, 1H, $-CH_2OH$), 2.03 (q, 4H), 3.54 (d, 2H, $-CH_2OH$), 4.96 (m, 4H, vinyl CH_2), 5.81 (m, 2H, vinyl CH); ^{13}C NMR ($CDCl_3$): δ (ppm) 15.25, 26.94, 28.99, 29.20, 29.57, 29.67, 30.14, 30.98, 33.88, 40.57, 65.61 ($-CH_2OH$), 114.13 (vinyl CH_2), 139.21 (vinyl CH); EI/LRMS: $[M + 1]^+$ calcd. for $C_{24}H_{46}O$: 351, found: 351; EI/HRMS: $[M + 1]^+$ calcd. for $C_{24}H_{46}O$: 351.3627, found: 351.3630; Elemental analysis calcd. for $C_{24}H_{46}O$: 82.20 C, 13.23 H; found: 82.15 C, 13.20 H.

2.4.4.4 Step 4 (Tosylation of the Alcohol)

6-*p*-toluenesulfonyl methyl-1,10-undecadiene (7a). In a flame dried and Ar purged 300 mL 3-neck flask equipped with a stir bar, 13.04 g (72 mmol) of distilled **6a** and 100 mL of $CHCl_3$ were added. This solution was cooled to 0 °C followed by the addition of

11.6 mL (11.3 g, 143 mmol) of pyridine. After stirring 20 min., 20.49 g (107 mmol) of *p*-toluenesulfonyl chloride (TsCl) was added with constant stirring. The solution changed from colorless to a yellow-brown hue after the addition. The solution was then allowed to warm to room temperature and stirred 12-24 h. (depending on the size of the diene). The reaction was stopped and washed with 3N HCl to neutralize any excess pyridine and dissolve pyridinium salts. The organic layer was washed with DI H₂O and saturated K₂CO₃ solution in order to remove unreacted tosyl chloride. The aqueous layers were extracted three times by CHCl₃, washed with DI H₂O, and combined with the original organic layer. The organic layer was dried with MgSO₄, filtered, and evaporated under reduced pressure to yield the crude tosylate (**7a**). The resulting product was a viscous yellow oil. Attempts to isolate the product were not pursued for fear of elimination of tosic acid. Therefore, yields for this reaction were not calculated. The following spectral properties were observed: ¹H NMR (CDCl₃): δ (ppm) 1.26 (m, br, 9H), 1.95 (d, br, 4H), 2.43 (s, 3H, methyl), 3.90 (d, 2H, -CH₂OTs), 4.94 (m, 4H, vinyl CH₂), 5.72 (m, 2H, vinyl CH), 7.33 (dd, 2H), 7.77 (dd, 2H); ¹³C NMR (CDCl₃): δ (ppm) 21.63, 25.70, 33.79, 37.41, 72.59 (-CH₂OTs), 114.62 (vinyl CH₂), 127.02, 127.90, 129.84, 130.27, 138.45 (vinyl CH), 144.67; EI/LRMS: [M]⁺ cald. for C₁₉H₂₈SO₃: 336, found: 336.

7-*p*-toluenesulfonyl methyl-1,12-tridecadiene (7b). Synthesized as above. The following spectral properties were observed: ¹H NMR (CDCl₃): δ (ppm) 1.25 (m, br, 13H), 1.98 (q, 4H), 2.47 (s, 3H, methyl), 3.91 (d, 2H, -CH₂OTs), 4.95 (m, 4H, vinyl CH₂), 5.76 (m, 2H, vinyl CH), 7.37 (dd, 2H), 7.85 (dd, 2H); ¹³C NMR (CDCl₃): δ (ppm) 14.71, 21.61, 25.91, 28.97, 30.40, 33.60, 37.56, 72.68 (-CH₂OTs), 114.47 (vinyl

CH₂), 127.05, 127.93, 129.80, 130.25, 133.12, 138.77 (vinyl CH), 144.66; EI/LRMS: [M]⁺ calcd. for C₂₁H₃₂SO₃: 364, found: 364.

9-*p*-toluenesulfonyl methyl-1,16-heptadecadiene (7c). Synthesized as above. The following spectral properties were observed: ¹H NMR (CDCl₃): δ (ppm) 1.26 (m, br, 21H), 2.02 (q, 4H), 2.45 (s, 3H, methyl), 3.91 (d, 2H, -CH₂OTs), 4.97 (m, 4H, vinyl CH₂), 5.78 (m, 2H, vinyl CH), 7.37 (dd, 2H), 7.79 (dd, 2H); ¹³C NMR (CDCl₃): δ (ppm) 21.63, 26.42, 28.88, 29.02, 29.64, 30.60, 33.79, 37.61, 72.81 (-CH₂OTs), 114.24 (vinyl CH₂), 127.06, 127.95, 129.80, 130.24, 133.10, 139.09 (vinyl CH), 144.66; EI/LRMS: [M]⁺ calcd. for C₂₅H₄₀SO₃: 420, found: 420.

11-*p*-toluenesulfonyl methyl-1,20-uneicosadiene (7d). Synthesized as above. The following spectral properties were observed: ¹H NMR (CDCl₃): δ (ppm) 1.24 (m, br, 29H), 2.04 (q, 4H), 2.47 (s, 3H, methyl), 3.91 (d, 2H, -CH₂OTs), 4.97 (m, 4H, vinyl CH₂), 5.83 (m, 2H, vinyl CH), 7.34 (dd, 2H), 7.79 (dd, 2H); ¹³C NMR (CDCl₃): not obtained; EI/LRMS: [M]⁺ calcd. for C₂₉H₄₈SO₃: 476, found: 476.

12-*p*-toluenesulfonyl methyl-1,22-trieicosadiene (7e). Synthesized as above. The following spectral properties were observed: ¹H NMR (CDCl₃): δ (ppm) 1.26 (m, br, 33H), 2.04 (q, 4H), 2.44 (s, 3H, methyl), 3.91 (d, 2H, -CH₂OTs), 4.96 (m, 4H, vinyl CH₂), 5.81 (m, 2H, vinyl CH), 7.37 (dd, 2H), 7.86 (dd, 2H); ¹³C NMR (CDCl₃): not obtained; EI/LRMS: [M + 1]⁺ calcd. for C₃₁H₅₂SO₃: 504, found: 504.

2.4.4.5 Step 5 (Reduction of the Tosylate to Yield the Methyl Branch).

6-methyl-1,10-undecadiene (1a). In a flame dried and Ar purged 500 mL 3-neck flask equipped with a stirbar, 20.50 g (61 mmol) of crude **7a** and 200 mL of anhydrous Et₂O were added. This mixture was then cooled to 0 °C and stirred for 30 min. To this

stirring, cooled solution, 91 mL (6 eq. of hydride) of 1.0M LAH in Et₂O was added slowly over a period of 15-20 min; bubbling was observed during the addition. The reaction was brought to reflux for a period of 24-36 h, cooled, and quenched with DI H₂O (Caution: dropwise initially). Upon formation of a viscous gel, 3N HCl was used to complete quenching, dissolving all precipitated salts. The reaction mixture was extracted three times with Et₂O, washed with DI H₂O, and dried over MgSO₄. Finally, the combined organic extracts were filtered and evaporated under reduced pressure. The crude monomer was distilled before performing flash column chromatography or HPLC (see Section 2.4.1). The crude monomer was placed over CaH₂, stirred overnight, and distilled by vigreux distillation apparatus (3 mm Hg). Crude monomer **1a** was distilled with a boiling point of 55-60 °C at 3.4 mm Hg. Yield of monomer **1a** (based on two steps from the isolated alcohol): 97.3% (Crude), 43.4% (Isolated). The following spectral properties were observed: ¹H NMR (CDCl₃): δ (ppm) 0.86 (d, 3H, methyl), 1.13 (m, 2H), 1.36 (m, br, 7H), 2.04 (q, 4H), 4.97 (m, 4H, vinyl CH₂), 5.81 (m, 2H, vinyl CH); ¹³C NMR (CDCl₃): δ (ppm) 19.66, 26.44, 32.59, 34.16, 36.53, 114.18 (vinyl CH₂), 139.22 (vinyl CH); EI/HRMS: [M]⁺ calcd. for C₁₂H₂₂: 166.1722, found: 166.1740; Elemental analysis calcd. for C₁₂H₂₂: 86.66 C, 13.34 H; found: 86.70 C, 13.30 H.

7-methyl-1,12-tridecadiene (1b). Crude monomer **1b** was distilled with a boiling point of 77-78 °C at 1.2 mm Hg. Yield of monomer **1b** (based on two steps from the isolated alcohol): 76.7% (Crude), 36.0% (Isolated). Synthesized as above. The following spectral properties were observed: ¹H NMR (CDCl₃): δ (ppm) 0.83 (d, 3H, methyl), 1.20 (m, 13H), 2.04 (q, 4H), 4.96 (m, 4H, vinyl CH₂), 5.80 (m, 2H, vinyl CH); ¹³C NMR (CDCl₃): δ (ppm) 19.70, 26.59, 29.32, 32.72, 33.89, 36.91, 114.15 (vinyl

CH_2), 139.22 (vinyl CH); EI/HRMS: $[\text{M}]^+$ calcd. for $\text{C}_{14}\text{H}_{26}$: 194.2035, found: 194.2019; Elemental analysis calcd. for $\text{C}_{14}\text{H}_{26}$: 86.51 C, 13.49 H; found: 86.70 C, 13.39 H.

9-methyl-1,16-heptadecadiene (1c). Crude monomer (**1c**) was distilled with a boiling point of 115-116 °C at 1.2 mm Hg. Yield of monomer **1c** (based on two steps from the isolated alcohol): 89.5% (Crude), 61.1% (Isolated). Synthesized as above. The following spectral properties were observed: ^1H NMR (CDCl_3): δ (ppm) 0.83 (d, 3H, methyl), 1.23 (m, br, 21H), 2.04 (q, 4H), 4.96 (m, 4H, vinyl CH_2), 5.81 (m, 2H, vinyl CH); ^{13}C NMR (CDCl_3): δ (ppm) 19.71, 27.04, 29.01, 29.21, 29.88, 32.80, 33.81, 37.11, 114.07 (vinyl CH_2), 139.21 (vinyl CH); EI/HRMS: $[\text{M}]^+$ calcd. for $\text{C}_{18}\text{H}_{34}$: 250.2661, found: 250.2666; Elemental analysis calcd. for $\text{C}_{18}\text{H}_{34}$: 86.31 C, 13.69 H; found: 86.43 C, 13.63 H.

11-methyl-1,20-uneicosadiene (1d). Crude monomer (**1d**) was distilled with a boiling point of 158-160 °C at 0.5mm Hg. Yield of monomer **1d** (based on two steps from the isolated alcohol): 80.4% (Crude), 57.2% (Isolated). Synthesized as above. The following spectral properties were observed: ^1H NMR (CDCl_3): δ (ppm) 0.83 (d, 3H, methyl), 1.13 (br, 2H), 1.27 (br, 27H), 2.03 (q, 4H), 4.96 (m, 4H, vinyl CH_2), 5.81 (m, 2H, vinyl CH); ^{13}C NMR (CDCl_3): δ (ppm) 19.73, 27.11, 28.99, 29.20, 29.57, 29.70, 30.05, 32.78, 33.86, 37.12, 114.10 (vinyl CH_2), 139.22 (vinyl CH); EI/LRMS: $[\text{M}]^+$ calcd. for $\text{C}_{22}\text{H}_{42}$: 306, found: 306; EI/HRMS: $[\text{M}]^+$ calcd. for $\text{C}_{22}\text{H}_{42}$: 306.3287, found: 306.3295; Elemental analysis calcd. for $\text{C}_{22}\text{H}_{42}$: 86.18 C, 13.82 H; found: 86.16 C, 13.84 H.

12-methyl-1,22-trieicosadiene (1e). Crude monomer (1e) was distilled with a boiling point of 170-172 °C at 0.5 mm Hg. Yield of monomer 1e (based on two steps from the isolated alcohol): 89.7% (Crude), 47.8% (Isolated). Synthesized as above. The following spectral properties were observed: ^1H NMR (CDCl_3): δ (ppm) 0.83 (d, 3H, methyl), 1.13 (br, 2H), 1.26 (br, 31H), 2.03 (q, 4H), 4.96 (m, 4H, vinyl CH_2), 5.81 (m, 2H, vinyl CH); ^{13}C NMR (CDCl_3): δ (ppm) 19.73, 27.12, 28.99, 29.20, 29.57, 29.67, 29.75, 30.07, 32.77, 33.86, 37.12, 114.09 (vinyl CH_2), 139.22 (vinyl CH); EI/HRMS: $[\text{M}]^+$ calcd. for $\text{C}_{24}\text{H}_{46}$: 334.3599, found: 334.3564; Elemental analysis calcd. for $\text{C}_{24}\text{H}_{46}$: 86.13 C, 13.87 H; found: 86.08 C, 13.92 H.

2.4.5 ADMET polymerizations of symmetrical methyl branch monomers 1a-1e.

All glassware was thoroughly cleaned and flame dried under vacuum prior to use. The monomers were degassed and distilled from CaH_2 prior to polymerization. All metathesis reactions were initiated in the bulk, inside an Argon atmosphere glove box. Monomers were placed in 25 or 50 mL round-bottomed flasks equipped with a magnetic TeflonTM stirbar. The flasks were then fitted with an adapter equipped with a TeflonTM vacuum valve. The adapter allows direct attachment to the vacuum line or Schlenk hose (depending on attachment design). Monomer to catalyst ratios typically used were 200-500:1. After addition of catalyst, slow to moderate bubbling of ethylene was observed. The sealed reaction vessel was removed from the drybox and immediately placed on the vacuum line. The reaction vessel was then exposed to intermittent vacuum while stirring in an oil bath at 40-50 °C until the viscosity increases. Generally after 4 h, the polymerization was exposed to full vacuum ($<10^{-1}$ mm Hg) and then high vacuum ($<10^{-3}$ mm Hg) for a period of 48 h at 60 °C. The reaction vessel is then cooled to room

temperature. The unsaturated polymer is hydrogenated using one of two methods (*vide infra*).

2.4.5.1 Polymerization of 6-methyl-1,10-undecadiene (2a)

Monomer **1a** was synthesized as previously described. 1.4g (8.4 mmol) of monomer **1a** was combined with 0.028g (3.41×10^{-5} mol) of Grubbs' benzylidene catalyst. The reaction was not quenched before proceeding to the hydrogenation reaction (246:1). The following spectral properties were obtained for the unsaturated polymer: ^1H NMR (CDCl_3): δ (ppm) 0.84 (d, 3H, methyl), 1.11 (br, 2H), 1.30 (br, 7H), 1.97 (br, 4H), 5.36 (m, br, 2H, internal olefin); ^{13}C NMR (CDCl_3): δ (ppm) 19.69, 27.12, 27.23, 27.53, 32.59, 32.95, 36.58, 36.70, 129.92 (cis olefin), 130.39 (trans olefin). ^{13}C NMR (CDCl_3) integration of cis:trans peaks gives: 23:77. GPC data: $M_n = 22\ 800$; P.D.I. (M_w/M_n) = 2.0.

2.4.5.2 Polymerization of 7-methyl-1,12-tridecadiene (2b)

Monomer **1b** was synthesized as previously described. 1.6g (8.2 mmol) of monomer **1b** was combined with 0.018 g (2.2×10^{-5} mol) of Grubbs' benzylidene catalyst (372:1). The reaction was not quenched before proceeding to the hydrogenation reaction. The following spectral properties were obtained for the unsaturated polymer: ^1H NMR (CDCl_3): δ (ppm) 0.83 (d, 3H, methyl), 1.19 (br, 13H), 1.97 (br, 4H), 5.36 (m, br, 2H, internal olefin); ^{13}C NMR (CDCl_3): δ (ppm) 19.72, 27.08, 29.26, 29.70, 29.81, 29.92, 32.65, 32.75, 37.11, 129.89 (cis olefin), 130.36 (trans olefin). ^{13}C NMR (CDCl_3) integration of cis:trans peaks gives: 25:75. GPC data: $M_n = 8000$; P.D.I. (M_w/M_n) = 1.7.

2.4.5.2 Polymerization of 9-methyl-1,16-heptadecadiene (2c)

Monomer **1c** was synthesized as previously described. 1.3 g (5.0 mmol) of monomer **1c** was combined with 0.021 g (2.6×10^{-5} mol) of Grubbs' benzylidene catalyst (192:1). The reaction was not quenched before proceeding to the hydrogenation reaction. The following spectral properties were obtained for the unsaturated polymer: ^1H NMR (CDCl_3): δ (ppm) 0.84 (d, 3H, methyl), 1.08 (br, 2H), 1.26 (br, 19H), 2.03 (br, 4H), 5.38 (m, br, 2H, internal olefin); ^{13}C NMR (CDCl_3): δ (ppm) 19.72, 27.08, 27.23, 29.26, 29.38, 29.70, 29.81, 29.92, 32.65, 32.75, 37.11, 129.89 (cis olefin), 130.36 (trans olefin). ^{13}C NMR (CDCl_3) integration of cis:trans peaks gives: 26:74. GPC data: $M_n = 15\,700$; P.D.I. (M_w/M_n) = 1.7.

2.4.5.4 Polymerization of 11-methyl-1,20-uneicosadiene (2d)

Monomer **1d** was synthesized as previously described. 2.1 g (6.8 mmol) of monomer **1d** was combined with 0.026 g (3.2×10^{-5} mol) of Grubbs benzylidene catalyst (215:1). The reaction was not quenched before proceeding to the hydrogenation reaction. The following spectral properties were obtained for the unsaturated polymer: ^1H NMR (CDCl_3): δ (ppm) 0.83 (d, 3H, methyl), 1.07 (br, 2H), 1.26 (br, 27H), 2.01 (br, 4H), 5.38 (m, br, 2H, internal olefin); ^{13}C NMR (CDCl_3): δ (ppm) 19.72, 27.11, 27.21, 29.22, 29.34, 29.58, 29.72, 30.05, 32.63, 32.77, 37.12, 129.89 (cis olefin), 130.36 (trans olefin). ^{13}C NMR (CDCl_3) integration of cis:trans peaks gives: 17:83. GPC data: $M_n = 11\,300$; P.D.I. (M_w/M_n) = 1.9.

2.4.5.5 Polymerization of 11-methyl-1,20-uneicosadiene (2ds)

Monomer **1d** was synthesized as previously described. 2.2 g (7.1 mmol) of monomer **1d** was combined with 0.011 g (1.4×10^{-5} mol) of Schrock's catalyst (507:1).

The reaction was quenched by exposing it to the air before proceeding to the hydrogenation reaction. The following spectral properties were obtained for the unsaturated polymer: ^1H NMR (CDCl_3): δ (ppm) 0.83 (d, 3H, methyl), 1.08 (br, 2H), 1.26 (br, 27H), 2.02 (br, 4H), 5.37 (m, br, 2H, internal olefin); ^{13}C NMR (CDCl_3): δ (ppm) 19.72, 27.09, 27.21, 29.21, 29.34, 29.57, 29.72, 30.05, 32.63, 32.76, 37.12, 129.89 (cis olefin), 130.36 (trans olefin). ^{13}C NMR (CDCl_3) integration of cis:trans peaks gives: 21:79. GPC data: $M_n = 78\ 100$; P.D.I. (M_w/M_n) = 1.9.

2.4.4.6 Polymerization of 12-methyl-1,22-trieicosadiene (2e)

Monomer **1e** was synthesized as previously described. 1.6 g (4.8 mmol) of monomer **1e** was combined with 0.028 g (3.4×10^{-5} mol) of Grubbs benzylidene catalyst (141:1). The reaction was not quenched before proceeding to the hydrogenation reaction. The following spectral properties were obtained for the unsaturated polymer: ^1H NMR (CDCl_3): δ (ppm) 0.83 (d, 3H, methyl), 1.08 (br, 2H), 1.26 (br, 31H), 2.02 (br, 4H), 5.37 (m, br, 2H, internal olefin); ^{13}C NMR (CDCl_3): δ (ppm) 19.73, 27.14, 29.22, 29.35, 29.58, 29.70, 29.76, 30.08, 32.65, 32.78, 37.14, 129.90 (cis olefin), 130.36 (trans olefin). ^{13}C NMR (CDCl_3) integration of cis:trans peaks gives: 20:80. GPC data: $M_n = 20\ 200$; P.D.I. (M_w/M_n) = 1.7.

2.4.6 Hydrogenation of polymers 2a-2e. Watson's supported catalyst system.

2.4.6.1 Synthesis and Characterization of 3a.

A supported catalyst system developed by Watson was used to complete the hydrogenation of these systems.^{33,45} Unsaturated polymer **2a** was taken into an argon atmosphere drybox. The tacky, rubbery polymer was removed from its original flask, sliced into smaller pieces, and placed into a high-pressure, glass-walled reactor with a

threaded top and equipped with a disposable magnetic stir bar. The unsaturated polymer and 2.8 g of silica gel were added (amount of silica gel is normally 100 times the weight of catalyst originally used). The three substances were then kneaded, mixed, and formed into a ball-like structure using a spatula. Finally 20 mL of dry toluene was added. The reaction vessel was then sealed with a TeflonTM cap affixed with a high-pressure valve attachment and pressure gauge. The reaction vessel was removed from the drybox, connected to a hydrogen tank, and charged with 125 psi of H₂. The reaction was then stirred and heated at 80-85°C for 48 h, then cooled to room temperature. The hydrogenated polymer **3a** was obtained by filtration of the silica and other particulate matter, and finally evaporation of the reaction solvent under reduced pressure. The polymer was then dried in vacuo (1 mm Hg) overnight. Polymer **3a** was then dissolved in toluene and precipitated into cold CH₃OH. **3a** Yield: 65% (after precipitation). The following spectral properties were obtained for the saturated polymer: ¹H NMR (CDCl₃): δ (ppm) 0.83 (d, 3H, methyl), 1.08 (br, 2H), 1.26 (br, 15H); ¹³C NMR (CDCl₃): δ (ppm) 19.73, 27.11, 29.78, 30.07, 32.77, 37.12. Elemental analysis calcd. for repeat unit (C₁₀H₂₀)_n: 85.62 C, 14.38 H; found: 85.58 C, 14.41 H. GPC data: M_n = 17 500; P.D.I. (M_w/M_n) = 1.7. Initial DSC Results (Samples Not Annealed): T_m(peak) = -12 °C, ΔH_f = 37 J/g. DSC Results (Annealed Samples): T_m(onset) = -18 °C, T_m(peak) = -14 °C, ΔH_f = 28 J/g; T_c(onset) = -22 °C, T_c(peak) = -24 °C, ΔH_f = 25 J/g. Glass Transition Temperature Data: T_g = -44 °C, ΔC_p = 28 J/g°C. Thermogravimetric Analysis (TGA) (onset of wt. loss) = 416.52 °C.

2.4.6.2 Synthesis and Characterization of 3b.

Synthesized as above. **3b** Yield: 69% (after precipitation). The following spectral properties were obtained for the saturated polymer: ^1H NMR (CDCl_3): δ (ppm) 0.83 (d, 3H, methyl), 1.08 (br, 2H), 1.26 (br, 19H); ^{13}C NMR (CDCl_3): δ (ppm) 19.73, 27.12, 29.76, 30.07, 32.77, 37.12. Elemental analysis calcd. for repeat unit $(\text{C}_{12}\text{H}_{24})_n$: 85.62 C, 14.38 H; found: 85.57 C, 14.38 H. GPC data: $M_n = 8500$; P.D.I. (M_w/M_n) = 1.8. Initial DSC Results (Samples Not Annealed): $T_m(\text{peak}) = 14\text{ }^\circ\text{C}$, $\Delta H_f = 51\text{ J/g}$. DSC Results (Annealed Samples): $T_m(\text{onset}) = -3\text{ }^\circ\text{C}$, $T_m(\text{peak}) = 11\text{ }^\circ\text{C}$, $\Delta H_f = 66\text{ J/g}$; $T_c(\text{onset}) = 0\text{ }^\circ\text{C}$, $T_c(\text{peak}) = -2\text{ }^\circ\text{C}$, $\Delta H_f = 63\text{ J/g}$. Glass Transition Temperature Data: $T_g = -44\text{ }^\circ\text{C}$, $\Delta C_p = 28\text{ J/g}^\circ\text{C}$. Thermogravimetric Analysis (TGA) (onset of wt. loss) = $435.27\text{ }^\circ\text{C}$.

2.4.6.3 Synthesis and Characterization of 3c.

Synthesized as above. **3c** Yield: 73% (after precipitation). The following spectral properties were obtained for the saturated polymer: ^1H NMR (CDCl_3): δ (ppm) 0.83 (d, 3H, methyl), 1.07 (br, 2H), 1.29 (br, 27H); ^{13}C NMR (CDCl_3): δ (ppm) 19.75, 27.12, 29.75, 30.08, 32.77, 37.14. Elemental analysis calcd. for repeat unit $(\text{C}_{16}\text{H}_{32})_n$: 85.62 C, 14.38 H; found: 85.43 C, 14.30 H. GPC data: $M_n = 17\ 100$; P.D.I. (M_w/M_n) = 1.7. Initial DSC Results (Samples Not Annealed): $T_m(\text{peak}) = 39\text{ }^\circ\text{C}$, $\Delta H_f = 71\text{ J/g}$. DSC Results (Annealed Samples): $T_m(\text{onset}) = 35\text{ }^\circ\text{C}$, $T_m(\text{peak}) = 39\text{ }^\circ\text{C}$, $\Delta H_f = 82\text{ J/g}$; $T_c(\text{onset}) = 32\text{ }^\circ\text{C}$, $T_c(\text{peak}) = 31\text{ }^\circ\text{C}$, $\Delta H_f = 83\text{ J/g}$. Thermogravimetric Analysis (TGA) (onset of wt. loss) = $447.32\text{ }^\circ\text{C}$.

2.4.6.4 Synthesis and Characterization of 3d.

Synthesized as above. **3d** Yield: 71% (after precipitation). The following spectral properties were obtained for the saturated polymer: ^1H NMR (CDCl_3): δ (ppm) 0.82 (d, 3H, methyl), 1.24 (br, 37H); ^{13}C NMR (CDCl_3): δ (ppm) 19.73, 27.12, 29.73, 30.06, 32.78, 37.13. Elemental analysis calcd. for repeat unit $(\text{C}_{20}\text{H}_{40})_n$: 85.62 C, 14.38 H; found: 85.39 C, 14.38 H. GPC data: $M_n = 17\,400$; P.D.I. (M_w/M_n) = 1.6. Initial DSC Results (Samples Not Annealed): $T_m(\text{peak}) = 57\text{ }^\circ\text{C}$, $\Delta H_f = 107\text{ J/g}$. DSC Results (Annealed Samples): $T_m(\text{onset}) = 53\text{ }^\circ\text{C}$, $T_m(\text{peak}) = 57\text{ }^\circ\text{C}$, $\Delta H_f = 96\text{ J/g}$; $T_c(\text{onset}) = 53\text{ }^\circ\text{C}$, $T_c(\text{peak}) = 51\text{ }^\circ\text{C}$, $\Delta H_f = 99\text{ J/g}$. Thermogravimetric Analysis (TGA) (onset of wt. loss) = $444.64\text{ }^\circ\text{C}$.

2.4.6.5 Synthesis and Characterization of 3e.

Synthesized as above. **3e** Yield: 77% (after precipitation). The following spectral properties were obtained for the saturated polymer: ^1H NMR (CDCl_3): δ (ppm) 0.84 (s, br, 3H, methyl), 1.25 (br, 41H); ^{13}C NMR (CDCl_3): δ (ppm) 19.73, 27.11, 29.73, 30.05, 32.75, 37.11. Elemental analysis calcd. for repeat unit $(\text{C}_{22}\text{H}_{44})_n$: 85.62 C, 14.38 H; found: 85.26 C, 14.32 H. GPC data: $M_n = 17\,500$; P.D.I. (M_w/M_n) = 1.7. Initial DSC Results (Samples Not Annealed): $T_m(\text{peak}) = 63\text{ }^\circ\text{C}$, $\Delta H_f = 100\text{ J/g}$. DSC Results (Annealed Samples): $T_m(\text{onset}) = 57\text{ }^\circ\text{C}$, $T_m(\text{peak}) = 62\text{ }^\circ\text{C}$, $\Delta H_f = 103\text{ J/g}$; $T_c(\text{onset}) = 60\text{ }^\circ\text{C}$, $T_c(\text{peak}) = 56\text{ }^\circ\text{C}$, $\Delta H_f = 102\text{ J/g}$. Glass Transition Temperature Data: $T_g = -42\text{ }^\circ\text{C}$, $\Delta C_p = 27\text{ J/g}^\circ\text{C}$. Thermogravimetric Analysis (TGA) (onset of wt. loss) = $448.35\text{ }^\circ\text{C}$.

2.4.7 Hydrogenation of polymer 2ds. Modified diimide method.

2.4.7.1 Synthesis and Characterization of 3ds.

The procedure given here has been adapted from a modified diimide reaction.^{38b,38c,46} The hydrogenation was performed in a flame dried, Ar purged 100 mL 3-neck round-bottom flask equipped with a reflux condenser and TeflonTM magnetic stirbar. To this vessel was added 400 mg (1.3×10^{-3} mol) of **2ds**, 40 mL of dry *o*-xylene, 608 mg (2.5 eq) of TSH, and 467 mg (or 0.62 mL, 2.5 eq) of TPA. The solution was heated to reflux and maintained for 6 h with vigorous stirring. Gas evolution was observed upon heating. The solution was then cooled to room temperature and an additional 2.5 eq. of TSH and TPA was added. The solution was brought to reflux for an additional 6 hr period and then cooled to room temperature. Finally, the reaction mixture was precipitated directly into cold CH₃OH giving a rubbery white solid. The polymer was placed in a flask under vacuum (1 mm Hg) overnight at 60 °C. The resultant product was cooled and isolated as a hard, milky film. **3ds** Yield: 92% (after precipitation). The following spectral properties were obtained for the saturated polymer: ¹H NMR (CDCl₃): δ (ppm) 0.83 (d, 3H, methyl), 1.24 (br, 37H); ¹³C NMR (CDCl₃): δ (ppm) 19.73, 27.11, 29.73, 30.07, 32.78, 37.12. Elemental analysis calcd. for repeat unit (C₂₀H₄₀)_n: 85.62 C, 14.38 H; found: 85.41 C, 14.26 H. GPC data: $M_n = 72,000$; P.D.I. (M_w/M_n) = 1.9. Initial DSC Results (Samples Not Annealed): $T_m(\text{peak}) = 57$ °C, $\Delta H_f = 84$ J/g. DSC Results (Annealed Samples): $T_m(\text{onset}) = 49$ °C, $T_m(\text{peak}) = 57$ °C, $\Delta H_f = 86$ J/g; $T_c(\text{onset}) = 51$ °C, $T_c(\text{peak}) = 49$ °C, $\Delta H_f = 82$ J/g. Thermogravimetric Analysis (TGA) (onset of wt. loss) = 447.50 °C.

CHAPTER 3

THERMAL BEHAVIOR OF MODEL ETHYLENE/PROPYLENE COPOLYMERS WITH PRECISE METHYL BRANCH PLACEMENT

3.1 Introduction

Polyethylene (PE), the most abundant synthetic macromolecule produced in the world today,⁶⁶ is a polymer which comprises a variety of commercial products such as low density polyethylene (LDPE);²⁵ high density polyethylene (HDPE);^{26,67} linear low density polyethylene (LLDPE);⁶⁸⁻⁷¹ as well as high and ultra high molecular weight polyethylene (HMWPE and UHMWPE).⁷² It is evident that the term polyethylene refers to not just a single structure but to a class of ethylene-based materials exhibiting a wide range of compositions and properties.

Ultimately, the enormous commercial success of this class of polymeric materials can be attributed to two main factors: (1) the raw materials on which these polymers are based are readily available and non-expensive, and (2) excellent opportunities exist for varying the chain macro- and microstructures merely by altering the process/polymerization conditions used to produce the end product. To be sure, the ability to fine-tune a given polymer's structure-property relationship remains an important academic and industrial aspiration. Without a doubt, the introduction of branch points (or defects) along the backbone provides the easiest method by which to modify the final physical properties of ethylene-based polymers.

Various possibilities exist during ethylene polymerization to insert a particular branch (or branches) along the chain stem(s), depending on the type of polymerization

method used. For example, LDPEs, or *high-pressure polyethylenes*, are produced radically under various reaction conditions and naturally contain a high branch content due to radical backbiting (30-60 branches/1000 carbons). On the other hand, HDPEs, or *low-pressure polyethylenes*, made by either Ziegler-Natta (Z-N) or metallocene catalyst systems, are materials containing very low branch contents (1-6 branches/1000 carbons); this lower branch content, when compared to LDPE, is due to both the lower pressures utilized during polymerization as well as the mechanistic differences during propagation (branch content is dependent on catalyst nature and the number of catalyst mistakes in HDPE). Recently, late transition metal catalysis, which also operates by chain-addition chemistry, has been used to create PEs with various architectures (different branch lengths and sequence distributions along the backbone).²⁸

The most facile method to place a branch of known identity along the backbone of PE is found in commercial LLDPE production via Ziegler-Natta⁷³⁻⁷⁹ or metallocene⁸⁰⁻⁹¹ catalysis. LLDPE is produced by the copolymerization of ethylene with a given *alpha*-olefin (i.e. propene, butene, hexene, and octene) to create a polymer with known branch length (methyl, ethyl, butyl, and hexyl branches; respectively). Because the physical properties of PE are heavily influenced by the nature and quantity of branching, considerable research over the last 60 years has been dedicated towards understanding the influence of branching on the final physical properties polyolefins.⁹²⁻⁹⁵

While such factors as mode of polymerization (radical, Z-N, etc.), choice of catalyst, reaction temperature, and molecular weight are important, ***the distribution and the amount of short-chain branching (SCB) content*** are the most influential factors in determining the final materials response for ethylene/ α -olefin copolymers.

Due to chain transfer, the formation of branches along the main chain of the polymer is an uncontrolled event in all of the aforementioned systems. Chain transfer (CT) leads to high molecular weight distributions, heterogeneous comonomer distribution, and unwanted branching, leading to both single-chain (intramolecular) and between-chain (intermolecular) structural variations. This is not to say that chain transfer is unwanted; in fact, CT is exploited industrially to create a library of LLDPEs possessing a plethora of final materials responses, with the branches created in this manner being random in nature. A number of thermal behavior studies concerning randomly branched ethylene/ α -olefin copolymers have attempted to understand how the branch content, size, and incorporation influence a given LLDPE's final physical properties.⁹⁶

Recently, we reported a method to eliminate CT as well as the random nature of branching in ethylene/ α -olefin materials by using the clean polycondensation chemistry offered by acyclic diene metathesis (ADMET).^{20,33,97,98} ADMET creates ethylene/ α -olefin systems with both a homogeneous composition distribution of branches and well-controlled polydispersity (P.D.I. \sim 2.0), which presents an opportunity to investigate the physical properties of ethylene/ α -olefin copolymers with narrow composition distribution. This chemistry facilitates study of the roles SCB and short-chain branching distribution (SCBD) play in the ultimate materials response of ethylene/ α -olefin systems. Most recently, a series of five ethylene/propylene (EP) copolymers was synthesized and studied in which a methyl branch was precisely placed on each and every 9th, 11th, 15th, 19th, and 21st carbon along the backbone of PE (**HP9**, **HP11**, **HP15**, **HP19**, and **HP21**). Here, *HP* is an acronym for *hydrogenated polymer* and the *number* refers to the *n*th

carbon on which the branch is precisely placed.²⁰ A general retro-synthetic scheme for this new class of E/P copolymers is shown below (Figure 3-1).

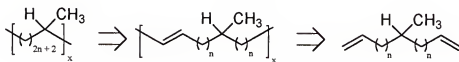


Figure 3-1. Retro-Synthetic Methodology to Produce E/P Model Copolymers via ADMET.

Herein, we examine thermal behavior for these model systems as measured by differential scanning calorimetry (DSC) analysis. In particular, topics addressed include the determination of the degree of mass crystallinity; importance of thermal aging/history; dependence of scan rate on melting and crystallization kinetics; and the estimation of ‘equilibrium’ melting and crystallization temperatures.

3.2 Experimental

3.2.1 Materials

All ADMET model EP copolymers were synthesized as previously described.²⁰ UHMWPE, HDPE, LDPE (Aldrich Chemical Company); and LLDPE (BASF) are used to demonstrate the difference in calorimetric traces for different types of PE. BASF 1800D (ill-defined number of methyl branches/1000 carbons) and BASF 1810H (33 methyls/1000 carbons) are commercial LLDPEs used to compare EP copolymers with statistically branched systems versus the precisely-placed methyl branched materials produced by ADMET.

3.2.2 Differential Scanning Calorimetry (DSC)

3.2.2.1 Initial studies on HP9, HP11, HP15, HP19, and HP21.

DSC analyses were performed using a Perkin-Elmer DSC 7 at a heating rate of 2 °C/min. Thermal calibrations were completed using indium and *p*-nitrotoluene as

standards for both onset melt temperature transitions as well as for heats of fusion. In order to destroy all thermal history, each sample was annealed for 5 h at 50 °C above the peak melting point found in the initial scans. Subsequently, the samples were cooled at 2 °C/min to approximately ten degrees below the onset melt temperature found in initial DSC measurements. Each sample was then annealed at this point for 5 h. The sample was next cooled at 2 °C/min to a point approximately 30 °C below the observed recrystallization temperature, followed by isothermal holding at 30 °C below the crystallization temperature for 5 min. After cooling, the sample was heated at 2 °C/min until reaching approximately 30 °C above the observed melting point, followed by isothermal heating for 5 min. Finally, the samples were scanned for multiple cycles through the same range to verify the results obtained on the first run. Data collection was taken on the first run. The results are listed in graphs or by tabular form within the text. Reported values are given as T_m (peak)(melting, first order transition peak position), T_m (onset), T_c (peak) (recrystallization, first order transition peak position). Glass transition temperatures (T_g 's) were taken in the following manner. Each sample was loaded and annealed for five hours at 50 °C above the observed melting temperature. Next the sample was rapidly quenched to -80 °C (from 50 °C above the melt to -80 °C in approximately 4 seconds) and isothermally held for fifteen minutes. Finally, the sample was heated at 2 °C/minute from -80 °C to 0 °C. Reported values are given as T_g (glass transition)(second order transition) and C_p (heat capacity in J/g °C).³⁷

3.2.2.2 Extended studies on HP9, HP15, HP21.

In order to further probe the thermal behavior of these systems, a detailed study was performed on three polymers in this series comprising the lowest, middle, and highest values for the methylene sequence length (MSL) between branch points. The E/P

model copolymers studied have a methyl branch on every 9th, 15th, and 21st carbons along the backbone.

Calorimetric analyses were again performed using a Perkin-Elmer DSC 7; however, measurements were made more efficient with both an upgrade from UNIX-based to Pyris Software for Windows (Copyright © 1999 Perkin Elmer LLC) as well as through the aid of an attached CCA 7 Controlled Cooling Accessory, thereby, enabling more efficient block heating/cooling. The measuring block and surrounding glove box were flushed with nitrogen (alumina column dried). Helium (alumina column dried) was used as the carrier gas due to the extreme subambient temperatures involved. Thermal calibrations were completed using indium and *n*-octane as standards for onset melting temperature transitions; indium was also used as the enthalpy calibration standard. In order to examine finer detail, sample weights were decreased greatly when compared to initial studies. Typically, weights ranged in the order of 1.40 to 2.50 (+/- 0.01) milligrams. No attempts were made to hot press the samples into thin films prior to the first heating/cooling scan; therefore, exact film thickness in the DSC sample pan was unknown. An empty pan measurement was subtracted from each DSC run. Scans were isothermally held for 1 minute at 60-120 °C below the peak melt found in Section 3.2.2.1. Subsequently, the sample was heated at 20 °C/min to a point 80 °C above the peak melting point and isothermally held for 1 minute. The cooling curve was performed in a similar manner to an endpoint where the sample was isothermally held at 60-120 °C below the peak crystallization temperature for 1 minute. This process was repeated for at least 3 scans with data collection taken on the 3rd scan (not the case for annealing experiments which are collected on the first scan). The scan rate of 20 °C/min was used

as the standard because observed heat flow differences were more dramatic concerning secondary endo/exothermic processes, thermal aging effects, etc. In fact, several scan rates were used and the differences are discussed below.

3.2.2.3 Crystallinity determination.

Degree of crystallinity values were derived on the basis of previous studies completed by Wunderlich.⁹⁹ Typically, olefin-based polymers with high comonomer content produce DSC endotherms that exhibit a flattened, broad characteristic. In fact, sometimes there is no discernable peak melt. This broad melting occurs as a result in the higher population of imperfect crystals; however, this leads to considerably larger deviations in baseline choice when calculating percent crystallinity. This greatly decreases accuracy when attempting calorimetric crystallinity determination for statistically branched materials with high defect contents. However, Mathot and coworkers have developed a second method using heat capacity measurements to obtain extrapolated values for crystallinity in this regard; and should be consulted for those attempting to calculate crystallinities for randomly branched systems.¹⁰⁰⁻¹⁰²

Fortunately, ADMET model systems exhibit sharp, distinct melting and crystallization curves when compared to equivalent counterparts produced by chain chemistry, as previously discussed.²⁰ The following relationship found by Wunderlich⁹⁹ (Eq. 3-1) was employed to calculate crystallinities (w_c) for the E/P copolymer models made via ADMET.

$$w_c = \frac{\Delta h'_f}{\Delta h_f} \quad \text{Equation [3-1]}$$

Where the melting peak area ($\Delta h'_f$) is determined above the baseline in an attempt to exclude the contribution from the heat capacity. This value is then compared to the

heat of fusion for completely crystalline PE (Δh_f). The Δh_f value for completely crystalline PE was found by extrapolation to be approximately 293 J/g (70 cal/g).⁹⁹

3.2.2.4 Scan rate dependence versus melting/crystallization temperature.

The melting behavior of a semicrystalline material is as important as crystallization in understanding the effect a material's structure has on the phase transition process. A material's melting behavior provides clues regarding the structure and characteristics of crystals formed during crystallization.

When consulting thermal behavior literature, scan rate dependence is highly overlooked when making calorimetric measurements. Different scan rates may make small changes in the peak values for endo/exotherms; however, by varying the scan rate, we have also noticed subtle differences in the non-isothermal crystallization and melting processes for the ADMET EP models studied herein. The melting curve for each sample (**HP9**, **HP15**, and **HP21**) was measured at 2 °C/min, 5 °C/min, 10 °C/min, and 20 °C/min. In turn, the cooling curves were obtained in a similar fashion. The peak melting/crystallization values were found at numerous scan rates in order to determine a value for the 'equilibrium melting point', T_m° , and 'equilibrium crystallization point', T_c° , for each polymer. These values become very important when attempting to crystallize these materials from solution.

3.2.2.5 Thermal history.

Thermal history/annealing effects for polyolefin materials have been observed previously,^{88,96h,103-106} but the exact structural changes which lead to perturbations in melting endotherms is still a highly debated topic. Thermal aging studies have been directed towards **HP15** and **HP21**. The thermal history of **HP15** and **HP21** were studied extensively at room temperature as a function of time (unlike preliminary measurements

where all thermal history was erased prior to calorimetric data collection). Measurements were taken at various annealing times ranging from 1-3 hours; 1-2 days; 1 week; and 10-18 months. Interestingly, the pre-melting region was highly affected; but most importantly, the presence of a secondary endotherm was also observed. This bimodal thermal behavior is discussed in further detail later in this text. **HP9** exhibits the same behavior; however, attempts to anneal this system at a controlled temperature for extended periods of time proved extremely difficult since the polymer has a melting point of -14°C .

3.2.2.6 Isothermal crystallization (annealing) time effect.

Nucleation and crystal growth are the initial mechanism by which crystal formation occurs. Annealing of a material describes the changes possible after this initial crystallization process has taken place. In fact, the plastics industry has used the annealing process to not only improve a material's ultimate heat resistance and impact strength but also as a method to decrease/prevent crazing and cracking for items used in extremely stressed applications. Most importantly, annealing has been shown to improve the overall dimensional stability of a polymer by exposure to elevated temperatures.

In this study, annealing of **HP15** and **HP21** was performed at or around the temperature at which the aforementioned secondary endotherm was observed. The effects of isothermal crystallization at various temperatures for times ranging in hours to days were studied. The change in the characteristic melting curve for both systems seems to be maximized after a four to five day period. The results found here are quite interesting and play a key role when obtaining x-ray diffraction data.

Prior to analysis, the samples have been: 1) melted at 50°C above the melt peak for 1 hour in order to destroy previous thermal history 2) annealed isothermally for a

given time period 3) quenched with liquid nitrogen (locking the sample in place) 4) transferred quickly to the DSC, cooled (-50 to -60 °C) and isothermally held for 30 minutes prior to the heating cycle.

3.3 Results and Discussion

3.3.1 Influence of Comonomer Content on Thermal Behavior and Morphology

In polymeric materials, imperfections give rise to changes in a system's overall entropy and enthalpy. As a consequence, calorimetry may be used as a tool to determine the degree of perfection in a crystallized polymer. For polymers, the broad melting peak encountered in differential scanning calorimetry (DSC), is usually attributed to the thickness distribution of crystalline lamellae and to the so-called "partial melting" as a function of heating rate. In the realm of ethylene-based polymers, several differences can be observed when comparing endothermic and exothermic traces not only between linear polyethylenes [high density polyethylene, HDPE and ultra high molecular weight polyethylene, UHMWPE] and branched materials [low density polyethylene, LDPE and linear-low density polyethylene, LLDPE] (Figure 3-2), but also within different kinds of LLDPEs (Figure 3-3).

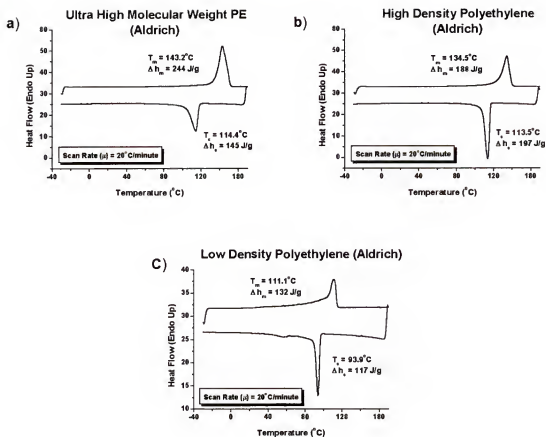


Figure 3-2. DSC trace comparison of (a) UHMWPE, (b) HDPE, and (c) LDPE samples. Polymers purchased from Aldrich Chemical Company. Calorimetry curves generated at the University of Florida.

The most noticeable feature in Figure 3-2 is the small range from onset to peak melting point for UHMWPE and HDPE when compared to LDPE. The LDPE endotherm is very broad compared to the linear polyethylenes (LPEs). After examining the exothermic curve differences, it is apparent that LDPE exhibits a secondary exotherm phenomenon in the 50-62 $^\circ\text{C}$ region. These differences are a consequence of the LDPE's high degree of branch content.

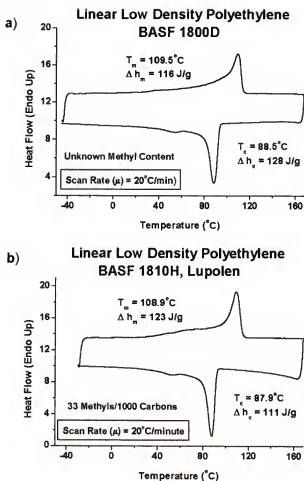


Figure 3-3. DSC trace comparison of (a) **BASF 1800D** and (b) **1810H**. Polymers provided by BASF Chemical Company (Germany). Calorimetry curves generated at the University of Florida.

Figure 3-3 compares two randomly branched EP copolymers from BASF. Both **1800D** and **1810H** show similar melting/crystallization kinetics as the LDPE sample in (Figure 3-2); however, **1810H**'s secondary exotherm is more prevalent, and the formation of a secondary endotherm at 40-78 $^{\circ}\text{C}$ is observed. An expanded-view comparison of multiple melting/crystallization events is provided in Figure 3-4 for LDPE, **1800D**, and **1800H**.

Although the samples contain varying degrees of branching, it is significant that all bare similarities in secondary endotherm/exotherm shape and placement. The secondary thermal events are important to note in relation to the perfection of the crystal and reorganization processes and will be discussed further, *vida infra*.

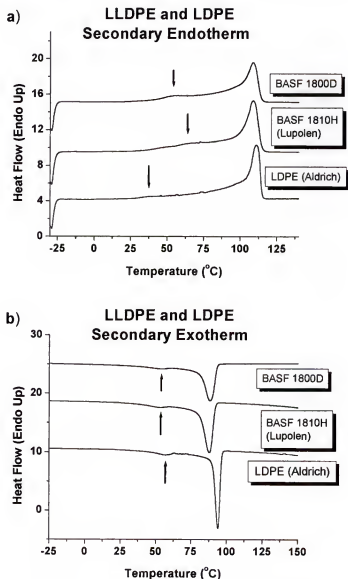


Figure 3-4. Expanded view of multiple a) endotherms and b) exotherms for branched PEs.

Figure 3-4 illustrates that variation in the amount and type of branch content imparts interesting changes in thermal behavior. As previously mentioned, reporting of

melting and structure studies for a number of ethylene/ α -olefin random copolymers has been described⁹²⁻⁹⁶ and reviewed,^{71,107} elsewhere. The calorimetric differences in broadness, lowered transition temperatures, and decreasing peak areas can be explained by the fact that increasing branch (defect) content reduces the capability to crystallize by shortening the average sequence length between crystallizable ethylene units. Consequently, crystallization takes place at progressively lower temperatures, where chain mobility decreases as well. And so, less perfect (smaller) crystallites form during crystallization.

3.3.2 Initial Calorimetry Data for ADMET Model EP Systems with Precise Methyl Branch Placement

Owing to the vast amount of literature concerning randomly branched systems, calorimetry was the first technique employed to examine the morphology and structure-property relationships in these model systems. Typical DSC plots for ADMET EP model compounds with a precise SCBD are illustrated in Figure 3-5, while Table 3-1 presents the information in graphical form as well as newly calculated crystallinities for these materials.

Our previous results verify the fact that with increasing propylene comonomer content (i.e. CH₃/1000 carbons increase), the melting point and heat of fusion decrease. This dependence is well established for polyethylenes and was first explained mathematically by Flory⁵⁵ and later by Sanchez and Eby.¹⁰⁸ The equations derived in each of these studies provide qualitative treatments with regard to how the number (Flory model) and/or chemical nature and number (Eby model) of comonomer units affect a material's melting behavior through the formation of crystal defects.

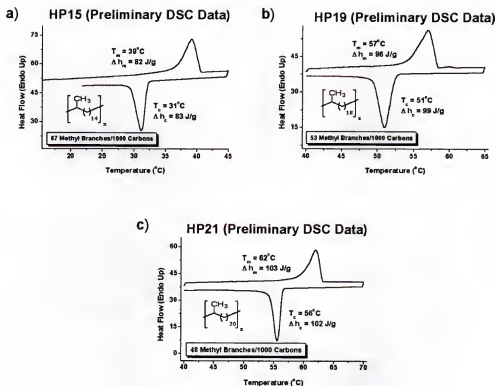


Figure 3-5. Initial DSC traces illustrating melting endotherm and crystallization exotherm for ADMET EP copolymer models with precise branching: a) **HP9** b) **HP15** and c) **HP21**.

Table 3-1. DSC and Crystallinity Data for ADMET EP Copolymer Models with Precise Methyl Branching.

ADMET polymers	methyls per 1000 carbons	T _m (peak) ^a (°C)	Δh _m (J/g)	Crystallinity ^b
HP9	111	-14	28	0.10
HP11	91	11	66	0.23
HP15	67	39	82	0.28
HP19	53	57	96	0.33
HP21	48	62	103	0.35

^a See Experimental Section 3.2.2 for details. Data obtained from thermally erased samples at scan rate of 2 °C/min. ^b Crystallinity determined by dividing the heat of fusion by 293 J/g.⁹⁹

3.3.3 Extended Thermal Behavior Studies for HP9, HP15, and HP21.

It was decided to further probe thermal transitions for ADMET EP copolymer models with the methyl branch placed on every 9th (**HP9**), 15th (**HP15**), and 21st (**HP21**) carbon along the backbone, thereby, taking 3 samples with the highest, middle, and lowest comonomer content, respectively. Great care has been taken concerning calibration; in accordance to the literature,¹⁰⁹⁻¹¹¹ indium and *n*-octane were used as standards to minimize the error in the relative deviation for onset melt values. In addition, *very low sample weights (approx. 1.40-2.50 mg)* were used to examine the finest detail possible while not sacrificing heat flow signal. The first results obtained in this light are illustrated in Figure 3-6 and Table 3-2.

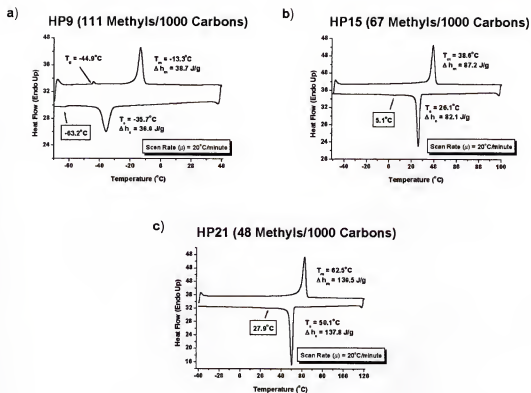


Figure 3-6. Extended DSC analysis for ADMET EP copolymer models with precise methyl branching: a) **HP9** b) **HP15** and c) **HP21**.

Table 3-2. DSC and Percent Crystallinity Data for ADMET E/P Models with Precise Methyl Branching—In Depth Analysis/Comparison.

ADMET polymers	methyls per 1000 carbons	T_m (peak) ^a (°C)	Δh_m (J/g)	Crystallinity ^b
HP9	111	-13.3	38.7	0.132
HP15	67	38.6	87.2	0.298
HP21	48	62.5	140	0.476

^a See Experimental Section 2.2 for details. Data obtained from thermally erased samples at scan rate of 20 °C/min. ^b Crystallinity determined by dividing the heat of fusion by 293 J/g.⁹⁹

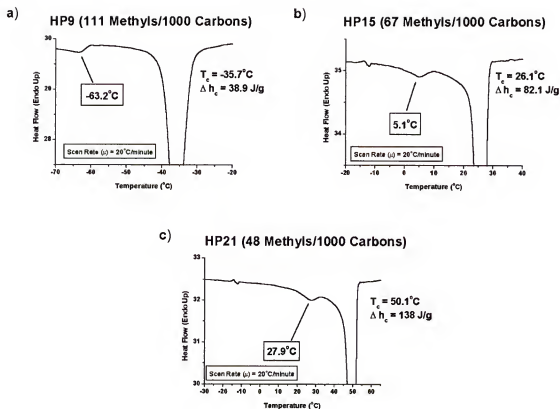


Figure 3-7. Expanded view of secondary exotherm event observed in Figure 3-6.

Distinct differences exist between these samples that are immediately evident—the enthalpy and percent crystallinity values for **HP9**, **HP15**, and **HP21** are higher than the results described earlier.²⁰ By using decreased sample weights (10 fold decrease from initial studies), much lower heat flow differentials are experienced when extrapolating the baseline from the pre-melting onset; therefore, deconvolution between the two is more facile during peak determination using Pyris Software©. This accounts for enthalpy measurement differences; however, additional attention-grabbing features are also manifested.

A secondary exotherm event was found for all three samples (Figure 3-6 and expanded view of 3-6 in Figure 3-7), a well-known phenomenon exhibited in randomly branched LDPE and LLDPE materials (see Figure 3-3 and 3-4). However, this was the

first observed presence of a secondary thermal event exhibited by ADMET model PEs with precise branch content. The secondary exotherm peak temperatures are labeled and indicated with an arrow (Figure 3-6 and 3-7). Immediate attention was focused on this phenomenon to examine if the secondary crystallization event could be exploited during sample preparation/crystallization for x-ray diffraction studies.

Upon closer inspection of Figure 3-7, the temperature difference between the primary and secondary endotherm peaks for **HP9** is 50 °C, while both **HP15** and **HP21** are approximately 35 °C (*notably, the difference in the LDPE, 1800D, and 1800H samples ranges 35-38 °C*). The difference in peak-to-peak variation exhibited by **HP9** may be due to a decreased ability for chain movement to occur when the comonomer content is increased to a given level. Clearly, with 111 methyl branches per 1000 carbons, **HP9's** ability to crystallize should be slowed when compared to **HP15** and **HP21**, owing to the fact that both of these materials contain comparatively lower branch contents. To further understand the nature of multiple thermal events, samples were analyzed at different scan rates and annealed at several temperatures to probe possible thermal behavior differences (See Section 3.4).

The presence of a well-defined melting behavior for **HP9** (111 methyls per 1000 carbons) is quite interesting. Previously, model studies for random systems have shown that lack of regularity in ethylene run lengths impacts the nature of melting transition to create broad, poorly-defined melting transitions;^{92c} and when the level of 150 methyls per 1000 carbons is reached, a completely amorphous polymer is formed (no observed melting event).^{92d,95a} If this same behavior held true for our precisely branched models, then **HP9** should exhibit either an ill-defined endotherm or none at all; however, as

illustrated earlier,²⁰ **HP9**, which contains a relatively high comonomer (defect) content, exhibits a sharp, well-defined melt (Figure 3-6a).

The presence of a visible relaxation event at $-44.9\text{ }^{\circ}\text{C}$ for **HP9** (Figure 3-6a) is also of note here. As previously studied in this group, the value found here verifies the number assigned as the β -relaxation for PE.²⁰ A surprising fact is the mere existence of this peak—previously, even when using a sample weight of 2.43 mg, this feature was not present unless **HP9** was first quenched rapidly from the melt. However, by decreasing sample weight to 1.40 mg, the relaxation appears in every scan of the material (quenching is not necessary) and is repeatable upon several successive scans. Again, the importance of using small sample weights in order to perceive fine detail in semicrystalline polymers is supported with this finding.

3.3.4 Dependence of Melting/Crystallization Temperature on Scan Rate.

Before further discussion of this material, the reader must be cautioned. Throughout the remainder of this chapter, the terms equilibrium, or true, melting point will be employed; however, it is for lack of a better terminology that these designations are used. The equilibrium melting point would be the solid to amorphous phase transition temperature for a sample which is composed of 100% crystallized material of infinitely long, fully extended chains. Therefore, the equilibrium melting point is always higher than that of any measured value. Clearly, with high defect levels, the ADMET EP copolymers examined here cannot have a true equilibrium melting point because a 100% crystalline material can never be achieved. The so-called true melting points presented for **HP9**, **HP15**, and **HP21** are the results of optimized annealing conditions. The attempt has been made to determine the melting points of these samples without the

influence of partial melting and recrystallization, thereby giving a melting transition for the crystalline material which is obtained at a more equilibrated state. Although not at true equilibrium, the melting points extrapolated here are the result of a sample with a distinct thermal history. So, one could say that these extrapolated values represent “pseudo-equilibrium points” of phase transition, but only at these defined conditions. This is the basis for the “true” designation used throughout the remainder of this text.

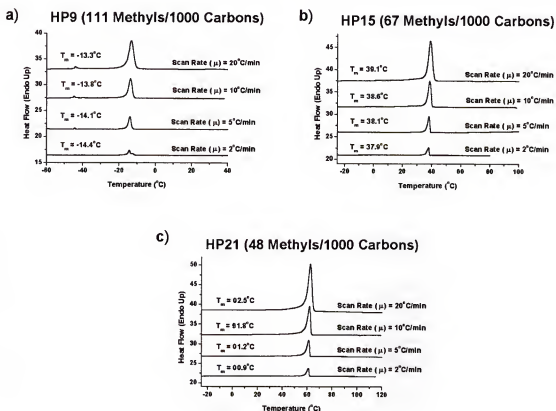


Figure 3-8. DSC melting curves as a function of heating rate.

The scan rate is a major contributing factor in determining the final shape and characteristic temperatures of a melting and/or crystallization peak.¹¹² Due to temperature gradient differences in a sample, the baseline height, peak area, and peak temperature (T_m) all increase with increasing scan rate during the melt process. However, when undergoing crystallization, an increase in the scan rate causes the

baseline height and peak area to increase while the peak crystallization temperature (T_c) decreases. These changes are demonstrated in Figure 3-8, which illustrates DSC melting curves generated at scan rates of 2, 5, 10, and 20 °C/min for **HP9** (3-8a), **HP15** (3-8b), and **HP21** (3-8c).

The peak melting point for all three polymers is dependent on the scan rate, μ , and the most significant value one can extrapolate from this is the true melting point, (T_m^{tr}) of a material.

The melting temperature may be the most important macroscopic quantity to characterize for a flexible, linear molecule. Unfortunately, it is one of the most difficult measurements to accurately obtain.

The T_m^{tr} has been determined by zero extrapolation of the plot for melting point versus the square root of the scan rate for **HP9**, **HP15**, and **HP21** (Figure 3-9). Additionally, to aid in crystallization studies, the true crystallization point, T_c^{tr} , may be found in a similar manner and has been extrapolated for all three polymers (Figure 3-10).

As indicated by the high R^2 values given in Figures 3-9 and 3-10, there is a high confidence level in data accuracy. Prior to undertaking this study, it was believed that performing this analysis for one of the polymers would suffice. Since all of the materials were related, it was envisioned that the slope obtained from one plot could be applied to all in order to derive the equilibrium values for melting and crystallization. Of the three possible materials, **HP15** (67 methyls/1000 carbons) was chosen because it possessed a median methyl branch content when compared to **HP9** (111 methyls/1000 carbons) and **HP21** (48 methyls/1000 carbons). After the T_m^{tr} and T_c^{tr} results for **HP15** were found by measuring the thermal transitions at five different scan rates, **HP9** and **HP21** peak

melting/crystallization points were to be analyzed at a single scan rate (2 or 5 °C/minute). Then, by using peak T_m/T_c values and the slope from **HP15**, a simple calculation would determine the T_m^{tr} and T_c^{tr} for **HP9** and **HP21**.

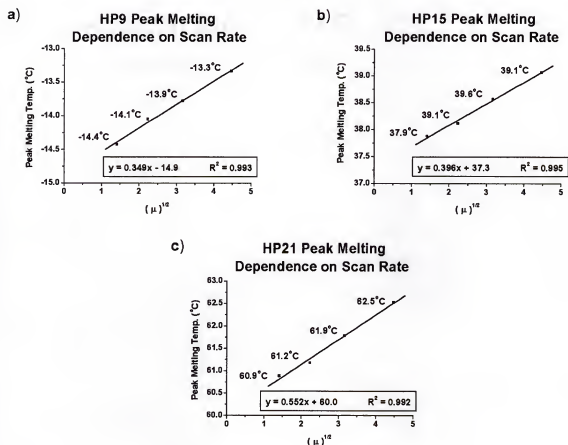


Figure 3-9. Linear regression plot for the influence of scan rate on peak melting temperature.

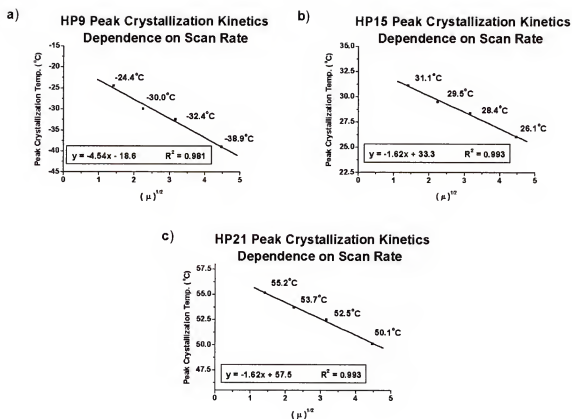


Figure 3-10. Linear regression plot for the influence of scan rate on peak crystallization temperature.

In curiosity, **HP21** was examined for the same series of scan rates to verify our original assumption. Notably, a vast difference in slope was found during extrapolation to find T_m^{tr} (Figure 3-9b vs. 3-9c) but not in T_c^{tr} , which lead to the subsequent individual analysis for all three polymers. Although counter-intuitive to initial prediction, the results can be explained on the basis of relative defect content and the contribution from crystal superheating and/or melt supercooling differences described earlier.

For example, when reviewing the melt process (Figure 3-9a vs 3-9b vs 3-9c), it is clear that the slope increases as the amount of defect content decreases (caused by higher variations in peak melt values in going from low to high scan rate). This is a direct result of an increased occurrence of supercooling/superheating due to the fact that there are

more nuclei available for phase transition initiation in a higher crystalline material (Crystallinity: **HP21>HP15>>HP9**). The effects of this are even more dramatic during the crystallization process in which one observes an approximate three-fold difference in **HP9's** slope when compared to **HP15** and **HP21**.

The question remains—how can **HP9** exhibit a sharp, clearly defined melting peak with such high levels of branching (defects)? This points to the presence of an ordered phase in the semicrystalline material that cannot be explained by simple thermal analysis. An increased branch content restricts crystallite formation to such an extent that the material must compensate both entropically and enthalpically for all of the crowding/bunching that arises when cooling from the melt. This is demonstrated by the large slope differentials observed during scan rate dependence studies (compare Figure 10a to 10b/c). The exact nature of this effect is unclear at this time.

3.3.5 Indication of Multiple Melting Endotherms for HP9.

Before discussing the affect annealing has on these polymers, an unexplained phenomenon occurred during the scan rate dependence studies made on **HP9**. When examining Figure 3-8 more closely, a discrepancy was notice in Figure 3-8a. For reasons that remain unclear, the endothermic process for **HP9** transitions from a monomodal to bimodal process when decreasing the scan rate from 5 to 2 °C/minute (Figure 3-11).

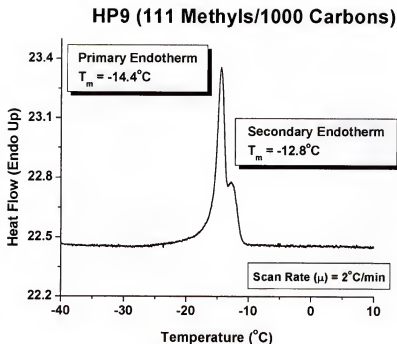


Figure 3-11. Magnified View of Bimodal Melting Process Observed for **HP9**.

A feasible explanation is that the very slow cooling/melting rate has given the material an increased ability to undergo reordering in the interfacial region during the melting—recrystallization—melting (MRM) process. Based on Flory's theory, one would expect that the crystalline domains formed at -12.8°C to have a higher order/perfection when compared to those at -14.4°C . The high branch content in **HP9** does not allow a great deal of freedom for chains (stems) to move, align, or slip in the amorphous and interfacial regions; therefore, the population for the higher melting crystallites is small when compared to the primary peak. No experiments were undertaken to optimize the secondary endotherm's size/position. Currently, experiments are underway to study this phenomenon in greater detail. This finding spurred interest to further investigate the multiple melting/crystallization process for these model materials;

however, the phenomenon of multiple thermal events deserves additional treatment before continuing this discussion.

A metastable state is a constrained system—defined relative to some unconstrained, thermodynamic equilibrium state. As discussed by Keller, it has been demonstrated many times that linear and branched polyethylenes exhibit a high degree of metastability.¹¹³ One must take into account the equilibrium state for PE has been determined to be perfect crystals made up of extended chains of infinite molecular weight. For linear PEs, it has been shown that crystals of this kind are only obtained under special conditions.¹¹⁴⁻¹¹⁶ This means that the crystallization process for polyolefin-based materials is far from ideal. Unless the aforementioned special conditions are met, a thermodynamic equilibrium situation dominates because the growth rate of metastable crystals exceeds that of their stable counterparts. For practical purposes, this means morphology changes are likely to occur during instances where chain mobility is increased (i.e. heating cycle in the DSC). Unfortunately, little is known about the metastable phenomenon. And until the recent development of high intensity synchrotron x-ray sources, a technology able to make time-resolved, dynamic measurements did not exist that could adequately examine the rapid reorganization processes encountered during heating/cooling cycles. Nevertheless, metastability in polyolefins is a real phenomenon and may possibly explain the existence of multiple endotherms/exotherms.

Multiple melting endotherms are observed in a wide variety of semicrystalline polymers. This behavior has been attributed to the following:

- 1) Melting of different polymorphic forms (in polypropylene, PP, this implies α , β , γ , and mesomorphic forms).
- 2) Segregation effects (by tacticity, composition, and molecular weight).

- 3) Reorganization effects (melting—recrystallization—melting) during the course of heating.
- 4) Melting of discrete morphological populations of the same crystallographic form, but differing in size and perfection.

Because crystallinity, crystallization, and melting behavior are all closely related to intrinsic polymer characteristics, they are important methods for studying chain structure. Consequently, understanding the mechanisms involved in multiple melting behavior is an important but challenging task.

3.3.6 Annealing Behavior

In a sense, one broad definition of annealing implies the introduction of a certain property by heat treatment, mechanical deformation, and/or chemical reaction without large-scale melting. In the case of semicrystalline polymers, the thermal history of annealing affects both the width and positions of endothermic transitions. According to one of the earliest theories of chain-folded crystallization made famous by Hoffman and Lauritzen,¹¹⁷ subjecting a sample to a given annealing temperature (T_A) should induce the melting of imperfect, thin lamellae crystals, thereby, allowing the growth of thicker PE lamellae through recrystallization and/or reorganization mechanisms of polymer chains. To prepare for x-ray diffraction studies of ADMET EP copolymer models with precise methyl branching, an investigation was undertaken in the hopes of maximizing crystallite perfection.

Owing to **HP9's** low melting point (approx. -14 °C), lengthy annealing studies on this material have not been attempted to date. The difficulty arises during transfer of the material from an isothermal bath to the DSC. Due to the fact that modern calorimetry instruments require a sample pan to be loaded at room temperature, there is no way to

ensure that **HP9** would not undergo melting during transfer to the DSC from an isothermal bath at low temperature, regardless if the sample is quenched prior to analysis. This would partially or completely destroy any annealing effects incurred at extremely low sub-ambient values. When compared to **HP9**, the same concerns do not apply here for **HP15** and **HP21** because their melting regions are above the load temperature of 25 °C.

Therefore, this study has concentrated on **HP15** and **HP21**—two samples that melt far enough above room temperature to allow for facile transfer and handling in the desired temperature range. To begin thermal aging studies, room temperature was chosen as the first annealing temperature to examine the ultimate endothermic effect for both **HP15** and **HP21**. All results given in this section are the result of a polymer sample, already encapsulated in an aluminum sample pan, being stored at room temperature, 21-25 °C, for a given time [all aluminum sample pans were placed in vials and stored in a desiccator in order to minimize exposure to outside elements]. Although the annealing temperature is imprecise, the results gained in these experiments gave a basis-set of knowledge with which to begin further studies.

Figure 3-12 depicts changes seen in the melt profile for **HP15** and **HP21** upon standing at room temperature for varying degrees of time. Attention should be focused on all scans in 3-12a and the top three scans in 3-12b—A close-up view for DSC heating cycles is provided in Figures 3-13 and 3-14.

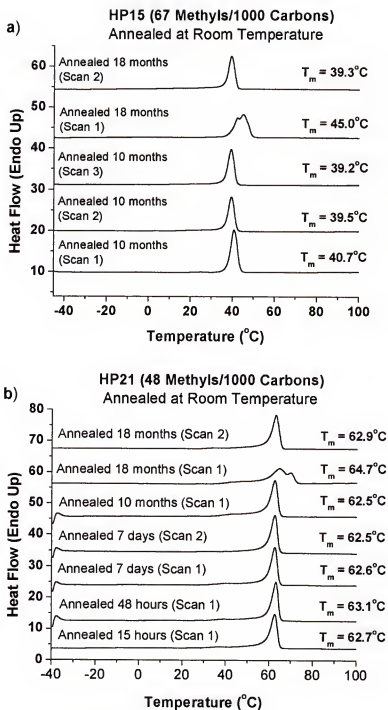


Figure 3-12. Annealing at room temperature for extended time periods—**HP15** (3-12a) vs. **HP21** (3-12b). [All measurements taken at a Scan Rate = 20 °C/minute.]

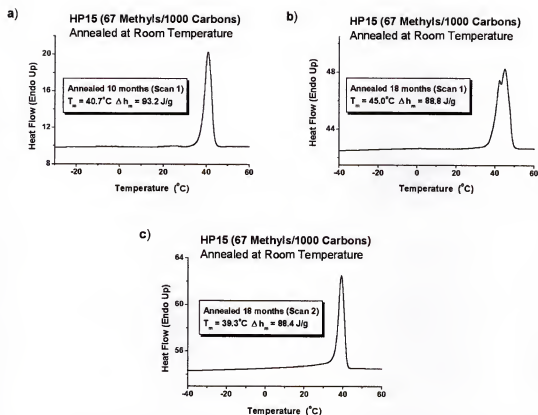


Figure 3-13. Annealing at room temperature for **HP15** at extended time periods—expanded view. [All measurements taken at a Scan Rate = $20^\circ\text{C}/\text{minute}$.]

There are a few features readily apparent upon closer observation. Referencing back to Figure 3-9b (linear regression plot for the influence of scan rate on peak melting temperature), one can find polymer peak melting temperatures for **HP15** and **HP21** after all thermal history has been erased and repeatedly cycled (data collection on the third scan). At a scan rate of $20^\circ\text{C}/\text{minute}$, **HP15's** peak melting point equaled 39.1°C while that for **HP21** equaled 62.5°C . In comparison to samples that have had all thermal history erased, an increase in peak melting point and enthalpy (i.e. crystallinity) for both materials was observed in the first scan after room temperature annealing for extended periods (Table 3-3). In fact, a significant increase in melting point was observed between 10 to 18 months with the added appearance of a bimodal endothermic event. The reason

for this bimodal anomaly is not apparent at this time nor is the drastic jump in melting point during annealing between the 10-18 month period when compared to equivalent measurements made for both materials throughout the course of this study. It is also unclear why the crystallinity (enthalpy) decreased slightly for the **HP15** sample when going from 10 to 18 months. One would expect the same trend as seen for **HP21**, in which the enthalpy remained constant; however, the difference is not alarming and is within experimental error of the DSC.

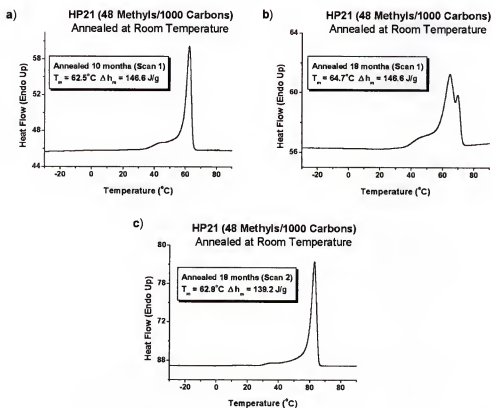


Figure 3-14. Annealing at room temperature for **HP21** at extended time periods—expanded view. [All measurements taken at a Scan Rate = 20 °C/minute.]

Table 3-3. Peak Melting Temperatures and Crystallinity after Annealing at Room Temperature for Extended Time Periods.

ADMET polymers	methyls per 1000 carbons	annealing 10 months T_m (peak) ^a (°C)	TIME 10 months Crystallinity ^b	annealing 18 months T_m (peak) ^a (°C)	TIME 18 months Crystallinity ^b
HP15	67	40.7	0.318	45.0	0.303
HP21	48	62.5	0.500	64.7	0.500

^a See Experimental Section 3.2.2 for details. Data obtained from thermally erased samples at scan rate of 20 °C/min. ^b Crystallinity determined by dividing the heat of fusion by 293 J/g.⁴¹

The increase in melting point illustrated in the Figures 3-12, 3-13, 3-14 and listed in Table 3-3 can be explained by well-known theory. The effect of annealing at room temperature, in this case, has allowed both **HP15** and **HP21** to undergo some degree of stabilization in the crystalline material. This is the cause of the increase in melting point and percent crystallinity when compared to a sample having all thermal history erased. In fact, the Thomson-Gibbs equation correlates a material's melting point as a function of lamellar thickness and heat of fusion.¹¹⁸ This relationship has been used to calculate the lamellar crystal thickness (l_c) for linear PEs as well as ethylene copolymers; however, its validity for copolymers has been questioned. Due to its complexity, a comparison of l_c values determined by both x-ray diffraction and calorimetric methods (**HP15** vs. **HP21**) will be treated in a later publication.

Another important factor to be addressed is the effect further cycling has on these materials after annealing has taken place. Paying attention to the differences in going from Scan 1 to Scan 2 to Scan 3 (Figure 3-12, 3-13, and 3-14), it can be seen that any changes induced by annealing have disappeared by the third consecutive heating cycle of the material. In fact, this erasure consistently happens more quickly for **HP15** (2nd scan)

than for **HP21** (3rd scan) for long annealing times, a result that has been repeated throughout the course of this study. Perhaps, this is a function of relative disorder as **HP15** and **HP21** enter into the melt. It is plausible that a material possessing high branch content would reorganize to minimize intra/intermolecular interactions, thereby lowering the system's free energy. Therefore, it is logical that "unlocking of the morphological memory" induced by annealing would be more quickly/easily disrupted in a system containing a higher number of defects. This may explain why the annealing effect is consistently erased more quickly in the case of **HP15** when compared to **HP21**.

The annealing effect at room temperature was further examined for time periods on the order of hours to one week (Figure 3-15). This illustrates the presence of a secondary endotherm for **HP21** even after 15 hours of annealing; however, the enthalpy does not reach an observed ceiling until day seven. The same peak melting/enthalpy trend was observed for **HP15**, but a secondary endotherm was not present in the material during room temperature annealing. Interestingly, even at the long annealing times (>10 months in Figures 3-12, 3-13, and 3-14), no secondary endotherm was observed for **HP15**. It is thought the close proximity of **HP15's** true melting point ($T_m^{\text{tr}} = 37.3\text{ }^{\circ}\text{C}$) to that of room temperature may lead to this difference.

Nevertheless, the trend for both **HP15** and **HP21** is clear—as annealing time is increased, the melting point and the enthalpy approach maximums. But it must be noted that these values are dependent on the particular temperature at which crystallization/annealing occurred. In other words, variation in annealing temperature should lead to observed differences in values obtained for peak melting point, enthalpy, and crystallinity. In order to work out optimal crystallization conditions, isothermal

annealing was carried out at several different temperatures in the hopes of finding a circumstance that allowed for the maximum crystal thickness to be obtained. The importance of this becomes evident when attempting to obtain x-ray diffraction patterns on melt crystallized material.

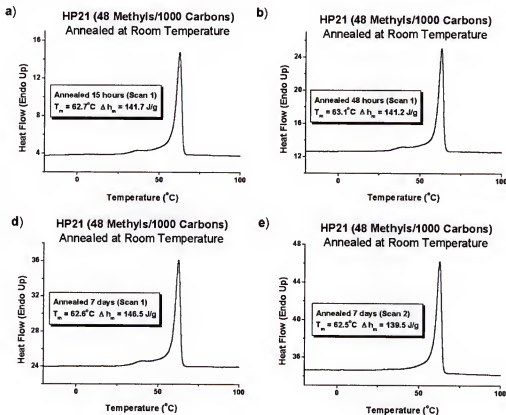


Figure 3-15. Annealing at room temperature for time periods on the order of 1 day to 1 week—HP21. [All measurements taken at a Scan Rate = 20 °C/minute.]

A considerable amount of time and effort went towards finding an annealing temperature that would induce the maximum crystallinity possible. Figure 3-16 illustrates the results for the temperature that ultimately satisfied this requirement for both **HP15** and **HP21**. As depicted in Figures 16a (**HP15**) and 16b (**HP21**), the annealing effect is completely erased after the second scan for **HP15** and the third for **HP21** which

agrees with the results obtained during room temperature annealing experiments. An enlarged view of this result is provided in Figure 3-17.

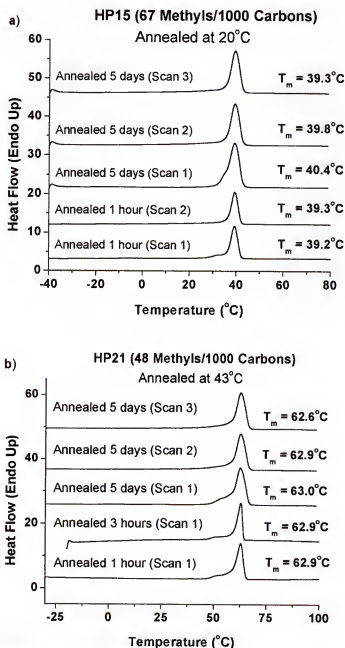


Figure 3-16. Optimizing crystallinity through isothermal annealing: a) **HP15** at 20 °C versus b) **HP21** at 43 °C. [All measurements taken at a Scan Rate = 20 °C/minute.]

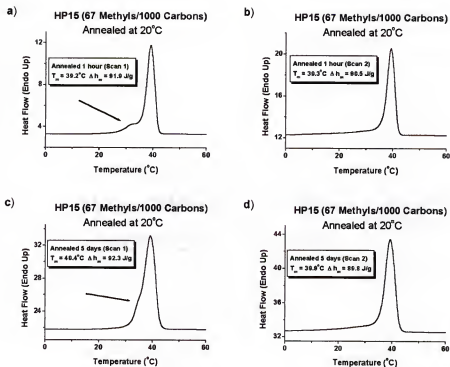


Figure 3-17. Optimizing crystallinity through isothermal annealing—**HP15** at 20 °C. Expanded view. [All measurements taken at a Scan Rate = 20 °C/minute.]

Only upon closer inspection can one really appreciate the differences given in Figure 3-16. Figure 3-17 depicts the effect annealing has on **HP15** at a temperature of 20 °C, while the same effect is provided for **HP21** at 43 °C (Figure 3-18) for several annealing times. An arrow denotes the location of a secondary endotherm when necessary. A few points should be reiterated here: 1) the annealing effect is erased after only the second or third heating cycle for both materials [see Figures 3-17a to 3-17b; 3-17c to 3-17d; 3-18c to 3-18d] 2) crystallite thickening can be monitored due an observed increase in melting point and/or enthalpy values as annealing time is increased [see Figures 3-17a to 3-17c; 3-18a to 3-18b to 3-18c]. Again, this result verifies the theoretical relationship regarding crystal thickening formulated by Thomson and Gibbs.¹¹⁸

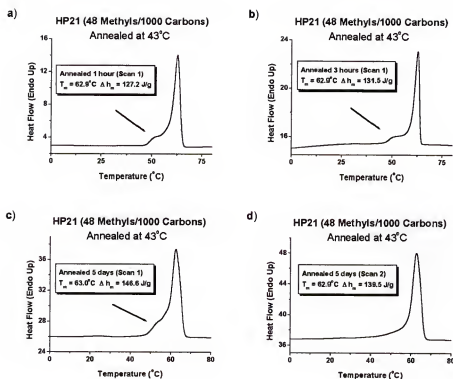


Figure 3-18. Optimizing crystallinity through isothermal annealing. **HP21** at 43 °C. Expanded view. [All measurements taken at a Scan Rate = 20 °C/minute.]

As a consequence of annealing, the premelting region has been changed dramatically—essentially disappearing after the annealing process. This harkens back to the idea that pristine packings of ethylene-based polymers commonly exhibit a high degree of metastability. So, a major conclusion of this discussion is that the ADMET model EP materials studied do not crystallize into an equilibrium structure under normal conditions. Annealing assists these materials to approach a state closer to equilibrium; however, it can be assumed that true equilibrium is far from being realized due to the high degree of metastability present in these branched systems when compared to a perfect PE crystal.

Nonetheless, the annealing process provides a method for a material to minimize non-favorable interactions between defects (branches), thereby, allowing a pathway for a system to achieve a lower free energy. Therefore, it is necessary to study the thermodynamic mechanism of change caused by annealing in order to better understand its impact on a plethora of nearest-neighbor hierarchy effects (bonding interactions, rotational isomerism, tacticity, and close packing).

3.3.7 Importance of Choosing Proper Annealing Condition

This discussion would not be complete without mentioning the variation observed when attempting annealing at three separate temperatures for **HP15**. Attention should be directed at Figure 3-19 (**HP15** annealed at 28 °C) and back to Figures 3-17a (**HP15** annealed at 20 °C) and 3-13a (**HP15** annealed at room temperature). It is true that the melting point and enthalpy increased at all three annealing temperatures which points to evidence for crystal thickening. However, one immediately recognizes that a secondary endotherm was exhibited only when annealing at 20 °C, whether the annealing took place at short or long periods of time. Again, as discussed for **HP21**, perhaps 20 °C annealing does not allow enough molecular motion for the ability of crystal thickening to extend into the preexisting primary crystal structure. The importance of choosing the proper annealing temperature cannot be stressed enough due to the results encountered during x-ray scattering experiments for these materials. For instance, all attempts to obtain suitable small angle x-ray scattering patterns for **HP15** failed for all annealing conditions except for the experiment in which the sample was annealed at 20 °C. In x-ray experiments, why is it so important to find a condition that yields a bimodal melt distribution for these model EP copolymer systems? And better yet, what mechanism leads to this difference?

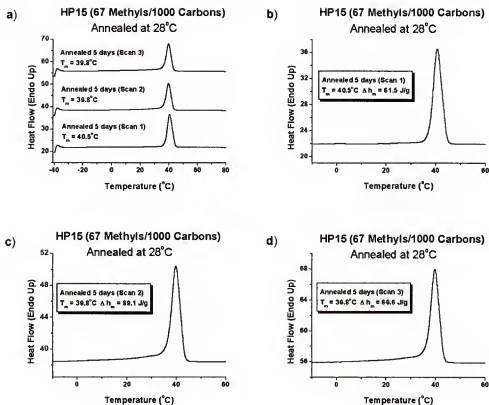


Figure 3-19. Importance of choosing proper annealing temperature—**HP15** annealed at 28 °C for 5 days. [All measurements taken at a Scan Rate = 20 °C/minute.]

The secondary endotherm is evidence for the formation of individual pockets of small crystallites. However, one may argue as to the exact location where crystal thickening has occurred. One plausible explanation for secondary endotherm existence is that homonucleation of stems in the amorphous region has created smaller domains of crystallites than those observed in the primary melting region.⁷³

One should not infer this to mean that the two thermal transitions cause differences in crystal packing—only that the size and location of the crystalline lamellae regions differ for the secondary and primary endotherm, or another possibility is that the entropy has been affected within the amorphous region. Of course, the picture is even more complicated by the question of whether the smaller crystalline regions are made through

the process of intramolecular heterogeneity (a bundling of chains that are tethered to existing crystals by tie-molecules, adjacent re-entry; etc.) or by intermolecular heterogeneity (consisting of several 'free stems/chains' from two or more crystallites that were previously unordered in the amorphous region).

In addition, these materials are not monodisperse, so one cannot exclude the possibility of the secondary endotherm arising from the segregation of material with differing molecular weights. In the hopes of better understanding the annealing phenomenon, x-ray diffraction and microscopy studies were undertaken.

3.4 Conclusions

Previously, thermal behavior studies on statistically branched LLDPE materials proved difficult due to catalyst mistakes made during chain propagation chemistry. For instance, Ziegler-Natta catalysis produces materials that contain high intra/intermolecular chain heterogeneity as well as an increased, and sometimes uncontrolled, polydispersity level. Metallocene systems, although touted for their superior control over polydispersity (P.D.I.s = 2.0) when compared to Ziegler-Natta systems, still produce ethylene/ α -olefin copolymers with intramolecular heterogeneity. Due to several thermal rising elution fractionation (TREF) and crystallization annealing fractionation (CRYTAF) studies,¹¹⁹ it has also been suggested that metallocene systems may also produce a small amount of intermolecular chain heterogeneity as well. Regardless of the method, until now, there has been no systematic way to examine the effect precise branch placement has on ethylene/ α -olefin copolymers. However, EP copolymers produced by ADMET step-condensation chemistry are homogeneous in SCBD both intramolecularly within a chain as well as intermolecularly between chains—the only variation occurring due to the

statistical distribution of chain molecular weights typical of a step condensation process (P.D.I. = 2.0).

For this reason, we feel that these systems provide excellent models to analyze the crystallization and melting behavior of ethylene-based copolymers to aid in determination of morphology and its relation to structure-property relationship. Therefore, a detailed study was performed in order to describe the thermal behavior for three model EP copolymers with methyl branches placed on each and every 9th (**HP9**), 15th (**HP15**), and 21st (**HP21**) carbon along the backbone.

Results have shown that the precisely branched ADMET EP copolymer model systems show a similar trend as statistically branched systems—namely, that as the comonomer (defect) content is increased, there is a resultant decrease in melting point, enthalpy, and crystallinity. Counter to randomly branched copolymers, the precise branch placement in these materials has induced a special order during chain packing that imparts well-defined crystallization and melting events to occur even at elevated defect contents (see results for **HP9**). Also, it has been shown that there is a significant annealing effect exhibited by all three polymers; in particular, this phenomenon has been examined for **HP15** and **HP21**, and later becomes important in obtaining small angle x-ray scattering (SAXS) patterns for these materials.

Annealing has provided a pathway by which to thicken the crystalline lamellae of these materials, and we believe that understanding the dynamic mechanism by which this is occurring in our ADMET EP model systems may provide a better comprehension in regard to LLDPE crystallization behavior exhibited by statistically branched materials—particularly those made by metallocene catalysis.

It has been said that one of the most influential factors governing the melting point (T_m) of an ethylene-based copolymer is the branch distribution in the copolymer system rather than the branch content. In other words, the crystallization, melting behavior, and morphology of said systems can only be understood in terms of the short chain branch distribution (SCBD). By utilizing ADMET chemistry, we have created the first experimental method by which to systematically study the effect a precise SCBD has on a polyolefin-based material. Through the study of these materials it is envisioned that a better understanding will be obtained for industrially produced LLDPE copolymers. In addition, precise branch placement provides an opportunity for increased control over final physical properties of the material; and if the control is robust enough, it may well produce advantages in material response not offered by present industrial chain propagation techniques. Consequently, if an inexpensive, more facile method for monomer synthesis is realized, these materials could well be used as the basis for a new class of commodity PEs.

CHAPTER 4
X-RAY DIFFRACTION AND MICROSCOPY INVESTIGATIONS OF MODEL
ETHYLENE/PROPYLENE COPOLYMERS WITH PRECISE METHYL BRANCH
PLACEMENT

4.1 Structure of Solids—Historical Perspective

A discussion of x-ray diffraction would not be complete without an introduction to the x-ray examination of crystals. In the solid-state, most pure elements and compounds are ordered (crystalline) as opposed to being disordered (amorphous). The central feature of any crystalline structure is that it is regular and repeating, *a priori*. In fact, any crystalline structure could be described as a geometrical pattern formed by various repeating 'structural units' which exhibit long-range order. By treating an element as a point particle, the structural unit of any crystalline compound may be represented by a *unit cell*. A general unit cell is given in Figure 4-1, where the lengths and angles between each crystallographic axis are referred to as lattice constants or lattice parameters. The key feature of a generalized unit cell is that it contains a full description of the structure as a whole; therefore, the repeated stacking of adjacent unit cells in a face-to-face manner throughout three-dimensional space can generate the complete structure.

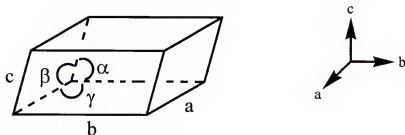


Figure 4-1. Geometry of a generalized unit cell.

Upon consideration, one would assume that the possible crystalline geometries in which individual substances may arrange are endless; however, due largely in part to energetic stability considerations, all possible structures reduce to a small number of basic unit cell geometries. In fact, presently, only 14 three-dimensional (space) lattices have been identified. These are referred to as the 14 Bravais lattices and were first derived by the 19th century French crystallographer, Auguste Bravais (Figure 4-2).¹²⁰

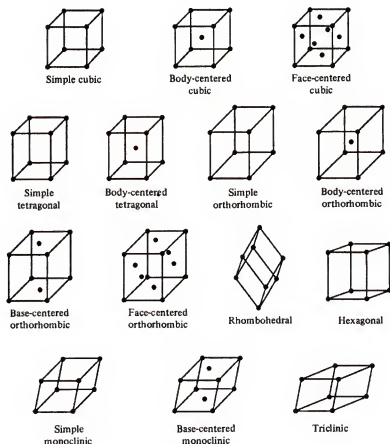


Figure 4-2. The fourteen crystal (Bravais) lattices.

Knowing that a crystal is built up by the repetition of a unit cell, one can explain the development various crystal planes or faces (Figure 4-3). Crystal planes, body-centered cubic in this case, are best described in terms of a set of translations along the x, y, and z axes. These translations are expressed as a set of integers, known as Miller

indices, developed by William Hallows Miller, a 19th century British crystallographer.¹²¹

The general notation for Miller indices is given as whole integer values (h , k , l) and can be used to describe the space planes of any crystal system.

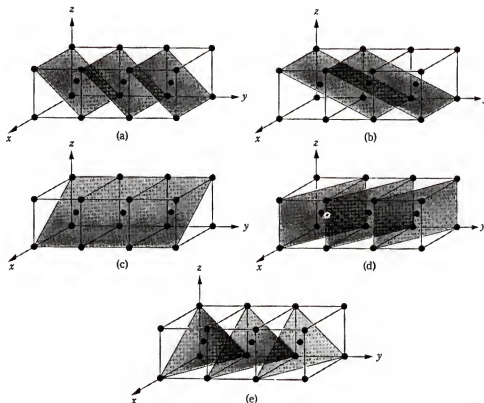


Figure 4-3. Crystallographic planes in the body-centered cubic lattice: (a) (0, 1, 1) planes (b) (0, 2, 1) planes (c) (1, 0, 1) planes (d) (1, 1, 0) planes (e) (1, 1, 1) planes.

However, obtaining Miller indices for a crystallographic plane is a more elaborate process when compared to giving a simple lattice direction. In actuality, these integers represent the inverse of the planes of axial intercepts within the unit cell. For example, the Miller indices (210) corresponds to a plane intercepting the a-axis at $(\frac{1}{2})a$, b-axis at b , and is parallel to the c-axis (in effect, intercepting it at infinity). So, in this example, the inverses of axial intercepts are $1/\frac{1}{2}$, $1/1$, and $1/\text{infinity}$, which gives 2, 1, and 0 integers leading to the (210) notation for a crystal plane. The distance (d) between two parallel

planes and is denoted as $d_{h,k,l}$ with h, k, l representing the Miller indices of a particular crystallographic plane.

4.2 X-ray Diffraction of Crystals

Wilhelm Roentgen first discovered x-rays in 1895.¹²² However, the exact identity of x-rays remained a mystery for some years after their discovery; that is why the term 'x' is still used to this day. It was found that this energy was very penetrating, could darken photographic film, and cause minerals to fluoresce; and since x-ray beam deflection could not be detected by an electric or magnetic field, it was assumed that the beam did not consist of charged particles. This led to the conclusion that x-rays consisted of short-wavelength (much smaller than visible light) electromagnetic radiation.

In 1912, this assumption led to Max von Laue's experiment that verified the wave nature of x-rays.¹²³ Von Laue pointed out that if x-rays have a wavelength, λ , approximately the same as the d spacing between crystallographic planes, then these impinging x-ray waves would exhibit interference effects. Afterwards, it was proven that translational repeat distances within crystals refract when subject to x-ray exposure, just as ordinary light is diffracted by gratings ruled with spacings of the same approximate wavelength as light. Almost immediately afterward, W. H. Bragg¹²⁴ improved on the Laue experiment by substituting monochromatic for polychromatic radiation and by providing a more physical interpretation of scattering data. Following this observation, Bragg was able to determine the structure for a number of simple crystals (i.e. NaCl, ZnS, and CsCl);¹²⁵⁻¹²⁷ and most importantly, he was able to explain the nature of x-ray diffraction by the relation that bears his name (Bragg's Law).¹²⁴ Bragg's law gives the angles that locate the maxima produced by the constructive interference of x-rays. Constructive interference is caused by the scattering of atoms in a parallel set of planes

and is shown as a two-dimensional representation of a three-dimensional crystal in Figure 4-4.

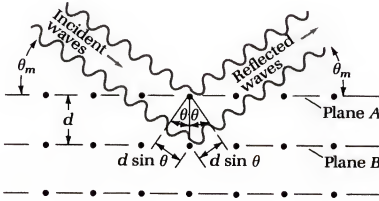


Figure 4-4. Bragg's theory of x-ray constructive interference.

As illustrated here, x-rays of a single wavelength are in phase before being scattered from the atoms in plane A and the atoms in plane B. For constructive interference to be achieved the angle of incidence for incoming x-rays must equal the angle of reflection; otherwise destructive interference ensues. To reach the detector (photographic film or rad counting detector), the waves scattered from the atoms in plane B travel a greater distance than those scattered from the atoms in plane A by the amount $2(d \sin \theta)$. Bragg proved that the angle θ_m is given by the following relation:

$$2d \sin \theta_m = m\lambda \quad [\text{Equation 4-1}]$$

where $m = 1, 2, \dots$ then the waves scattered from the atoms in plane A will arrive at the detector in phase with the waves scattered from the atoms in plane B. Thus, the waves will constructively interfere to produce a maximum—commonly referred to as a reflection. Similarly, the waves reflected on each of the many planes that are parallel to

planes A and B will cause constructive interference of the scattered x-rays. The relationship given in Equation 4-1 may be rewritten as:

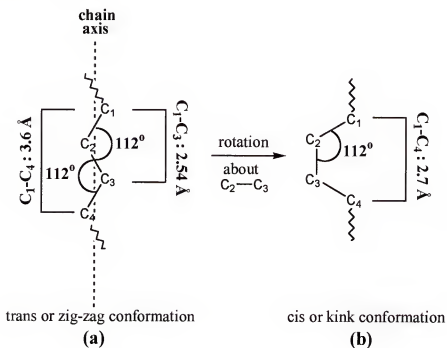
$$d = \frac{m\lambda}{2\sin\theta_m} \quad [\text{Equation 4-2}]$$

Accordingly, the distance, d , in Braggs' law corresponds to any of the numerous interplanar spacings that exist in a crystal. This d value is equivalent to the $d_{h,k,l}$ notation mentioned earlier during the discussion of Miller indices. Therefore, it is possible to designate Miller indices h, k, l for each set of diffracted planes, causing the constructive reflections observed during the examination of a given crystal. This process is known as the indexing of reflections. For metals, salts, ceramics and simple organic/inorganic compounds, deducing the proper lattice and indexing reflections is a rather straightforward process; however, when considering oligomers and/or polymers, the situation becomes highly complex.

4.3 Towards the Structure of Polyethylene—Linear Paraffins

Linear or *normal*-paraffins (n -paraffins) consist of a simple class of structures in the form of $\text{CH}_3\text{—}[\text{CH}_2\text{CH}_2]_n\text{—CH}_3$ (where $n = 1, 2, \dots \sim 34$). These low-molecular weight materials (oligomers) serve as the most simplistic compounds with which to investigate/model the structural differences in large, purely hydrocarbon substances. By far, Alex Müller¹²⁸⁻¹³¹ completed the most prolific structural investigations on n -paraffins. X-ray diffraction of a $n\text{-C}_{29}\text{H}_{60}$ single crystal in the mid-1920s showed that the material packs to form parallel planes of zig-zag (trans) stems of carbon atoms. Planes normal to the axes can be drawn through the end-groups, which separate one layer of molecules from another. Additionally, the structure was shown to be composed of two layers (i.e.

every second layer is translationally identical to one another). Müller determined the unit cell to be orthorhombic (Figure 4-2), a geometry later observed for higher order *n*-paraffins by Hengstenberg,¹³² Kohlhaas and Soremba,¹³³ and Smith.¹³⁴ A plethora of studies concerning *n*-paraffins followed Müller's initial work,¹³⁴⁻¹⁴¹ with the most complete compilation of the phase behavior exhibited by these materials being provided by Schaerer, *et al.*¹⁴²



**All C—C bond distances are 1.54 Å.

Figure 4-5. Bond distances and angles in a completely aliphatic-based chain—(a) all trans (b) occurrence of a cis linkage.

Figure 4-5 illustrates noteworthy differences in bond angles and distances for a purely hydrocarbon-based chain (the H—C—H bond angles have been omitted for simplicity). Previously studied by spectroscopic and thermal methods,^{143,144} this configuration was later verified, with slight modification, by diffraction^{135,136} and modeling studies.¹³⁷ The minimum potential energy is obtained when the carbon atoms

arrange themselves into an all trans configuration (Figure 4-5a). As indicated by the dotted line in Figure 4-5a, the imaginary chain axis passes through the mid-points of C—C bonds. The hydrogen atoms (not shown) lay in planes normal to the main chain axis, with the angles between H—C—H bonds being approximately tetrahedral ($108\text{--}109^\circ$).¹³⁸ Interestingly, diffraction studies elucidated that the C—C—C bond angle to be 112° ,^{135,136} a significant departure from ideal tetrahedral geometry (109.5°). Angular variation between carbons can be ascribed to the energy minimization of non-bonded repulsion interactions between hydrogen atoms.

The cis configuration is also considered (Figure 4-5b); however, it can be seen that the C₁—C₄ distance becomes 2.7 Å. This distance is substantially smaller than that of the C₁—C₄ trans configuration distance of 3.6 Å. Further, non-bonding repulsions between the hydrogen atoms bonded to C₂ and C₃ are severely strained here (Figure 4-5b); therefore, it is clear from this comparison that the trans configuration is the most favorable conformation for a linear hydrocarbon chain, both energetically and sterically.

4.4 Structural Morphology of Linear Polyethylene.

In contrast to small organic molecules and oligomers, polymers offer a distinct advantage during x-ray diffraction studies. If a linear molecule contains 1000 atoms or more, it may be considered infinitely long; therefore, the influences of chain end-to-end packing can be safely ignored. By utilizing this concept, C. W. Bunn published his landmark powder diffraction study that deduced the structure of the simplest synthetic macromolecule known—polyethylene (PE).¹⁴⁵ Bunn found that the PE unit cell was practically identical to that for a single layer of the paraffin molecules studied earlier, save the influence from end-group interactions. Just as Müller had observed for *n*-C₂₉H₆₀, Bunn found an orthorhombic unit cell for PE. By Fourier transformation of the

x-ray data, Bunn was also able to map the electron crystal density for the PE unit cell, giving a method to deduce how the methylene chain stems align in PEs unit cell. In order to provide a technique by which to compare and contrast the unit cell for different materials more easily, Vand introduced the concept of mapping an individual subcell in accordance to the positions of methylene groups.¹⁴⁶ This type of model is given for the *ab* face of orthorhombic PE below (Figure 4-6).

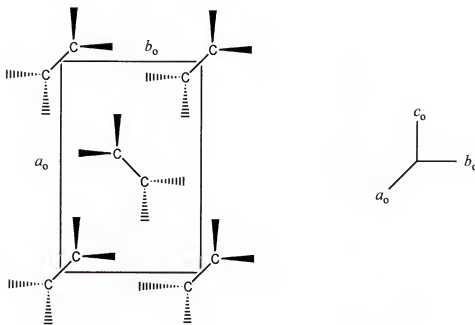


Figure 4-6. PE orthorhombic unit cell (*ab* face shown in plane).

By far, the orthorhombic unit cell presented here is the most commonly encountered for polyethylene, with the main features being that 1) the cell parameters are: $a_0 = 7.45 \text{ \AA}$, $b_0 = 4.97 \text{ \AA}$, and $c_0 = 2.54 \text{ \AA}$ and 2) each cell contains 2 complete ethylene (monomer) units. The c_0 value is the repeat distance for a single plane of aliphatic molecules in an all zig-zag (trans) conformation. In Figure 4-6, the chain axes are normal to the page, and the position of methylenes is shown with each C—H bond designated as a solid black (out-of-plane) or dashed (into-plane) line to indicate three-dimensional

positioning with respect to the plane of the page. The distance between levels is $c_0/2 = 1.27 \text{ \AA}$.

Upon inspection of the unit cell in Figure 4-6, the structure for PE seems quite simple. Indeed, for metals, ceramics, and small organic molecules, knowledge of the unit cell structure implies knowledge of the crystal structure over a large volume. However, the picture for PE, or most commercial polymers for that matter, is much more complicated because these substances contain a high degree of non-crystalline (amorphous) material. So, polymers (i.e. some PEs, nylons, polyester, etc.) exhibiting a melting point are semicrystalline in nature; that is, polymers containing ordered material (crystal) encapsulated in a disordered matrix (amorphous). For a number of years, this fact complicated the deduction of the long-range structure for PE; this was mainly due to the belief that single crystal growth in polymers was improbable.

4.5 Long Range Order in Linear Polyethylene

Early investigations of crystal morphology in high polymers led to the creation of two schools of thought in regard to crystallite formation in macromolecules. The key question to be answered was: what is the fate of a long molecular chain at the surface during crystallization of the material? Sauter first proposed the concept of a polymer being able to form ideally grown single crystals in the early 1930s.¹⁴⁷ Subsequent work by Storks on *gutta percha* [trans-1,4-poly(2-methylbutadiene)] found evidence for orientation in solution crystallized material.¹⁴⁸ He presumed that the orientation was a result of the polymer chain folding back and forth upon itself to create relatively large crystallites ($\sim 270 \text{ \AA}$).¹⁴⁸ Despite these initial findings, the work of Sauter and Stork was overlooked for almost three decades in favor of a concept that supported the formation of

small crystallites because it was believed that construction of a chain-folded single crystal was unlikely due to the deleterious effects caused by molecular entanglement(s).

In 1930, Herrmann, et al. postulated the fringed-micelle crystallization model (Figure 4-7),¹⁴⁹ which proposes that single, chain-extended polymer stems can contribute to several different crystallite and amorphous regions. This crystallization concept was based on x-ray diffraction observations in which the Bragg reflections appeared broad and diffuse when compared to those obtained from well-developed simple crystals. Diffraction theory predicts these broad, diffuse reflections to occur from either small crystallite size or lattice defects. Unfortunately, scattering patterns from polymers are normally too weak to discriminate between the two possibilities. Herrmann assumed that the hypothesis of small crystallite size was the more probable,¹⁴⁹ thus, leading to the fringed-micelle concept. Although the fringed-micelle composite-based structure could explain mechanical property and percent crystallinity trends, it tended to draw attention away from fine structural details (i.e. interface, tie molecules, etc.) and gave little insight to larger structural entities such as helices or spherulites.

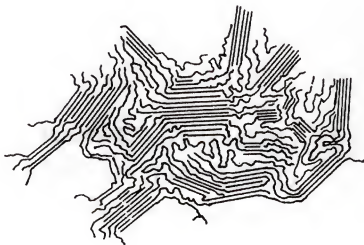


Figure 4-7. Fringed-micelle model for the crystalline-amorphous composite interface found in polymeric materials.

Several groups in the early 1950s showed that it was possible to grow chain-folded single crystals in a polymeric material,¹⁵⁰⁻¹⁵⁴ sparking attention back to the initial studies by Sauter and Stork. Soon thereafter, Keller,¹⁵⁵ Fischer,¹⁵⁶ and Till,¹⁵⁷ independently published the first evidence for the presence of a chain-folded macroconformation in solution-grown single crystals of polyethylene. In these studies, electron diffraction measurements yielded evidence that PE single crystals form into thin platelets (~100 Å in thickness). Although the thickness of the chain-folded lamellae proposed by Keller, Fischer, and Till has been shown to be dependent on both crystallization and and/or annealing treatments,¹⁵⁸ the measure of 100-250 Å is a typical lateral growth dimension for both linear and branched PEs. Several models of chain-folding have been postulated and are given in Figure 4-8, which includes the famous switchboard model proposed by Flory (Figure 4-8b).¹⁵⁹

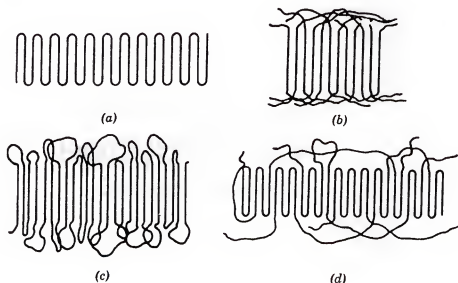


Figure 4-8. Two-dimensional pictorial representation of possible fold surfaces (normal to the plane of the page) in polymer lamellae. (a) sharp folds (b) "switchboard" model (c) adjacent reentry with loose loops (d) combination of features shown in a, b, and c.

Since the lamellae thickness for a PE single crystal was found to be on the order of 100-200 Å and the fact that a typical polymer chain would be at least 1000 Å, Keller contended that the only plausible explanation was for chain folding to occur. This concept is illustrated more clearly in Figure 4-9. This pictorial representation provides an idea of the wave-like pattern created during the growth of a PE single crystal. Also, to further explain the geometrical origins of the orthorhombic unit cell depicted in Figure 4-6, a group of six adjacent PE unit cells have been outlined in Figure 4-9. Most importantly, this model was finally able to explain larger structural observations including spherulites, dendrites, corrugations, and twinning. To be sure, the chain-folded lamellar concept paved the way towards a quantum leap in the theories of polymer crystallization^{117,160,161} and still maintains its stature as a significant influence in the ever-evolving concepts^{117,160-166} surrounding macromolecular crystal growth.

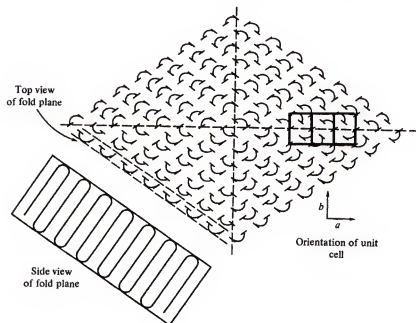


Figure 4-9. Chain-folded lamellae in linear polyethylene—top and side view of the wave-like pattern formed by polymeric stems (on the far right, the arrangement of 6 adjacent orthorhombic unit cells are indicated by the rectangular boxes).

4.6 Wide-Angle X-ray Diffraction (WAXD): Powder Diffraction—The Debye-Scherrer Technique

Obtaining interplanar (d) spacings, using the Bragg equation, has the disadvantage that mounting a single crystal on a precise axis is time consuming. As a consequence, the rotating crystal method is normally used to obtain a diffraction pattern. Another disadvantage is the prerequisite of growing a single crystal of sufficient x-ray quality. It is well known that synthetic polymers can seldom be obtained as macroscopic single crystals, even if they are grown at low supercoolings from highly dilute solutions. For macromolecules, the length and frequently appreciable amount of irregularities (branches, etc.) hinders the attainment of the three-dimensional regularity required for growing macroscopic single crystals.¹⁶⁷

Consequently, the powder method was developed independently by Debye and Scherrer in Germany (1916)¹⁶⁸ and Hull in the United States (1917)¹⁶⁹ in order to gain structural data from a source (polycrystalline powder) other than a single crystal. The method was little used until after the First World War and did not receive marked attention until the advent of the Debye-Scherrer camera based on the design of Buerger (Figure 4-10).¹⁷⁰

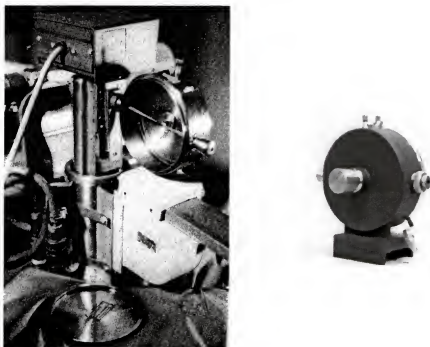


Figure 4-10. Debye-Scherrer powder diffraction camera, [mounted (left); un-mounted, opposite view (right)].

One of the simplest ways of obtaining interplanar spacings is the Debye-Scherrer method. The camera consists of a cylindrical chamber, tight cover, incident beam collimator, beam stop, and a rotatable specimen holder. Detection of x-rays is accomplished by the blackening of a strip of photographic film surrounding the sample (Note: To obtain suitable films, typical exposure times are on the order of 2-6 hours).

The crystalline sample, ground into a powder or cut into a thin sliver, is placed into a thin-walled glass (or quartz) tube and mounted in the middle of the circular chamber. The sample consists of a very large number of tiny crystals that present essentially all the possible angles θ to the incident beam. So, every plane satisfies Bragg's Law and may diffract the beam onto the film. If only one crystal that satisfied the Bragg equation were present, the exposure would only exhibit a small, singular spot, which corresponds to the intersection of the diffracted beam with the film. However, in a powder, many tiny

crystals offer a vast number of possible angles with respect to the beam axis. Thus, for the planes that satisfy Bragg's law, the rotation of one of these tiny crystals about the beam axis will generate a cone of reflection that intersects the nearly planar film in a circle (Figure 4-11). This film is too narrow to encompass the entire circle; therefore, one observes a reflection circle that is placed symmetrically about the beam axis (Figure 4-12).

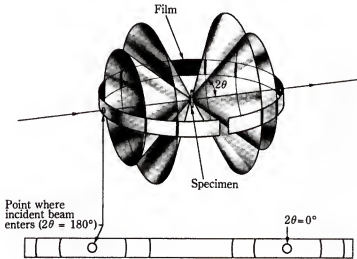


Figure 4-11. Reflected cones generated by the Debye-Scherrer powder method.

The geometry of the camera is set so that the reflected x-ray beam has an angle of 2θ with respect to the incident beam. The incident beam has been diffracted from an arbitrary crystal plane within the sample; thus, the sum of the two halves of a given reflection cone subtend 4θ of angle (Figure 4-12) which gives the relation $[2s/4\theta] = [2\pi/360]$.

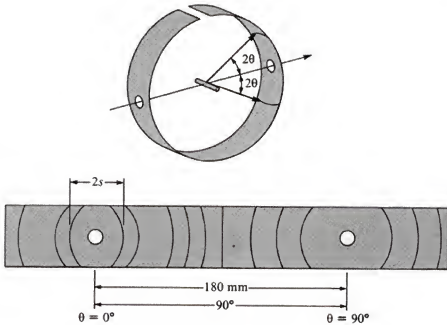


Figure 4-12. Geometry of a Debye-Scherrer Camera and relation to interplanar spacings found on exposed photographic film.

All films presented in this work were generated on a small diameter camera with an internal radius of 57.296 mm ($r = 180/\pi$). This corresponds to 1 degree (40) being equal to a measured distance of 1 mm on the film. Therefore, the three-dimensional spacings for inter-crystalline planes (d values) can be calculated for an exposed film by rewriting Braggs' law as:

$$d = \frac{\lambda}{2 \sin\left(\frac{2s}{4}\right)} \quad [\text{Equation 4-3}]$$

4.7 Small-Angle X-ray Scattering (SAXS)

Unlike WAXD, SAXS is only concerned with scattering at small angles.¹⁷¹ Most importantly, this technique provides structural information in the dimensional range of 10-1000 times greater than that which is obtained by WAXD. So, information obtained by SAXS provides a method to investigate the interactions between stacks of crystalline

lamellae, microfibrils, growth spirals, and any other macromolecular structure able to exhibit long-range regularity. The main requirement for SAXS is that an extremely efficient collimation technique is needed. Unfortunately, this cannot be easily accomplished using the slit collimation technique unless a mathematical procedure known as desmearing is employed;¹⁷² thus, pinhole collimation has become a favored technique.

Pinhole collimation of x-rays is accomplished by passing the beam through a set of sequential pinholes that are separated by defined distances. The advantage of this technique is the avoidance of smearing effects encountered during slit collimation; however, the drawback is that extremely long exposure times are needed in order to compensate for the severe drop in resolution during scattering measurements. Kiessig developed one of the earliest pinhole collimation cameras.¹⁷³

A commercially available Kiessig camera is shown in Figure 4-13. The sample is mounted inside the sample holder (rectangular-shaped box mounted on the triangular base). The collimator, capable of containing several interchangeable pinholes, is the thin metal tube situated between the sample holder and x-ray source (far right). The body of the camera (far left) is capable of being interchanged in order to vary the distance between the sample and the recording film. For this particular camera, distances of 100 mm, 200 mm, and 400 mm are readily accessible. At the beginning of each measurement, the entire camera chamber is evacuated by an oil rotation pump ($\sim 10^{-6}$ to 10^{-8} mm Hg) to avoid parasitic air scattering; without this, the film would blacken due to the long exposure times. Scattering patterns are taken on flat film that has been

previously cut to match the inner diameter of the sample holder's base plate. (Note: Exposure times for this method are generally on the order of 72-100+ hours).

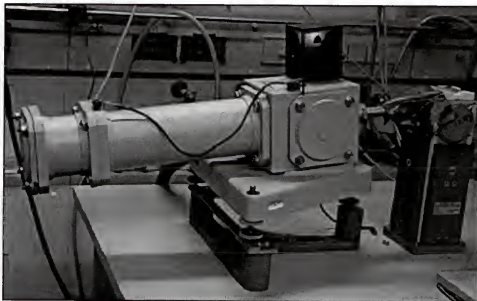


Figure 4-13. Commercially available small-angle x-ray scattering device—Kiessig Camera.

4.8 Three-Dimensional Structure Determination in Polymeric Materials— Additional Techniques

Analysis by x-ray diffraction is probably the most standard and straightforward method used to study a polymer's crystalline structure; however, there are many alternative experimental tools that provide opportunities to elucidate a gambit of structural information for a given material when used in tandem with the aforementioned diffraction techniques. In this light, various methods have been employed: infrared spectroscopy (IR), Raman spectroscopy, solid-state NMR (SSNMR), neutron scattering, scanning electron microscopy (SEM), optical (light) microscopy (OM), and transmission electron microscopy (TEM). Findings for the latter two techniques will be presented and discussed later in this text.

Although both analytical methods are similar in theoretical basis, there are distinct differences between the two. The TEM is similar in design to a conventional optical microscope due to the wave-like nature of the electron. But in TEM, the typical electron beam operates at a constant voltage of 120 keV with a monochromatic wavelength, λ , of 3.7 pm, a value that is *five orders of magnitude lower* than the visible light ($\sim 380\text{-}770$ nm) used in OM. In other words, OM allows practical magnification resolutions of up to 2000 \times (roughly 500 nm), whereas magnifications on the order of 100,000 \times are routinely examined in TEM (resolution < 1 nm is typical in conventional instruments). The result is that TEM allows for the structural examination of substantially smaller details when compared to OM. The utility of the aforementioned techniques during the structural characterization of macromolecular materials cannot be stressed enough; but, a detailed description regarding the theory, use, and limitations for these instruments is not in the scope of the current discussion. However, the reader is referred to several recent texts, and references therein, that provide an adequate treatment concerning the newer techniques and developments used to characterize polymeric materials.¹⁷⁴⁻¹⁸¹

4.9 Introduction—Morphological Studies of EP Copolymers Containing Precise Methyl Branching

A semicrystalline polymer may be considered to be a composite material consisting of an amorphous matrix with dispersed deposits of rigid filler in the form of crystals. However, the picture is slightly more complicated since there are also supermolecular structures to be considered (morphology, crystallinity, entanglements, interfacial region between amorphous and crystalline regions, etc.). Due to its simplicity, linear polyethylene (PE) has been one of the most thoroughly studied materials in attempting to understand the morphology and packing nature exhibited by a

macromolecule.^{96a,107,114,182-185} However, the ability to accurately study the morphology of an ethylene-based material is complicated when branches (defects) are introduced into the backbone.

Industrially, the vast number of structural differences exhibited by ethylene-based materials make them ideal systems for studying the impact small changes in molecular-level architecture have on the polymer's larger-scale structure, and thereby, its final physical properties. In particular, variation in branch content, type, and distribution along the PE backbone provide the most facile methods to vary the physical properties of these materials. The most useful materials to study this phenomenon are prepared by the copolymerization of ethylene with various *alpha*-olefins (1-alkenes) to produce a class of polyethylenes (PEs) known as linear-low density polyethylene (LLDPE).

To date, structural studies concerning branching in LLDPE have focused on how branch type and content influence molecular-level structure,^{71,92c,92d,95a,96a,107,114,182,186-206} while the topic of how the branch sequence length distribution affects the final morphology/physical properties has not been heavily addressed.²⁰⁷⁻²⁰⁹ In large part, the deficiency in obtaining experimental data has been due to synthetic limitations encountered during chain propagation chemistry (i.e. radical backbiting, chain transfer, chain walking, etc.). As a direct consequence of these side reactions as well as differences in reactivity between ethylene and a given 1-alkene, the placement of the branch is a random event. In order to address the question of what the true impact a given branch has on final materials response, a synthetic method was needed to create a series of linear low-density polyethylenes (LLDPEs) in which branch placement occurs

in a precise methylene sequence length distribution (MSLD), thereby, creating a completely homogenous microstructure.

Recently, a method was reported that eliminates chain transfer reactions as well as the random nature of branching in ethylene/ α -olefin materials by using the clean polycondensation chemistry offered by acyclic diene metathesis (ADMET).²⁰ ADMET creates ethylene/ α -olefin systems with both a homogeneous composition distribution of branches and well-controlled polydispersity (P.D.I. ~ 2.0). This presents an opportunity to investigate the physical properties of ethylene/ α -olefin copolymers with narrow composition distribution, attributes that lend well to the modeling of the material responses for classes of LLDPE made by metallocene catalysis. Therefore, ADMET facilitates examination of the influence(s) short chain branching (SCB) and short-chain branching distribution (SCBD) play in the ultimate response of ethylene/ α -olefin materials. Most recently, a series of five ethylene/propylene (EP) copolymers was synthesized and studied in which a methyl branch was precisely placed on each and every 9th, 11th, 15th, 19th, and 21st carbon along the backbone of PE (**HP9**, **HP11**, **HP15**, **HP19**, and **HP21**). Here, *HP* is an acronym for *hydrogenated polymer* and the *9,11,15, etc.* refers to the *n*th carbon on which the branch is precisely placed.²⁰ The general structure for this new class of EP copolymers is shown below (Figure 4-14).



Where:

<u>m</u>	<u>Polymer</u>
8	HP9
10	HP11
14	HP15
18	HP19
20	HP21

Figure 4-14. EP Copolymers possessing precise methyl branch placement.

Herein, we describe the first wide-angle x-ray diffraction (WAXD), small-angle x-ray scattering (SAXS), optical microscopy (OM), transmission electron microscopy (TEM), and electron (e-) diffraction observations made during macromolecular, crystal morphology studies for two of these materials, **HP15** and **HP21**. The most important question to answer here is what effect precise branch placement has had on chain packing? Does the material still allow for methyl branch incorporation both inside the crystalline lamellae as well as within the amorphous region (Model A, Figure 4-15; based on Eby's model¹⁰⁸), or does the precise branch placement lead to deliberate ejection of the methyl branch into the amorphous region (Model B, Figure 4-15; based on Flory's exclusion principle⁵⁵)?

For the two-phase model illustrated in Figure 4-15, ω_a and ω_c represent the amorphous and crystalline regions, respectively. The long period (spacing), d_l , encompasses the combined thickness of the crystalline and amorphous region. It is also worthy to note that the crystalline region, ω_c , is sometimes referred to as L , which is an alternative shorthand used to represent the crystalline core material.

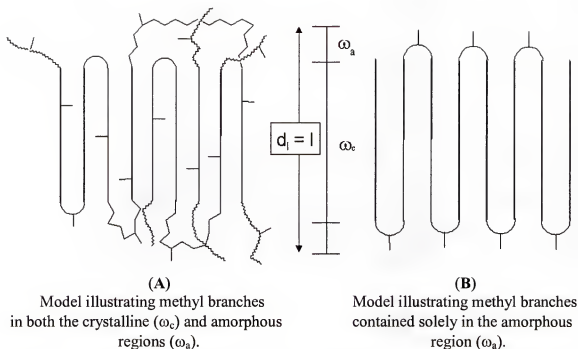


Figure 4-15. 2-Dimensional representation of possible fold surfaces postulated for model ADMET EP copolymers prior to x-ray studies (based on folded-chain lamellae theory for a two-phase model).

Numerous studies on EP copolymer systems containing random methyl branches have pointed to **Model A** (Figure 4-15) as being the correct chain-folding mechanism. Indeed, it is well established that propylene units may be included within the orthorhombic lattice of polyethylene, due to the pioneering work of W. C. Bunn¹⁴⁵ and others that have followed.

Model B depicts a chain-folded surface containing sharp folds. Due to the precise placement of the methyl branch in ADMET EP copolymers, it was postulated that induced folding at the branch point could occur during crystallization of these materials. The main aim of this study is to deduce which structural model best describes the morphology of this new class of EP copolymers.

4.10 Experimental

4.10.1 Materials

Model ethylene-propylene (EP) copolymers (**HP15** and **HP21**) possessing precise methyl branch placement were synthesized as previously described.²⁰ The sample of Lupolen 1810H, possessing a branch content of 33 methyls/1000 carbons, was provided by the BASF Company (BASF AG; Ludwigshafen, Germany).

4.10.2 Differential Scanning Calorimetry (DSC)

Calorimetric analyses were performed using a Perkin-Elmer DSC 7 equipped with Pyris Software for Windows (Copyright © 1999, Perkin Elmer LLC) and a Controlled Cooling Accessory (CCA 7). The measuring block and surrounding glove box were flushed with nitrogen (alumina column dried). Helium (alumina column dried) was used as the carrier gas due to the subambient temperature ranges. Thermal calibrations were completed using indium and *n*-octane standards for onset melting temperature transitions; indium was also used as the enthalpy calibration standard. In order to examine finer detail, sample weights were decreased greatly when compared to initial studies.²⁰ Typically, weights ranged in the order of 1.40 to 2.50 (+/- 0.01) milligrams. In this case, exact film thickness in the DSC sample pan is unknown. An empty pan measurement was subtracted from each DSC run. Scans were isothermally held for 1 minute at 60-120 °C below the peak melt found in initial studies. Subsequently, the sample was heated at 20 °C/min to a point 80 °C above the peak melting point and isothermally held for 1 minute. The cooling curve was performed in a similar manner to an endpoint where the sample was isothermal held (60-120 °C below the peak crystallization temperature) for 1 minute. This process was repeated for at least 3 scans with data collection taken on the 3rd scan (not the case for annealing experiments which are collected on the first scan).

Crystallinity values were derived on the basis of previous studies by Wunderlich.⁹⁹ However, Mathot and coworkers have developed a method using heat capacity measurements to obtain extrapolated crystallinity values in this regard and should be consulted for those attempting to calculate crystallinities for randomly branched systems.¹⁰⁰⁻¹⁰²

Fortunately, ADMET EP copolymer model systems exhibit sharp, distinct melting and crystallization curves when compared to counterparts synthesized by chain chemistry, as described earlier.²⁰ The following relationship found by Wunderlich⁹⁹ (Eq. 4-4) was employed to calculate crystallinity (w_c) values for the EP copolymer models made via ADMET.

$$w_c = \frac{\Delta h'_f}{\Delta h_f} \quad [\text{Equation 4-4}]$$

Where the melting peak area ($\Delta h'_f$) is determined above the baseline in an attempt to exclude the contribution from the heat capacity. This value is then compared to the heat of fusion for completely crystalline PE at the same average temperature (Δh_f). The Δh_f value for completely crystalline PE was found by extrapolation to be approximately 293 J/g (70 cal/g).⁹⁹

4.10.3 Wide-Angle X-ray Diffraction (WAXD)

4.10.3.1 Debye-Scherrer camera

A Philips Debye-Scherrer camera was used to generate wide-angle film patterns. The source was Ni-filtered Cu K_{α} - radiation with a wavelength of 1.5418 Å. The diameter of the camera was designed so that a 1 mm distance between reflections (4 θ) corresponds to 1 degree. Samples were prepared from melt-crystallized material with approximate dimensions of 1mm x 15mm x 1mm. Samples were not annealed prior to making this measurement. All measurements were made at room temperature.

4.10.3.2 ENRAF-NONIUS Diffractus 586

This instrument was equipped with a banana-shaped detector for $2\theta = 120^\circ$, an Inel detector CPS 120 (produced in-house, MPI-P), and variable temperature controller (in-house, MPI-P). The source was Cu $K_{\alpha 1}$ - radiation monochromatized by a germanium monochromator to produce a wavelength of 1.5406 Å. Temperature dependent wide-angle diffractograms were recorded between room temperature and 118 °C for **HP15** and room temperature and 140 °C for **HP21**. Calibration was performed using ZnO (NBS-Standard). Data evaluation was accomplished with commercial software from ENRAF-NONIUS (GUF1 3.0/ENFRAF-GUF1 1.05).

4.10.4 Small-Angle X-ray Scattering (SAXS)

4.10.4.1 Sample preparation—annealing

To obtain optimal results, melt crystallized samples were annealed for extended periods of time before x-ray analysis. Both **HP15** and **HP21** were annealed in an isothermal bath for five days at 20.0 °C (+/-0.5 °C) and 43.0 °C (+/- 0.5 °C), respectively. These temperatures, which produce a maximum in both enthalpy and peak melting point for **HP15** and **HP21**, were pre-determined by in-depth DSC analysis.

4.10.4.2 Kiessig camera

A SEIFERT (Germany) Kiessig camera was used to produce small-angle film patterns. The source was Ni-filtered Cu K_{α} - radiation with a wavelength of 1.5418 Å. Unoriented samples (thin fibers) have been annealed (see 2.4.1, above) prior to the x-ray measurement. The Kiessig camera is a pinhole collimated small-angle device with photographic recording. The collimation is performed by a set of four apertures. Measurements were taken at several camera lengths (100 mm, 200 mm, 400 mm). Note, for example: at 400 mm, the apertures have diameters of 0.4, 0.6, 0.4, and 0.7 mm (beginning at the x-ray tube) with a 4 mm diameter beam stop. Suitable films were obtained by exposing the sample to source x-rays for 3-5 days, depending on camera length. All measurements were made *in vacuo* in order to reduce air scattering effects.

4.10.5 Optical (Light) Microscopy.

4.10.5.1 Sample preparation

All samples were prepared by solution crystallization from tetrachloroethylene (TCE) at room temperature. Dilute solutions of the polymer were transferred to microscope slides by pipette. After evenly depositing a thin layer of the solubilized material, the microscope slide was placed into a petri dish containing a pool of TCE (the microscope slide was elevated above the solution by placement on top of a cut piece of glass; referred to as the mote technique). The petri dish was covered and the solvent was allowed to slowly evaporate (9-10 days) in the attempt to obtain the thinnest sample specimen possible.

4.10.5.2 Instrumentation

A Zeiss Axiophot equipped with Differential Interference Contrast (DIC) facility in reflected light was used to obtain all light microscopy images. Samples, previously

crystallized on a microscope slide were mounted between crossed-polarizers and observed with transmitted light. Crystallization kinetic(s) observations were made using a LINKAM TH600 heating stage equipped with a LINKAM TMS90 controller. The heating stage was mounted between the crossed-polarizers.

4.10.6 Transmission Electron Microscopy (TEM) and Electron Diffraction (e-diffraction).

4.10.6.1 Sample preparation

Dilute solutions of **HP15** and **HP21** were made using TCE as solvent. Some drops of a suspension of PE growth spirals were brought onto glass where the solvent (tetrachloroethylene) was allowed to evaporate. This sample was subsequently shadowed with Pt and covered by a carbon supporting film giving an estimated thickness of 10-20 nm.

4.10.6.2 Instrumentation

TEM images were recorded on a Zeiss EM 902 equipped with a Castaing-Henry Spectrometer (2 magnetic sectors and an electrostatic mirror) at a maximum voltage of 80 keV. Electron diffraction measurements were obtained using a LEO EM 912 equipped with an OMEGA Spectrometer (contains magnetic parts only) at a maximum voltage of 120 keV.

4.10.7 Infrared (IR) Spectroscopy

Fourier transform infrared (FT-IR) spectroscopy was performed on a Bio-Rad FTS-40A spectrometer. Rapid scan mode was employed at rate of 0.15 sec/scan with a 1 cm^{-1} spectral resolution. Complete hydrogenation of the unsaturated ADMET prepolymer was verified by the absence of the out-of-plane C-H bend for the internal olefin at 967 cm^{-1} . All solution cast polymer films were prepared by evaporation from tetrachloroethylene

onto a KBr salt plate. Melt cast films were prepared by melting/recrystallization of the thin film originally cast from solution.

4.10.8 Raman Spectroscopy

Raman Spectra were obtained at the resolution of 2 cm^{-1} by a Dilor XY-800 spectrometer equipped with a silicon chip charge-coupled device (CCD) detector (Type CCD05, Wright Instruments). Laser sources were an Ar⁺ (10W, INNOVA 400; Coherent Palo Alto CA, USA), Kr⁺ (1W, INNOVA 90; Coherent), HeNe (633 nm, 30 mW; Siemens Munich, Germany), and a diverse HeNe (633 nm/NIR with a laser line from 330 to 1152 nm). All data was produced with 1.800 nm^{-1} as the fixed grating (grid) distance. Data manipulation was achieved using PC Pentium, Windows 95 Software
* Version 2.08.

4.11 Results and Discussion

4.11.1 Thermal Behavior

Several calorimetric studies relative to the crystallinity of statistically branched EP copolymers have been performed and shown that the introduction of methyl branches along the backbone of PE causes a decrease in the total crystalline population with an increase in propylene content;²¹⁰⁻²¹² and it is also well established that ethylene-based copolymers are essentially amorphous when the ethylene content is lower than 60-65 mole percent.^{92d,94d,210,213,214} Randomly branched LLDPEs exhibit broad, and sometimes multi-modal, endothermic peaks whose melting peak maximum is normally positioned in the range of 30-105 °C.^{88,92d,94d,211-222} In contrast to statistically branched EP copolymers, initial calorimetric analysis on thermally erased ADMET EP copolymer models gave distinct, sharp melting points for the entire series studied;²⁰ in fact, the breadth of all endothermic events for EP copolymers with precise methyl branching were more narrow

than those reported for statistically branched EP copolymers with comparable comonomer contents.^{92d,214}

In summary, the perfect control of methyl branch sequence length distribution had a profound influence on the thermal behavior of these new ethylene-*co*-propylene materials. Also, as in industrially made EP copolymers, it was found that the melting point, heat of fusion, and percent crystallinity decrease as the amount of defect content is increased for ADMET EP copolymer models, a trend that is predicted by the Flory relationship.⁵⁵

Recently, more in-depth calorimetric analysis of **HP15** and **HP21** showed the existence of bimodal melting and crystallization kinetics after the samples were aged and/or annealed.²²³ It is noteworthy that the thermal history of these materials becomes important during WAXD/SAXS studies. In order to exploit this phenomenon, a series of annealing conditions were investigated in order to find melting point and heat of fusion maximums for both **HP15** and **HP21** (Table 4-1). Attaining a state that maximizes crystallinity becomes vital when attempting to generate suitable SAXS films for these model materials, particularly during long-spacing (d_l) measurements. When found, the proper annealing condition will generate a maximum percent crystallinity for a given material, thereby, increasing the opportunity for source x-rays to be scattered.

Table 4-1. Optimized Peak Melting Temperatures and Crystallinity Found After Annealing Experiments for Extended Time Periods.

ADMET polymers	methyls per 1000 Carbons	T_m (peak) ^a (°C)	Δh_m (J/g)	Crystallinity ^b
HP15	67	40.4	92.3	0.315
HP21	48	63.0	146.6	0.500

^a See Experimental Section 4.10.2 for details. Data obtained from samples that were thermally erased, quenched with liquid nitrogen, and finally annealed for 5 days below the melt at 20.0 °C (**HP15**) and 5 days at 43.0 °C (**HP21**). All calorimetric curves obtained at scan rate of 20 °C/min. ^b Crystallinity determined by dividing the experimentally found heat of fusion by 293 J/g (theoretical value for completely linear PE).⁹⁹

By annealing both **HP15** and **HP21** at approximately 19.5 °C below the peak melt (found for a thermally erased sample) for 5 days, a maximum in the crystallinity for each compound was achieved. The physiochemical result of annealing is illustrated in Figure 4-16. As illustrated below in Figure 4-16, a thermally erased sample exhibits a small pre-melting region and sharp melting transition, whereas, the annealing process leads to bimodal melting kinetics. As predicted by the Thomson-Gibbs relationship (Eq. 4-5),¹¹⁸ an increase in melting point and enthalpy induced by annealing are evidence that crystal thickening is taking place. The Thomson-Gibbs Equation is written as:

$$T_m = T_m^0 \left(1 - \frac{2\sigma_e}{L(\Delta h'_f)} \right) \quad [\text{Equation 4-5}]$$

where T_m^0 is the equilibrium melting point (Kelvin) of an infinitely large crystal of PE ($T_m^0 = 418.65$ K); σ_e is the top and bottom specific free energy per unit area of the PE basal face ($\sigma_e = 87 \times 10^{-3}$ J/m²); $\Delta h'_f$ is the bulk enthalpy of fusion for an infinitely large crystal of PE ($\Delta h'_f = 293 \times 10^6$ J/m³); and the observed melting temperature, T_m (Kelvin), gives a lamella thickness of L (crystalline core in Angströms). Using this relationship,

the predicted lamellar thickness, L , for both **HP15** and **HP21** has been calculated by using the observed melting temperatures (peak) found during annealing optimization studies (Table 4-2).

The calculated values for **HP15** and **HP21**, presented in Table 2, are also compared to theoretical long-spacings calculated for a typical commercial HDPE (observed $T_m = 132$ - 135 °C) and LDPE (BASF 1810; observed $T_m = 108.9$ °C). When comparing LDPE and HDPE, it is evident that the lamellar thickness increases markedly as the SCB content decreases; however, in going from **HP15** (67 methyls/1000 carbons) to **HP21** (48 methyls/1000 carbons), there is only a relatively small increase in the lamellar thickness, a trend that has been observed before when defect content is greater than 15 SCBs/1000 carbons.^{224,225} The theoretical lamellar thicknesses obtained here will later be compared to experimental values obtained during SAXS.

It must be cautioned that the Thomson-Gibbs relationship has been used as a basis of discussion only. There are inherent difficulties encountered when deriving theoretical values from Equation 4-5; namely, this stems from the fact that small crystals are not stable when subjected to varying annealing conditions. In fact, Wunderlich²²⁶ and Lauritzen and Hoffman¹⁶⁰ were the first experimentalists to apply the Thomson-Gibbs Equation (Eq. 4-5) in efforts to explain the metastability encountered during small crystal melting. In addition to Wunderlich's initial work, several groups attempted to examine the metastability phenomenon for less perfect crystals of flexible, linear macromolecules, specifically those containing internal defects (branches, tie-molecules, etc.).²²⁷⁻²³⁷ Although much information was gathered from these studies, a definitive explanation of crystal thickening was unable to be formulated for non-ideal systems (defect containing)

because of the existence of 1) nonequilibrium and equilibrium defects and 2) the unknown nature and SCBD of point defects along the polymer backbone. Despite possible shortcomings, recently, several authors have efficiently utilized this relationship in a qualitative manner when comparing different grades of branched PE.^{224,225,238}

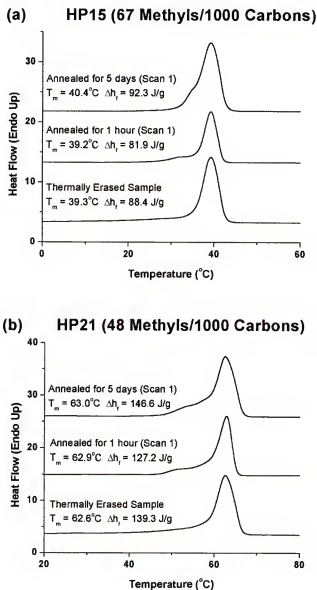


Figure 4-16. Optimizing crystallinity through isothermal annealing—**HP15** (4-16a) at 20°C vs. **HP21** (4-16b) at 43°C —Expanded view comparison. [All measurements taken at a Scan Rate = $20^\circ\text{C}/\text{minute}$.]

At present, the exact mechanism that leads to metastability and bimodal thermal events in polyolefins is still debated; however, a logical postulate for the EP copolymer models presented here is that the melting of discrete morphological populations of the same crystallographic form, differing only in size and perfection, is taking place. Regardless of the reason, thermal behavior studies for **HP15** and **HP21** have produced very surprising results when compared to normally observed trends for randomly branched EP copolymers. These findings spurred interest to gain further behavioral information for ADMET EP copolymer models with a precise SCBD of methyl groups by gathering microscopy and x-ray diffraction data in order to deduce secondary and tertiary structural information.

Table 4-2. Crystal Thickness (L): Theoretical Calculation Based on the Thomson-Gibbs Equation.

ADMET polymers	methyls per 1000 carbons	T _m (peak) ^a (°C)	L ^b (Å)	crystallinity ^c
HP15	67	40.4	24	0.315
HP21	48	63.0	30	0.500
LDPE^d	33	108.9	68	0.419
HDPE^e	< 5	132-135	130-250	0.6-0.8

^a See Experimental Section 4.10.2 for details. Data obtained from samples that were thermally erased, quenched with liquid nitrogen, and finally annealed for 5 days below the melt at 20.0 °C (**HP15**) and 5 days at 43.0 °C (**HP21**). All calorimetric curves obtained at scan rate of 20 °C/min. ^b Theoretical long-spacing values calculated by inserting observed melting points (peak value) into Equation 5 and solving for L.¹¹⁸ ^c Percent crystallinity determined by dividing the experimentally found heat of fusion by 293 J/g (theoretical value for completely linear PE).⁹⁹ ^d **BASF 1810H**, acquired from BASF (Germany). ^e Commonly encountered values for HDPE made by Ziegler-Natta or metallocene catalysis.

4.11.2 X-ray Diffraction

As previously described, numerous thermal behavior studies have been performed for chain produced EP copolymers with statistical methyl branching,^{88,92d,94d,210-222} however, there have also been numerous morphological studies devoted to these materials. In particular, there exists a great deal of x-ray diffraction data for a variety of EP copolymers synthesized by way of both Ziegler-Natta (vanadium or titanium-based) and metallocene catalysis.^{92d,210,212,239-251} From these studies, data has been garnered supporting the fact that propylene units can be incorporated into the PE orthorhombic unit cell;^{210,239-244,247} although, there are literary examples that purport methyl branch exclusion from the crystal lattice.^{92d} Thus, the influence of branch size on branch location has provoked a wide range of opinions. In addition, one study by Swan has even reported that branches of up to five carbon atoms in length may be included into the polyethylene lattice.²³⁹

Although several varying opinions have been formulated, it is now generally accepted that EP copolymers allow methyl branch inclusion into the crystal and are semicrystalline materials whenever the propylene content falls below 35-40 mol %.^{210-212,217,240} In order to compensate for methyl branch inclusion, normal PE lattice dimensions [$a_0 = 7.45 \text{ \AA}$, $b_0 = 4.97 \text{ \AA}$, and $c_0 = 2.54 \text{ \AA}$] have been shown to undergo expansion or distortions within the ab plane but remain relatively unaltered in the direction running along the stem axes of nearly zig-zag (trans) planar stems.^{92d,239-241,244,248-251}

Indeed, diffraction data obtained for an array of ethylene-co-propylene materials have revealed that the b and c axes basically retain the same dimensions regardless of propylene content; whereas, the a axis of the polyethylene unit cell increases more or less

proportionally with an increase in propylene content.^{210,241,247} For high propylene contents (>40 mol %), EP copolymers are essentially amorphous under normal conditions,^{210,247} however, successful crystallization of EP materials, with high propylene content, has been induced by stretching under high-pressure to give a pseudo-hexagonal lattice, as determined by x-ray diffraction measurements.^{210,249,250} It is important to note that nearly all of this 'induced crystallinity' disappears upon removal of the applied pressure at room temperature. Nonetheless, the crystalline nature for these materials has been successfully analyzed by diffraction techniques when a given sample, immediately after pressure removal, is examined at low temperatures (at or below $-30\text{ }^{\circ}\text{C}$). For the pseudo-hexagonal unit-cell of EP materials with elevated defect contents, it should also be noted that the a parameter becomes approximately equivalent to $[b \times (3)^{1/2}]$, the product of b parameter and the square root of 3.

The conversion from the orthorhombic to pseudo-hexagonal form has also been observed at elevated temperatures/pressures for oriented PE; and as a result of number of structural studies performed on oriented samples of linear²⁵²⁻²⁷⁰ and branched polyethylenes,^{202,210,249,250} the pseudo-hexagonal form for polyolefin-based materials has been described as being a conformationally disordered (condis) mesophase that mimics the orientation and physical properties normally encountered on the periphery of the substance's melting point.^{260,261,271,272} Without a doubt, orthorhombic and pseudo-hexagonal are not the only three-dimensional structural possibilities for PEs—evidence also exists for the monoclinic²⁷³ and triclinic^{139,274,275} forms; however, emphasis has been placed on the discussion of the pseudo-hexagonal phase in light of the results found for the ADMET EP copolymer model compounds discussed herein, *vida infra*.

4.11.2.1 Debye-Scherrer camera—powder diffraction (WAXD)

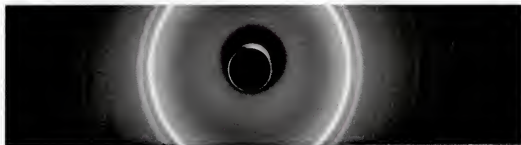
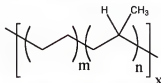


Figure 4-17. WAXD—Debye-Scherrer film from powder diffraction of an EP copolymer with random methyl branching (**BASF 1810H**; 33 methyls per 1000 carbons as determined by ^{13}C NMR).

Figure 4-17 depicts the unoriented powder diffraction pattern produced by an EP copolymer with random methyl branching. Attention should be directed towards the two reflections with the highest intensity; the elevated intensities indicate that these two planes are the most closely packed in the material. Fortunately, a plethora of data exists for the diffraction patterns of PE-based systems, so one is able to index the reflections given by this material through the substitution of measured values into the general relations valid for all crystal systems (a knowledge of the relations between the direct and reciprocal lattices is also required).²⁷⁶⁻²⁷⁹ The two innermost reflections correspond to the (1 1 0) and (2 0 0) crystal planes for the PE orthorhombic unit cell. These reflections are the normal benchmarks for any PE-based material's diffraction measurement because they account for the majority of x-ray scattering. Upon further examination, additional reflections are also present, albeit much weaker. A complete listing of d spacing information for **BASF 1810H** is provided in Table 4-3.

A few points are evident when examining the data more closely. First, all of the reflections are weak or very weak in intensity except those corresponding to the (1 1 0), (2 0 0), and (0 2 0) planes—a direct result from the varying electron densities of crystallographic planes. By using d -values obtained from the three most intense reflections, the lattice parameters for this EP copolymer are roughly: [$a = 7.68 \text{ \AA}$, $b_o = 5.08 \text{ \AA}$, and $c_o = 2.54 \text{ \AA}$]. As expected, the a parameter for the unit cell of the EP copolymer (7.68 \AA) is larger than that for linear PE (7.45 \AA). As noted previously,^{92d,239-241,244,245,248-251} the change in this dimension of the unit cell results from the minimization of lattice free energy whenever defects are incorporated into the crystalline material.

Table 4-3. Debye-Scherrer Scattering Data for EP Copolymer with Random Methyl Branching (**BASF 1810H**; 33 methyls/1000 carbons as determined by ^{13}C NMR).

2θ (mm)	d value (Angströms)	$h k l$	Relative Intensity
$19^\circ 2\theta$	--	Amorphous Halo	dark
20.9	4.26	1 1 0	v. strong
23.2	3.84	2 0 0	strong
29.6	3.02	2 1 0	v. weak
35.4	2.54	0 2 0	Medium
38.8	2.32	3 1 0	Weak
42.9	2.11	2 2 0 or 2 0 1	v. weak
46.2	1.97	2 1 1	v. weak
51.7	1.77	4 2 0, 3 2 1?	v. weak

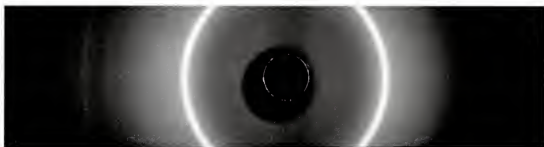


Figure 4-18. WAXD—Debye-Scherrer film from powder diffraction of **HP15** (theoretically 67 methyls/1000 carbons).

Table 4-4. Debye-Scherrer Scattering Data for **HP15**: EP Copolymer with Precise Methyl Branching (67 methyls/1000 carbons).

2θ	d value	$h k l$	Relative
(mm)	(Angströms)		Intensity
20.3	4.39		v. strong*
35.5	2.53		Weak
40.3	2.24		medium
50.5	1.81		v. weak

*Result of 2 overlapping reflections.

Debye-Scherrer patterns and scattering data in tabular form are presented in Figure 4-18/Table 4-4 for **HP15** and Figure 19/Table 4-5 for **HP21**. Initially, it was hoped that scattering patterns from the two model EP copolymers with precise branching could be indexed in a similar manner as the randomly branched EP copolymer, **BASF 1810H** (Figure 4-17); however, after studying both sets of data, it became immediately apparent that the geometry for **HP15** and **HP21** was not orthorhombic. An attempt was made to correlate the observed reflections to experimental and literature values given for the

monoclinic²⁷³ and triclinic^{139,274,275} unit cells of PE; but, it was determined that neither geometry was applicable in relation to the observed Bragg reflections for **HP15** or **HP21**.



Figure 4-19. WAXD—Debye-Scherrer Film from Powder Diffraction of **HP21** (Theoretically 48 methyls/1000 carbons).

Table 4-5. Debye-Scherrer Scattering Data for **HP21**: EP Copolymer with Precise Methyl Branching (48 methyls/1000 carbons).

2θ	<i>d</i> value	<i>h k l</i>	Relative
(mm)	(Angströms)		Intensity
18.8	4.72		v. strong
21.8	4.09		v. strong
25.1	3.55		Strong
34.7	2.59		medium/strong
38.1	2.36		medium
40.4	2.23		Strong
48.1	1.89		v. weak
53.5	1.71		Weak
75.0	1.27		v. weak

Despite these facts, there are some initial points that must be made here. For one, there are many more observed reflections for **HP21** when compared to **HP15**. This most likely is a direct result of defect content. It could be postulated that the **HP21** lattice,

with 48 methyls/1000 carbons is less distorted (contains a higher crystalline content) than **HP15** (67 methyls/1000 carbons), a fact that is supported by the crystallinity differences obtained by differential scanning calorimetry. Also, with less defects, **HP21** does not have as many free energy barriers to overcome during crystal formation as does **HP15**, thereby, allowing the **HP21s** crystal planes to pack more densely. Secondly, attention should be directed at the very strong inner reflection for **HP15** with a d value of 4.39 Å. As denoted in Table 4, a faint indication of two unresolved peaks was observed; unfortunately, the resolution of the film did not allow for deconvolution of the two peaks so the d -value provided in Table 4-4 is the result of an average. In order to possibly investigate the unresolved reflections for **HP15** and to conduct temperature dependent studies, both samples were analyzed using a complimentary WAXD instrument equipped with a position-sensitive counter.

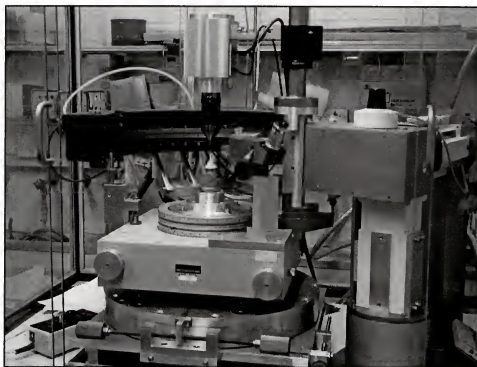


Figure 4-20. DiffRACT Model 586—Powder Diffraction (WAXD).

4.11.2.2 ENRAF-NONIUS Diffractus 586—powder diffraction (WAXD)

Figure 4-20 illustrates the second instrument utilized to obtain WAXD for **HP15** and **HP21**. The instrument was equipped with a banana-style detector, rotating sample holder, and a controlled heating accessory. The attached heating device made temperature-dependent WAXD measurements possible. Data collection for all samples was taken for acquisitions times on the order of 2-3000 seconds.

The first goal was to elucidate the overlapping reflections obtained by the Debye-Scherrer camera exposure of **HP15**. To begin, a comparison of **HP15** versus **HP21** was made at room temperature in order to mimic the same sample condition employed during the camera exposures. As depicted in Figure 4-21, the computer generated measurement proved to be a fine compliment to the film measurements made earlier. Although the reflections still overlap one another, the resolution was sufficient to enable assignment of two distinct d values (4.34 and 4.25 Å) to the previously unresolved peak in **HP15**. Additionally, as in the Debye-Scherrer exposures, **HP21** appears to contain a higher percentage of crystalline material when compared to **HP15** on the basis of intensity differences. So, relative crystallinity differences found by x-ray diffraction tend to concur with calorimetry findings with respect to the observed enthalpic differences found for **HP15** and **HP21**.

Owing to the previous thermal aging and annealing effects found for both **HP15** and **HP21**, a series of temperature-resolved WAXD experiments were carried out in order to determine the possible influence(s) to d spacings during crystallization of material from the melt.

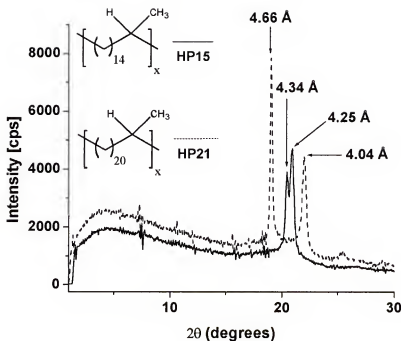


Figure 4-21. WAXD—Powder diffraction of **HP15** versus **HP21** at room temperature.

Figure 4-22 depicts temperature-dependent WAXD measurements during cooling for **HP15**. During each step of melt crystallization, the sample was isothermally held (± 1 °C) at the elevated temperatures (Figure 4-22a-c) for a period of 1 hour prior to collection of diffraction data; however, the final measurement was taken after holding the sample at room temperature for a 24 hours period (Figure 4-22d). From Figure 4-22a, the amorphous halo was estimated by profile fitting to be 18.2° (2θ), a value much lower than that normally observed for linear and branched PEs (typically 19 – 20° 2θ). As shown here, the intensities of both reflection maximums ($d = 4.34$ and 4.25 Å) increase as the material is crystallized from the melt. This trend is reversible during the melting cycle for these materials, also. In fact, the comparison of several heating and cooling cycles clearly show that these results are reproducible, both in position and relative intensities for each observable peak reflection and/or the amorphous halo region.

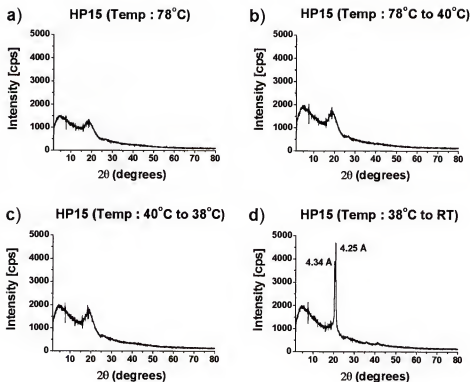


Figure 4-22. WAXD—Temperature dependent measurements during cooling for **HP15** at: a) 78 °C (40 °C above peak melting temperature found calorimetrically) b) 40 °C c) 38 °C d) room temp.

A similar temperature-dependent WAXD study was carried out for **HP21**. Here, the amorphous halo was found to be 18.5° (2θ), a slightly higher but comparable angular value found during the analysis of **HP15**. Accordingly, as observed in **HP15**, the two reflection maximums for **HP21** ($d = 4.66$ and 4.04 Å) exhibited intensity increases as the material was crystallized from the melt. However, in contrast to the overlapped reflection maximums in **HP15**, the definitive separation of **HP21**'s two reflection maxima provided a more advantageous opportunity to study any possible lattice distortions encountered during crystallization from the melt. Upon a decrease in temperature (Figure 4-23b to 4-23c to 4-23d), the lower intensity reflection remains relatively constant (average d value = 4.04 Å), while the higher intensity reflection shifts

to lower angles of 2θ (i.e. higher d values: 4.55 to 4.56 to 4.66 Å, respectively). Qualitatively, this change to lower-angled reflections is most probably due to distortions in the ab dimensions of the unit cell during the crystal thickening process; although, in regards to the influence(s) on a specific crystallographic plane, a quantitative assessment is impossible at this time since reflection indices have not been assigned.

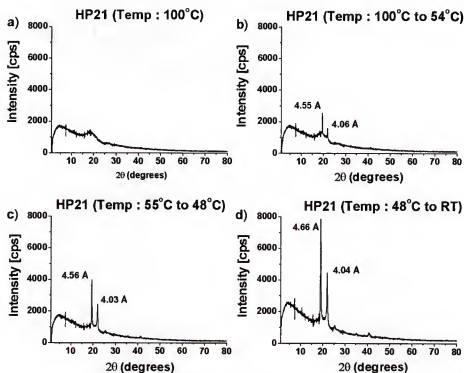


Figure 4-23. WAXD—Temperature dependent measurements during cooling for **HP21** at: a) 100 °C (40 °C above peak melting temperature found calorimetrically) b) 54 °C c) 48 °C d) room temp.

Despite indexing difficulties and the differences in defect content, a number of similarities exist in the diffraction data for **HP15** and **HP21**. First, both samples exhibit an increase in intensity of primary reflections during cooling from the melt; and although not presented here, **HP15** and **HP21** show an increase in primary reflection intensities

during room temperature annealing which verifies findings found during thermal behavior experiments in regard to annealing effects.

Secondly, during temperature-dependent WAXD heating experiments, an inverse effect was observed in relation to the relative reflection intensity for primary maxima that was found during the cooling process—as the samples were heated from the crystallized form, a continuous decrease was observed for all reflection maxima. This is unequivocal proof that the intensity increase, during cooling from the melt, is not caused by further crystallization (i.e. secondary amorphous to crystalline phase changes), but rather an improvement of overall crystalline organization in the existing matrix. So, the WAXD for the ADMET EP model systems presented here indicate that these materials do not conform to a strict two-phase model when considering the chain-folding crystallization process. In concurrence with calorimetry results, the diffraction data for **HP15** and **HP21** give credence for the operation of a bimodal crystallization mechanism. The development of a primary crystalline phase is followed by the creation of a second, either less-ordered or smaller-domained phase; however, each individual crystalline segment should possess independent behavior in regard to its crystallization kinetics and melting behavior, a result that is enhanced during annealing of said materials (See **Section 4.11.1**). A similar bi-phasic crystallization process has recently been postulated for a LLDPE commercial material with hexyl branches {ethylene-*co*-octene (EO)}.^{201,202}

Thirdly, in going from **HP15** (67 methyls/1000 carbons) to **HP21** (48 methyls/1000 carbons), an increase in defect content resulted in a drastic change in the position of the two primary reflections. Intuitively, this is most likely due to changes in relative spacing of the *ab* dimensions within the unit cell. When comparing the lattice parameters for a

uniform PE unit cell and that for a randomly methyl-branched EP copolymer, an increase in propylene content typically results in an increase in the unit cell's a dimension [1 0 0] but very little change in the b [1 1 0] and c [0 2 0] directions.^{92d,239-241,244,245,248-251} If the assumption is made for **HP15** and **HP21** that the reflections with primary intensity and secondary intensity correspond to the (1 1 0) and (2 0 0) planes, respectively, there is an immense effect made upon both the a and b dimensions for EP copolymers with precise methyl branch placement. Of course, this is speculative at best; and without assignment of Miller indices, final comments cannot be made concerning the exact nature of unit-cell long-range order (c dimension) or amorphous halo location in comparison to existing ethylene-based materials.

The two-phase structural model for semicrystalline polymers divides the three-dimensional state of these systems into 1) the amorphous (disordered) phase and 2) the crystalline (ordered) phase; however, experimental results have shown that the crystallinity range for known semicrystalline polymers is limited to 5-95%. From the phase rule theory in regard to a one-component system (a composite in this case), it is understood that attaining equilibrium is impossible for either phase. Since both phases exist simultaneously in the material below the melting point and a polymer with 100% crystallinity has never been observed, it is logical that there must also be an intermediate phase, or even several phases (mesophases), between the two. These regions have customarily been dubbed as interstitial crystalline/amorphous regions or simply as amorphous defects.¹¹⁴

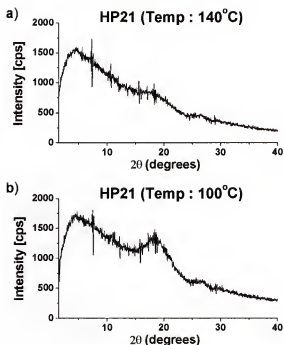


Figure 4-24. WAXD—Suggested evidence for an ordered mesophase in the amorphous region (**HP21**).

Figure 4-24 suggests the existence for some type of ordered mesophase in **HP21**.

Evidence for a mesophase can be attributed to the significant intensity decrease in the amorphous halo for **HP21** upon heating the material from 100 to 140 °C. Normally, ethylene-based materials, even at 0.5-1 °C above the peak melting point, produce a singular, broad/Gaussian-shaped amorphous halo that is very weak in intensity. Figure 4-24a depicts the characteristic shape generally observed during the x-ray diffraction of linear and statistically branched PEs when completely in the melt. But as illustrated above, on cooling from 78 to 38 °C above the peak melting point (~62 °C), **HP21** exhibits a noticeable increase in amorphous halo peak intensity when measured at the lower temperature (Figure 4-24b; **HP21** at 100 °C).

During temperature-resolved WAXD experiments, crystallization of the **HP21** was qualitatively monitored by the initial development and subsequent increase in primary

crystal plane reflections when cooling the material from the melt. Using increasing intensity as a basis for an increase in relative structural order, *it is postulated that HP21 undergoes some degree of ordering while in the melt at 100 °C*. The significance of this ordering at 100 °C is counter to the entropic barriers that normally prevent such an event to take place. The organization of this EP copolymer at such an elevated melt temperature is most probably a consequence of the precise methyl branch placement along the polymer backbone. Although **HP21** was heated to almost 40° C above the peak melt, x-ray diffraction results have revealed that the polymer apparently undergoes some type of chain rearrangement in preparation for the crystallization process—this is a new finding for any polyolefin-based material while being maintained at such an elevated temperature above the peak melting point. Although not discussed here, the same ordering phenomenon was observed for **HP15** as well.

Upon further inspection of the amorphous halo region for **HP15** and **HP21**, the presence of a secondary halo is also evident (Figure 4-25)—a similar finding has recently been observed for an EO copolymer synthesized by Dow Chemical's INSITE™ technology.^{201,202} The relative position of both amorphous halos is comparable for each ADMET EP copolymer; however, the position of the second halo occurs at a much higher angle when compared to the values typically observed for linear or branched polyethylenes in the molten state. The occurrence of a secondary halo at a higher angle indicates some form of additional short-range ordering in the melt. This finding is indeed interesting and merits further study; however, as previously stated, the exact nature of short-range order in these model EP copolymers is unknown at this time.

Amorphous Halo Comparison

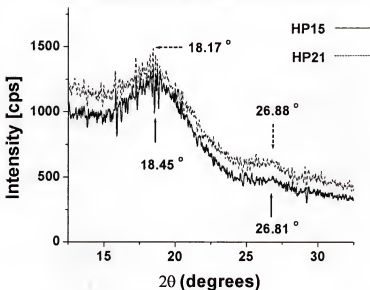


Figure 4-25. WAXD—Further evidence for a secondary ordered mesophase in the amorphous region (HP15 at 78 °C vs. HP21 at 100 °C).

4.11.2.3 Small-angle x-ray scattering (SAXS)—Kiessig camera

Wide-angle x-ray diffraction has established a relative idea of short-range order differences for **HP15** and **HP21**, but small-angle measurements are needed to explore the influence precise branching has on long-range structure(s). Turning attention back to Figure 4-15, it was postulated that two possible scenarios could exist: 1) Eby's model¹⁰⁸ of methyl branch inclusion in the crystal (see Figure 4-15a) and 2) Flory's exclusion model⁵⁵ in which the branches (defects) are ejected from the lattice at the terminus of sharp-folded run-lengths of methylene units (see Figure 4-15b). The lamellar thickness, or long-spacing (d_l) as it is sometimes referred, can be measured through the use of SAXS. Determination of the long-spacing for **HP15** and **HP21** provides an opportunity to examine the nature of the fold-distance in each macromolecule, thereby, allowing possible discrimination between the branch inclusion or branch exclusion models (Figure

4-15). Small-angle measurements were performed using a Kiessig camera; this instrument is capable of adjusting the path-length between the sample and film by distances of 100, 200, and 400 mm. Increasing the path-length distance affords the opportunity to study larger structural information, eventually gaining the ability to measure the long-spacings that would be typical for an ethylene-based material (400 mm path-length).

The SAXS film exposures for **HP15** are illustrated in Figure 4-26. The corresponding numerical data is provided in Tables 4-6a and 4-6b for the 100 mm and 200 mm exposure distances, respectively. Initially, focus will be directed at Figure 4-26a (100 mm). With the small exposure distance, information at higher angles of 2θ is still maintained. This is demonstrated by the reoccurrence of the reflections at 4.35 and 4.26 Å that were measured earlier in WAXD; however, two new weak reflections are now observed at 13.47 and 11.29 Å—periodic reflections that were not visible in the WAXD measurements.

New reflections observed at 100 mm (Figure 4-26a) were verified by developing a 200 mm exposure (Figure 4-26b); at this time, an additional reflection appeared at approximately 27 Å (Table 4-6b). All three of the reflections resolved by SAXS are important because they indicate long-range order at various distances with the crystal. To this author's knowledge, this is the first time that periodic distances of this scale have been recorded for any ethylene-based material and most likely stem from the influence of a more ordered placement of defect points (methyl branches) within the crystal lattice.

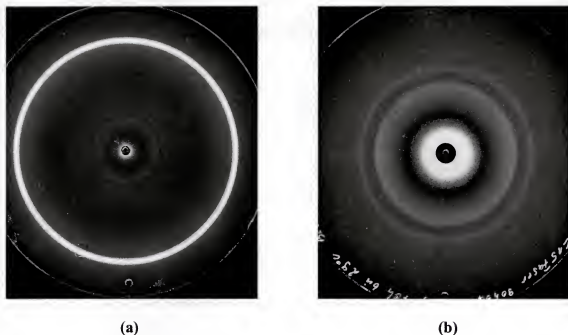


Figure 4-26. SAXS of **HP15**: (a) 100 mm camera-length, unoriented thin film (cut sliver), sample annealed at 5 °C for 3 months prior to measurement with a 72 h exposure time (b) 200 mm camera-length, unoriented thin fiber, sample annealed at 26 °C for 90 h with a 96 h exposure time.

Table 4-6a. Kiessig Camera: SAXS of **HP15**, 100 mm Exposure Distance: EP Copolymer with Precise Methyl Branching (67 methyls/1000 carbons).

2θ (degrees)	d value (Å)	relative intensity
6.56	13.5	very, very weak
7.83	11.3	very, very weak
20.4	4.35	medium
20.9	4.26	strong

Table 4-6b. Kiessig Camera: SAXS of **HP15**, 200 mm Exposure Distance: EP Copolymer with Precise Methyl Branching (67 methyls/1000 carbons).

2θ (degrees)	d value (Å)	relative intensity
3.28 (3.27)	26.96 (27.0)	weak
6.55	13.5	medium
7.82	11.3	weak
10.8	8.22	very weak

Figure 4-27 illustrates two possible periodic long-spacing values p if **HP15** were to crystallize according to either the fringed-micelle theory (Figure 4-27a) or Flory's defect exclusion model of chain folding (Figure 4-27b). Figure 4-27a assumes that the chains are extended in a planar zigzag conformation and would give a long-spacing value of 11.9 Å only if a number of 14 carbon long methylene segments, from differing chain stems, were to coalesce to form small bundles of crystallites (fringed-micelles). Of course, if methyl branches are included into the crystal as has commonly been observed, the long-spacing would be greater in a fringed-micelle, but the smallest value possible would be 11.9 Å

If the switchboard model is actually at work in **HP15** (Figure 4-27b), then a number of methylene units must be involved in the folding process, and therefore, will be ejected into the amorphous region as well. It is commonly accepted that a total of five carbon atoms are involved in the fold itself, this includes both the methine carbon and the alpha and beta carbons on either side of the branch.

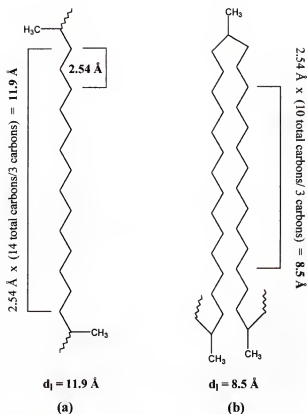


Figure 4-27. Possible periodic distances for **HP15**: (a) smallest integer of an extended zigzag chain of methylenes between methyl branches (b) long-spacing derived from the switchboard model with all methyl branches excluded from the crystal.

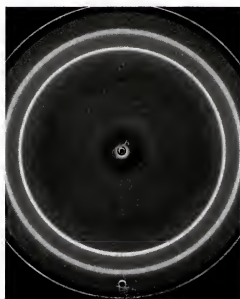
At this stage, the fringed-micelle possibility cannot be completely ignored, but focus of the discussion will center on whether or not the model depicted in Figure 4-27b is viable for the crystal structure of **HP15**. When comparing the d spacings obtained in the 100 and 200 mm Kiessig exposures to the predicted d_1 value of 8.5 \AA (Figure 4-27b), a near match was found in the 200 mm exposure at 8.22 \AA . This may be an indication that some of the material may indeed fold according to Flory's exclusion principle; however, upon inspection, it is evident that this reflection was the weakest of all those measured. From earlier discussion, it is well understood that a higher electron density in a given crystal plane will scatter x-rays more intensely. Therefore, if the model given in Figure 4-27b were the dominant crystal form, a reflection at or around 8.5 \AA would

dominate the landscape of any SAXS exposure. In this instance, the reflection observed at 8.22 Å does not dominate; even so, the mere presence of this periodic distance suggests that the structure illustrated in Figure 4-27b may contribute to the crystallization mechanism of **HP15**. It is a fair assumption that **HP15** does not contain a significant population of material (if any) that is chain-folded in this manner; however, if all the methyl branches have been excluded from the lamella, then the periodic distances observed at 27.0, 13.5, and 11.3 Å would likely be possible. Identical methods were used to examine **HP21** as well and are presented in Figure 4-28 and Table 4-7.

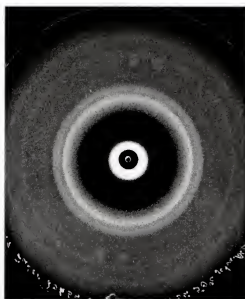
As was seen in WAXD, an increase in the crystallinity leads to the evolution of a greater number of visible reflections in the SAXS measurements for **HP21** when compared to **HP15**. And as was the case with **HP15**, SAXS photographic exposures of **HP21** yielded several new reflections that indicate longer-range order in the material. After annealing at 50 °C for 3 days, SAXS at a 100 mm exposure (Figure 4-28a) distance gave reflections corresponding to longer-range periodicities at 15.3, 13.4, 11.9, and 9.04 Å. The reflections at 4.63 and 4.03 Å were also observed during WAXD and correspond to the most densely packed crystallographic planes in the unit cell of **HP21**. Subsequent analysis at 200 mm (Figure 4-28b) gave measured reflections with *d* values of 26.8, 14.5, 12.6, 9.89, 9.04, 8.91 and 7.80 Å.

There are noticeable differences when comparing the 100 mm to 200 mm exposure; for instance, *d* values 15.3, 13.4, and 11.9 Å in the 100 mm exposure are thought to emanate from the same crystal planes at 14.5, 12.6, and 9.89 Å observed in the 200 mm exposure. The difference in the two being the annealing temperature: 1) 50 °C for the 100 mm exposure and 2) 45 °C for the 200 mm exposure. In other words, a decrease in

annealing temperature led to a decrease in 3 long-range periodicities in **HP21**. The absence of Miller indices makes any speculation of whether this contraction occurs in the *a*, *b*, or *c* dimension of the unit cell a mute point. Also in reference to annealing, it is curious as to why the reflection observed at 9.04 Å was not effected during the different annealing conditions employed here. Logic would dictate that this *d* spacing would decrease in a similar manner as the three cases mentioned above. The results are quite puzzling, and many additional tandem annealing/diffraction experiments are required to make any quantitative assessment for the perturbations observed here.



(a)



(b)

Figure 4-28. SAXS of **HP21**: (a) 100 mm camera-length, unoriented thin film (cut sliver), sample annealed at 50 °C for 72 h prior to measurement with a 72 h exposure time (b) 200 mm camera-length, unoriented thin fiber, sample annealed at 45 °C for 120 h with a 120 h exposure time.

Table 4-7a. Kiessig Camera: SAXS of **HP21**, 100 mm Exposure Distance: EP Copolymer with Precise Methyl Branching (48 methyls/1000 carbons).

2θ (degrees)	d value (Å)	relative intensity
5.77	15.3	very, very weak
6.62	13.4	very, very weak
7.41	11.9	very, very weak
9.78	9.04	weak halo (center)
19.2	4.63	strong
22.1	4.03	medium

Table 4-7b. Kiessig Camera: SAXS of **HP21**, 200 mm Exposure Distance: EP Copolymer with Precise Methyl Branching (48 methyls/1000 carbons).

2θ (degrees)	d value (Å)	relative intensity
3.30	26.8	v. Weak
6.10	14.5	medium
7.02	12.6	medium/Weak
8.94	9.89	very, very weak
9.78	9.04	very, very weak
9.93	8.91	weak
11.3	7.80	weak

Of particular significance is the d value measured at 26.8 Å for **HP21** (Table 4-7b) because a reflection plane was reported for **HP15** at approximately 27.0 Å as well (Table 4-6b). This represents the only periodic SAXS distance that was found common to both

HP15 and **HP21**. The origin of this reflection is still in question; but it is fascinating why approximately 27 Å would be a shared lattice repeating distance for both **HP15** and **HP21**. This is the only periodic distance found thus far that does not depend on the annealing condition employed or on the amount of defect content. Further observations made during electron diffraction of these materials may offer additional insight into this matter, *vida infra*.

The relations given in Figure 4-29 have been compared to d values obtained in SAXS exposures (Table 4-7a and 4-7b). For **HP21**, only a single, very weak reflection at $d = 13.4$ Å was found to possibly satisfy the exclusion model requirement of a $d_1 = 13.5$ Å given in Figure 4-29b. However, care must be taken in the interpretation of this result due to the concerns with the annealing effects already discussed above. If the reflection observed at 13.4 Å in the 100 mm exposure (annealed at 50 °C) were proven to correspond to the same crystallographic plane as 12.6 Å does in the 200 mm measurement (annealed at 45 °C), there would be indiscriminate proof that neither value indicates a true long-spacing measurement for **HP21**. If the switchboard model were true, the theoretical long-spacing distance of 13.5 Å would never be contracted to such a degree, if at all.

It is worthy to note here that this entire argument is contingent on the fact that the chain axes of these materials arrange themselves in a zigzag type fashion (all trans). In defect containing materials, the occurrence of gauche conformations along the chain stems are known to exist and would certainly skew the chain-folding models presented in Figures 4-27 and 4-29. In order to attempt a measurement of the 'true' long-spacing

distance, SAXS experiments were performed at an exposure distance of 400 mm with the Kiessig camera.

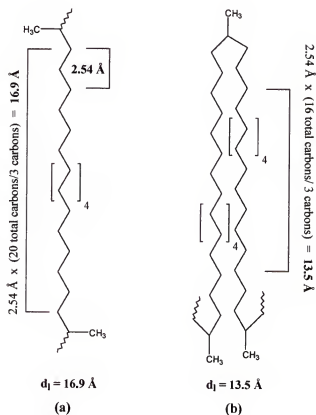


Figure 4-29. Possible periodic distances for **HP21**: (a) smallest integer of an extended zigzag chain of methylenes between methyl branches (b) long-spacing derived from the switchboard model with all methyl branches excluded from the crystal.

4.11.2.4 Small-angle x-ray scattering (SAXS)—Long-period measurements

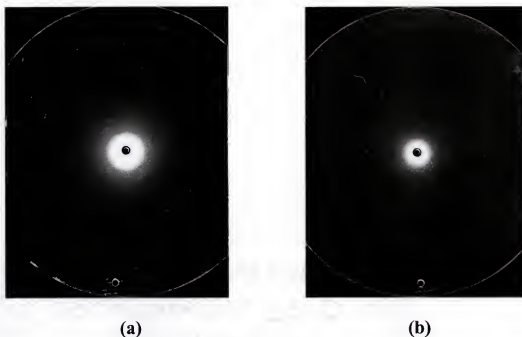


Figure 4-30. Long-spacing measurement from SAXS (a) **HP15**—400 mm path-length, unoriented thin fiber, sample annealed at 20 °C for 120 h prior to measurement with a 120 h exposure time (b) **HP21**—400 mm path-length, unoriented thin fiber, sample annealed at 45 °C for 120 h with a 120 h exposure time.

Figure 4-23 depicts the photographic exposures for **HP15** (4-30a) and **HP21** (4-30b). Although not clear from the scanned image, two overtone reflections can be seen in each measurement. The resolution of the first order reflection responsible for these overtones is slightly visible and contained within the bright white circular pattern that is created due to the errant scattering of x-rays upon hitting the beam stop. Therefore, the second and third order reflections have been used as a basis to calculate the long spacing for each of the model EP copolymers studied here (see Table 4-8).

Table 4-8. SAXS Long-Spacing Measurements for ADMET Model EP Copolymers with Precise Methyl Branching.

polymer	order of reflection	<i>d</i> value (Å)
HP15	1 st	197.4*
	2 nd	98.7
	3 rd	63.3
HP21	1 st	164.4*
	2 nd	82.2
	3 rd	53.6

*1st order reflection *d*-value obtained by multiplying the 2nd order reflection by 2.

By SAXS, lamella long-spacing values for **HP15** and **HP21** were measured at 197 and 164 Å, respectively. The values obtained are in the typical range of long-spacing distances normally measured for commercially produced branched and linear PEs (100-250 Å). The significance of this finding is two-fold: 1) the length obtained here suggests that the switchboard chain-folding is most likely improbable (i.e. Eby's model of branch inclusion is the determinate manner of crystallization here) and 2) long-spacing values obtained by SAXS are 6-8 orders of magnitude higher than those predicted by the Thomson-Gibbs equation, which is based on the melting points obtained for **HP15** and **HP21** during DSC analysis (see Table 2, Section 4.11.1).

For both **HP15** and **HP21**, long-spacing measurements were unsuccessful until the proper annealing condition was determined. As discussed in Section 4.11.1, a variety of annealing conditions and times were investigated until an apparent maximum crystallinity for each polymer was observed. In other words, the long-spacing values of

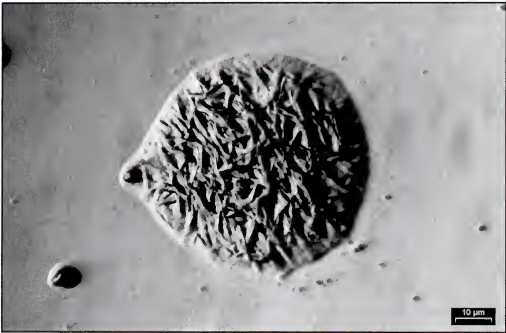
197 Å (**HP15**) and 164 Å (**HP21**) have been attained from materials at a metastable state. The maximum in the crystallinity obtained by annealing approaches the true equilibrium state of the crystal only at the annealing temperature itself. Further, one should not assume that the values stated here are absolute for either system. Although the exact influence of precise branch placement on long-spacing is unknown at the moment, it is quite evident from the x-ray diffraction findings for **HP15** and **HP21** that ADMET model EP copolymers appear to conform to Eby's crystallization model which allows for the inclusion of methyl branch into the PE lattice—an important issue when attempting to utilize these materials as behavior models for randomly branched LLDPEs.

After having completed a battery of x-ray diffraction studies, attention was then directed towards the study of larger structural detail for **HP15** and **HP21** through the use of OM, TEM, electron diffraction, IR, and Raman Spectroscopy.

4.11.3 Optical Microscopy (OM) of **HP15** and **HP21**.

Sample preparation is an important consideration in microscopy, but it is not always a straightforward process for polymeric materials. In microscopy, a variety of solution crystallization methods have been employed to create suitable specimens.¹⁷⁴⁻¹⁷⁸ Definitely, the growth of a polymer single crystal from solution provides the most regular (perfected) structure for the morphological elucidation of any given material. Polymer single crystals may be found as faceted platelets of regular shape for polymers containing a low degree of imperfections; however, in contrast, the attempt to grow a single crystal for a macromolecule with a sizeable defect concentration inevitably leads to crystals with a less perfect microstructure. Although single crystals have been readily prepared for PE during cooling from dilute solutions,^{155-157,280-283} all attempts failed to grow single crystals for both ADMET model EP copolymers examined here.

ADMET model EP copolymers are very peculiar materials in relation to their solution properties. Normally, higher boiling solvents are required to dissolve and grow suitable x-ray quality crystals of ethylene-based materials (xylenes, chlorobenzenes, tetrachloroethylene, etc.). On the other hand, **HP15** and **HP21** are soluble at room temperature, or with slight heating, in most common organic solvents (chloroform, dichloromethane, tetrahydrofuran, hexanes, benzene, toluene, xylenes, etc.). Additionally, three good non-solvents were found to be methanol, isopropanol, and acetone. In order to form single crystals, a single solvent crystallization environment is most desirable, since a homogenous crystallization medium precludes any thermodynamic and entropic obstacles encountered during solvent mixing. The situation is highly complicated when a second solvent is introduced due to mixing problems and solubility differences that materials encounter during crystal growth from a heterogeneous medium.

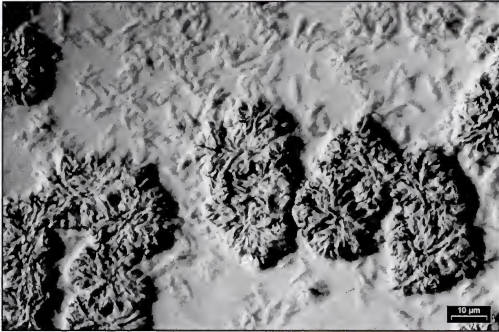


(a)

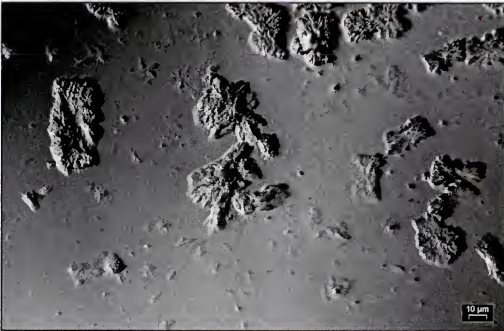


(b)

Figure 4-31. Representative optical microscopy images for **HP15** (image produced under reflected differential interference contrast, DIC); (a) objective = 100X, aperture = 0.9 (b) objective = 50X, aperture = 0.9 (in reflected light).



(a)



(b)

Figure 4-32. Representative optical microscopy images for **HP21** (image produced under differential interference contrast, DIC); (a) objective = 100X, aperture = 0.9 (b) objective = 50X, aperture = 0.9 (in reflected light).

The ability for **HP15** and **HP21** to dissolve in common solvents at room temperature allows easier transferal/handling when compared to other PEs of similar crystallinity. The lowered melting point is a definite contributing factor to the ease at which these materials are taken up into solution; however, there must also be a structural explanation as to why all attempts failed to produce single crystals. Additional discussion concerning this issue is presented below and in the sections detailing IR and Raman findings.

After attempts to grow single crystals proved for naught, suitable samples were prepared for OM by casting thin films onto a glass slide from a dilute solution of tetrachloroethylene at room temperature. Figures 4-31 and 4-32 depict representative OM images taken for **HP15** and **HP21**, respectively.

Figure 4-31 and 4-32 illustrate the predominant structural features observed for **HP15** and **HP21**. The two sets of images provide evidence for the occurrence of dendritic formations in both systems, a deviation from polyhedral growth. Dendrites are branched crystals that sometimes form tree-like shapes. The formation of dendrites here is a direct result of a perturbation in local concentration differences of the polymer in dilute solution. During crystal formation, the leading edge of the growth-plane experiences deviations in its concentration compared to the remainder of material in solution; and as a result of variations in local concentration, a temperature gradient ensues in an effort to disperse the superheating of crystals. A major influencing factor in the formation of concentration gradients is the rejection of defect or non-crystallizable species from the material in the quest to minimize the free energy of the system.

Both **HP15** and **HP21** contain a considerable amount of defects; so the formation of dendrites is a logical result for these materials. Although both materials crystallize to form dendrites, each polymer exhibits topological characteristics that are unique in regards to one another. Figure 4-31 illustrates that the typical shape of **HP15** is spheroidal or globular in appearance, while Figure 4-32 depicts a repeating rectangular structural feature for **HP21**. Without a doubt, this relative change in geometrical shape is a function of the defect content differences between the two materials.

A recent molecular modeling study may provide evidence for the topological differences observed here.²⁸⁴ In early 2002, Ze-sheng Li and coworkers published a molecular dynamics (MD) simulation that examined a series of single copolymer chains containing precisely controlled methyl branching [methyl was placed on every 10th, 14th, 16th, 22nd, 52nd, and 101st backbone carbon].²⁸⁴ They found that as the defect content is decreased, a more perfect lamellar structure is formed, and the crystallinity of the copolymer increases—both points have been confirmed by the calorimetric and diffraction data obtained for **HP15** and **HP21**.

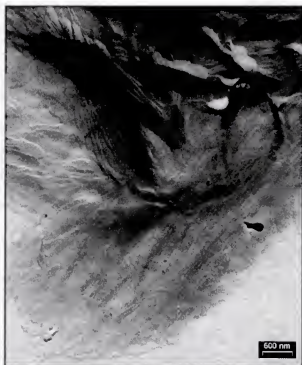
Most important was their discussion of chain morphology. The EP copolymer chain model with a methyl on every 10th branch collapsed from an extended-chain to a globular-shaped random coil containing many gauche conformations and chain kinks. This molecule was determined to be amorphous, but as the defect content was decreased, more regular zigzag (trans) segments were created, thereby, leading to more perfect lamellar structures. The MD models obtained for an EP copolymer chain with a methyl branch placed on every 14th carbon was found to collapse into a similar globular shape, while the material with a methyl every 22nd took on a more rectangular contour. It is

worthy to note that differences in the morphological shape of the models (methyl every 14th and 22nd) studied by Li, et al. because they bear an uncanny resemblance to the topological differences observed under the OM for **HP15** and **HP21**.

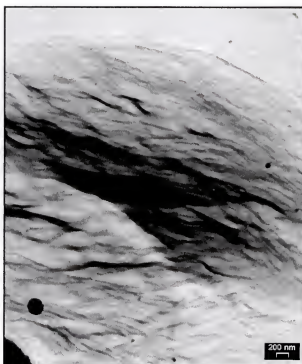
Further, the MD simulations found that a majority of methyl branches were located at the fold surfaces of the lamellae, especially in the materials containing a higher concentration of defects. This result is pertinent to the earlier discussion of dendrite formation and seems to suggest that **HP15** and **HP21s** relatively elevated defect content may be the principal factor causing the deviation from polyhedral crystal growth in these materials.

4.11.4 Transmission Electron Microscopy (TEM) and Electron (e-) Diffraction of HP15 and HP21.

Transmission electron microscopy is a powerful tool in the analysis of polymer morphology and offers superior resolution over images generated by OM. This image enhancement is demonstrated for model ADMET EP copolymers, **HP15** and **HP21**, in the exemplary graphic depictions given in Figures 4-33 and 4-34, respectively. The reader is reminded that neither ADMET EP model material afforded a single crystal. So, images shown here are the direct result of analysis on carbon—platinum (C—Pt) shadowed solution-grown crystals.^{177,178,285} TEM investigations were carried out in order to examine fine structure for ADMET EP copolymers with precise methyl branching; in particular, interest lay in whether or not any differences existed in the molecular ordering and orientation of these model systems.

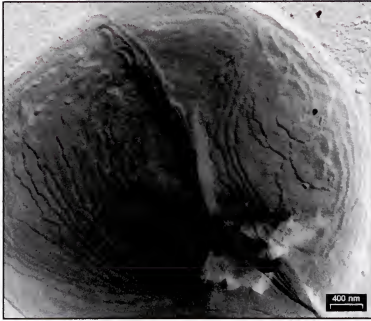


(a)

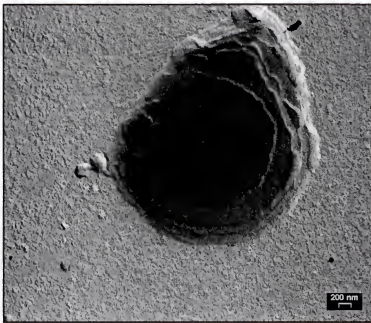


(b)

Figure 4-33. Representative transmission electron microscopy images for **HP15**.



(a)



(b)

Figure 4-34. Representative transmission electron microscopy images for **HP21**.

As found in OM, clear-cut differences exist in the TEM images obtained for **HP15** (Figure 4-33) and **HP21** (Figure 4-34). Images of **HP15** show visible signs of oriented

polymer chains; however, the stems do not seem to be organized into a cohesive pattern within a given area. One reason for the disorganization may have been caused by difficulties encountered during attempts to crystallize **HP15** from solution. On the other hand, the argument of defect content differences presented in the discussion of dendrite formation is the most probable explanation.

This viewpoint is substantiated from the results obtained for **HP21** (Figure 4-34). TEM images obtained for **HP21** indicate, without question, definitive evidence of chain-folded lamellae (Figure 4-34a). Moreover, Figure 4-34b illustrates direct proof that successive layers of lamellae are able to stack on top of one another, a result that follows the two-phase model for interactions between the crystalline and amorphous regions in a chain-folded material.

Figure 4-34a depicts the possible occurrence of a crystallization phenomenon known as twinning. Twinning describes the plane of symmetry encountered in Figure 4-34a if one bisects the chain-folded lamellae along the diagonal of the image. A twinned crystal is formed in a symmetrical fashion when two crystals are joined macroscopically along their respective growth faces to form a single entity. Thus, the twin contains an additional element of symmetry beyond that normally possessed by either of the individual components that make up the single substance. This phenomenon was first examined for polyethylene by electron diffraction in the late 1950s.^{286,287} The formation of twinned crystals during mechanical deformation, thermal treatment, phase transition, and crystal growth of PE has been studied by several authors.²⁸⁸ Although an interesting finding, the twinning encountered during the crystallization of **HP21** has not been studied further, mainly due to the lack of obtaining Miller indices for this material.



Figure 4-35. Representative electron diffraction image for ADMET model EP copolymer with precise methyl branching, **HP15**, produced under a tilt angle of approximately 36.5° θ at -130°C .

The electron diffraction images presented in Figure 4-35 (**HP15**) and Figure 4-36 (**HP21**) are the result of the inversion of dark field images. Even though single crystals were not available for analysis, replicated specimens of both materials did produce suitable diffraction patterns. Privy to the same scattering theories as x-ray diffraction, the use of e- diffraction enables the mapping of spatial frequencies within an object. However, because the electron has a small wavelength ($\lambda = 3.7\text{ pm}$), Bragg's law is only satisfied at very small angles of 2θ . This means that crystal lattice planes will only diffract if they are almost parallel to the incident electron beam, making the geometry of

an electron diffraction pattern easier to analyze than the equivalent x-ray diffraction blueprint. Thus, the geometry of a single pattern is enough to determine orientation or distinguish between different phases within the crystal.^{289,290} For an unknown material, it is possible to use the geometry of the diffraction pattern to determine both the unit cell identity as well as the symmetry elements associated for varying motifs within the crystal.²⁹¹

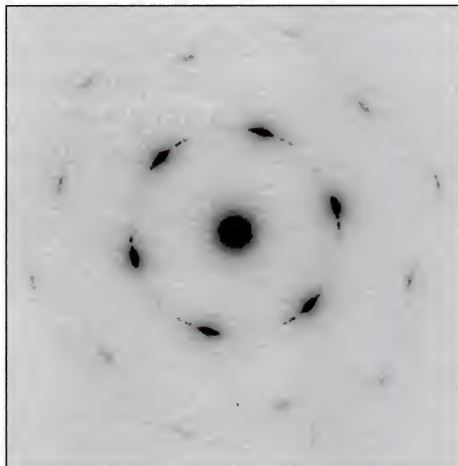


Figure 4-36. Representative electron diffraction image for ADMET model EP copolymer with precise methyl branching, **HP21**, produced under a tilt angle of approximately $0^\circ \theta$ at room temperature.

From e- diffraction, the unit cell for both **HP15** and **HP21** was determined to be pseudo-hexagonal. This was a surprising result when first obtained. As discussed in

Section 4.11.2, the occurrence of the hexagonal phase has only been observed after induced crystallization at higher pressures and/or the stretching of linear PE²⁵²⁻²⁷⁰ and ethylene/ α -olefin materials.^{202,210,249,250} By all accounts, this is the first documented occurrence of the hexagonal phase for an ethylene-based material crystallized at room temperature and pressure.

The presence of the hexagonal phase was quite fascinating, but there are additional features in Figure 4-35 and 4-36 that merit further attention. First is that the reflections generated in both patterns satisfy an even reflection selection rule [i.e. the sum of the Miller indices are even; $(1\ 1\ 0) = 2$; $(2\ 0\ 0) = 2$; and so on]. This means that the unit cell is centered and possesses a relatively high degree of symmetry.

Second, a number of additional reflections were observed for both **HP15** and **HP21**. These reflections convey information concerning the three-dimensional repeating distance of methyl groups within the lattice.

Third, for both materials, the lattice parameter cannot be defined in the c-dimension. From the measure of contour lengths in the e- diffraction imaging of both samples, it is suggested that chain axes cannot be defined in terms of a zigzag (trans) conformation of 2.54 Angströms. In other words, with the data obtained thus far, there are still many uncertainties as to the exact long-range dimensional order along the chain axes for both **HP15** and **HP21**; however, it has been established that each material chain packs in a pseudo-hexagonal arrangement within the crystal.

As described earlier, the hexagonal phase for PE-based materials has been described as being a crystal in a high state of conformational disorder (i.e. the so-called CONDIS crystal).^{260,261,271,272} This mesophase, as it is sometimes referred, mimics the

orientation and physical properties normally encountered at the boundary of a substance's transition from the solid to melt phase.

It is well understood that melting is a process that always leads to an increase in disorder, in other words, an increase in entropy. So how could **HP15** and **HP21** undergo any kind of spatial ordering while in the melt, as was postulated from x-ray diffraction results? A plausible explanation revolves around theories of defect incorporation. There are many point defects that can disrupt the crystallization of a molecule including branches, tie molecules, edge/screw dislocations, chain distortions, etc. When considering **HP15** and **HP21**, the two most likely contributions that may lead to defects within the crystal are not only the branches themselves but also distortions in the planar zigzag direction of the chain axes. The introduction of gauche conformations is by far the most common method for perturbations to occur along the chain axis (*c* direction in the unit cell). Common names for mistakes made along the polymer main chain include twists, kinks, knots, or jogs.

Contrary to chain-produced EP model materials with equivalent levels of random methyl branching, the precise methyl branch placement in **HP15** and **HP21** has allowed enough molecular symmetry in these LLDPE models to allow for an ordered unit cell to occur (*ab* dimension only). However, in an effort to minimize lattice energy associated with defect incorporation, multiple mistakes have been made in the chain axes (*c* dimension) during collapse of the random coil and/or extended chains of these materials during crystallization.

The argument for a CONDIS crystal best explains the ordered phases observed in the amorphous halo regions during temperature-resolved WAXD measurements for

HP15 and **HP21**. In particular, the deviation from an ideal zigzag chain conformation found by e- diffraction sheds light on the solution properties of ADMET EP model materials. For example, an elevated level of gauche conformations leads to kinks, twists, etc. along an individual chain axis, thereby affecting all the nearest neighbor chains in the molecule. The existence of a high degree of non-trans conformations was predicted by MD modeling on a series of EP copolymers with levels of precise methyl branching comparable to the ADMET models examined within this text. Without a doubt, this structural argument is the most likely explanation as to why all ADMET EP copolymers examined to date are soluble in a range of common organic solvents at room temperature. In light of this finding, additional structural information for **HP15** and **HP21** was gathered utilizing infrared (IR) and Raman Spectroscopy.

4.11.5 Raman and Infrared (IR) Spectroscopy of HP15 and HP21.

4.11.5.1 Raman spectroscopy

Raman scattering results from the same type of quantized vibrational changes that are associated with IR absorption. Indeed, Raman and IR absorption spectrum analyses performed on the same material often resemble one another quite closely. However enough differences exist in the IR and Raman activities to make the techniques complimentary rather than competitive. Over the years, numerous structural studies on *n*-paraffins, PE, and PE-based materials have been performed using Raman scattering,²⁹²⁻³⁰⁶ IR spectroscopy,³⁰⁷⁻³¹⁷ and combinations of the two.^{265,318,319} The subject matter treated in these studies has examined a variety of topics including the conformation, mobility, and chain-packing ability for the extended chain(s) of ethylene-based materials. In the search to obtain additional structural information for ADMET model EP copolymers, qualitative Raman and IR spectroscopy have been performed.

The structure of **HP15** and **HP21** is pseudo-hexagonal, a fact already determined by e- diffraction. While there have been a number of Raman absorption studies on the hexagonal phase of *n*-paraffins,^{304,319-325} few experimental investigations have thoroughly examined the hexagonal phase, or rotator phase as it is sometimes called, of PE-based materials.^{265,311,326-328} This is not surprising because of the difficulty of performing such experiments—for PE-based materials, the orthorhombic to hexagonal phase transition is affected only under conditions of drawing and/or high temperatures and pressures. Nonetheless, it is of interest to study such vibrational data in the hopes that it may provide concrete information regarding the conformational disorder of chain stems. Because the rotator phase exists at room temperature and pressure for **HP15** and **HP21**, these substances provide the first opportunity to study the hexagonal phase for an undrawn ethylene-based polymer at ambient conditions.

Upon first inspection of Figure 4-37 and Table 4-9, it is apparent that **HP15** and **HP21** exhibit similar vibration modes; yet, closer evaluation of the data provides a great deal of structural information for each polymer. The *C—H stretching region* for these materials exhibit two maxima at 2876 (**HP15** and **HP21**) and 2842 (**HP15**) to 2841 (**HP21**) wavenumbers. For crystalline alkanes, the asymmetric and symmetric C—H stretch for the orthorhombic and hexagonal phase have been shown to occur at 2882/2848 cm^{-1} and 2898/2850 cm^{-1} , respectively.³¹⁹ The difference between the fundamental C—H stretching frequencies for ADMET EP copolymer models and those normally found in the hexagonal phase is unclear here. This may be linked to the differing temperatures and pressures at which the 'hexagonal phase' measurements were taken, but more experiments will be required to ascertain the nature of this shift. The origin of the

frequency at 2717 cm^{-1} (HP15 and HP21) is unknown at this time; and no literature precedent has been found for this remarkable result.

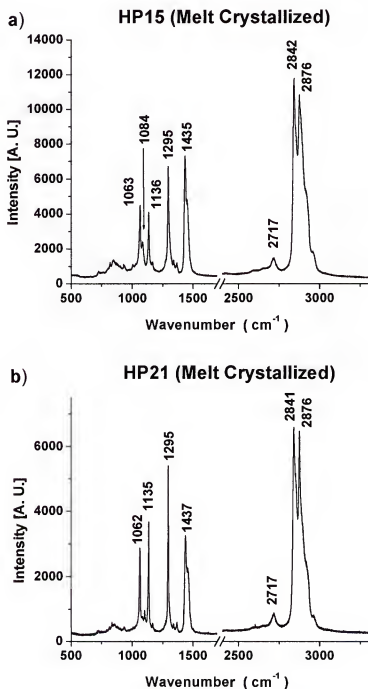


Figure 4-37. Raman spectral data for (a) HP15 (b) HP21. Samples crystallized from the melt and analyzed at room temperature.

Table 4-9. Raman Frequency Assignments for EP Copolymer Models with Precise Methyl Branching.

Polymer	Frequency	Vibration
	(cm ⁻¹)	Mode
HP15	2876	C—H asymmetric stretch
	2842	C—H symmetric stretch
	2717	?
	1435	CH ₂ —bending
	1295	CH ₂ —twisting
	1136	C—C asymmetric stretch
	1084	C—C gauche conformers
	1063	C—C symmetric stretch
HP21	2876	C—H asymmetric stretch
	2841	C—H symmetric stretch
	2717	?
	1437	CH ₂ —bending
	1295	CH ₂ —twisting
	1135	C—C asymmetric stretch
	1062	C—C symmetric stretch

The *CH₂-bending region* for PE has been thoroughly studied and oft used to study the nature of chain folding and molecular packing. Three bands at 1460, 1441, and 1417 cm⁻¹ are indicative of the orthorhombic unit cell—the two bands at 1460 and 1441 cm⁻¹

arise from Fermi-resonance,^{329,330} while the band at 1417 cm^{-1} is only characteristic of the orthorhombic unit cell (not seen in any other crystal form). However, the methylene bending region of the pseudo-hexagonal phase was shown to contain a single band at $1438\text{--}1440\text{ cm}^{-1}$.^{326,328} The bending region for **HP15** and **HP21** clearly shows a single band at 1435 and 1437 cm^{-1} , respectively, thus verifying the molecular packing result obtained by e- diffraction for these materials. The shift of 2 cm^{-1} between the two polymers may be the result of the differences in the sequence length between the methyl branches, but this is purely speculative at the moment.

The CH_2 -twisting region is not remarkable in its differences and the band at 1295 cm^{-1} is a typical feature in all Raman spectra for semicrystalline polyethylenes.

The C—C stretching region may offer the most specific information in regards to conformation of polyethylene-based materials. Normally, for orthorhombic PE, two narrow bands are shown at 1131 and 1063 cm^{-1} , which represents the asymmetric and symmetric stretching vibrations, respectively. This set of frequencies is characteristic of the trans zigzag conformation. The same two frequencies in the monoclinic phase of PE were determined to be 1136 and 1061 cm^{-1} . However, in the case of both the rotator phase and a semicrystalline PE in the melt, the Raman spectrum only yields a broad scattering region around 1080 cm^{-1} (*Note: these frequencies do not exist in a completely melted semicrystalline material, whereas they do exist, although depressed, in the pseudo-hexagonal phase*).^{319,328} The characteristic C—C stretches found for EP copolymers with precise methyl branching were $1136/1063\text{ cm}^{-1}$ for **HP15** and $1135/1062\text{ cm}^{-1}$ for **HP21**. The asymmetric stretch in both polymers relates more closely to that generated by the monoclinic cell of polyethylene, while the symmetric stretch is

comparable to either the monoclinic or orthorhombic unit cell. Further experiments are required to interpret the shift in the asymmetric stretch; however, it is highly likely that the cause is somehow related to a perturbation in the unit cell's *ab* dimension, as was postulated during the WAXD studies.

For either sample, the most interesting feature in the C—C stretching region is the spectral frequency at 1084 cm^{-1} in **HP15**. This broadened scattering peak has been previously been observed at 1080 cm^{-1} by several authors and unambiguously assigned as an amorphous-like area containing many gauche-conformers caused by supermolecular structural impact on the folding region.^{265,319,328} No presence of this vibration is found in the Raman spectra for **HP21**, an extremely significant result. The absence of this peak in **HP21** and the presence of it in **HP15** imply that the amorphous (or conformationally disordered gauche-conformer) content is higher in **HP15**, supporting observations/theories made during the diffraction and microscopy studies on these materials.

A short time ago, Kobayashi, et al. determined values for the methylene sequence lengths required to produce several Raman regularity-sensitive bands (Table 4-10) from the analysis of random copolymers of ethylene and deuterated ethylene.³³¹

Table 4-10. Methylene Sequence Length (n) Needed to Obtain Planar—Zigzag PE Chains.³³¹

Frequency (cm ⁻¹)	Vibration Mode	—(CH ₂) _n — # of methylenes (n)
2883	C—H asymmetric stretch	4-6
1295	CH ₂ —twisting	6
1130	C—C asymmetric stretch	18
1062	C—C symmetric stretch	6-8

Gauche bonds would be distributed along the entire macromolecular backbone of both **HP15** and **HP21**, unlike the majority surface distribution known to exist for the pseudo-hexagonal phase in *n*-paraffins. From Table 4-10, a minimum of six to eight sequential methylene units in an all trans-zigzag are required to produce the vibration at 1062 cm⁻¹. Both **HP15** and **HP21** show this characteristic vibration; therefore, both materials must contain sequences of at least 6-8 methylenes in a zigzag (trans) conformation. This is an exciting finding because it means that ADMET EP copolymer models contain significant order in a larger portion of methylene run-lengths than was initially thought. Nonetheless, as demonstrated by the vibration found at 1084 cm⁻¹ for **HP15**, there is still a large enough population of gauche-conformational defects (in **HP15** and to a lesser extent in **HP21**) to disrupt the crystal packing, thereby forcing these model materials to crystallize in a pseudo-hexagonal array of conformationally disordered parallel chains.

The Raman data gathered thus far on ADMET EP copolymer models has given a greater understanding into the nature of chain-packing and orientation for a polyethylene-based material containing precise methyl branches.

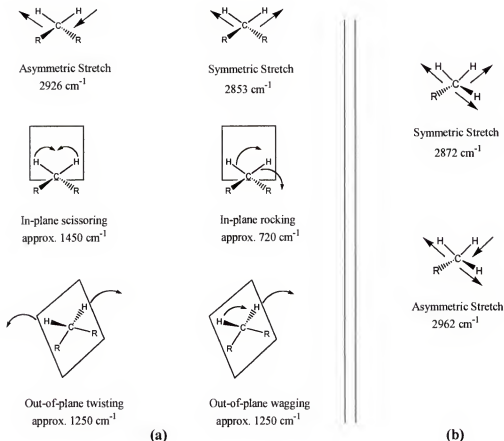


Figure 4-38. Examples of molecular vibrations encountered in the infrared absorption spectroscopy for simple hydrocarbon-based materials: (a) methylene modes (b) methyl group.

4.11.5.2 Infrared spectroscopy

Like Raman scattering, IR spectroscopy also provides detailed information regarding the fine structure of a purely hydrocarbon substrate, albeit by a different mechanism. Figure 4-38 illustrates typically observed fundamental vibration modes for purely aliphatic substances and is provided for readers who may not be familiar

with/recall the directional amplitudes for the twisting, scissoring, rocking, and wagging vibrations.

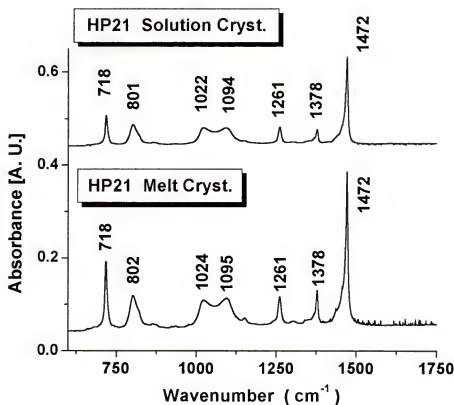


Figure 4-39. IR Spectroscopy of **HP21**—fingerprint region (700 to 1200 cm^{-1}) and beyond for solution crystallized material (top) and 2) melt crystallized material (bottom). All spectral data collection was performed at a resolution of 1 cm^{-1} .

Stacked interferograms are provided in Figure 4-39 (fingerprint region) and 4-40 (entire spectrum) for both the solution and melt crystallized thin films of **HP21**, while a complete listing of assignable vibrations is presented in Table 4-11. The analysis of solution versus melt crystallized material was done in order to investigate possible structural differences incurred during the chain packing of **HP21**. The treatment of **HP15** is omitted here, but the same absorption trends were observed in this material. As was previously performed for Raman data, the discussion of IR results is best broken down into the various regions of the spectrum.

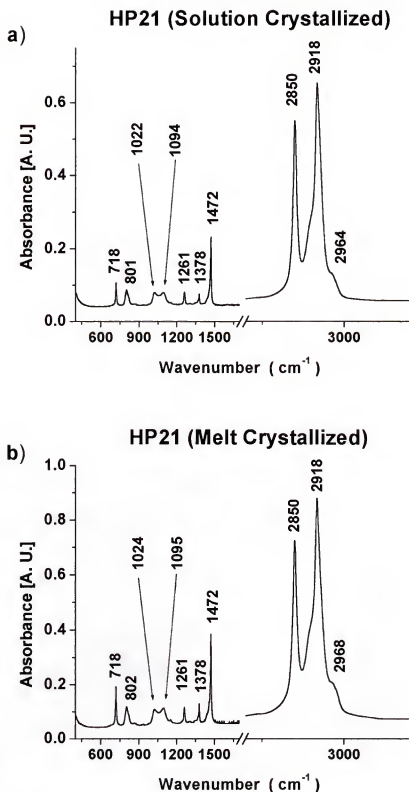


Figure 4-40. IR Spectroscopy of **HP21**—entire middle IR spectrum (600 to 4000 cm^{-1}) for (a) solution crystallized material and (b) melt crystallized material. All spectral data collection was performed at a resolution of 1 cm^{-1} .

Table 4-11. Infrared Frequency Assignments for Solution and Melt Crystallized EP Copolymer Models with Precise Methyl Branching.

Vibrational Frequency		Relative Intensity	Vibration Mode
Solution Cast Film (cm ⁻¹)	Melt Cast Film (cm ⁻¹)		
2964	2968	w (shoulder)	-CH ₃ asymmetric stretch
2918	2918	s	-CH ₂ - asymmetric stretch
2850	2850	s	-CH ₂ - symmetric stretch
1472	1472	s (singlet)	-CH ₂ - scissoring (i.e. bending)
1378	1378	m	-CH ₃ symmetrical bending
1349	1350	v. w (shoulder)	double gauche (TTGGTT)
1306	1304	v. w	kink (TTGTG*TT)
1261	1261	m	-CH ₂ - wagging
1153	1151	w (shoulder)	-CH ₂ - twisting/wagging (?)
1094	1095	m (broad)	-CH ₂ - twisting/rocking (??)
1022	1024	m (broad)	-CH ₂ - twisting/rocking (??)
867	867	w (shoulder)	-CH ₂ - rocking/twisting (??)
801	802	m (broad)	unknown rocking (???)
718	718	m—s (singlet)	-CH ₂ - rocking region (all methylenes rock in phase)

Where s = strong; m = medium; w = weak; v. w = very weak; T = trans conformation of 4 adjacent carbons; G = gauche conformation of 4 adjacent carbons; and the number of question marks (?) denotes the confidence level in assignment.

As in Raman scattering, the IR *C—H stretching region* is characteristic of two fundamental maxima that correspond to the methylene asymmetric and symmetric

stretches. For **HP21**, these maxima occur at 2918/2850 cm^{-1} for both solution and melt crystallized material. The presence of a shoulder evident at 2964 cm^{-1} (solution) and 2968 cm^{-1} (melt) in Figure 40a and 40b, respectively, corresponds to a methyl asymmetric stretch. There is a distinct difference in these two frequencies, but why? The most likely explanation concerns the differences in crystallization kinetic encountered during the solution versus melt crystallization of this material. Solution crystallization gives more opportunity for the realignment/reorganization of chain stems during the solidification of the material from solvent. Whereas during melt crystallization, the chain stems are much more sterically crowded (less degrees of freedom in the chain and/or an increase in free energy).

This is clearly evident by the observed increase of the methyl asymmetric stretch at 2964 cm^{-1} (solution) going to 2968 cm^{-1} (melt). In IR spectroscopy, an increase in wavenumber translates into an increase in energy; therefore, the methyl branches in the melt crystallized material lie at a higher energetic state than that encountered by solution crystallized material. This suggests that the methyl branches in the melt crystallized material are more sterically crowded in their local environment or that the chain defects are more pronounced around the methyl branch in the melt crystallized material. This finding is quite important and is evident in other regions of the spectrum, *vide infra*.

The *C—H bending region* for the orthorhombic phase would contain the same splitting of the methylene bending modes as observed in Raman scattering. So, for linear PE, two maxima at 1463 and 1471/1472 cm^{-1} arise from Davydov-splitting, which is typical for orthorhombic unit cells. The bending vibration at 1471/1472 cm^{-1} is only characteristic of the orthorhombic unit cell, present in *n*-paraffins or linear PE, and is

sometimes referred to as the crystalline band because of its use in PE percent crystallinity calculations by IR spectroscopy. Previous studies have shown a dramatic change in the methylene bending region during an orthorhombic to hexagonal phase change. Essentially, the Davydov-splitting of bands at 1463 and 1472 cm^{-1} is destroyed in favor of single band growth centered somewhere between 1466-1468 cm^{-1} , corresponding to the conformationally-disordered hexagonal rotator phase.^{265,319} As illustrated in Figure 4-39, **HP21** produces a single-peaked fundamental bending (scissoring) vibration at 1472 cm^{-1} , which indicates the presence of the pseudo-hexagonal phase. The increase in bending energy, when compared to values previously reported for the hexagonal phase of PE, is unclear at this time and requires further investigation.

The symmetrical deformation vibration for the methyl group is dominant in the bending region as well and shows up at 1378 cm^{-1} for **HP21**. This band has been investigated and used as a quantitative tool in the determination of short-chain branching in LLDPE;³¹⁴ however, special correction factors must be used in order to differentiate between methyl terminus short-chain branches and end-group methyls.³³²

The *C—H twisting/wagging region* (1180-1300 cm^{-1}) contains a considerable series of bands that are sometimes difficult to interpret due to the many overtones and overlapping frequencies encountered in this vicinity of the infrared spectrum. This area has been investigated quite well for *n*-paraffins³⁰⁷⁻³¹⁰ and has been shown to exhibit greatly reduced intensities when compared to the same area studied for long-chain fatty acids and/or other crystals containing long methylene sequences.^{333,334} Only one remarkable peak at 1261 cm^{-1} was observed for both solution and melt crystallized **HP21** (Figure 4-39) and has been assigned as the principle methylene wagging band. Further, a

weak shoulder present at 1153 (solution) to 1151 (melt) cm^{-1} was observed at the fringe of this region and tentatively assigned as a methylene twisting vibration; however, the possibility of this excitation arising from a wagging motion cannot be ruled out, hence the notation given in Table 4-11.

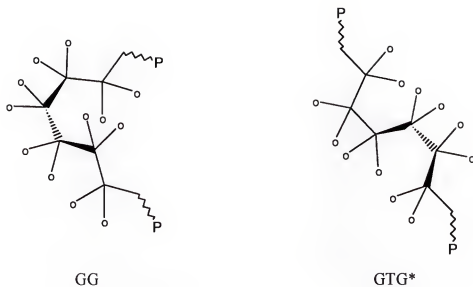
The *C—H twisting/rocking region* (700-1065 cm^{-1}) for **HP21** contains a great deal of structural information, some of which is unknown at this time because no precedence exists in the studies made on *n*-paraffins and other ethylene-based materials. For instance, two broad, overlapped peaks with medium intensity were found to have peaks at 1094/1022 cm^{-1} and 1095/1024 cm^{-1} for both solution and melt crystallized material. No literature precedence has been found for this particular overlap; hence, it must be assumed that the occurrence of this frequency phenomenon is the result of the precise methyl branching in these EP model materials. This is most likely the case for the broad, single-peaked absorption found at 801 (solution)/802 (melt) cm^{-1} as well; however, the exact mode or origin of this remarkable excitation is unknown. In addition, the precise origin of the weak shoulder found at 867 cm^{-1} is unknown at this time, but it could be assumed to arise from a predominately rocking motion due to its location in the interferogram.

In the methylene rocking region of **HP21**, the most dominant fundamental vibration is found as a singlet band at 718 cm^{-1} . Due to the interchain interactions found in linear alkanes and polyethylene alike, an orthorhombic lattice gives rise to a splitting pattern of slightly overlapped bands at 720 and 730 cm^{-1} . The band at 730 cm^{-1} is only found for the orthorhombic unit cell, while that at 720 cm^{-1} is characteristic of stem segments with both *trans* and *gauche* conformations. Deconvolution and integration of

these two bands is the common method by which to quantitatively determine the degree of crystallinity in an ethylene-based polymer by IR spectroscopy. During the orthorhombic to pseudo-hexagonal phase transition of PE, it has been demonstrated that this splitting pattern disappears in favor of a single-peaked band centered around 719-720 cm^{-1} for the rotator phase;²⁶⁵ therefore, using this analysis, the chain configuration for **HP21** has been assigned as the hexagonal rotator phase.

Sandwiched between the C—H wagging and bending regions are subtle absorptions which have been verified during *n*-alkane analysis^{320,321,324} but have only recently been studied in regards to polyethylene.²⁶⁵ During the analysis of *n*-paraffins, the weak shouldered band at 1352 cm^{-1} was found to correspond to a double gauche conformation (—TTGGTT—) within the chain, while the weak bands at 1366 and 1306 cm^{-1} were assigned to the kink structure (—TTGTG*TT—). Tashiro, et al. have verified these values as characteristic absorptions exhibited by the conformationally disordered hexagonal phase of PE.²⁶⁵ A pictorial representation of the double gauche and kink conformation is provided in Figure 4-41 (below).

As indicated in Table 11, absorptions were found at 1349-1350 cm^{-1} and at 1304-1306 cm^{-1} for **HP21**. Using the findings of Tashiro, et al.,²⁶⁵ these peaks have been unambiguously assigned as the double gauche and kink components arising in the disordered chain conformation regions of **HP21**. This is the first documented observance of these defect absorptions in a LLDPE. The infrared analysis is currently underway for a series of five ADMET EP copolymers with precise methyl branching as well as their randomly branched analogs (made by ADMET copolymerization of a methyl branched monomer with 1,9-decadiene) in order to further explore the ramifications of this finding.

1352 cm⁻¹ double gauche [...TGGT...]

1366, 1306 cm⁻¹ kink [...TGTG*T...]

(a)

(b)

Figure 4-41. Defect conformations: (a) double gauche, GG and (b) kink, GTG* defects with all trans (planar zigzag) polymer chains on either side.

4.12 Final Comments on the Structure of the Hexagonal Phase Determined for ADMET EP Copolymers Containing Precise Methyl Branching.

If the chain-flóded lamellae theory for the two-phase model given in Figure 4-15 is correct, then **HP15** and **HP21** would most closely follow Model A, which is based on the diffraction, microscopy, and spectroscopy findings presented herein. This model depicts methyl branch inclusion in both the amorphous and crystalline regions. An important factor considered in this chain-flóded surface model is based on the fact that the majority of stems take on a planar zigzag (all trans) conformation along the polymer chain axes. However, as detailed in this work, the actual structure of these materials is far more complicated than either of the two-phase models presented in Figure 4-15.

From the e-diffraction, infrared spectroscopy, and Raman spectroscopy, the structure of **HP15** and **HP21** may be considered to be the pseudo-hexagonal or conformationally-disordered (Condis) rotator phase. This is a significant finding since it is the first verified existence of this phase for an ethylene-based material without having first applied high pressures/temperatures to the sample and/or stretching the material prior to analysis.

The crystalline region of **HP15** and **HP21** can be considered to consist of parallel-packed conformationally disordered chains in which the trans-gauche conformations are distributed randomly throughout the stems; however, Raman spectroscopy findings suggest that both materials must contain a number of sequential sequences of at least 6-8 methylenes in a zigzag (trans) conformation distributed along the polymer backbone. Additionally, infrared analysis has indicated that a portion of the defect content in these materials has a kink or double gauche conformation; however, a quantitative assessment of total gauche defect content in these materials has not been attempted.

From differential scanning calorimetry, WAXD, and OM results, it may qualitatively be stated that **HP21** contains a higher percent crystallinity when compared to **HP15**; therefore, on this basis, it may be assumed that **HP21** most likely would have a decreased number of gauche conformational defects when compared to **HP15**.

The structural evidence presented here can also explain the unique solubility properties of these polymers when compared to normal PE-based materials (i.e. the elevated gauche content enables ADMET EP copolymer models to be soluble at room temperature in a variety of common organic solvents). This study has laid the groundwork for the further analysis of the effect precise branching has on the final

physical properties of an ethylene-*co*-propylene material. Future work in this area would benefit by the production of LLDPE models with lower defect contents (on the order of 12-15 branches per 1000 carbons) in order to better approximate industrially produced LLDPEs with random branching. Nonetheless, as hoped during the early stages of this project, it is apparent that the findings presented here have provided a basis for a better understanding of the morphology, crystalline structure, and crystallization process for the most abundant synthetic macromolecule in the world, polyethylene. As to what the future holds for this project...only time will tell.

CHAPTER 5
SYNTHESIS AND THERMAL BEHAVIOR OF A MODEL ETYLENE/BUTYLENE
COPOLYMER WITH PRECISE ETHYL BRANCH PLACEMENT

5.1 Introduction

Without question, ethylene-based macromolecules, both homo and copolymers, constitute the highest volume of synthetically produced polymers in world. The structural simplicity and industrial importance have led to these materials being some of the most thoroughly studied polymers on earth. Although such factors as mode of polymerization (radical, Ziegler-Natta, metallocene, etc.), catalyst choice, reaction temperature/pressure, and molar mass bare significant importance to the end product, the short-chain branching (SCB) content and its distribution are the most prominent factors in determining the final physical properties of ethylene/ α -olefin copolymers, commonly referred to a class of materials known as linear low density polyethylenes (LLDPEs).

Recently, we have discovered a way to obviate the random nature of branching in polyethylene. This has been accomplished using the clean, step polymerization chemistry offered by acyclic diene metathesis (ADMET). This mild chemistry avoids chain transfer and other catalyst mistakes encountered during chain propagation processes, thereby producing a branched polymer with a homogenous composition distribution.

A short time ago, we reported the synthesis and thermal behavior for a series of five model ethylene/propylene (EP) copolymers in which the methyl branch was precisely placed on each and every 9th, 11th, 15th, 19th, and 21st carbon along the backbone

respectively.²⁰ The general synthetic methodology used to accomplish this task is illustrated in Figure 5-1, where the pendant R group is equal to methyl.

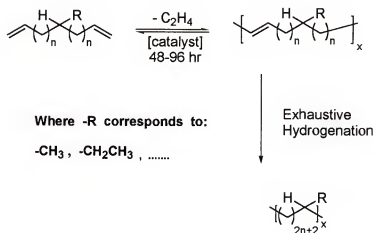


Figure 5-1. General scheme for the synthesis of precisely branched ethylene/ α -olefin copolymer models by ADMET.

The thermal behavior²⁰ and morphological analysis (see Chapter 4) for this series of EP copolymers have yielded fascinating results, and in an effort to extend our LLDPE structural library, a methodology was sought to lengthen the alkyl branch in these model materials (Figure 5-1, where R is equal to ethyl, propyl, etc.). We now report the successful synthesis of an α,ω -diene monomer in which the ethyl branch has been symmetrically substituted on the hydrocarbon backbone. The ADMET polymerization of this monomer and subsequent hydrogenation reaction has yielded the first ADMET model ethylene/butylene (EB) copolymer wherein the ethyl branch is placed on each and every 9th carbon along the backbone (see Figure 5-1, where R is equal to ethyl and Figure 5-2). Herein we present the monomer/polymer synthesis, characterization, and thermal analysis for this new LLDPE model material.

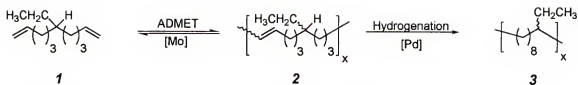


Figure 5-2. Synthesis of the first ADMET model ethylene/butylene (EB) copolymer.

5.2. Results and Discussion

5.2.1 Monomer Synthesis and Design

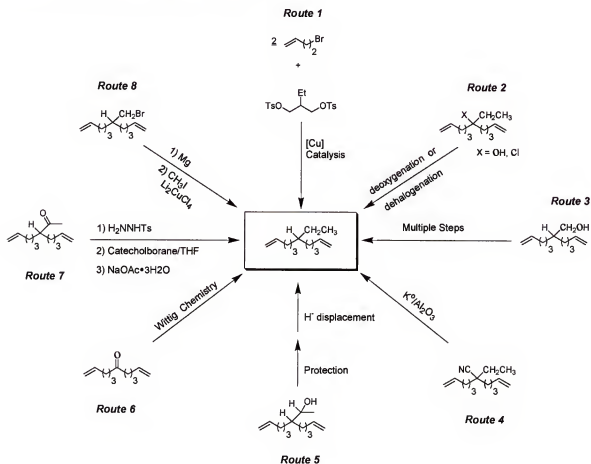


Figure 5-3. Synthetic pathways attempted to reach the target symmetrical α,ω -diene monomer with symmetrical ethyl branch placement. *Route 1*: Copper mediated coupling of a tosylate and Grignard reagent [ref 335]. *Route 2*: Deoxygenation of a secondary alcohol [ref 336] or dehalogenation of a secondary chloride [ref 337]. *Route 3*: Several coupling methods were attempted [ref 335, 338]. *Route 4*: Decyanation reaction affected by a potassium on alumina dispersion [ref 339]. *Route 5*: Hydride displacement of a secondary tosylate/mesilate ligand [ref 340]. *Route 6*: Wittig reaction of a primary ylide to a secondary ketone [ref 341]. *Route 7*: A modified Wolff-Kishner reduction of the tosyl hydrazone [ref 342]. *Route 8*: Coupling of a Grignard and a primary alkyl iodide through copper mediation [ref 338].

A great deal of effort went into formulating a synthetic pathway that would successfully extend the "R-group" in Figure 5-1 from a methyl²⁰ to an ethyl branch.

As illustrated Figure 5-3, several methodologies were investigated in pursuit of synthesizing the target monomer, 6-ethyl-1,10-undecadiene, depicted in the center of Figure 5-3. To date, Route 5 has been the only synthetic pathway that has proven useful in this regard. This success stems from using a modified acetoacetate-based route, which is a process similar to the synthetic pathway used to create the analogous series of methyl-branched monomers; albeit, there have been two significant modifications made to the procedure. The first successful synthetic strategy to produce an α,ω -diene monomer with a symmetrically substituted ethyl branch is presented in Figure 5-4.

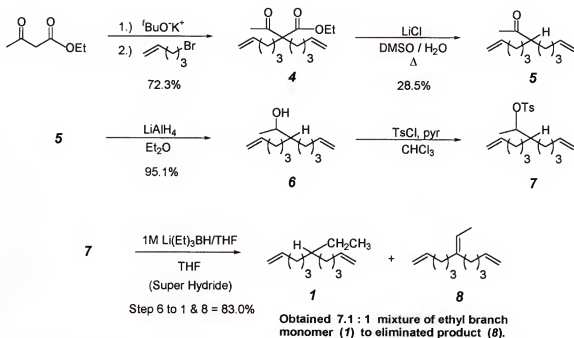


Figure 5.4. Synthesis of an ADMET α,ω -diene monomer with a symmetrically placed ethyl branch [All yields are reported as isolated percentages].

Ethyl acetoacetate is deprotonated with base and readily effects the $\text{S}_{\text{N}}2$ displacement of bromide upon addition of 5-bromo-1-pentene. Subsequently, in the same

pot, the reaction of the monosubstituted product with a second equivalent of base and alkenyl halide affords the disubstituted β -keto ester (**4**). Compound **4** is successfully decarboxylated using a dimethylsulfoxide (DMSO)/water/salt mixture³⁴³ to yield an α,ω -diene with a methyl ketone pendant group that is symmetrically substituted along the monomer backbone (**5**). Reduction using lithium aluminum hydride yields the secondary alcohol (**6**), which is tosylated (**7**) and finally reduced via Super Hydride displacement³⁴⁴ to yield a mixture of the symmetrical diene of interest (**1**) and eliminated by-product (**8**).

Although monomer was successfully produced by the method given in Figure 5-4, two difficulties were encountered during the development of this synthetic blueprint that requires further attention. The first complications arose during attempts to decarboxylate compound **4**. The conditions utilized in this conversion were modified from the work of Krapcho, et al.³⁴³

The mechanism for decarboxylation of the ethyl ester is thought to first proceed to the acid (Figure 5-5, D) and then through a six-center transition state to give the enol (Figure 5-5, E), which immediately undergoes tautomerization to yield the keto product (Figure 5-5, F).³⁴⁵ Normally, this organic transformation is accomplished by heating the substrate in an aqueous acid-containing medium; however, Krapcho's method was utilized because decarboxylation is accomplished under mild, neutral conditions. This approach obviates unwanted side reactions such as acyl group cleavage and/or acid addition to the alkene. Therefore, the continuity of the terminal olefins is preserved in the desired monomer, which is a key factor in the ultimate success of the ADMET reaction.

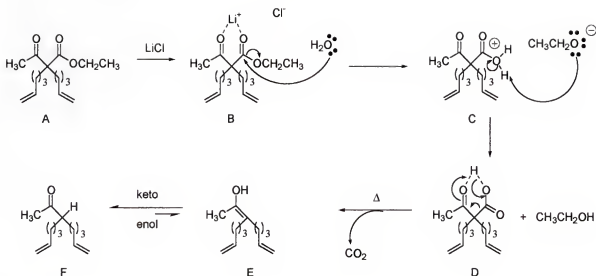


Figure 5-5. Mechanism for the decarboxylation of compound 4.

A great deal of effort focused on the optimization of reaction conditions for the decarboxylation step. Table 5-1 furnishes the yields of **5** in relation to the various times, temperatures, and equivalents of LiCl /water used for a number of representative reactions investigated during this study. The results in Table 5-1 reveal that the reaction occurs more readily when employing either a) large initial equivalents of LiCl /water while maintaining the reaction temperature at approximately 149-150 °C or b) 3 equivalents of LiCl /water while maintaining an approximate reaction temperature of 160-170 °C.

The sensitivity of this reaction cannot be stressed enough. For example, the slightest deviation in reaction temperature (± 5 °C) beyond or below the window of the conditions listed above resulted in either the full recovery of starting material (**4**) at lower temperatures or complete decomposition of all material at the higher temperatures (Table 5-1, entry number 3). By far, this reaction is the bottleneck of the five-step synthesis given in Figure 5-4; and current research is underway in the hopes to either further optimize this reaction or to abandon altogether the 5-step process presented here in favor of a completely different/higher yielding synthetic approach.

Table 5-1. Decarboxylation of Compound 4 to Yield 5: Representative Optimization Reactions.

rxn #	equiv. LiCl	equiv. H ₂ O	time hours	rxn temp. (°C)	% conv. ^a	rxn appearance remarks/changes
1	2	2	16	149	20	clear to yellow/brown
	4	4	36	149	68	no change
	4	4	63	149	82	orange/brown
	4	4	88	149	91	orange-brown/auburn
2	20	20	120	149-152	90	orange/brown
3 ^b	20	20	120	170-184	--	dark brown solution w/solid gel
4	1.1	1.1	0	0	0	clear, colorless
			2	97	0	clear, colorless
			17	99	0	clear to yellow/brown
			89	118	7	yellow/brown
			96	130	6-7	yellow/brown
	2	2	112	137	10	yellow/brown
			139	135	25	yellow/brown
			166	153	38	yellow/orange
			243	172	78	yellow/orange

Table 5-1. Continued.

rxn #	equiv. LiCl	equiv. H ₂ O	time hours	rxn temp. (°C)	% conv. ^a	rxn appearance remarks/changes
5	3	3	16	168	76	clear to yellow/brown
			40	170	86	clear to yellow/orange
			47	170	86	clear to yellow/orange
6	1.1	1.1	21	152	--	clear to light brown
			45	164	63	clear to yellow/orange
			53	164	71	clear to yellow/orange
	2	2	125	156	78	yellow/orange
			149	156	82	yellow/orange

^a The percent conversion as determined by GC relative to peak of starting material (4).

^b Complete decomposition without reclaim of any starting material.

The second complication in this synthesis surfaced during the transformation of the secondary tosylate (compound 7, Figure 5-4) to the desired ethyl-branched α,ω -diene of interest, 1. The reaction was first performed with lithium aluminum hydride in diethyl ether (Et₂O) as the reducing agent. Workup of this reaction yielded not only the desired ethyl-branched diene (1) but also the undesired elimination product, 8. Fortunately, the separation of the two products is easily affected by flash column chromatography in pure hexanes; however, upon purification, it was found that the ratio of eliminated (8) to ethyl-branched (1) monomer was approximately 3:2, which is not highly unfavorable when seeking gram quantities of material—as we were in this instance. Therefore, a method was sought to either completely circumvent or suppress the evolution of eliminated side

product, **8**, during the reduction of the tosylate. In the hope to improve upon our initial result, a series of scout reactions were performed using a variety of reducing agents and solvent combinations, results of which are presented in Table 5-2.

Table 5-2. Reduction of the Secondary Tosylate (**4**) to Ethyl-Branched (**1**) and Eliminated (**8**) Monomers with Various Hydride Reducing Agents.

Reagent ^a		% 1	% 8
(1M solution)	solvent	(by GC)	(by GC)
LiAlH ₄ /Et ₂ O ^b	Et ₂ O	42	58
LiAlH ₄ /Et ₂ O	Et ₂ O	40	60
LiAlH ₄ /Et ₂ O	THF	0 ^c	0 ^c
LiAlH ₄ /THF	THF	0 ^c	0 ^c
Li(<i>sec</i> -Bu) ₃ BH/THF	Et ₂ O	41	59
Li(Et) ₃ BH/THF	Et ₂ O	0 ^c	0 ^c
Li(<i>sec</i> -Bu) ₃ BH/THF	THF	38	62
Li(Et) ₃ BH/THF	THF	86	14

^a All reactions conducted at room temperature except entry 1. ^b Reaction ran under reflux conditions. ^c No product was detected by GC or NMR analysis.

As shown in Table 5-2, the reduction of **4** to yield the desired ethyl-branched monomer, **1**, is most effective when using Li(Et)₃BH as the reducing agent and THF as the solvating medium. This reducing agent, coined a Super Hydride, was first employed by H.C. Brown and coworkers in the deoxygenation of cyclic and acyclic alcohols in the late 1970s.³⁴⁴

No attempts have been made to optimize this reaction further, and as mentioned previously, the unwanted eliminated side-product, **8**, is easily separated from the ethyl-branched monomer, **1**, by utilizing flash column chromatography.

5.2.2 Continuing Research in Regard to Ethyl Monomer Synthesis

Thus far, Route 5 (Figure 5-4) has been the sole successful synthetic pathway used to produce the ethyl branch monomer; however, current research is still centered on exploring Routes 4 and 6 as viable candidates to produce the desired ethyl-branched dienes. In particular, attention will be given to Route 4, involving decyanation chemistry, in the following discussion (Figure 5-6, below).

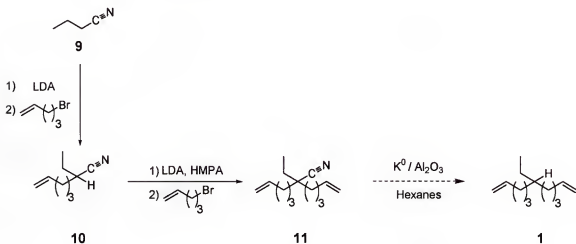


Figure 5-6. Ethyl monomer synthesis via decyanation chemistry; LDA (lithium diisopropyl amide) and HMPA (hexamethylphosphoramide).

If successful, this synthetic process offers important advantages over the ethyl acetoacetate-based route given earlier. First, the steps required for overall monomer synthesis would be reduced from a total of five to only three. Also, the starting nitrile, **9**, and its longer alkyl analogs are all inexpensive, readily available materials. This is important because the availability of longer alkyl nitriles lends well to the future

synthesis of longer-branched monomers (i.e. propyl, butyl, hexyl, etc.) if this synthetic methodology proves feasible.

The alkylation of **9** is readily accomplished by deprotonation at the alpha carbon by lithium diisopropyl amide (LDA) and subsequent reaction with 5-bromo-1-pentene. The monoalkylated nitrile is then isolated and purified before proceeding to the next reaction. The conversion of **10** to **11** proved more difficult. After the addition of LDA to **10**, a white salt immediately began to precipitate from solution, a point not encountered previously in the literature.³³⁹ However, the addition of a small amount of HMPA dissipated the salt formation and allowed for the successful completion of the reaction to yield compound **11**.

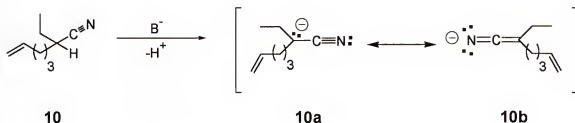


Figure 5-7. Possible resonance structures for anion formation in compound **10**.

It is thought that the complexation of lithium cations to nitrile salts led to the salt formation. Figure 5-7 depicts the possible resonance structures after deprotonation of **10**. It is thought that compound **10b** is the most likely candidate for the observed salt formation.

After the successful synthesis and purification of compound **11**, attention was turned towards the decyanation reaction that would yield the desired ethyl-branched diene (**1**). However, the desired product was not obtained in this instance.

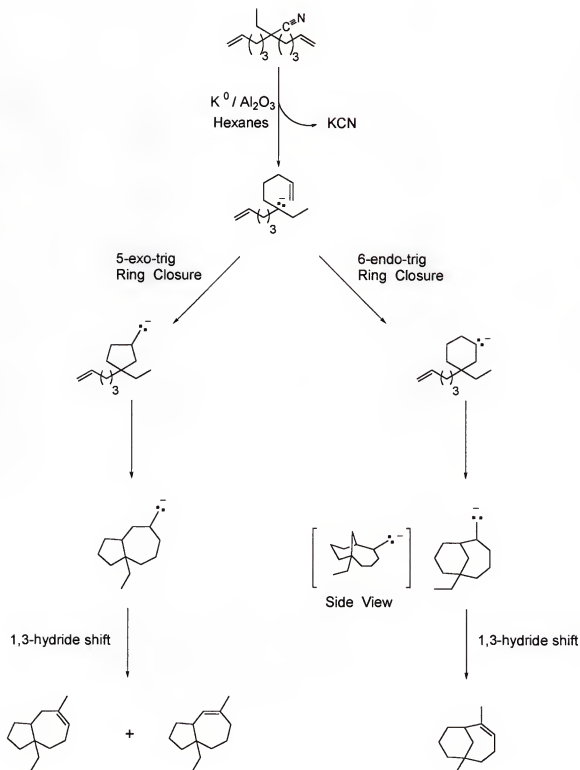


Figure 5-8. Proposed ring closing mechanism for the decyanation reaction of 11.

Figure 5-8 depicts a proposed mechanism for what may have actually occurred during the attempted conversion of **11** to **1**. The decyanation reaction is thought to occur by an anionic mechanism; therefore, the possibility exists for the anion to take part in ring closure to form the stable five-membered ring before it can be quenched.

Following workup, ^1H and ^{13}C NMR analysis indicated that only internal olefin was present in what appeared to be a mixture of products. Further, gas chromatography (GC) and thin-layer chromatography results suggested the presence of three distinct products. These findings suggest that a double ring closure occurs to yield the three bicyclic rings illustrated in Figure 5-8. In order to substantiate this mechanism, attempts are currently underway to purify the product mixture obtained during the decyanation of monomer **11**.

Even though the reaction failed to produce the desired monomer, it is still felt that this methodology requires further exploration as a viable candidate to produce a plethora of alkyl-branched α,ω -diene monomers. With regards to the conversion of monomer **11** to **1**, the result may be improved if lower reaction temperature and reduced times of reaction are used in the attempt to sway the kinetics of reaction away from ring closure.

However, the problem may exist in the length of the alkenyl branch itself. Perhaps the use of this methodology would require the distance between the anion formation and terminal olefins consist of more than 6 carbons, thereby avoiding favorable ring closure conditions. Regardless, it is felt that further research is required in this area before this methodology is abandoned as a viable route to a series of ethyl-branched monomers and beyond (i.e. propyl, butyl, pentyl, hexyl, etc.).

5.2.3. ADMET Polymerization and Hydrogenation Chemistry

Monomer **1** was exposed to Schrock's catalyst⁷ under mild ADMET step polymerization conditions (see Figure 5-2). The chemistry proceeds cleanly to yield a linear, unsaturated polymer (Figure 5-2, **2**) that is comprised of only one type of repeat unit plus the usual amount of cyclics (<1-2%) found in bulk polycondensation conversions. Exhaustive hydrogenation of unsaturated prepolymer was accomplished using palladium on carbon (10 wt% Pd/C) as the method of choice, leading to creation of an ethylene-based material with an ethyl branch precisely placed on each and every 9th backbone carbon, **3**. This is the first example of an ADMET model EB copolymer. No side reactions are detectable by TLC, NMR. Complete hydrogenation has been verified by both infrared (IR) spectroscopy and NMR analysis.

5.2.4. Molecular Weight Analysis

Table 5-3. Molecular Weight Data for Unsaturated and Saturated Ethyl Branched ADMET Polyethylene Polymers

polymer	\overline{M}_n ^a	polydispersity
	(grams/mole)	index (PDI) ^a
2 (unsaturated)	31 400	1.83
3 (saturated)	32 600	1.78

^a Molecular weight data obtained in THF and is relative to polystyrene standards.

Table 5-3 confirms that the hydrogenation process does not alter the molecular weight of the unsaturated polymers in this study, which is an observation consistent with our earlier experiments.^{20,23,39} For both the unsaturated and saturated polymers, the polydispersities are somewhat more narrow than the typical step polymerization value of

2.0. This is a direct consequence of the small degree of fractionation that takes place during precipitation of these materials prior to GPC analysis. As previously discussed for EP copolymer models,²⁰ this ADMET model EB copolymer exhibits a molecular weight and polydispersity index within a sufficient range to make it an excellent model for commercial grades of LLDPE produced via metallocene catalysis.

5.2.5. Structural Determination Data

Figure 5-9 shows the ¹H NMR spectra for the conversion of monomer, **1**, to unsaturated polymer, **2**, and then on to the fully saturated ADMET model EB copolymer possessing an ethyl branch on every 9th carbon, **3**. The conversion of terminal alkene peaks at 4.96 and 5.81 ppm in monomer (Figure 5-9a) to growth of a single internal alkene resonance at 5.40 ppm in the unsaturated polymer (Figure 5-9b) gives clear indication that the ADMET reaction has taken place, and the absence of visible end-groups implies that high polymer has been obtained—a result consistent with the GPC results given earlier. Subsequently, the internal olefin resonance at 5.40 ppm (Figure 5-9b) completely vanishes upon exhaustive hydrogenation of the double bonds. In a like manner when going from Figure 5-10b to 5-10c in the ¹³C NMR spectra, the disappearance of unsaturated olefin resonances at 130.62 ppm (trans) and 130.15 ppm (cis) further substantiates the success of exhaustive hydrogenation to produce the desired model EB copolymer. The clean nature and clear transformation processes depicted in the spectra are typical for all ADMET model LLDPEs synthesized thus far²⁰ and illustrate the level of structural control that is possible when utilizing step condensation chemistry as the choice method to model ethylene-*co*-alpha-olefin systems.

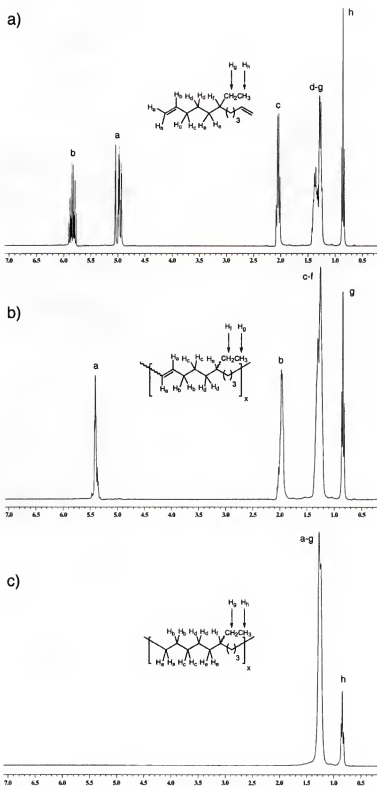


Figure 5-9. ^1H NMR: (a) monomer, **1**; (b) unsaturated polymer, **2**; (c) saturated polymer, **3**.

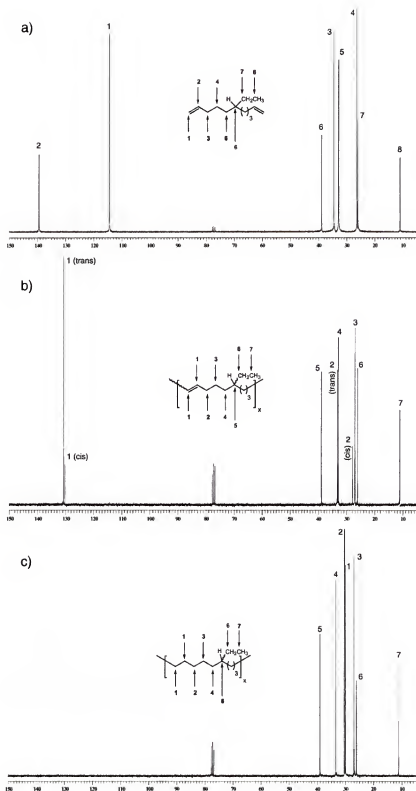


Figure 5-10. ^{13}C NMR: (a) monomer, 1; (b) unsaturated polymer, 2; (c) saturated polymer, 3.

Moreover, the ^{13}C NMR spectra in Figure 5-10c reveals that there are seven distinct sp^3 carbon signals present in the fully saturated ADMET model EB copolymer. The chemical shifts observed for polymer 3 are 11.12, 26.12, 39.09, 30.01, 30.43, 26.99, and 33.45 ppm, values that are in very good agreement with experimental³⁴⁶ and predicted values.³⁴⁷ For comparison, a table of calculated and observed values for ethyl branches in polyethylene is provided in Table 5-4. However, in order to simplify the discussion, the individual carbons in the polymer repeat unit will be labeled based on a modified version of nomenclature defined by Randall.³⁴⁸

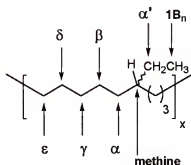


Figure 5-11. Generalized nomenclature for ^{13}C NMR analysis of branched polyethylenes.

Table 5-4 provides an interesting comparison of the various chemical shift values for the repeat unit given in Figure 5-11. Although the chemical shifts of the ADMET model EB copolymer coincide very well with all of the values presented in Table 5-4, the ADMET model correlates most closely with that of the experimental data presented by Rinaldi. It is interesting that Rinaldi's chemical shift values were generated on the highest field NMR of all data presented in Table 5-4. This suggests that ADMET model LLDPEs, in conjunction with high field NMR experiments, could be used to derive new and improved mathematical parameters in the structural study of branched polyethylenes.

To be sure, the precisely-branched ADMET PEs, synthesized thus far, offer a tremendous potential to study/model the exact impact a short-chain branch and its distribution have on the final structure-property relationships in ethylene-based materials. And nowhere is this more evident than in the NMR results presented here.

Table 5-4. Observed and Calculated Chemical Shifts for an ADMET Model EB Copolymer with an Ethyl Branch on Every 9th Carbon.

	ADMET EB	exp	exp	calcd	calcd
carbon	copolymer ^a	Rinaldi ^b	Mandelkern ^c	G-P ^d	L-A ^e
α	33.45	34.15	34.26	34.33	34.30
β	26.99	27.36		28.16	28.10
γ	30.43	30.49		30.34	30.30
δ	30.01	30.00		29.92	29.90
methine	39.09	39.79	39.86	37.77	37.70
α'	26.12	26.80	27.15	27.42	27.40
1B_n	11.12	11.16	10.94	11.33	11.40

^a Data obtained in this study; spectra taken in CHCl₃ on a 75 MHz Varian Associates 300 spectrometer. ^b [See ref 346a] Data obtained from commercial LLDPE samples; spectra taken in a 40% benzene-d₆/60% 1,2,4-trichlorobenzene mixture on a 188.6 MHz Varian Unityplus 750 MHz spectrometer. ^c [See ref 346b] Data obtained from commercial LDPE samples; spectra taken in 1,2,4-trichlorobenzene on a 67.905 MHz Bruker-HX-270 spectrometer. ^d [See ref 347a] Calculated values based on the work of Grant and Paul. ^e [See ref 347b] Calculated values based on the work of Lindeman and Adams.

While there are several analytical techniques to examine successful hydrogenation (¹H NMR, ¹³C NMR, bromine uptake, and IR), IR spectroscopy offers the most sensitive method to observe whether or not exhaustive hydrogenation has occurred. Analogous to the NMR comparisons presented earlier, Figure 5-12 illustrates the conversion of

The sharp peaks at 1380 cm^{-1} (unsaturated) and 1379 cm^{-1} (saturated) correspond to the symmetrical methyl bend. Several differences are immediately apparent. In going from unsaturated to saturated polymer, the internal olefin's characteristic out-of-plane (oop) C—H bending vibration (966 cm^{-1}) completely disappears, thereby signifying the successful completion of the hydrogenation reaction. Contrary to this is the appearance of many more characteristic absorptions in the saturated polymer. A plausible explanation is that the hydrogenated polymer perhaps has a decreased number of conformational defects along the chain stems (no cis/trans issues), thereby producing a more ordered material. A higher level of structural order could lead to the observed increase in vibration frequencies; however, this phenomenon was not observed in the series of EP copolymers produced earlier, at least to this noticeable extent. The exact reasons for this anomaly are unclear at this time; however, a detailed IR study for a series of melt and solution crystallized ADMET LLDPEs is currently underway in the hopes of deducing these structural differences.

As previously discussed (Chapter 4), Tashiro et al. carried out a detailed study on the IR response of differing polyethylene crystal structures. They concluded that a single-peaked scissoring vibration at 1466 cm^{-1} in combination with a single-peaked rocking absorption at 721 cm^{-1} was indicative of the pseudo-hexagonal structure for polyethylene.²⁶⁵ In Figure 5-12b, the saturated ADMET EB copolymer model (3) clearly exhibits the characteristic shapes and absorption values (two single peaks at 1462 and 721 cm^{-1}) which point to it having a pseudo-hexagonal packing structure. The pseudo-hexagonal, or rotator phase as it is sometimes called, lies somewhere on the periphery of the melt and solid phase; therefore, a strict determination of the ability (or inability) of

hydrogenated polymer 3 to crystallize cannot be based on IR information alone. In order to delineate this problem further, the thermal behavior of these materials must be explored.

5.2.6. Thermal Analysis

A number of thermal behavior studies have been performed on commercial EB copolymers containing a statistical distribution of ethyl branches.^{88,349} Similar to the results obtained for EP copolymers, studies on randomly-branched EB copolymer systems have shown that the density, enthalpy, degree of crystallinity, and peak melting/crystallization points all decrease as the amount of defect content (ethyl branches) is increased.

Like EP copolymers, the melting behavior of EB systems is influenced by the amount of short-chain branching (SCB); however, the SCB distribution (SCBD) is by far the more determinate factor on the final physical properties of a given material. An especially difficult problem arises during modeling studies on ethylene-based polymers due to the compositional heterogeneity normally encountered for these statistically branched materials. Elaborate precautions are required to synthesize materials that approach a uniform composition, and detailed physical characterization studies are required to confirm the existence of a well-defined material. Without definitive knowledge of the distinct polymer architecture in a given material, any theoretical interpretation concerning the final structure-property relationship dependence on defect content and distribution is severely compromised. This is a major advantage in ADMET EB copolymers because they are well-defined materials with a homogenous distribution of defects along the backbone, thereby making them excellent substances with which to

model the effect that SCB and SCBD have on the final materials response of ethylene-based materials.

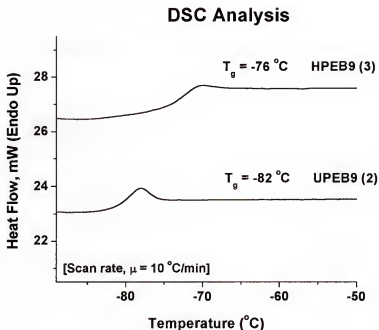


Figure 5-13. DSC comparison of unsaturated polymer (2) to fully hydrogenated EB copolymer model (3). Relaxations are given as onset glass transition values.

In Figure 5-13, a calorimetric comparison is depicted for the unsaturated (2) versus fully saturated polymer (3). Both materials possess a precise ethyl branch distribution along the hydrocarbon backbone; however, the relaxation onset of the hydrogenated polymer ($-76\text{ }^{\circ}\text{C}$) is a full six degrees higher than its unsaturated counterpart ($-82\text{ }^{\circ}\text{C}$), a direct result of the conformational disordering caused by the random distribution of cis/trans olefins. Due to their hybridization and energetic differences, points of unsaturation are more easily unlocked from a rigid state than their fully saturated counterparts.

It is worthy to note that neither material showed any sign of melting in the range studied here (-95 to $140\text{ }^{\circ}\text{C}$). Previously, model EB copolymers, made from

hydrogenated poly(butadienes), have exhibited ill-defined melts for branch contents as high as 106 ethyls/1000 carbons.^{349f} In contrast, the ADMET model EB copolymer (3) possessing 111 ethyls/1000 carbons studied here shows no detectable melting point. Therefore, it can be assumed that this material (**HPEB9**) is completely amorphous, an interesting result when compared to the thermal behavior exhibited by the ADMET model EP copolymer (**HPEP9**) with the same branch content (Figure 5-14).

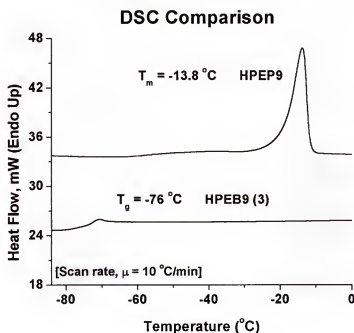


Figure 5-14. DSC comparison of 1) **HPEP9**: ADMET model ethylene/propylene copolymer with a methyl on each and every 9th carbon and 2) **HPEB9**: ADMET model ethylene/butylene copolymer with an ethyl on each and every 9th carbon.

The only viable explanation of this result is that methyl branches are readily incorporated into the crystal lattice, whereas the steric demands of the ethyl branch preclude its ability to take part in the crystallization process at this level of precise branch distribution. In this light, it has been shown that approximately 95% of the ethyl branches are excluded from the crystalline region in statistically branched EB

copolymers.^{349d} This may give insight into the differences observed in the thermal behavior of the statistically branched EB copolymer with 106 ethyls/1000 carbons and the ADMET EB copolymer (111 ethyls/1000 carbons) model studied here. The plausible explanation centers on the SCBD differences in these materials. Although care is taken during the creation of ideal random EB copolymers, slight differences in either monomer reactivity and/or polymerization conditions allows the evolution of a substantial amount of methylene sequence lengths (MSLs) to be present in these materials. These regions are devoid of branching and allow crystallization to take place in much the same manner as in linear polyethylene, but only to a lesser degree. However, ADMET model EB materials possess the same MSL between every ethyl branch, and it is evident from the thermal behavior results obtained here that a MSL of eight carbons between ethyl branches is not sufficient enough to allow this material to crystallize. These findings are quite interesting and merit further exploration.

5.3. Conclusions

The synthetic methodology to produce the first α,ω -diene monomer possessing a symmetrically substituted ethyl branch (**1**) has been disclosed. The ADMET polymerization and subsequent exhaustive hydrogenation of this substrate has created the first ADMET model ethylene/butylene (EB) copolymer wherein there is placed an ethyl branch on each and every 9th carbon along the hydrocarbon backbone (**3**). Both NMR and IR spectroscopy have been utilized to verify the structure of this new ethylene-based polymer.

Calorimetric analysis has shown that **3** is a completely amorphous material with a glass transition of -76 °C. This result lies in stark contrast to the semicrystalline nature

exhibited by its sister ADMET ethylene/propylene (EP) copolymer. The EP copolymer with a methyl branch on each and every 9th carbon was shown to exhibit a sharp, well-defined melting point and $-13.8\text{ }^{\circ}\text{C}$ and a β -relaxation observed at $-45\text{ }^{\circ}\text{C}$. The initial thermal behavior findings for this new model EB copolymer are indeed interesting and provide a basis to better understand the precise influence that SCB content and distribution have on the final physical properties of polyethylene. In order to enhance our understanding of these materials, research is currently underway to produce a series of ADMET model EB copolymers within the same regime of varying methylene sequence lengths studied for their EP copolymer predecessors (i.e. a short chain branch on every 15th, 19th, and 21st carbon). Synthetic work is also being directed at further decreasing the branch (defect) content in these precisely branched materials in the hopes of modeling SCB levels commonly encountered in commercial LLDPEs (15-18 SCBs/1000 carbons or a SCB on every 57-67th carbon).

5.4. Experimental

5.4.1. Instrumentation and Analysis.

All ^1H NMR (300 MHz) and ^{13}C NMR (75 MHz) spectra were recorded on either a General Electric QE-Series NMR Superconducting spectrometer system or Varian Associates Gemini 300 spectrometer. Chemical shifts for ^1H and ^{13}C NMRs were referenced to residual signals from CDCl_3 with 0.03% v/v TMS as an internal reference. Reaction conversions and relative purity of crude reactions were monitored by chromatography. Gas chromatography (GC) was performed on a Shimadzu GC-17 gas chromatograph equipped with a 25 m capillary column packed with a 5% crosslinked PH ME and flame ionization detector. Thin layer chromatography (TLC) was performed on WatmanTM aluminum backed, 250 mm silica gel coated plates. TLC plates were

developed with mixtures of hexanes and ethyl acetate as the mobile phase. TLC plates for UV inactive olefin monomers were stained with either potassium permanganate (2%) in an aqueous solution of sodium bicarbonate (4%) or phosphomolybdic acid (10%) in ethanol after development to produce a visible signature. Low and high-resolution mass spectral (LRMS and HRMS) data were obtained on a Finnegan 4500 gas chromatograph/mass spectrometer using the electron ionization (EI) mode. Elemental analyses were carried out by Atlantic Microlabs Inc., Norcross, GA.

Methyl ketone and secondary alcohol intermediates were purified by vacuum distillation from calcium hydride. Initial purification of monomer was accomplished by simple short path vacuum distillation. Final purification to yield pure monomer was accomplished by either flash chromatography⁶¹ using 100% hexanes as the eluent or high performance liquid chromatography (HPLC) using 99.5% hexanes and 0.5% ethyl acetate as the mobile phase. HPLC was accomplished using a Ranin instrument equipped with Dynamax SD1 pumps, Dynamax UV-1 variable wavelength UV/VIS absorbance detector and a Varian Star 9042 Refractive Index (RI) detector in series, and Dynamax FC-1 fraction collector. Two columns were utilized: 1) analytical or scout scale column with dimensions of 10.0 mm (inner diameter) by 250.0 mm. 2) preparative scale with dimensions of 41.4 mm (inner diameter) by 250.0 mm. Both columns were silica packed with a particle size of 8 μ m and a pore size of 60 Å. Crude samples were diluted in a 25% solution (w/v) of HPLC grade hexanes and filtered prior to injection.

Gel permeation chromatography (GPC) was performed using a Waters Associates liquid chromatography U6K injector equipped with a tandem ABI Spectroflow 757 UV absorbance/Hewlett-Packard 1047-A RI detectors and a TC-45 Eppendorf column heater

set to 35 °C. All molecular weights are relative to polystyrene standards. Polymer samples were dissolved in HPLC grade tetrahydrofuran, THF, (approximately 0.1% w/v) and filtered before injection (a volume of 20 μ L). The GPC was equipped with two 300 mm Polymer Laboratories gel 5 μ m mixed-C columns. HPLC grade THF was used as the eluent at a constant flow rate of 1.0 mL/min. Retention times were calibrated against narrow molecular weight polystyrene standards (Polymer Laboratories; Amherst, MA). All standards were selected to produce M_p or M_w values well beyond the expected polymer's range. A minimum of five data points has been used to obtain calibration curves.

Fourier transform infrared (FT-IR) spectroscopy was performed using a Bio-Rad FTS-40A spectrometer. The hydrogenation of the unsaturated ADMET prepolymer was monitored by the disappearance of the out-of-plane bend C-H bend for the internal olefin at 967 cm^{-1} . Monomer was prepared by droplet deposition and sandwiched between two KCl salt plates. Unsaturated and hydrogenated polymer samples were prepared by solution casting a thin film from tetrachloroethylene onto a KCl salt plate.

Differential scanning calorimetry (DSC) analysis was performed using a Perkin-Elmer DSC 7 equipped with a controlled cooling accessory (CCA-7) at a heating rate of 10 °C/min. Calibrations were made using indium and freshly distilled *n*-octane as the standards for peak temperature transitions and indium for the enthalpy standard. All samples were prepared in hermetically sealed pans (5-10 mg/sample) and were run using an empty pan as reference and empty cells as a subtracted baseline. Prior to each measurement, each sample was first quenched from 50 °C into liquid nitrogen in order to maximize the relaxation event. Data collection was taken on the 3rd run.

Thermogravimetric analysis (TGA) was also performed. Polymers were heated from room temperature to 800 °C in nitrogen at a scan rate of 10 °C/min. The onset of weight loss was taken as the initial value. The results are listed in the experimental and in tabular form within the text. Relaxations (T_g 's) are given as onset T_g (glass transition) (second order transition) and C_p (heat capacity in J/g°C).

5.4.2. Materials.

Schrock's molybdenum catalyst $[(CF_3)_2CH_3CO]_2(N-2,6-C_6H_3-i-Pr_2)Mo=CHC(CH_3)_2Ph$ (Figure 2-1), was also synthesized via literature procedure.³⁶

Tetrahydrofuran (THF), dimethoxyethane (DME), toluene, and diethyl ether (Et_2O) were freshly distilled from Na/K alloy using benzophenone as the indicator. A solution of 2M potassium *tert*-butoxide ($KOt-Bu$) was prepared in a flame dried, argon purged Schlenk tube by combining the salt (Aldrich) with DME freshly distilled from Na/K alloy. 5-bromo-1-pentene was distilled from CaH_2 prior to use. Ethyl acetoacetate (Aldrich) was also distilled from CaH_2 prior to use. 1H NMR and ^{13}C NMR spectra for ethyl acetoacetate and 5-bromo-1-pentene are provided under the listing of starting materials. All other reagents mentioned in the experimental were used as received.

5.4.3. Characterization of Starting Materials.

Ethyl acetoacetate (Aldrich): 1H NMR ($CDCl_3$): δ (ppm) 1.29 (t, 3H, -C(O)OCH₂CH₃), 2.29 (s, 3H, -C(O)CH₃), 3.46 (s, 2H), 4.21 (q, 2H, -C(O)OCH₂CH₃), 12.17 (s, 0.06H, enol contributor); ^{13}C NMR ($CDCl_3$): δ (ppm) 14.12 (-C(O)OCH₂CH₃), 30.10 (-C(O)CH₃), 50.10, 61.30 (-C(O)OCH₂CH₃), 167.22 (-C(O)OCH₂CH₃), 200.74 (-C(O)CH₃).

5-bromo-1-pentene (Aldrich): ^1H NMR (CDCl_3): $\delta(\text{ppm})$ 1.95 (m, 2H), 2.21 (m, 2H), 3.41 (t, 2H), 5.05 (m, 2H), 5.79 (m, 1H); ^{13}C NMR (CDCl_3): $\delta(\text{ppm})$ 31.80, 32.06, 33.06, 115.91, 136.74.

5.4.4. Symmetrical Monomer Synthesis and Characterization.

5.4.4.1. Step 1: Dialkylation of ethyl acetoacetate (one-pot, two-step synthesis).

Ethyl-2-acetyl-2-(4-pentenyl)-hept-6-en-oate (4). Synthesized according to literature procedure.²⁰ **Note:** 4 batches of the disubstituted β -keto product (4) were combined before proceeding with the next reaction. The product was then placed in a roundbottom flask over CaH_2 and stirred overnight. The flask was next transferred to a vigreux distillation apparatus, placed under vacuum, and stirred overnight (5×10^{-1} mm Hg). Crude disubstituted β -keto ester (4) was distilled with a boiling point of 131-133 °C at 5×10^{-1} mm Hg. Average yield of keto-ester 4 (*for 4 batches*): 89.2% (Crude), 72.3% (Isolated). The following spectral properties were observed: ^1H NMR (CDCl_3): $\delta(\text{ppm})$ 1.18 (m, br, 4H), 1.28 (t, 3H, $-\text{C}(\text{O})\text{OCH}_2\text{CH}_3$), 1.82 (m, br, 4H), 2.06 (q, 4H), 2.11 (s, 3H, $-\text{C}(\text{O})\text{CH}_3$), 4.18 (q, 2H, $-\text{C}(\text{O})\text{OCH}_2\text{CH}_3$), 4.98 (m, 4H, vinyl CH_2), 5.74 (m, 2H, vinyl CH); ^{13}C NMR (CDCl_3): $\delta(\text{ppm})$ 14.04, 23.09, 26.60, 30.57, 33.80, 61.10, 63.25, 115.04 (vinyl CH_2), 137.88 (vinyl CH), 172.43 ($-\text{C}(\text{O})\text{OCH}_2\text{CH}_3$), 205.20 ($-\text{C}(\text{O})\text{CH}_3$); EI/LRMS: $[\text{M} + 1]^+$ calcd. for $\text{C}_{16}\text{H}_{26}\text{O}_3$: 267, found: 267. Elemental analysis calcd. for $\text{C}_{16}\text{H}_{26}\text{O}_3$: 72.14 C, 9.84 H 18.02 O; found: 71.98 C, 9.95 H, 18.22 O.

5.4.4.2. Step 2: Decarboxylation of the disubstituted β -keto ester.

2-alkoxy-3-(4-pentenyl)-7-octene (5). A 21.81 g sample of 4 (82 mmol) and 200 mL of dimethylsulfoxide (DMSO) were placed in flame dried, Ar purged 500 mL 3-neck round bottom flask equipped with a condenser and stirbar. To this solution was added

1.1 equivalents of anhydrous LiCl (3.82 g, 90 mmol) and 1.1 equivalents of D.I. H₂O (1.62 mL, 90 mmol). The reaction mixture was gently heated with a temperature-controlled hot plate. **Important:** the temperature control was set to maintain an oil bath temperature of 149-152 °C throughout the reaction. A reaction time of 20 h yielded a reaction mixture that was light brown in color (transparent). At this point, the reaction vessel was cooled to room temperature and an aliquot was taken for GC analysis. The mixture was returned to the 149-152 °C bath and reacted for an additional 21 h, upon which a second aliquot was taken. After 41 h of reaction time, the color of the mixture had changed to dark yellow/orange in color. The mixture was again stirred at 149-152 °C for an additional 31 h (72 h), after which a final aliquot was taken. After a total of 5 days (120 h), the reaction was cooled to room temperature and quenched with 200 mL of D. I. H₂O over a period of 15 minutes. An additional 100 mL of D. I. H₂O was then added and the reaction mixture was extracted (1 x 300 mL and 2 x 150 mL) with dichloromethane (CH₂Cl₂). The organics were combined, washed with DI H₂O (3 x 200 mL), and dried over MgSO₄. This mixture was stirred overnight, filtered and the dichloromethane was evaporated under reduced pressure. The product was then placed over CaH₂ and stirred overnight. The crude product over CaH₂ was then placed into a vigreux distillation apparatus, exposed to vacuum (5 x 10⁻¹ mm Hg), and stirred overnight. Crude methyl ketone (**5**) was then distilled with a boiling point of 55-60 °C at 5 x 10⁻¹ mm Hg to give 4.5 g of pure product. Yield of ester **5**: 54.1% (Crude), 28.5% (Isolated). The following spectral properties were observed: ¹H NMR (CDCl₃): δ(ppm) 1.35 (m, br, 6H), 1.43 (m, br, 2H) 1.57 (m, br, 2H), 2.02 (q, 4H), 2.11 (s, 3H, -C(O)OCH₃), 2.44 (m, 1H, R₂CHC(O)OCH₃), 4.97 (m, 4H, vinyl CH₂), 5.77 (m, 2H, vinyl CH); ¹³C NMR (CDCl₃):

δ (ppm) 26.77, 28.91, 31.15, 33.91, 53.12 ($-C(O)CH_3$), 114.99 (vinyl CH_2), 139.18 (vinyl CH), 212.99 ($-C(O)CH_3$); CI/HRMS: $[M + 1]^+$ calcd. for $C_{13}H_{23}O$: 195.1749, found: 195.1773; Elemental analysis calcd. for $C_{13}H_{23}O$: 79.94 C, 11.87 H, 8.19 O; found: 79.70 C, 12.01 H, 8.29 O.

5.4.4.3. Step 3: Reduction of the alkyl methyl ketone to the secondary alcohol.

3-(4-pentenyl)-7-octen-2-ol (6). (Two additional batches of Steps 1 and 2 were prepared and combined prior to undertaking this procedure). An 11.40 g (59 mmol) sample of purified **5** and 350 mL of dry diethyl ether were combined in a flame dried and Ar purged 3-neck 1000 mL round bottom flask equipped with a stir bar and condenser. This mixture was then cooled to 0°C and stirred for 30 min. To this stirring, cooled solution was added 176 mL (3 eq. of LAH; 12 eq. of hydride) of 1.0M lithium aluminum hydride (LAH) in Et_2O over a period of 45-60 min. Bubbling was observed during addition. The reaction was allowed to warm to room temperature and stirred for a period of 18 h. After transferring to a beaker (blanketed with a nitrogen and/or argon purge via a funnel), DI H_2O was added (**Caution:** dropwise initially) with stirring to quench the reaction. Upon formation of a gel-like solution that hinders stirring, 3N HCl was added to complete the quenching, dissolving all precipitated salts. The reaction mixture was extracted 3 x with Et_2O , washed with DI H_2O , and dried over $MgSO_4$. The combined organic extracts were filtered and evaporated under reduced pressure to yield a clear, oily substance with a trace of precipitated white salts. The product was then purified by column chromatography using a 90:10 mixture of hexane/ethyl acetate as eluent. Yield of alcohol **6**: 99.6% (Crude), 95.1% (Isolated). The following spectral properties were observed: 1H NMR ($CDCl_3$): δ (ppm) 1.38 (m, br, 9H), 1.74 (s, 1H, $-CH_2OH$), 2.04 (q,

4H), 3.53 (d, 2H, $-\text{CH}_2\text{OH}$), 4.98 (m, 4H, vinyl CH_2), 5.81 (m, 2H, vinyl CH); ^{13}C NMR (CDCl_3): $\delta(\text{ppm})$ 26.23, 30.40, 34.16, 40.36, 65.48 ($-\text{CH}_2\text{OH}$), 114.46 (vinyl CH_2), 138.90 (vinyl CH); EI/HRMS: $[\text{M} + 1]^+$ calcd. for $\text{C}_{12}\text{H}_{22}\text{O}$: 183.1749, found: 183.1796; Elemental analysis calcd. for $\text{C}_{12}\text{H}_{22}\text{O}$: 79.05 C, 12.17 H; found: 79.11 C, 12.19 H.

5.4.4.4. Step 4 (Tosylation of the alcohol).

6-(4-pentenyl)-7-(*p*-toluenesulfonyl)-1-octene (7). In a flame dried and Ar purged 250 mL 3-neck flask equipped with a stir bar, 10.94g (56 mmol) of pure **6** and 50 mL of CHCl_3 were added. This solution was cooled to 0 °C followed by the addition of 11.3 mL (11.0 g, 139 mmol) of pyridine. After stirring 20 min., 12.21 g (64 mmol) of *p*-toluenesulfonyl chloride (TsCl) was added with constant stirring. The solution changed from colorless to a yellow-brown hue after the addition. The solution was then allowed to warm to room temperature and stirred 36 h. The reaction was stopped and washed with 3N HCl to neutralize any excess pyridine and dissolve pyridinium salts. The organic layer was washed with DI H_2O and saturated K_2CO_3 solution in order to remove unreacted tosyl chloride. The aqueous layers were extracted three times by CHCl_3 , washed with DI H_2O , and combined with the original organic layer. The organic layer was dried with MgSO_4 , filtered, and evaporated under reduced pressure to yield the crude, viscous yellow oil (**7**). Attempts to isolate the product were not further pursued for fear of tosic acid elimination; therefore, yield was not calculated. The following spectral properties were observed: ^1H NMR (CDCl_3): $\delta(\text{ppm})$ 1.34 (m, br, 12H), 1.95 (d, br, 4H), 2.44 (s, 3H, methyl), 4.66 (m, 1H, $-\text{CH}(\text{OTs})\text{CH}_3$), 4.94 (m, 4H, vinyl CH_2), 5.73 (m, 2H, vinyl CH), 7.31 (dd, 2H), 7.77 (dd, 2H); ^{13}C NMR (CDCl_3): $\delta(\text{ppm})$ 17.34 ($-\text{CH}_3$), 22.07 ($-\text{CH}(\text{OTs})\text{CH}_3$), 26.86, 26.93, 29.02, 29.61, 34.19, 34.36, 43.17 (-

C(H)CH(OTs)CH_3), 82.58 ($-\text{CH(OTs)CH}_3$), 114.97 and 115.08 (vinyl CH_2), 128.12 ($-\text{SO}_2\text{CC(H)-}$), 130.13 ($-\text{SO}_2\text{CC(H)C(H)-}$), 135.03 ($-\text{SO}_2\text{C-}$), 138.88 and 139.00 (vinyl CH), 144.67; EI/LRMS: $[\text{M}]^+$ calcd. for $\text{C}_{20}\text{H}_{30}\text{SO}_3$: 350, found: 350.

5.4.4.5. Step 5: Reduction of the tosylate to yield the ethyl branch monomer (1).

3-(4-pentenyl)-7-octene [or 6-ethyl-1,10-undecadiene] (1). **Note:** Before using **7**, the monomer was dissolved in 100 mL of anhydrous diethyl ether, dried overnight by stirring over MgSO_4 , filtered, and evaporated under reduced pressure to yield a colorless, oily substance. In a flame dried and Ar purged 250 mL 3-neck flask equipped with a stirbar and 250 mL addition funnel, 6.98 g (20 mmol) of crude **7** and 100 mL of anhydrous THF were added. The stirred mixture was then cooled to -78°C (acetone/dry ice) and stirred for 30 min. To this stirring, cooled solution, 40 mL (2 eq. of hydride) of 1.0M lithium tri-ethyl borohydride (Super-Hydride®) in THF was slowly dropped into the reaction vessel via addition funnel over a period of 30-40 min; constant bubbling was observed during the addition. The reaction was gradually brought to room temperature and subsequently stirred for a period of 20 h. The mixture was then cooled to -78°C (acetone/dry ice) and an additional 20 mL of Super-Hydride® was added, the temperature brought back to room temperature, and the mixture stirred for an additional 24 h (44 h total). The reaction vessel was next cooled to 0°C and quenched with 180 mL of EtOH (vigorous evolution of gas, **Caution:** dropwise initially). The residual organoborane was then oxidized by addition of 300 mL of a 15% NaOH solution and 180 mL of a 30% hydrogen peroxide (H_2O_2). The reaction was let stand overnight due to persistent gas evolution. With a small amount gas evolution still present, the aqueous layer was separated and successively washed with diethyl ether (3 x 75 mL) and once with 50 mL of brine. The combined organics were then washed 3 x 50 mL of D. I., dried on MgSO_4

with stirring (1 h), filtered, and evaporated under reduced pressure to yield a light yellow oil that still contained trace salts. These were removed by dissolving the crude product in pentane to precipitate all remaining salts. Subsequent filtration and evaporation of pentane under reduced pressure yielded 3.00g of **1** and **8**. Yield of **1** and **8**: 83.0% (Crude mixture of products; Overall crude yield for 5 steps: 39.9%). **Purification of the mixture of 1 and 8.** A mixture of *ethyl branched (1) to eliminated monomer (8)* (7.1 : 1, by GC and NMR analysis) was formed during the reaction of the tosylate with Super-Hydride®. The crude product was purified by flash chromatography using 100% hexanes as eluent (R_f values: 0.608 ethyl branched monomer; 0.525 eliminated monomer) to yield 2.50g of **1** (Step 2.3 to 2.5: 83.3%, isolated; Overall 5 Step isolated yield: 13.6%) and 0.400 g of **8** (Step 2.3 to 2.5: 13.3%, isolated; Overall 5 Step isolated yield: 2.17%). The ethyl monomer was further purified by vacuum vigreux distillation from CaH_2 with a boiling point of 56-58 °C at 1.5 mm Hg. Monomer **1** was additionally dried via vacuum transfer to a sodium mirror. A second vacuum transfer to a storage flask equipped with a TeflonTM vacuum valve was performed followed by three successive freeze-pump-thaw degassing cycles. Finally, this flask was placed in an argon atmosphere glovebox for storage prior to polymerization.

The following spectral properties were observed for the ethyl monomer **1**: ^1H NMR (CDCl_3): $\delta(\text{ppm})$ 0.82 (t, 3H, $-\text{CH}_2\text{CH}_3$), 1.30 (m, 12H), 1.36 (m, br, 7H), 2.05 (m, 4H), 4.96 (m, 4H, vinyl CH_2), 5.81 (m, 2H, vinyl CH); ^{13}C NMR (CDCl_3): $\delta(\text{ppm})$ 10.86 ($-\text{CH}_2\text{CH}_3$), 25.95 ($-\text{CH}_2\text{CH}_3$) 26.18, 32.78, 34.23, 38.80 ($-\text{C}(\text{H})(\text{CH}_2\text{CH}_3)$), 114.14 (vinyl CH_2), 139.19 (vinyl CH); EI/HRMS: $[\text{M}]^+$ calcd. for $\text{C}_{13}\text{H}_{24}$: 180.1878, found:

180.1871; Elemental analysis calcd. for $C_{13}H_{24}$: 86.58 C, 13.42 H; found: 86.78 C, 13.50 H.

The following spectral properties were observed for the eliminated monomer **8**: 1H NMR ($CDCl_3$): δ (ppm) 1.44 (m, 7H, contains encapsulated doublet for methyl on tri-substituted alkene $R_2CC(CH_3)(H)$), 1.95 (m, 8H), 4.95 (m, 4H, vinyl CH_2), 5.21 (dd, 1H, $-CC(CH_3)(H)$), 5.82 (m, 2H, vinyl CH); ^{13}C NMR ($CDCl_3$): δ (ppm) 13.14 ($R_2CC(CH_3)(H)$), 27.49, 27.57, 29.24, 33.52, 33.78, 36.42, 114.26 (vinyl CH_2 : terminal olefin), 114.38 (vinyl CH_2 : terminal olefin), 118.88 (vinyl CH : internal olefin), 138.88 (vinyl CH : terminal olefin), 138.98 (vinyl CH : terminal olefin) 139.84 (quaternary carbon : $R_2CC(CH_3)(H)$); EI/HRMS: $[M]^+$ calcd. for $C_{13}H_{22}$: 178.1722, found: 178.1720; Elemental analysis calcd. for $C_{13}H_{22}$: 87.56 C, 12.44 H; found: 87.70 C, 12.53 H.

5.4.4.6. General Metathesis Conditions.

All glassware was thoroughly cleaned and flame dried under vacuum prior to use. The monomer was dried over CaH_2 and Na mirror and subsequently degassed prior to polymerization. All metathesis reactions were initiated in the bulk, inside an Argon atmosphere glove box. Monomer **1** was placed in a 50 mL round-bottomed flasks equipped with a magnetic TeflonTM stirbar. The flasks were then fitted with an adapter equipped with a TeflonTM vacuum valve. The adapter allows direct attachment to the vacuum line or Schlenk hose (depending on attachment design). Typical monomer to catalyst ratios are 1000-1500:1 with Schrock's $[Mo]$ catalyst. After addition of catalyst, slow to moderate bubbling of ethylene was observed. The sealed reaction vessel was removed from the drybox and immediately placed on the vacuum line. The reaction

vessel was then exposed to intermittent vacuum while stirring in an oil bath at 30 °C until the viscosity increases. Generally after 4 h, the polymerization is exposed to full vacuum ($<10^{-1}$ mm Hg) for 24 h and then high vacuum ($<10^{-3}$ mm Hg) for a period of 96 h, gradually increasing temperature to a final value of 50 °C during the last 24 h of polymerization. The reaction vessel is then cooled to room temperature. The unsaturated polymer is characterized and subsequently hydrogenated using a Parr bomb with 10% palladium on carbon using toluene as solvent, *vida infra*.

5.4.4.7. Polymerization of 3-(4-pentenyl)-7-octene (1) to give UPEB9 (2).

Monomer 1 was synthesized as described above. Schrock's [Mo] catalyst, (0.052g, 6.79×10^{-3} mmol), was added to monomer 1, (1.21 g, 6.6 mmol), in a 50 mL roundbottom flask while moderately stirring the monomer; monomer to catalyst ratio (980:1). Immediate evolution of gas ensued. The roundbottom flask was capped with a TeflonTM vacuum valve, removed from the drybox, and placed on a high vacuum line to aid in the polymerization reaction. The polymerization was continued for 120 h at which time the reaction vessel was cooled to room temperature. The flask was exposed to air and toluene was added. The mixture was heated to 80 °C in order to dissolve the resultant polymer and decompose any remaining active catalyst. The polymer/toluene solution (25 ml total) was taken up and precipitated dropwise into a vigorously stirred beaker containing 1500 ml of acidic methanol (1N stock solution prepared with HCl) that was chilled to -78 °C. Precipitation yielded an off white, stringy material that adhered to the stir bar. The unsaturated polymer was removed from the chilled solution and transferred to a pre-weighed flask. Residual methanol was removed *in vacuo* while constantly heating (50 °C) for a period of three days to yield 1.01g of a clear, tacky solid (2). Yield: 98.9% (after precipitation). [Note: 150 mg of this material was taken for characterization prior

to the hydrogenation reaction.]. The following spectral properties were obtained for the unsaturated polymer (**2**): ^1H NMR (CDCl_3): $\delta(\text{ppm})$ 0.84 (t, 3H, methyl), 1.28 (m, br, 11H), 1.97 (m, br, 4H), 5.40 (m, br, 2H, internal olefin); ^{13}C NMR (CDCl_3): $\delta(\text{ppm})$ 11.11, 26.06, 27.00, 27.12, 27.88, 32.92, 33.08, 33.27, 38.89, 130.15 (cis olefin), 130.62 (trans olefin). ^{13}C NMR (CDCl_3) integration of cis:trans peaks gives: 16:84. **GPC data (THF vs. polystyrene standards):** $M_n = 31\,400$; P.D.I. (M_w/M_n) = 1.83. **DSC Results:** Glass Transition Temperature: $T_g = -82\text{ }^\circ\text{C}$, $\Delta C_p = 0.51\text{ J/g}^\circ\text{C}$.

5.4.4.8. Hydrogenation of UPEB9 (**2**) to produce HPEB9 (**3**).

Hydrogenation was performed using a 150 mL Parr high-pressure stainless steel reaction vessel equipped with a glass liner and TeflonTM stirbar. Unsaturated polymer (**2**) was first taken up into 35 mL of toluene (80 $^\circ\text{C}$). To the pre-tared glass liner equipped with a magnetic TeflonTM stirbar was added 0.870 g of palladium (10% wt.) on activated carbon followed by the pipette addition of the 35 mL toluene solution containing 0.870 g of **2**. The glass liner was placed into the bomb and the bomb sealed. The Parr vessel was purged 3 x with 150 p.s.i. of Grade 5 hydrogen gas (H_2) in order to minimize oxygen and water introduced from the atmosphere. The bomb was charged to 500 p.s.i. and the mixture stirred for 24 h at 50 $^\circ\text{C}$ and 96 h at 80 $^\circ\text{C}$ (120 h or 5 days total). *Note:* The bomb was cooled, pressure released, and liner removed after 72 h. The glass liner was washed with hot toluene to wash down splattered carbon/polymer. Subsequently, the bomb was submitted to the same hydrogenation conditions described above for an additional 48 h. The resultant polymer was taken up into hot toluene and precipitated into $-78\text{ }^\circ\text{C}$ acidic methanol (1N stock solution prepared with HCl) to obtain a finely dispersed white solid. The polymer was filtered and reclaimed by dissolving into

chloroform in order to recover material that adhered to the glass filter. Transfer to a 50 mL roundbottom flask, evaporation under reduced pressure for 6 h, and further drying under high vacuum (3×10^{-4} mm Hg) at 70 °C for 5 days yielded 0.800 g (90.7%, after precipitation) of a translucent, tacky material at room temperature. The following spectral properties were obtained for saturated polymer 3: ^1H NMR (CDCl_3): $\delta(\text{ppm})$ 0.84 (t, 3H, methyl), 1.25 (br, 19H); ^{13}C NMR (CDCl_3): $\delta(\text{ppm})$ 11.12, 26.12, 26.99, 30.01, 30.43, 33.45, 39.09. Elemental analysis calcd. for repeat unit $(\text{C}_{11}\text{H}_{22})_n$: 85.62 C, 14.38 H; found: 84.93 C, 14.36 H. **GPC data (THF vs. polystyrene standards):** $M_n = 32\,600$; P.D.I. (M_w/M_n) = 1.78. **DSC Results:** Glass Transition Temperature Data: $T_g = -76$ °C, $\Delta C_p = 0.63$ J/g°C. Thermogravimetric Analysis (TGA) (onset of wt. loss) = 426.7 °C.

REFERENCES

1. (a) Calderon, N.; Ofstead, E. A.; Judy, W. A. *J. Poly. Sci., Part A* **1967**, *5*, 2209. (b) Calderon, N.; Chen, H. Y.; Scott, K. W. *Tet. Lett.* **1967**, 3327. (c) Calderon, N.; Ofstead, E. A.; Ward, J. P.; Judy, W.A.; Scott, K. W. *J. Am. Chem. Soc.* **1968**, *90*, 4133. (d) Scott, K. W.; Calderon, N.; Ofstead, E. A.; Judy, W. A.; Ward, J. P. *Am. Chem. Soc. Adv. Chem. Ser.* **1969**, *91*, 399. (e) Herrison, J.L.; Chauvin, Y. *Makromol. Chem.* **1970**, *141*, 161. (f) Calderon, N.; Ofstead, E. A.; Judy, W. A. *Angew. Chem., Int. Ed. Engl.* **1976**, *15*, 401.
2. Ivin, K. J.; Mol, J. C. *Olefin Metathesis and Metathesis Polymerization*, Academic Press: San Diego, 1997.
3. Metathesis reviews: *I*. [General]: Furstner, A. *Angew. Chem., Int. Ed. Engl.* **2000**, *39*, 3012 [Ring Closing Metathesis, RCM]: (a) Grubbs, R. H.; Miller, S. J.; Fu, G. C. *Acc. Chem. Res.* **1995**, *28*, 446. (b) Furstner, A. *Topic Catal.* **1997**, *4*, 285. (c) Schuster, M.; Blechert, S. *Angew. Chem., Int. Ed. Engl.* **1997**, *36*, 2037. (d) Grubbs, R. H.; Chang, S. *Tetrahedron* **1998**, *54*, 4413. *II*. [Ring Opening Metathesis Polymerization, ROMP]: (a) Schrock, R. R. *Acc. Chem. Res.* **1990**, *23*, 158. (b). Schrock, R. R. Ring Opening Metathesis Polymerization. In *Ring Opening Polymerization*; Bruneile, D. J., Ed.; Hanser: Munich, 1993, p 129. (c) Grubbs, R. H.; Khosravi, E. Ring Opening Metathesis Polymerization (ROMP) and Related Processes. In *Synthesis of Polymers, Materials Science and Technology Series*; Schluter, A. D., Ed.; Wiley: Weinheim, 1999, p 65. *III*. [Acyclic Diene METathesis, ADMET]: (a) Tindall, D. T.; Pawlow, J. H.; Wagener, K. B. Recent Advances in ADMET Chemistry. In *Topics in Organometallic Chemistry: Alkene Metathesis in Organic Synthesis*, Furstner, A., Ed.; Springer: Berlin, 1998, p 184. (b) Davidson, T. A.; Wagener, K. B. Acyclic Diene Metathesis (ADMET) Polymerization. In *Synthesis of Polymers, Materials Science and Technology Series*, Schluter, A.D., Ed.; Wiley: Weinheim, 1999.
4. Eleuterio, H. S. U.S. Patent 3,074,918, 1963.
5. Crabtree, R. H. *The Organometallic Chemistry of the Transition Metals*, 3rd ed.; Wiley and Sons: New York, 2001.

6. (a) Natta, G.; Dall'Asta, G.; Mazzanti, G. *Angew. Chem., Int. Ed. Engl.* **1964**, *3*, 723. (b) Günther, P.; Haas, F.; Marwede, G.; Nützel, K.; Oberkirch, W.; Pampus, G.; Schön, N.; Witte, J. *Die Angew. Makro. Chem.* **1970**, *14*, 87. (c) Dall'Asta, G. *Makromol. Chem.* **1972**, *154*, 1. (d) Dall'Asta, G. *Rubber Chem. Tech.* **1974**, *47*, 510.
7. (a) Sharp, P. R.; Holmes, S. J.; Schrock, R. R. *J. Am. Chem. Soc.* **1981**, *103*, 965. (b) Schrock, R. R. *Science* **1983**, *219*, 13. (c) Schrock, R. R.; DePue, R. T.; Feldman, J.; Schaverien, C. J.; Dewan, J. C.; Liu, A. H. *J. Am. Chem. Soc.* **1988**, *110*, 1423. (d) Schrock, R. R.; Murdzek, J. S.; Bazan, G. C.; Robbins, J.; DiMare, M.; O'Regan, M. *J. Am. Chem. Soc.* **1990**, *112*, 3875. (e) Schrock, R. R.; DePue, R. T.; Feldman, J.; Yap, K. B.; Yang, D. C.; Davis, W. M.; Park, L.; DiMare, M.; Schoefield, M.; Anhaus, J.; Walborsky, E.; Evitt, E.; Kruger, C.; Betz, P. *Organometallics* **1990**, *9*, 2262. (f) Feldman, J.; Schrock, R. R. *Prog. Inorg. Chem.* **1991**, *39*, 1.
8. (a) Lindmark-Hamburg, M.; Wagener, K. B. *Macromolecules* **1987**, *20*, 2949. (b) Wagener, K. B.; Nel, J. G.; Konzelman, J.; Boncella, J. M. *Macromolecules* **1990**, *23*, 5155.
9. (a) Nguyen, S. T.; Grubbs, R. H.; Ziller, J. W. *J. Am. Chem. Soc.* **1993**, *115*, 9858. (b) Schwab, P.; France, M. B.; Ziller, J. W.; Grubbs, R. H. *Angew. Chem., Int. Ed. Engl.* **1995**, *34*, 2039. (c) Schwab, P.; Grubbs, R. H.; Ziller, J. W. *J. Am. Chem. Soc.* **1996**, *118*, 100. (d) Grubbs, R. H.; Marsella, M. J.; Maynard, H. D. *Angew. Chem., Int. Ed. Engl.* **1997**, *36*, 1101. (e) Dias, E. L.; Nguyen, S. T.; Grubbs, R. H. *J. Am. Chem. Soc.* **1997**, *119*, 3887. (f) Dias, E. L.; Grubbs, R. H. *Organometallics* **1998**, *17*, 2758. (g) Trnka, T. M.; Grubbs, R. H. *Acc. Chem. Res.* **2001**, *34*, 18 and references therein.
10. (a) Scholl, M.; Ding, S.; Lee, C. W.; Grubbs, R. H. *Org. Lett.* **1999**, *1*, 953. (b) Scholl, M.; Trnka, T. M.; Morgan, J. P.; Grubbs, R. H. *Tet. Lett.* **1999**, *40*, 2247. (c) Chatterjee, A. K.; Grubbs, R. H. *Org. Lett.* **1999**, *1*, 1751. (d) Sanford, M. S.; Henling, L. M.; Day, M. W.; Grubbs, R. H. *Angew. Chem., Int. Ed. Engl.* **2000**, *39*, 3451. (e) Bielawski, C. W.; Grubbs, R. H. *Angew. Chem., Int. Ed. Engl.* **2000**, *39*, 2903.
11. (a) Herrmann, W. A.; Kocher, C. *Angew. Chem., Int. Ed. Engl.* **1997**, *36*, 2162. (b) Weskamp, T.; Schattenmann, W. C.; Spiegler, M.; Herrmann, W. A. *Angew. Chem. Int. Ed. Engl.* **1998**, *37*, 2490. (c) Weskamp, T.; Kohl, F. J.; Hieringer, W.; Gleich, D.; Herrmann, W. A. *Angew. Chem., Int. Ed. Engl.* **1999**, *38*, 2416. (d) Huang, J.; Stevens, E. D.; Nolan, S. P.; Peterson, J. L. *J. Am. Chem. Soc.* **1999**, *121*, 2674.
12. Wagener, K. B.; Brzezinska, K.; Anderson, J. D.; Younkin, T. R.; Steppe, K.; DeBoer, W. *Macromolecules* **1997**, *30*, 7363.

13. Wagener, K. B.; Boncella, J. M.; Nel, J. G.; Duttweiler, R. P.; Hillmyer, M. A. *Makromol. Chem.* **1990**, *191*, 365.
14. (a) Wagener, K. B.; Boncella, J. M.; Nel, J. G. *Macromolecules* **1991**, *24*, 2649. (b) Wagener, K. B.; Brzezinska, K. *Macromolecules* **1991**, *24*, 5273. (c) Wagener, K. B.; Smith, D. W., Jr.; *Macromolecules* **1991**, *24*, 6073. (d) Wagener, K. B.; Patton, J. T.; Boncella, J. M. *Macromolecules* **1992**, *25*, 5273. (e) Wagener, K. B.; Patton, J. T. *Macromolecules* **1993**, *26*, 249. (f) Cummings, S. K. Smith, D. W., Jr.; Wagener, K. B. *Macromol. Rapid Comm.* **1995**, *16*(5), 347. (g) Portmess, J. D.; Wagener, K. B. *J. Polym. Sci., Part A* **1996**, *34*(7), 1353. (h) Wolfe, P. S.; Wagener, K. B. *Macromol. Rapid Comm.* **1998**, *19*(6), 305. (i) Wolfe, P. S.; Wagener, K. B. *Macromolecules* **1999**, *32*, 7961. (j) Brzezinska, K. R.; Schitter, R. Wagener, K. B. *J. Poly. Sci., Part A* **2000**, *38*, 1544.
15. (a) Ingold, C. K. *J. Chem. Soc.* **1921**, *119*, 305. (b) Thorpe, J. F.; Deshapande, S. S. *J. Chem. Soc.* **1922**, *121*, 1430. (c) Eliel, E. L. *Stereochemistry of Carbon Compounds*; McGraw-Hill: New York, 1962, p 197.
16. Odian, G. *Principles of Polymerization*, 3rd ed.; John Wiley & Sons: New York, 1991, pp 74-77; 87.
17. Hadjichristidis, N.; Iatrou, H.; Pispas, S.; Pitsikalis, M. *J. Poly. Sci., Part A* **2000**, *38*, 3211.
18. (a) Shriver, D. F.; Drezdzon, M. A. *The Manipulation of Air-Sensitive Compounds*, 2nd ed.; Wiley and Sons: New York, 1986. (b) Perrin, D. D.; Armarego, W. L. F.; *Purification of Laboratory Chemicals*, 3rd ed.; Pergamon Press: New York, 1988. (c) Furniss, B. S.; Hannaford, A. J.; Smith, P. W. G.; Tatchell, A. R. *Vogel's Textbook of Practical Organic Chemistry*, 5th ed.; Longman Group and Wiley and Sons: New York, 1989.
19. Maynard, H. D.; Grubbs, R. H. *Tet. Lett.* **1999**, *40*, 4137.
20. Smith, J. A.; Brzezinska, K. R.; Valenti, D. J.; Wagener, K. B. *Macromolecules* **2000**, *33*, 3781.

21. (a) Natta, G.; Dall'Asta, G.; Bassi, I. W.; Carella, G.; *Die Angew. Makro. Chem.* **1966**, *91*, 87. (b) Scott, K. W.; Calderon, N.; Ofstead, E. A.; Judy, W. A.; Ward, J. P. *Rubber Chem. Technol.* **1971**, *44*, 1341. (c) Kormer, V. A.; Polcabaera, I. A.; Yufa, T. L. *J. Polym. Sci., Polym. Chem. Ed.* **1972**, *10*, 251. (d) Glenz, W.; Holtrup, W.; Kupper, F. W.; Meyer, H. H. *Die Angew. Makro. Chem.* **1974**, *37*, 97. (e) Porri, L.; Piversi, P.; Lucherini, A.; Rossi, R. *Makromol. Chem.* **1975**, *176*, 3121. (f) Katz, T. J.; Lee, S. J.; Acton, N. *Tet. Lett.* **1976**, 4247. (g) Sato, H.; Okimoto, K.; Tanaka, Y.; *J. Macromol. Sci., Chem.* **1977**, *A11*, 767. (h) Syatkowsky, A. J.; Denisova, T. T.; Buzina, N. A. Babitsky, B. O. *Polymer* **1980**, *21*, 1112. (i) Finter, J.; Wegner, G.; Nagel, E. J.; Lenz, R. W. *Makromol. Chem.* **1980**, *181*, 1619. (j) Hocker, H.; Reimann, W.; Reif, L.; Riebel, K. *J. Mol. Cat.* **1980**, *8*, 191.
22. (a) Katz, T. J.; Lee, S. J.; Acton, N. *Tet. Lett.* **1976**, 4247. (b) Katz, T. J.; Acton, N. *Tet. Lett.* **1976**, 4251.
23. O'Gara, J. E.; Wagener, K. B.; Hahn, S. F. *Makromol. Chem. Rapid Commun.* **1993**, *14*(10), 657.
24. (a) Meerwein, H. *Angew. Chem.* **1948**, *60*, 78. (b) Buckley, G. D.; Cross, L. H.; Ray, N. H. *J. Chem. Soc.* **1950**, 2714. (c) Kantor, S. W. Osthoff, R. C. *J. Am. Chem. Soc.* **1953**, *75*, 931. (d) Mandelkern, L.; Hellmann, M.; Brown, D. W.; Roberts, D. E.; Quinn, F. A., Jr. *J. Am. Chem. Soc.* **1953**, *75*, 4093. (e) Von Pechmann, H. *Ber. Dtsch. Chem. Ges.* **1989**, *31*, 2640.
25. Fawcett, E. W.; Gibson, R. Q.; Perrin, M. H.; Patton, J. G.; Williams E. G. Br. Pat. 2,816,883, Sept. 6, 1937 (to Imperial Chemical Industries, Ltd.).
26. (a) Ziegler, K. *Kunststoffe* **1955**, *45*, 506. (b) Ziegler, K. Belg. Pat. 533,326, May 5, 1955.
27. (a) Sinn, H.; Kaminsky, W. Ziegler-Natta Catalysts. In *Advances in Organometallic Chemistry*; Academic Press Inc.: London, 1980, pp 99-149. (b) James, D. E. *Ethylene Polymers: Encyclopedia of Polymer Science and Engineering*, 2nd ed.; Wiley-Interscience: New York, 1986, p 329.

28. (a) Keim, W.; Kowaldt, F. H.; Goddard, R.; Krüger, C. *Angew. Chem., Int. Ed. Engl.* **1978**, *17*, 466. (b) Peuckert, M.; Keim, W. *Organometallics* **1983**, *2*, 594. (c) Schmidt, G. F.; Brookhart, M. *J. Am. Chem. Soc.* **1985**, *107*, 1443. (d) Möhring, V. M.; Fink, G. *Angew. Chem., Int. Ed. Engl.* **1985**, *24*, 1001. (e) Klabunde, U. Ittel, S. D. *J. Mol. Cat.* **1987**, *41*, 123. (f) Wilke, G. *Angew. Chem., Int. Ed. Engl.* **1988**, *27*, 185. (g) Brookhart, M.; Volpe, A. F., Jr.; Lincoln, D. M.; Horvath, I. T.; Millar, J. M. *J. Am. Chem. Soc.* **1990**, *112*, 5634. (h) Rix, F.; Brookhart, M. *J. Am. Chem. Soc.* **1995**, *117*, 1137. (i) Johnson, L. K.; Killian, C. M.; Brookhart, M. *J. Am. Chem. Soc.* **1995**, *117*, 6414. (j) Johnson, L. K.; Killian, C. S.; Author, S. D.; Feldman, J.; McCord, E. F.; McLain, S. J.; Kreutzer, K. A.; Bennett, M. A.; Coughlin, E. B.; Ittel, S. D. Parthasarathy, A.; Tempel, D. J.; Brookhart, M. S. Intl. Pat. Appl. WO96/23010, 1996. (k) Long, D. P.; Bianconi, P. A. *J. Am. Chem. Soc.* **1996**, *118*, 12453. (l) Feldman, J.; McLain, S. J.; Parthasarathy, A.; Marshall, W. J.; Calabrese, J. C.; Arthur, S. D. *Organometallics* **1997**, *16*, 1514. (m) Kim, J. S.; Pawlow, J. H.; Wojcinski, L. M., II; Murtuza, S.; Kacker, S.; Sen, A. *J. Am. Chem. Soc.* **1998**, *120*, 1932. (n) Small, B.L.; Brookhart, M.; Bennett, A. M. A. *J. Am. Chem. Soc.* **1998**, *120*, 4049. (o) Younkin, T. R.; Connor, E. F.; Henderson, J. I.; Friedrich, S. K.; Grubbs, R. H.; Bansleben, D. A. *Science* **2000**, *287*, 460.
29. Wunderlich, B. *Macromolecular Physics: Crystal Melting*; Academic Press: New York, 1980, Vol. 3, pp 275-278.
30. (a) Wunderlich, B.; Poland, D. *J. Poly. Sci., Part A* **1963**, *1*, 357. (b) Gutzler, F.; Wegner, G. *Colloid Polym. Sci.* **1980**, *258*, 776. (c) Mirabella, F. M., Jr.; Ford, E. A. *J. Poly. Sci., Part B: Polym. Phys.* **1987**, *25*, 777. (d) Alamo, R. G.; Mandelkern, L. *Macromolecules* **1989**, *22*, 1273. (e) Failla, M. D.; Lucas, J. C.; Mandelkern, L. *Macromolecules* **1994**, *27*, 1334. (f) Lambert, W. S.; Phillips, P. J. *Polymer* **1996**, *37*, 3585.
31. (a) Gutzler, F.; Wegner, G. *Coll. Polym. Sci.* **1980**, *258*, 776. (b) Bowmer, T. N.; Tonelli, A. E. *Polymer* **1985**, *26*, 1195. (c) Bowmer, T. N.; Tonelli, A. E. *Macromolecules* **1986**, *19*, 498. (d) Tonelli, A. E.; Valenciano, M. *Macromolecules* **1986**, *19*, 2643. (e) Buerger, D. E.; Boyd, R. H. *Macromolecules* **1989**, *22*, 2694. (f) Buerger, D. E.; Boyd, R. H.; *Macromolecules* **1989**, *22*, 2699. (g) Gomez, M. A.; Tonelli, A. E.; Lovinger, A. J.; Schilling, F. C.; Cozine, M. H.; Davis, D. D. *Macromolecules* **1989**, *22*, 4441. (h) Smith, G. D.; Boyd, R. H. *Macromolecules* **1991**, *24*, 2725. (i) Smith, G. D.; Boyd, R. H. *Macromolecules* **1991**, *24*, 2731. (j) Smith, G. D.; Liu, F.; Devereaux, R. W.; Boyd, R. H. *Macromolecules* **1992**, *25*, 703. (k) Smith, G. D.; Boyd, R. H. *Macromolecules* **1992**, *25*, 1326. (l) Pourahmady, N.; Bak, P. I. *J. Macromol. Sci.-Pure Appl. Chem.* **1992**, *A29(11)*, 959. (m) Chowdhury, F.; Haigh, J. A.; Mandelkern, L.; Alamo, R. G. *Polym. Bull.* **1998**, *41*, 463. (n) Bistac, S.; Kunemann, P.; Schultz, J. *Polymer* **1998**, *39*, 4875.

32. (a) Yakota, K.; Hirabayashi, T. *Macromolecules* **1981**, *14*, 1613. (b) Yakota, K.; Kouga, T.; Hirabayashi, T. *Polym. J.* **1983**, *15*, 349. (c) Hirabayashi, T.; Yamauchi, K.; Yakota, K. *Macromolecules* **1991**, *24*, 4543. (d) Yakota, K.; Miwa, M.; Hirabayashi, T.; Inai, Y. *Macromolecules* **1992**, *25*, 5821. (e) Gerum, W.; Höhne, G. W. H.; Wilke, W.; Arnold, M.; Wegner, T. *Macromol. Chem. Phys.* **1995**, *196*, 3797.
33. Watson, M. D.; Wagener, K. B. *Macromolecules* **2000**, *33*, 3196-3201.
34. Valenti, D.; Wagener, K. B. *Macromolecules* **1998**, *31*, 2764.
35. Watson, M. D.; Wagener, K. B. *Macromolecules* **2000**, *33*, 5411 (2000).
36. Reisch, M. S. *Chem. and Eng. News* **1997**, *75*, 14.
37. (a) Mandelkern, L.; Glotin, M.; Benson, R. A. *Macromolecules* **1981**, *14*, 22. (b) Alamo, R. G.; Chan, E. K. M.; Mandelkern, L.; Voight-Martin, I. G. *Macromolecules* **1992**, *25*, 6381. (c) Alamo, R. G.; Viers, B. D.; Mandelkern, L. *Macromolecules* **1993**, *26*, 5740. (d) Schumacher, M.; Lovinger, A. J.; Agarwal, P.; Wittmann, J. C. Lotz, B. *Macromolecules* **1994**, *27*, 6956. (e) Hachimoto, T.; Prud'homme, R. E.; Stein, R. S.; *J. Polym. Sci., Polym. Phys. Ed.* **1973**, *11*, 709. (f) Kawaguchi, T.; Ito, T.; Kawai, H.; Keedy, D.; Stein, R. S. *Macromolecules* **1968**, *1*, 126.
38. (a) Kim, Y.; Kim, C.; Park, J.; Kim, J.; Min, T. *J. Appl. Polym. Sci.* **1996**, *60*, 2469, and references therein. (b) Gerum, W.; Höhne, G. W. H.; Wilke, W.; Arnold, M.; Wegner, T. *Macromol. Chem. Phys.* **1996**, *197*, 1691. (c) Shroff, R.; Prasad, A.; Lee, C. *J. Polym. Sci., Part B: Polym. Phys.* **1996**, *34*, 2317. (d) Pieski, E. T. *Polyethylene*; Renfrew, A.; Morgan, P.; Eds. Interscience Publishers, Inc.: New York, 1960. (e) Ke, B. *J. Polym. Sci.* **1960**, *42*, 15. (f) Ke, B. *J. Polym. Sci.* **1962**, *61*, 47. (g) Alamo, R. G.; Mandelkern, L.; Stack, G. M.; Krönke, C.; Wegner, G. *Macromolecules* **1994**, *27*, 147. (h) Mirabella, F. M., Jr.; Ford, E. A. *J. Polym. Sci., Part B: Polym. Phys.* **1987**, *25*, 777.
39. (a) Valenti, D. J.; Wagener, K. B.; Hahn, S.F. *Macromolecules* **1997**, *30*, 6688. (b) Valenti, D. J.; Wagener, K. B. *Macromolecules* **1997**, *30*, 6688. (c) Valenti, D. J. Ph.D. Dissertation, University of Florida, 1997.
40. O'Gara, J. E.; Portmess, J. D.; Wagener, K. B. *Macromolecules* **1993**, *26*, 2831; and references therein.
41. Newkome, G. R.; Baker, M. B.; Caruso, A.; Greewald, M. M.; Hanson, P. G.; Mangogna, G. A.; Mathes, P. D.; Pascal, R. A.; Rigby, H. O.; Riser, J. M.; Schnabel, J. J.; Sonnier, J. A.; Steinkampf, M. P.; Johnson, J. L. *Synthesis* **1975**, 517.
42. Petraghani, N.; Massami, Y. *Synthesis* **1982**, 521.

43. (a) Eliel, E. L. *Stereochemistry of Carbon Compounds*; McGraw-Hill: New York, 1962; 197. (b) Jung, M. E.; Garvey, J. *J. Am. Chem. Soc.* **1991**, *113*, 224. (c) Kirby, A. J. *Adv. Phys. Org. Chem.* **1980**, *17*, 183.
44. Hill, E. A.; Link, D. C.; Donndelinger, P. *J. Org. Chem.* **1981**, *46*, 1177; and references therein.
45. Watson, M. D. Ph.D. Dissertation, University of Florida, 1999.
46. Hahn, S. F. *J. Polym. Sci., Part A* **1992**, *30*, 397.
47. (a) Kaminsky, W. *Macromol. Chem. Phys.* **1996**, *197*, 3907. (b) Zucchini, U.; Cecchin, G. *Adv. Polym. Sci.* **1983**, *51*, 101.
48. (a) Wunderlich, B.; Czorny, G. *Macromolecules* **1977**, *10*, 906. (b) Wilski, H. *Kunststoffe* **1964**, *54*, 90. (c) Buckley, C. P.; Kovacs, A. J. *Prog. Colloid Polym. Sci.* **1975**, *58*, 44. (d) Wunderlich, B. "The Basis of Thermal Analysis." *Thermal Characterization of Polymeric Materials*; Academic Press Inc.: Orlando, FL; 1981, p 181.
49. Carman, C. J.; Tarpley, A. R., Jr.; Goldstein, J. H. *Macromolecules* **1973**, *6*, 719.
50. (a) Hoffman, J. D. *Polymer* **1983**, *24*, 3. (b) Hoffman, J. D. *Polymer* **1982**, *23*, 656.
51. Quirk, R. P.; Alsamarraie, M. A. A. In *Polymer Handbook*, 3rd ed.; Brandrup, J.; Immergut, E. H., Eds. John Wiley & Sons: New York, 1989; Section V, pp 15-26; and references therein.
52. Gopalan, M.; Mandelkern, L. *J. Phys. Chem.* **1967**, *71*, 3833.
53. Mandelkern, L.; Prasad, A.; Alamo, R. G.; Stack, G. M. *Macromolecules* **1990**, *23*, 3696.
54. Griskey, R.; Foster, G. *J. Polym. Sci., Polym. Chem. Ed.* **1970**, *8*, 1623.
55. (a) Flory, P. J. *J. Chem. Phys.* **1947**, *15*, 684. (b) Flory, P. J. *Trans Farad. Soc.* **1955**, *51*, 848.
56. Kline, D. E.; Sauer, J. A.; Woodward, A. E. *J. Poly. Sci.* **1956**, *22*, 455.
57. Stehling, F. C.; Mandelkern, L. *Macromolecules* **1970**, *3*, 242; and references therein.
58. Boyer, R. F. *Encyclopedia of Polym. Sci. and Tech.* Mark, H. F.; Bikales, N. M., Eds., Supplemental No. 2, **1977**, p 745.
59. Davis, G. T.; Eby, R. K. *J. Appl. Phys.* **1973**, *44*, 4274-4281.

60. Chang, S. S. *J. Polym. Sci., Polym. Symp.* **1973**, 43, 43-54.
61. (a) Illers, K. H. *Kolloid-Z. Z. Polym.* **1969**, 231, 622. (b) Illers, K. H. *Kolloid-Z. Z. Polym.* **1974**, 252, 1. (c) Illers, K. H. *Kolloid-Z. Z. Polym.* **1973**, 251, 394. (d) Illers, K. H. *Kolloid-Z. Z. Polym.* **1963**, 190, 16.
62. Hendra, P. J.; Jobic, H. P.; Holland-Moritz, K. *J. Polym. Sci., Polym. Lett. Ed.* **1975**, 13, 365.
63. Boyer, R. F. *J. Polym. Sci.* **1966**, C14, 3.
64. Still, W. C.; Kahn, M.; Abhijit, M. *J. Org. Chem.* **1978**, 43, 2923.
65. Katritzky, A. R.; Nowak-Wydra, B.; Marson, C. M. *Chemica Scripta* **1987**, 26.
66. Univation_Technologies—Market_Information.<http://www.univation.com/markets/market.asp> (accessed Feb 2002).
67. (a) Mellbring, O.; Øiseth, S. K.; Krozer, A.; Lausmaa, J.; Hjertberg, T. *Macromolecules* **2001**; 34; 7496-7503. (b) Wilkes, G. *Macromolecules* **1997**, 30, 2412-2421.
68. Nowlin, T. E.; Kissin, Y.V.; Wagener, K. P. *J. Polym. Sci., Part A.* **1988**, 26, 755.
69. Escalona, A. M.; Fuentes, A.; Liscano, T.; Alboronoz, A. *Stud. Surface Sci. Catal.* **1990**, 56, 377.
70. Chu, K. J.; Park, T. H.; Ha, J. W. *Mater. Lett.* **1997**, 30, 115.
71. Alamo, R. G.; Mandelkern, L. *Thermochim. Acta.* **1994**, 238, 155.
72. Murakami, S. *Macromolecules* **1996**, 29, 1540-1547.
73. Mathot, V. B. F., ed. *Calorimetry and Thermal Analysis of Polymers*; Hanser Publishers: New York, 1994; ch. 9, p 231.
74. Defoor, F.; Groeninckx, G.; Schouterden, P.; Van der Heijden, B. *Polymer* **1998**, 39, 4541.
75. Starck, P. *Polym. Int.* **1996**, 40, 111.
76. Hosoda, S. *Polym. J.* **1988**, 20, 383.
77. Crist, B.; Howard, P. R. *Macromolecules* **1999**, 32, 3057.
78. Wild, L. *Adv. Polym. Sci.* **1990**, 98, 1.

79. Schouterden, P.; Groeninckx, G.; Van der Heijden, B.; Jansen, F. *Polymer* **1987**, *28*, 2099-104.
80. Guathier, X-V. *Informations Chimie* **1996**, *375*, 83.
81. Soares, J. B. P.; Penlidis, A. *J. Polym. Sci., Part A: Polym. Chem.* **1998**, *36*, 831.
82. Sinn, H.; Kaminsky, W.; Vollmer, H. J.; Woldt, R. *Angew. Chem., Int. Ed. Engl.* **1980**, *19*, 390.
83. Reddy, S. S.; Sivaram, S. *Prog. Polym. Sci.* **1995**, *20*, 309.
84. Kaminsky, W.; Kulper, K.; Brintzinger, H. H.; Wild, F. R. W. P. *Angew. Chem.* **1985**, *24*, 507.
85. Reddy, S. S.; Sivaram, S. *Prog. Polym. Sci.* **1995**, *20*, 309.
86. Huang, J.; Rempel, G. L. *Prog. Polym. Sci.* **1995**, *20*, 459.
87. Hsieh, E. T.; Tso, C. C.; Byers, J. D.; Johnson, T. W.; Fu, Q.; Cheng, S. Z. D. *J. Macromol. Sci., Part B: Phys.* **1997**, *36*, 615.
88. Kim, M. -H.; Phillips, P. J. *J. Appl. Polym. Sci.* **1998**, *70*, 1893-1905.
89. Mathot, V. B. F.; Scherrenberg, R. L.; Pijpers, M. F. J.; Bras, W. *J. Thermal Anal.* **1996**, *46*, 681.
90. Peeters, M.; Goderis, B.; Vonk, C.; Reynaers, H.; Mathot, V. B. F. *J. Polym. Sci., Part B: Polym. Phys.* **1997**, *35*, 2689.
91. Xu, X.; Xu, J.; Feng, L.; Chen, W. *J. Appl. Polym. Sci.* **2000**, *77*, 1709.
92. (a) Kc, B. *J. Polym. Sci.* **1962**, *61*, 47. (b) Alamo, R. G.; Mandelkern, L.; Stack, G. M.; Krönke, Wegner, G. *Macromolecules* **1994**, *27*, 147. (c) Gutzler, F.; Wegner, G. *Colloid and Polym. Sci.* **1980**, *258*, 776. (d) Mirabella, F. M., Jr.; Ford, E. A. *J. Polym. Sci., Part B: Polym. Phys.* **1987**, *25*, 777-790. (e) Wunderlich, B.; Poland, D. *J. Polym. Sci., Part A: Polym. Chem.* **1963**, *1*, 357-372. (f) Alamo, R. G.; Mandelkern, L. *Macromolecules* **1989**, *22*, 1273.

93. (a) Mandelkern, L.; Glotin, M.; Bensen, R. A. *Macromolecules* **1981**, *14*, 22. (b) Alamo, R. G.; Chan, E. K. M.; Mandelkern, L.; Voight-Martin, I. G. *Macromolecules* **1992**, *25*, 6381. (c) Alamo, R. G.; Viers, B. D.; Mandelkern, L. *Macromolecules* **1993**, *26*, 5740. (d) Schumacher, M.; Lovinger, A. J.; Agarwal, P.; Wittmann, J. C.; Lotz, B.; *Macromolecules* **1994**, *27*, 6956. (e) Hachimoto, T.; Prud'homme, R. E.; Stein, R. S. *J. Polym. Sci., Polym. Phys. Ed.* **1973**, *11*, 709.
94. (a) Kawaguchi, T.; Ito, T.; Kawai, H.; Keedy, D.; Stein, R. S. *Macromolecules* **1968**, *1*, 126. (b) Lambert, W. S.; Phillips, P. J. *Polymer* **1996**, *37*, 3585. (c) Kim, Y.; Kim, C.; Park, J.; Kim, J.; Min, T. *J. Appl. Polym. Sci.* **1996**, *60*, 2469; and references therein. (d) Gerum, W.; Hohne, G. W. H.; Wilke, W.; Arnold, M.; Wegner, T. *Macromol. Chem. Phys.* **1995**, *196*, 3797.
95. (a) Gerum, W.; Hohne, G. W. H.; Wilke, W.; Arnold, M.; Wegner, T. *Macromol. Chem. Phys.* **1996**, *197*, 1691-1712. (b) Shroff, R.; Prasad, A.; Lee, C. *J. Polym. Sci., Part B: Polym. Phys.* **1996**, *34*, 2317. (c) Pieski, E. T. *Polyethylene*; Renfrew, A.; Morgan, P., eds. Interscience Publishers, Inc.: New York, 1960. (d) Ke, B. *J. Polym. Sci.* **1960**, *42*, 15.
96. (a) Ungar, G.; Zeng, X-b. *Chem. Rev.* **2001**, *101*, 4157-4188 (232 references). (b) Bracco, S.; Comotti, A.; Simonutti, R.; Camurati, I.; Sozzani, P. *Macromolecules* **2002**, *35*, 1677-1684. (c) DesLauriers, P. J.; Rohlfing, D. C.; Hsieh, E. T. *Polymer* **2002**, *43*, 159-170. (d) Zhang, F.; Song, M.; Lü, T.; Liu, J.; He, T. *Polymer* **2002**, *43*, 1453-1460. (e) DesLauriers, P. J.; Rohling, D. C.; Hsieh, E. T. *Polymer* **2002**, *43*, 159-170. (f) Starck, P.; Malmberg, A.; Löfgren, B. *J. Appl. Poly. Sci.* **2002**, *83*, 1140-1156. (g) Sun, T.; Brant, P.; Chance, R. R.; Graessley, W. W. *Macromolecules* **2001**, *34*, 6812-6820. (h) Jokela, K.; Väänänen, A.; Torkkeli, M.; Starck, P.; Serimaa, R.; Löfhren, B.; Seppälä, J. *J. Poly. Sci., Part B: Poly. Phys.* **2001**, *39*, 1860-1875. (i) Wright, K. J.; Lesser, A. J. *Macromolecules* **2001**, *34*, 3626-3633. (j) Pak, J.; Wunderlich, B. *Macromolecules* **2001**, *34*, 4492-4503. (k) Zhang, X-b.; Li, Z-s.; Lu, Z-y.; Sun, C-c. *J. Chem. Phys.* **2001**, *115*, 3916-3922. (l) Walter, P.; Heinemann, J.; Ebeling, H.; Mader, D.; Trinkle, S.; Rolf, M. *Organomet. Catal. Olefin Poly.* **2001**, 317-326. (m) Haigh, J. A.; Nguyen, C.; Alamo, R. G.; Mandelkern, L. *J. Therm. Anal. Calorim.* **2000**, *59*, 435-450. (n) Hadjichristidis, N.; Xenidou, M.; Iatrou, H.; Pitsikalis, M.; Poulos, Y.; Avgeropoulos, A.; Sioula, S.; Paraskeva, S.; Velis, G.; Lohse, D. J.; Schulz, D. N.; Fetters, L. J.; Wright, P. J.; Mendelson, R. A.; Garcia-Franco, C. A.; Sun, T.; Ruff, C. J. *Macromolecules* **2000**, *33*, 2424-2436.
97. Watson, M. D.; Wagener, K. B. *Macromolecules* **2000**; *33*; 8963-8970.
98. Watson, M. D.; Wagener, K. B. *Macromolecules* **2000**; *33*; 5411-5417.
99. Wunderlich, B. *Macromolecular Physics: Crystal Structure, Morphology, Defects*, 1, Academic Press, Inc.: New York, 1980; Vol. 1, pp 401-407.

100. Mathot, V. B. F.; Pijpers, M. F. J. *J. Polym. Sci., Part B: Polym. Phys.* **1990**, *39*, 979.
101. Mathot, V. B. F.; Pijpers, M. F. J. *J. Thermal. Anal.* **1983**, *28*, 349.
102. Mathot, V. B. F., ed. *Calorimetry and Thermal Analysis of Polymers*; Hanser Publishers: New York, 1994, Ch. 5, p 105.
103. Keating, M. Y.; McCord E. F. *Thermchim. Acta.* **1994**, *243*, 129.
104. Phillips, P. J.; Vatansever, A. *Polymer* **1989**, *30*, 711.
105. Gohil, R. M.; Phillips, P. J. *Polymer* **1986**, *27*, 1687.
106. Gohil, R. M.; Phillips, P. J. *Polymer* **1986**, *27*, 1696.
107. Wunderlich, B. *Macromolecular Physics: Crystal Melting*, 1, Academic Press, Inc.: New York, 1980; Vol. 3.
108. Sanchez, I. C.; Eby, R. K. *J. Res. Nat. B. Stand.* **1973**, *77*, 353.
109. Finke, H. L.; Gross, M. E.; Waddington, G.; Huffman, H. M. *J. Am. Chem. Soc.* **1954**, *76*, 331-341.
110. Hakvoort, G. *J. Thermal Anal.* **1994**, *43*, 1551-1555.
111. Emsley, J. *The Elements*, Oxford University Press: New York, 1998; pp 1-292.
112. Illers, K. -H. *Eur. Polym. J.* **1974**, *10*, 911-916.
113. Keller, A. *Macromol. Symp.* **1995**, *98*, 1.
114. Wunderlich, B. *Macromolecular Physics: Crystal Structure, Morphology, Defects*, 1, Academic Press, Inc.: New York, 1980; Vol. 1.
115. Wunderlich, B. *Macromolecular Physics: Crystal Nucleation, Growth, and Annealing*, 1, Academic Press, Inc.: New York, 1980; Vol. 2.
116. Keller, A.; Hikosaka, M.; Rastogi, S.; Toda, A.; Barham, P. J.; Godbeck-Wood, G. *J. Mater. Sci.* **1994**, *29*, 2579.
117. Hoffman, J. D.; Lauritzen, J. J., Jr. *J. Res. Natl. Bur. Stand., Sect. A* **1961**, *65*, 297.
118. Wunderlich, B. *Macromolecular Physics: Crystal Melting*, 1, Academic Press, Inc.: New York, 1980; Vol. 3., p 30.

119. (a) Wild, L.; Ryle, T. R.; Knobeloch, D. C.; Peat, I. R. *J. Polym. Sci., Part B: Polym. Phys.* **1982**, *20*, 441-455. (b) Wild, L. *Adv. Polym. Sci.* **1990**, *98*, 1. (c) Karoglanian, S. A.; Harrison, I. R. *Thermochimica Acta* **1996**, *288*, 239-245. (d) Gabriel, C.; Lilge, D. *Polymer* **2001**, *42*, 297-303. (e) Xu, J.; Xu, X.; Feng, L. *Eur. Polym. J.* **2000**, *36*, 685-693. (f) Zhang, M.; Lynch, D. T.; Wanke, S. E. *J. Appl. Polym. Sci.* **2000**, *75*, 960-967. (g) Zhang, M.; Lynch, D. T.; Wanke, S. E. *Polymer* **2001**, *42*, 3067-3075. (h) Xu, J.; Xu, X.; Feng, L.; Chen, L.; Chen, W. *Macromol. Chem. Phys.* **2001**, *202*, 1524-1530. (i) Wang, C.; Chu, M. -C.; Lin, T. -L.; Lai, S. -M.; Shih, H. -H.; Yang, J. -C. *Polymer* **2001**, *42*, 1733-1741. (j) Brüll, R.; Pasch, H.; Raubenheimer, H. G.; Sanderson, R.; Van Reenen, A. J.; Wahner, U. M. *Macromol. Chem. Phys.* **2001**, *202*, 1281-1288.
120. Bravais, A. *J. Ecole Polytech.* **1850**, *19*, 1-128 [English Transl.: Shaler, A. *Cryst. Soc. Amer. Memoir* **1949**, n1].
121. Miller, W. H. *A Treatise on Crystallography*, Cambridge Pitt Press: London, 1839.
122. Röntgen, W. C. *Zh. Russ. Fiz. Kim. Ova., Chast. Fiz.* **1896**, *28*, 1B, 12.
123. Fredrich, W., Knipping, P., Laue, M. *Sitzungber. Math.-Phys. Klasse Bayer Akad. Wiss. München* **1912**, *5*, 303-322; reprinted with slight changes in *Ann. Phys.* **1913**, *41*, 971.
124. Bragg, W. H. *Proc. Camb. Phil. Soc.* **1913**, *17*, 43.
125. Bragg, W. H. *Phil. Mag.* **1914**, *27*, 881.
126. Bragg, W. H.; James, R. W.; Bosanquet, C. H. *Phil. Mag.* **1921**, *41*, 309.
127. Bragg, W. H.; James, R. W.; Bosanquet, C. H. *Phil. Mag.* **1921**, *42*, 1.
128. Müller, A. *J. Chem. Soc.* **1925**, *127*, 599.
129. Müller, A. *Proc. Roy. Soc.: Ser. A* **1928**, *120*, 437.
130. Müller, A. *Proc. Roy. Soc.: Ser. A* **1930**, *127*, 805.
131. Müller, A. *Proc. Roy. Soc.: Ser. A* **1932**, *138*, 514.
132. Hengstenberg, J. *Z. Kristallogr.* **1928**, *67*, 583.
133. Kohlhaas, R.; Soremba, K. H. *Z. Kristallogr.* **1938**, *100*, 47.
134. Smith, A. E. *J. Chem. Phys.* **1953**, *21*, 2229.
135. Shearer, H. M. M.; Vand, V. *Acta Crystallogr.* **1956**, *9*, 379.
136. Brathovde, J. R.; Lingafelter, E. C. *Acta Crystallogr.* **1958**, *11*, 729.

137. Kitaigorodsky, A. I. *Tetrahedron* **1960**, *9*, 183.
138. Vainshtein, B. K.; Pinsker, Z. G. *Dokl. Akad. Nauk SSSR* **1950**, *72*, 53.
139. Müller, A.; Lonsdale, K. *Acta Crystallogr.* **1948**, *1*, 129.
140. (a) Piper, S. H.; Brown, D.; Dymont, S. *J. Chem. Soc.* **1925**, *127*, 2194. (b) Schoon, T. *Z. Phys. Chem., Abt. B* **1938**, *39*, 385.
141. Schoon, T. *Z. Phys. Chem., Abt. B* **1938**, *39*, 385.
142. Schaerer, A. A.; Bayle, G. G.; Mazel, W. H. *Rec. Trav. Chim. Pays-Bas* **1956**, *75*, 513.
143. Pitzer, K. S. *Discuss. Faraday Soc.* **1951**, *10*, 66-73.
144. Taylor, W. J. *J. Chem. Phys.* **1948**, *16*, 257-267.
145. Bunn, W. C. *Trans. Faraday* **1939**, *35*, 482.
146. Vand, V. *Acta Crstallogr.* **1951**, *4*, 104.
147. Sauter, E. *Z. Phys. Chem.* **1932**, *B18*, 417.
148. Storks, K. H. *J. Am. Chem. Soc.* **1938**, *60*, 1753.
149. Herrmann, K.; Gerngross, O.; Abitz, W. *Z. Phys. Chem.* **1930**, *10*, 371.
150. Yundt, A. P. *Tappi* **1951**, *34*, 89.
151. Schlesinger, W.; Leeper, H. M. *J. Polym. Sci.* **1953**, *11*, 203.
152. Keller, A.; Waring, J. R. S. *J. Polym. Sci.* **1955**, *17*, 447.
153. Jaccondine, R. *Nature* **1955**, *176*, 305.
154. Peck, V.; Kaye, W. *J. Appl. Phys.* **1954**, *25*, 1465.
155. Keller, A. *Phil. Mag.* **1957**, *2*, 1171-1175.
156. Fischer, E. W. *Z. Naturforsch.* **1957**, *12a*, 753-754.
157. Till, P. H., Jr. *J. Polym. Sci.* **1957**, *24*, 301-306.
158. Hendra, P. J. "The Measurement of Lamellar Thickness by Raman Methods." In *Structural Studies of Macromolecules by Spectroscopic Methods*; Ivin, K. J., Ed.; John Wiley & Sons: New York, 1976, Chapter 6.
159. Flory, P. J. *J. Am. Chem. Soc.* **1962**, *84*, 2857-2867.

160. Lauritzen, J. I., Jr.; Hoffman, J. D. *J. Res. Natl. Bur. Stand.* **1960**, A 64, 73.
161. Sadler, D. *Polymer* **1983**, 24, 1401.
162. Strobl, G. *Eur. Phys. J.* **2000**, E 3, 165-183.
163. Lotz, B. *Eur. Phys. J.* **2000**, E 3, 185-194.
164. Cheng, S. Z. D.; Li, C. Y.; Zhu, L. *Eur. Phys. J.* **2000**, E 3, 195-197.
165. Wagener, J.; Phillips, P. J. *Polymer* **2001**, 42, 8999-9013.
166. Muthukumar, M. *Eur. Phys. J.* **2000**, E3, 199-202.
167. Geil, P. H. *Polymer Single Crystals*, Interscience: New York, 1963.
168. Debye, P.; Scherrer, P. *Physik. Zeit.* **1916**, 17, 277.
169. Hull, A. W. *Phys. Rev.* **1917**, 10, 661.
170. Buerger, M. J. *J. Appl. Phys.* **1945**, 16, 501.
171. Kratky, O.; Laggner, P. *Encyclopedia of Physical Science and Technology*; Academic Press: New York, 1987, Vol. 14, pp 693-742.
172. Glatter, O. In *Small Angle X-ray Scattering*; Glatter, O.; Kratky, O., Eds.; Academic Press: New York, 1982, Chapter IV.
173. Kiessig, H. *Kolloid Z. Z. Polymere* **1942**, 98, 213.
174. *Applied Polymer Light Microscopy*; Hemsley, D. A., Ed.; Elsevier Applied Science: New York, 1989.
175. Maksymilian, P. *Advanced Light Microscopy*, Elsevier Science Publishing Company: New York, Vol.1, 1988.
176. Maksymilian, P. *Advanced Light Microscopy*, Elsevier Science Publishing Company: New York, Vol.2, 1989.
177. Sawyer, L. C.; Grubb, D. T. *Polymer Microscopy*, Chapman and Hall: New York, 1987.
178. Goodhew, P. J. *Specimen Preparation in Materials Science*, American Elsevier: New York, 1973.
179. *Physics of Polymer Surfaces and Interfaces*; Sanchez, I. C.; Fitzpatrick, L. E., Eds.; Manning: Greenwich, Connecticut, 1992.

180. Urban, M. W. *Attenuated Total Reflectance Spectroscopy of Polymers: Theory and Practice*, American Chemical Society: Washington, D.C., 1996.
181. *Characterization of Solid Polymers: New Techniques and Developments*; Spells, S. J., Ed.; Chapman & Hall: New York, 1994.
182. Mandelkern, L. *Crystallization of Polymers*, McGraw-Hill, Inc.: New York, 1964.
183. Baker, A. M. E.; Windle, A. H. *Polymer* **2001**, *42*, 667-680; and 83 references therein.
184. Voight-Martin, I. G.; Fischer, E. W. *J. Polym. Sci.: Part B, Polym. Phys.* **1980**, *18*, 2347-2367.
185. Fischer, E. W. *Makromol. Chem, Macromol. Symp.* **1988**, *20/21*, 277-291.
186. Slichter, W. P. *J. Polym. Sci.* **1956**, *21*, 141-143.
187. Walter, E. R.; Reding, F. P. *J. Polym. Sci.* **1956**, *21*, 561-562.
188. Mathot, V. B. F.; Scherrenberg, R. L.; Pijpers, T. F.; Bras, W. *Polym. Prepr. (Am. Chem. Soc., Div. Polym. Chem.)* **1995**, *36*, 302-303.
189. Sun, Z; Yu, F; Qi, Y. *Polymer* **1991**, *32*, 1059-60.
190. Simanke, A. G.; Alamo, R. G.; Galland, G. B.; Mauler, R. S. *Macromolecules* **2001**, *34*, 6959-6971.
191. Guerra, G.; Galimberti, M.; Piemontesi, F.; de Ballesteros, O. R. *J. Am. Chem. Soc.* **2002**, *124*, 1566-1567.
192. Eichhorn, R. M. *J. Polym. Sci.* **1958**, *31*, 197-198.
193. Preedy, J. E. *Br. Polym. J.* **1973**, *5*, 13-19.
194. Howard, P. R.; Crist, B. *J. Polym. Sci., Part B: Polym. Phys.* **1989**, *27*, 2269-2282.
195. Baker, C. H.; Mandelkern, L. *Polymer* **1966**, *7*, 71-83.
196. Holdworth, P. J.; Keller, A. *Polym. Lett.* **1967**, *5*, 605-612.
197. Swan, P. R. *J. Polym. Sci.* **1962**, *56*, 409-416.
198. Bodily, D.; Wunderlich, B. *J. Polym. Sci.: Part A2.* **1966**, *4*, 25-40.
199. Vonk, C. G. *J. Polym. Sci.: Part C.* **1972**, *38*, 429-35.

200. Burfield, D. R.; Kashiwa, N. *Makromol. Chem.* **1985**, *186*, 2657-2662.
201. Androsch, R. *Polymer* **1999**, *40*, 2805-2812.
202. Androsch, R.; Blackwell, J.; Chvalun, S. N.; Wunderlich, B. *Macromolecules* **1999**, *32*, 3755-3740.
203. Richardson, M. J.; Flory, P. J.; Jackson, J. B. *Polymer* **1963**, *4*, 221-236.
204. Cole, E. A.; Holmes, D. R. *J. Polym. Sci.* **1960**, *46*, 245-256.
205. Shirayama, K.; Kita, S-I.; Watabe, H. *Makromol. Chem.* **1972**, *151*, 97-120.
206. Kavesh, S.; Schulz, J. M. *J. Polym. Sci.: Part A2*. **1970**, *8*, 243-276.
207. Baker, A. M. E.; Windle, A. H. *Polymer* **2000**, *42*, 667-680.
208. Baker, A. M. E.; Windle, A. H. *Polymer* **2000**, *42*, 681-698.
209. Baker, A. M. E.; Windle, A. H. *Polymer* **2001**, *42*, 651-665.
210. Bassi, I. W.; Corradini, P.; Fagherazzi, G.; Valvassori, A. *Eur. Polym. J.* **1970**, *6*, 709-718.
211. Guerra, G.; Ilavský, M.; Biroš, J.; Dušek, K. *Colloid Polym. Sci.* **1981**, *259*, 1190.
212. Ver Strate, G.; Wichinsky, Z. W. *J. Polym. Sci.: Part A-2* **1971**, *9*, 127.
213. Baldwin, F. P.; Ver Strate, G. *Rubber Chem. Technol.* **1972**, *45*, 709.
214. Griskey, R.; Foster, G. *J. Polym. Sci., Polym. Chem. Ed.* **1970**, *8*, 1623.
215. Gilbert, M; Briggs, J. E.; Omana, W. *Br. Polym. J.* **1979**, *11*, 81.
216. Koivumäki, J.; Seppälä, J. V. *Eur. Polym. J.* **1994**, *30*, 1111.
217. Scholtens, B. J. R.; Riande, E.; Mark, J. E. *J. Polym. Sci., Polym. Phys. Ed.* **1984**, *22*, 1223.
218. Jokela, K.; Väänänen, A.; Torkkeli, M.; Starck, P.; Serimaa, R.; Löfhren, B.; Seppälä, J. *J. Poly. Sci., Part B: Poly. Phys.* **2001**, *39*, 1860-1875.
219. Keating, M. Y.; McCord E. F. *Thermchim. Acta.* **1994**, *243*, 129.
220. Phillips, P. J.; Vatansever, A. *Polymer* **1989**, *30*, 711.
221. Gohil, R. M.; Phillips, P. J. *Polymer* **1986**, *27*, 1687.

222. Gohil, R. M.; Phillips, P. J. *Polymer* **1986**, *27*, 1696.
223. Smith, J. A.; Wagener, K. B.; Lieser, G.; Wegner, G. *Thermal Behavior of Model Ethylene/Propylene Copolymers with Precise Methyl Branch Placement*, Full manuscript submitted to *Macromolecules*.
224. Defoor, F.; Groeninckx, G.; Reynaers, H.; Schouterden, P.; Van der Heijden, B. *J. Appl. Polym. Sci.* **1993**, *47*, 1839-1848.
225. Zhang, M.; Lynch, D. T.; Wanke, S. E. *Polymer* **2001**, *42*, 3067-3075.
226. Wunderlich, B.; Sullivan, P.; Arakawa, T.; DiCyan, A. B.; Flood, J. F. *J. Polym. Sci.: Part A1*. **1963**, *1*, 3581.
227. Ueberreiter, K.; Orthmann, H. J. *Kolloid Z.* **1953**, *132*, 61.
228. Stuart, H. *Ann. N. Y. Acad. Sci.* **1959**, *83*, 1.
229. Rohleder, J. *Makromol. Chem.* **1960**, *41*, 124.
230. Zachmann, H. G.; Stuart, H. A. *Macromol. Chem.* **1960**, *8*, 131.
231. Roe, R. -J. *J. Chem. Phys.* **1970**, *53*, 3026.
232. Zachmann, H. G.; Stuart, H. A. *Macromol. Chem.* **1960**, *8*, 148.
233. Eby, R. K. *J. Appl. Phys.* **1962**, *33*, 2253.
234. Zachmann, H. G. *Fortschr. Hochpolym.-Forsch.* **1964**, *3*, 581.
235. Ewers, W. M.; Zachmann, H. G.; Peterlin, A. *J. Macromol. Sci.* **1972**, *B6*, 695.
236. Zachmann, H. G.; Peterlin, A. *J. Macromol. Sci.* **1969**, *B3*, 495.
237. Gasparyan, K. A.; Borokonovskii, V. A.; Sevast'yanov, L. K.; Mirzoyev, R. G.; Baranov, V. G. *Polym. Sci. USSR* **1976**, *18*, 628.
238. Crist, B.; Williams, D. N. *J. Macromol. Sci.: Physics* **2000**, *B39*, 1-13.
239. Swann, P. R. *J. Polym. Sci.* **1962**, *56*, 409-416.
240. Walter, E. R.; Reding, E. P. *J. Polym. Sci.* **1956**, *21*, 561.
241. Crespi, G.; Valvassori, A.; Zamboni, V.; Flisi, U. *Chim. Ind. (Milan)* **1973**, *55*, 130.
242. Eichorn, R. M. *J. Polym. Sci.* **1958**, *31*, 197.
243. Baker, C. H.; Mandelkern, L. *Polymer* **1965**, *7*, 71.

- 244. Cole, E. A.; Holmes, D. R. *J. Polym. Sci.* **1960**, *46*, 245.
- 245. Preedy, J. E. *Br. Polym. J.* **1973**, *5*, 13.
- 246. Gilbert, M.; Briggs, J. E.; Omana, W. *Br. Polym. J.* **1979**, *11*, 81.
- 247. Baldwin, F. P.; Ver Strate, G. *Rubber Chem. Technol.* **1972**, *45*, 709.
- 248. Scholtens, B. J. R.; Riande, E.; Mark, J. E. *J. Polym. Sci.: Part B, Polym. Phys.* **1984**, *22*, 1223.
- 249. Ruiz de Ballesteros, O.; Auriemma, F.; Guerra, G.; Corradini, P. *Macromolecules* **1996**, *29*, 7141.
- 250. Guerra, G.; Ruiz de Ballesteros, O.; Venditto, V.; Galimberti, M.; Sartori, F.; Pucciariello, R. *J. Polym. Sci., Part B: Polym. Phys.* **1999**, *37*, 1095-1103.
- 251. Richardson, M. J.; Flory, P. J.; Jackson, J. B. *Polymer* **1963**, *4*, 221-236.
- 252. Bassett, D. C.; Block, S.; Piermarini, G. J. *J. Appl. Phys.* **1974**, *45*, 4146-4150.
- 253. Bassett, D. C.; Turner, B. *Phil. Mag.* **1974**, *29*, 925.
- 254. Yasuniwa, M.; Nakafuku, C.; Takemura, T. *Polymer J.* **1973**, *4*, 526.
- 255. Maeda, Y.; Keanetsuna, H. *J. Polym. Sci.: Part A-2* **1974**, *12*, 2551.
- 256. Maeda, Y.; Keanetsuna, H. *J. Polym. Sci.: Part A-2* **1975**, *13*, 637.
- 257. Yasuniwa, M.; Takemura, T. *Polymer* **1974**, *15*, 661.
- 258. Yasuniwa, M.; Enoshita, R.; Takemura, T. *Jap. J. Appl. Polym. Phys.* **1976**, *15*, 1421-1428.
- 259. Ungar, G. *Macromolecules* **1986**, *19*, 1317-1324.
- 260. Noid, D. W.; Sumpter, B. G.; Wunderlich, B. *Macromolecules* **1990**, *23*, 664-669.
- 261. Sumpter, B. G.; Noid, D. W.; Wunderlich, B. *J. Chem. Phys.* **1990**, *93*, 6875-6889.
- 262. Rastogi, S.; Hikosaka, M.; Kawabata, H.; Keller, A. *Macromolecules* **1991**, *24*, 6384-6391.
- 263. Galeski, A.; Bartczak, Z.; Argun, A. S.; Cohen, R. E. *Macromolecules* **1992**, *25*, 5705-5718.
- 264. Kavassalis, T. A.; Sundararajan, P. R. *Macromolecules* **1993**, *26*, 4144-4150.

265. Tashiro, K.; Sasaki, S.; Kobayashi, M. *Macromolecules* **1996**, *29*, 7460-7469.
266. Bartczak, Z.; Galeski, A.; Argun, A. S.; Cohen, R. E. **1996**, *37*, 2113-2123.
267. Fujiwara, Tetsuya, S. *J. Chem. Phys.* **1997**, *107*, 613.
268. Rastogi, S.; Kurelec, L.; Lemstra, P. J. *Macromolecules* **1998**, *31*, 5022-5031.
269. Kuwabara, K.; Horii, F. *Macromolecules* **1999**, *32*, 5600-5605.
270. Kurelec, L.; Rastogi, S.; Meier, R. J.; Lemstra, P. J. *Macromolecules* **2000**, *33*, 5593-5601.
271. Wunderlich, B.; Grebowicz, J. J. *Adv. Polym. Sci.* **1984**, *60/61*, 1-59.
272. Sumpter, B. G.; Noid, D. W.; Liang, G. L.; Wunderlich, B. *Adv. Polym. Sci.* **1984**, *116*, 27-72.
273. Seto, T.; Hara, T.; Tanaka, K. *Jpn. J. Appl. Phys.* **1968**, *37*, 31-42.
274. Teare, P. W.; Holmes, D. R. *J. Polym. Sci.* **1957**, *24*, 496.
275. Turner-Jones, A. *J. Polym. Sci.* **1962**, *62*, 174.
276. Ewald, P. P. *Zeit. f. Krist.* **1921**, *56*, 129.
277. Ewald, P. P. *Krist.* **1936**, *93*, 396.
278. International Union of Crystallography. *International Tables for X-ray Crystallography*; Kynock Press: Birmingham, U.K., 1952, Vol 1-4.
279. International Union of Crystallography. *International Tables for X-ray Crystallography*; Kluwer Academic Publishers Group: Boston, M.A., 1984-present, Vols. B & F.
280. Kieth, H. D.; Padden, F. J. *J. Appl. Phys.* **1963**, *34*, 2409.
281. Ward, I. M., Ed. *Structure and Properties of Oriented Polymers*; Applied Science: London, 1975.
282. Bassett, D. C. *Principles of Polymer Morphology*; Cambridge University Press: Cambridge, 1981.
283. Bassett, D. C. *CRC Crit. Rev. Solid State Mater. Sci.* **1984**, *12*, 97.
284. Zhang, X-b.; Ze-sheng, L.; Lu, Z-y.; Sun, C-C. *Macromolecules* **2002**, *25*, 106-111.

285. Bradley, D. E. Replica and Shadowing Techniques. In *Techniques for Electron Microscopy*; Kay, D. H., Ed.; Blackwell: Oxford, U. K., 1965, 96.
286. Keller, A.; O'Conner, A. *Discuss. Faraday Soc.* **1958**, 25, 114.
287. Sella, C.; Trillat, J. -J. *Compt. Rend.* **1959**, 248, 410.
288. Wunderlich, B. *Macromolecular Physics: Crystal Structure, Morphology, Defects*, 1, Academic Press, Inc.: New York, 1980; Vol. 1, pp 283-295; and references therein.
289. Allen, P.; Bevis, M. *Proc. Roy. Soc.* **1974**, A341, 75.
290. Lovinger, A. J.; Keith, H. D. *Macromolecules* **1979**, 12, 919.
291. Geiss, R. H.; Street, G. B.; Volksen, W.; Economy, J. *IBM J. Res. Develop.* **1983**, 27, 321.
292. Boerio, F. J.; Koenig, J. L. *J. Chem. Phys.* **1970**, 52, 3425.
293. Barnes, J. D.; Fanconi, B. M. *J. Chem. Phys.* **1972**, 56, 5190-5192.
294. Khoury, F.; Fanconi, B.; Barnes, J. D.; Bolz, L. H. *Bull. Am. Phys. Soc.* **1973**, 18, 403-404.
295. Wu, C.; Nicol, M. *J. Chem. Phys.* **1973**, 58, 5150-5162.
296. Takeuchi, H.; Shimanout, T.; Tasumi, M.; Vergoten, G.; Fleury, G. *Chem. Phys. Lett.* **1974**, 28, 449-453.
297. Fonconi, B. M.; Crissman, J. *J. Polym. Sci., Polym. Lett. Ed.* **1975**, 13, 421-426.
298. Rabolt, J. F.; Fanconi, B. M. *J. Polym. Sci., Polym. Lett. Ed.* **1977**, 15, 121-127.
299. Chang, C.; Krimm, S. *J. Polym. Sci., Polym. Lett. Ed.* **1979**, 17, 2163-2170.
300. Strobl, G. R. *Colloid and Polym. Sci.* **1976**, 254, 170-189.
301. Zerbi, G.; Gussoni, M. *Bull. Am. Phys. Soc.* **1979**, 24, 347.
302. Chang, C.; Krimm, S. *J. Polym. Sci.: Part B., Polym. Phys.* **1979**, 17, 2163-2170.
303. Strobl, G. R.; Eckel, R. *Colloid and Polym. Sci.* **1980**, 258, 570-577.
304. Lee, K-S; Wegner, G. *Makromol. Chem. Rapid Commun.* **1985**, 6, 203-208.
305. Sano, K.; Shimoyama, M.; Ohgane, M.; Higashiyama, H.; Watari, M.; Tomo, M.; Ninomiya, T.; Ozaki, Y. *Appl. Spectr.* **1999**, 53, 551-556.

306. Ungar, G.; Zeng, X. B.; Spells, S. J. *Polymer* **2000**, *41*, 8775-8780.
307. Ferguson, E. E. *J. Am. Chem. Soc.* **1956**, *78*, 1115.
308. Martin, J. M., Jr.; Johnston, R. W. B.; O'Neal, M. J. *Spectrochim. Acta* **1958**, *12*, 12-16.
309. Snyder, R. G.; Schachtschneider, J. H. *Spectrochim. Acta* **1963**, *19*, 85-116.
310. Snyder, R. G.; Schachtschneider, J. H. *Spectrochim. Acta* **1963**, *19*, 117.
311. Snyder, R. G. *J. Chem. Phys.* **1979**, *71*, 3229-3235.
312. Grossmann, H. P.; Arnold, R.; Bürkle, K. R. *Polym. Bull.* **1980**, *3*, 135-142.
313. Zerbi, G.; Gussoni, M. *Polymer* **1980**, *21*, 1129-1134.
314. Blitz, J. P.; McFaddin, D. C. *J. Appl. Polym. Sci.* **1994**, *51*, 13-20.
315. Ungar, G.; Organ, S. J. *Polym. Commun.* **1987**, *28*, 232-235.
316. Hastie, G. P.; Roberts, K. J. *J. Mater. Sci.* **1994**, *29*, 1915-1919.
317. Lee, J-S.; Chung, H. *Vibrational Spectr.* **1998**, *17*, 193-201.
318. Theimer, O. *J. Chem. Phys.* **1957**, *27*, 1041-1048.
319. Lee, K-S; Wegner, G.; Hsu, S. L. *Polymer* **1987**, *28*, 889-896.
320. Snyder, R. G.; Maroncelli, M.; Qi, S. P.; Strauss, H. L. *Science* **1981**, *214*, 188.
321. Maroncelli, M.; Qi, S. P.; Strauss, H. L.; Snyder, R. G. *J. Am. Chem. Soc.* **1982**, *104*, 6327.
322. Strobl, G.; Ewen, B.; Fischer, E. W.; Piesczek, W. *J. Chem. Phys.* **1974**, *61*, 5257.
323. Ewen, B.; Fischer, E. W.; Piesczek, W.; Strobl, G. *J. Chem. Phys.* **1974**, *61*, 5265.
324. Kim, Y.; Strauss, H. L.; Snyder, R. G. *J. Phys. Chem.* **1989**, *93*, 7520.
325. Sirota, E. B.; King, H. E., Jr.; Singer, D. M.; Shao, H. H. *J. Chem. Phys.* **1995**, *98*, 5809.
326. Boerio, F. J.; Koenig, J. L. *J. Chem. Phys.* **1970**, *52*, 3425.
327. Tanaka, H.; Takemura, T. *Polym. J.* **1980**, *12*, 355.

328. Strobl, G. R.; Hagedorn, W. *J. Polym. Sci.: Part B, Polym. Phys.* **1978**, *16*, 1181-1193.
329. Snyder, R. G.; Shu, S. L.; Krimm, S. *Spectrochim. Acta* **1978**, *34*, 395.
330. Snyder, R. G.; Scherer, J. *J. Chem. Phys.* **1979**, *71*, 3221-3228.
331. Cho, Y.; Kobayashi, M.; Tadkkoro, H. *Polym. Prepr. Jpn.* **1986**, *30*, 1842.
332. Baker, C.; Maddams, W. *Makromol. Chem.* **1976**, *177*, 437.
333. Jones, R. N.; McKay, A. F.; Sinclair, R. G. *J. Am. Chem. Soc.* **1952**, *74*, 2575-2578.
334. Sinclair, R. G.; McKay, A. F.; Myers, G. S.; Jones, R. N. *J. Am. Chem. Soc.* **1952**, *74*, 2578-2585.
335. (a) Sowinski, A. F.; Whitesides, G. M. *J. Org. Chem.* **1979**, *44*, 2369-2376. (b) Fouquet, G.; Schlosser, M. *Angew. Chem., Int. Ed. Engl.* **1974**, *13*, 82-83. (c) Normant, J. F. *Synthesis* **1972**, 63-80. (d) Corey, E. J.; Posner, G. H. *J. Am. Chem. Soc.* **1967**, *89*, 3911-3912. (e) Corey, E. J.; Posner, G. H. *J. Am. Chem. Soc.* **1968**, *90*, 5615-5616. (f) House, H. O.; Respass, W. L.; Whitesides, G. M. *J. Org. Chem.* **1966**, *31*, 3128-3141. (g) Tochtermann, W. *Angew. Chem., Int. Ed. Engl.* **1966**, *5*, 351-371. (h) Gilman, H.; Jones, R. G.; Woods, L. A. *J. Org. Chem.* **1952**, *17*, 1630-1634.
336. (a) Ireland, R. E.; Muchmore, D. C.; Hengartner, U. *J. Am. Chem. Soc.* **1972**, *94*, 5098-5100. (b) Ireland, R. E.; Pfister, G. *Tet. Lett.* **1969**, 2145-2148. (c) Barton, D. H. R.; McCombie, S. W. *J. Chem. Soc., Perkin Trans. I* **1975**, 1574. (d) Barton, D. H. R.; Subramanian, R. *J. Chem. Soc., Perkin Trans. I* **1977**, 1718. (e) Acton, E. M.; Goener, R. N.; Uh, H. S.; Ryan, K. J.; Henry, D. W.; Cass, C. E.; LePage, G. A. *J. Med. Chem.* **1979**, *22*, 518. (f) Robins, M. J.; Wilson, J. S.; Hansske, F. *J. Am. Chem. Soc.* **1983**, *105*, 4059.
337. (a) Marchland, A. P.; Madhava Sharma, G. V.; Annapurna, G. S.; Pednekar, P. R. *J. Org. Chem.* **1987**, *52*, 4784-4788. (b) Krishnamurthy, S.; Brown, H. C. *J. Org. Chem.* **1980**, *45*, 849-856. (c) Bryce-Smith, D.; Wakefield, B. J.; Blues, E. T. *Proc. Chem. Soc., London* **1963**, 219. (d) Toi, H.; Yamamoto, Y.; Sonoda, A.; Murahashi, S. -I. *Tetrahedron* **1981**, *37*, 2261-2267.
338. Tamura, M.; Kochi, J. *Synthesis* **1971**, 303-305.
339. (a) Watt, D. S. *Tet. Lett.* **1974**, *n9*, 707-710. (b) Savoia, D.; Tagliavini, E.; Trombini, C.; Umani-Ronchi, A. *J. Org. Chem.* **1980**, *45*, 3227-3229.
340. (a) Krishnamurthy, S. *J. Org. Chem.* **1980**, *45*, 2551-2553. (b) Brown, H. C.; Krishnamurthy, S. *Tetrahedron* **1979**, *35*, 567-607.

341. (a) Wittig, G.; Geissler, G. *Justus Liebigs Ann. Chem.* **1953**, *44*, 580. (b) Maercker, A. *Org. React.* **1965**, *14*, 270.
342. (a) Hutchins, R. O.; Milewski, C. A.; Maryanoff, B. E. *J. Am. Chem. Soc.* **1973**, *95*, 3662-3668. (b) Kabalka, G. W.; Baker, J. D., Jr. *J. Org. Chem.* **1975**, *40*, 1834-1835. (c) Kabalka, G. W.; Yang, T. C.; Baker, J. D., Jr. *J. Org. Chem.* **1976**, *41*, 574-575. (d) Kabalka, G. W.; Summers, S. T. *J. Org. Chem.* **1981**, *46*, 1217-1218.
343. (a) Krapcho, A. P.; Weimaster, J. F.; Eldridge, J. M.; Jahngen, G. E., Jr.; Lovey, A. J.; Stephens, W. P. *J. Org. Chem.* **1978**, *43*, 138-147. (b) Krapcho, A. P. *Synthesis* **1982**, 805-822. (c) Krapcho, A. P. *Synthesis* **1982**, 893-914. (d) Krapcho, A. P.; Gowrikumar, G. *J. Org. Chem.* **1987**, *52*, 1880-1881.
344. Krishnamurthy, S.; Brown, H. C. *J. Org. Chem.* **1976**, *41*, 3064-3066.
345. House, H. O. *Modern Synthetic Reactions*, 2nd ed.; W. A. Benjamin: Menlo Park, CA, 1972.
346. (a) Liu, W.; Ray, D. G., III; Rinaldi, P. L. *Macromolecules* **1999**, *32*, 3817-3819. (b) Axelson, D. E.; Levy, G. C.; Mandelkern, L. *Macromolecules* **1979**, *12*, 41-52.
347. (a) Grant, D. M.; Paul, E. G. *J. Am. Chem. Soc.* **1964**, *86*, 2984-2990. (b) Lindeman, L. P.; Adams, J. Q. *Anal. Chem.* **1971**, *43*, 1245-1252.
348. Randall, J. C. *Rev. Macromol. Chem. Phys.* **1989**, *C29* (2 & 3), 201.
349. (a) Vanden Eynde, S.; Mathot, V.; Koch, M. H. J.; Reynaers, H. *Polymer* **2000**, *41*, 3437-3453. (b) Zang, M.; Lynch, D. T.; Wanke, S. E. *Polymer* **2001**, *42*, 3067-3075. (c) Crist, B.; Howard, P. R. *Macromolecules* **1999**, *32*, 3057-3067. (d) Pérez, E.; VanderHart, D. L.; Crist, B., Jr.; Howard, P. R. *Macromolecules* **1987**, *20*, 78-87. (e) Krigas, T. M.; Carella, J. M.; Struglinski, M. J.; Crist, B.; Graessley, W. W. *J. Polym. Sci., Polym. Phys. Ed.* **1985**, *23*, 509-520. (f) Crist, B.; Williams, D. N. *J. Macromol. Sci.—Phys.* **2000**, *B39*, 1-13. (g) Crist, B.; Claudio, E. S. *Macromolecules* **1999**, *32*, 8945-8951. (h) Xu, J. T.; Xu, X. R.; Chen, L. S.; Feng, L. X. *J. Mater. Sci. Lett.* **2000**, *19*, 1541-1543. Xu, X.; Xu, J.; Feng, L.; Chen, W. *J. Appl. Polym. Sci.* **2000**, *77*, 1709-1715. (i) Xu, J.; Xu, X.; Feng, L. *Eur. Polym. J.* **1999**, *36*, 685-693.

BIOGRAPHICAL SKETCH

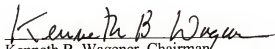
Jason Alan Smith was born in Columbia, South Carolina, on July 4, 1973. Shortly thereafter, he relocated to Joanna, South Carolina, where he was reared for the next eighteen years. Upon graduation from Clinton High School in May 1991, he entered Clemson University where he received a Bachelor of Science degree in December 1995. While at Clemson, he conducted research not only in the synthesis of polychalcogen-based complexes but also in the study of supercritical depolymerization reactions under the supervision of Dr. Joseph W. Kolis.

During the summers of his undergraduate career, he worked for the Monsanto Chemical Company in Greenwood, South Carolina, as a result of being chosen a Monsanto Scholar. After graduating from Clemson, he accepted an eight-month position at the Monsanto Chemical Company in Pensacola, Florida, where he carried out research in the areas of nuclear magnetic resonance, near-infrared spectroscopy, and finish-on-fiber analysis under the direction of Dr. James E. Rodgers.

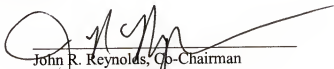
He began his graduate studies in organic/polymer chemistry at the University of Florida in August 1996 under the guidance of Professor Kenneth B. Wagener. Beginning in March 2000, while at Florida, he traveled to Europe in order to conduct x-ray scattering and microscopy investigations at the Max-Planck-Institut für Polymerforschung (MPI-P) in Mainz, Germany, under the co-direction of Professor Dr. Gerhard Wegner and Dr. Günter Lieser. After returning in December 2000, he completed the degree requirements for the Doctor of Philosophy and received his Ph.D. in organic

chemistry on August 10, 2002. In early September 2002, he relocated to Spartanburg, South Carolina and began his post-graduate career with the Research and Development Group for Milliken Chemical's Chemical Performance Business as a Development Chemist.


I certify that I have read this study and that in my opinion it conforms to acceptable standards of scholarly presentation and is fully adequate, in scope and quality, as a thesis for the degree of Doctor of Philosophy.


Kenneth B. Wagener, Chairman
George B. Butler Professor of Polymer
Chemistry

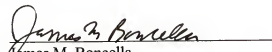
I certify that I have read this study and that in my opinion it conforms to acceptable standards of scholarly presentation and is fully adequate, in scope and quality, as a thesis for the degree of Doctor of Philosophy.


John R. Reynolds, Co-Chairman
Professor of Chemistry

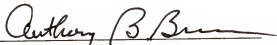
I certify that I have read this study and that in my opinion it conforms to acceptable standards of scholarly presentation and is fully adequate, in scope and quality, as a thesis for the degree of Doctor of Philosophy.


J. Eric Enholm
Professor of Chemistry

I certify that I have read this study and that in my opinion it conforms to acceptable standards of scholarly presentation and is fully adequate, in scope and quality, as a thesis for the degree of Doctor of Philosophy.


James M. Boncella
Professor of Chemistry

I certify that I have read this study and that in my opinion it conforms to acceptable standards of scholarly presentation and is fully adequate, in scope and quality, as a thesis for the degree of Doctor of Philosophy.

A handwritten signature in dark ink, appearing to read "Anthony B. Brennan", written over a horizontal line.

Anthony B. Brennan
Professor of Materials Science and
Engineering

This thesis was submitted to the Graduate Faculty of the Department of English in the College of Liberal Arts and Sciences and to the Graduate School and was accepted as partial fulfillment of the requirements for the degree of Doctor of Philosophy.

August 2002

Dean, Graduate School